NUREG/CR-4599
BMI-2173
Vol. 2, No. 1

Short Cracks in Piping and Piping Welds

Semiannual Report
April–September 1991

Prepared by
G. M. Wilkowski, F. Brust, R. Francini,
N. Ghadiali, T. Kilinski, P. Krishnaswamy, M. Landow,
C. W. Marschall, S. Rahman, P. Scott

Battelle

Prepared for
U.S. Nuclear Regulatory Commission

AVAILABILITY NOTICE

Availability of Reference Materials Cited in NRC Publications

Most documents cited in NRC publications will be available from one of the following sources:

1. The NRC Public Document Room, 2120 L Street, NW., Lower Level, Washington, DC 20555
2. The Superintendent of Documents, U.S. Government Printing Office, P.O. Box 37082, Washington, DC 20013-7082
3. The National Technical Information Service, Springfield, VA 22161

Although the listing that follows represents the majority of documents cited in NRC publications, it is not intended to be exhaustive.

Referenced documents available for inspection and copying for a fee from the NRC Public Document Room include NRC correspondence and internal NRC memoranda; NRC bulletins, circulars, information notices, inspection and investigation notices; licensee event reports; vendor reports and correspondence; Commission papers; and applicant and licensee documents and correspondence.

The following documents in the NUREG series are available for purchase from the GPO Sales Program: formal NRC staff and contractor reports, NRC-sponsored conference proceedings, international agreement reports, grant publications, and NRC booklets and brochures. Also available are regulatory guides, NRC regulations in the *Code of Federal Regulations*, and *Nuclear Regulatory Commission Issuances*.

Documents available from the National Technical Information Service include NUREG-series reports and technical reports prepared by other Federal agencies and reports prepared by the Atomic Energy Commission, forerunner agency to the Nuclear Regulatory Commission.

Documents available from public and special technical libraries include all open literature items, such as books, journal articles, and transactions. *Federal Register* notices, Federal and State legislation, and congressional reports can usually be obtained from these libraries.

Documents such as theses, dissertations, foreign reports and translations, and non-NRC conference proceedings are available for purchase from the organization sponsoring the publication cited.

Single copies of NRC draft reports are available free, to the extent of supply, upon written request to the Office of Administration, Distribution and Mail Services Section, U.S. Nuclear Regulatory Commission, Washington, DC 20555.

Copies of industry codes and standards used in a substantive manner in the NRC regulatory process are maintained at the NRC Library, 7920 Norfolk Avenue, Bethesda, Maryland, for use by the public. Codes and standards are usually copyrighted and may be purchased from the originating organization or, if they are American National Standards, from the American National Standards Institute, 1430 Broadway, New York, NY 10018.

DISCLAIMER NOTICE

NUREG/CR-4599
BMI-2173
Vol. 2, No. 1

Short Cracks in Piping and Piping Welds

Semiannual Report
April–September 1991

Manuscript Completed: May 1992
Date Published: September 1992

Prepared by
G. M. Wilkowski, F. Brust, R. Francini,
N. Ghadiali, T. Kilinski, P. Krishnaswamy, M. Landow,
C. W. Marschall, S. Rahman, P. Scott

Battelle
505 King Avenue
Columbus, OH 43201

Prepared for
Division of Engineering
Office of Nuclear Regulatory Research
U.S. Nuclear Regulatory Commission
Washington, DC 20555
NRC FIN B5702

ABSTRACT

This is the third semiannual report of the U.S. Nuclear Regulatory Commission's Short Cracks in Piping and Piping Welds research program. This 4-year program began in March 1990. The overall objective of this program is to verify and improve fracture analyses for circumferentially cracked large-diameter nuclear piping with crack sizes typically used in leak-before-break analyses or in-service flaw evaluations.

Progress for through-wall-cracked pipe involved: (1) evaluation of a 4-inch-diameter French TP316 pipe which showed high anisotropy, (2) completion of a matrix of FEM analyses to determine the GE/EPRI functions for short TWC pipe, and (3) examination of a 28-inch-diameter TP316 stainless steel SAW test, which showed that the crack grew significantly farther in the fusion line, indicating a lower toughness region. A significant finding to date is that shorter cracks fail closer to net-section-collapse predicted loads than long cracks, hence there is greater margins for short cracks than long cracks in SRP 3.6.3 for LBB which is based on the ASME Section XI code source equations for long crack behavior.

For surface-cracked pipe, a comparison of pipe experiments with Net-Section-Collapse predictions showed the limitation of the Net-Section-Collapse analysis as a function of the pipe R/t.

The investigation of dynamic strain aging (DSA) involved: (1) an examination of a carbon steel SAW it had different high temperature fracture properties from the base metals examined, (2) measurement of crack velocities during an unstable crack jump due to DSA, (3) an examination of fracture surfaces in stable and unstable crack jump regions, and (4) a comparison of the occurrence of crack jumps in pipe tests relative with those in laboratory specimen tests.

For anisotropic fracture evaluations, a literature review on microstructural aspects that affect anisotropic fracture properties in carbon steel was conducted. A correlation between the degree of anisotropy and angled crack growth in past pipe experiments showed more scatter than anticipated.

Crack-opening area analyses involved validation of deterministic analyses for probabilistic evaluations to provide a technical basis for changes to NRC Regulatory Guide 1.45 on leakage detection systems.

A new version of the NRCPIPE code, containing numerous circumferential through-wall-cracked pipe J-estimation schemes, was compiled and released to the NRC. Other efforts involved: (1) numerical evaluations of residual stress on elastic plastic fracture (conducted at the University of Michigan), and (2) several ASME Section XI activities on pipe flaw evaluation criteria.

CONTENTS

CONTENTS

CONTENTS

CONTENTS

CONTENTS

LIST OF FIGURES

LIST OF FIGURES

LIST OF FIGURES

LIST OF TABLES

LIST OF TABLES

PREVIOUS REPORTS IN SERIES

Previous Reports from this Program

"Short Cracks in Piping and Piping Welds," First Semiannual Report, NUREG/CR-4599, Vol. 1, No. 1, March 1991.

"Short Cracks in Piping and Piping Welds," Second Semiannual Report, NUREG/CR-4599, Vol. 1, No. 2, April 1992.

Previous Related Documents from NRC's Degraded Piping Program

"Degraded Piping Program - Phase II," Semiannual Report, NUREG/CR-4082, Vol. 1, October 1984.

"Degraded Piping Program - Phase II," Semiannual Report, NUREG/CR-4082, Vol. 2, June 1985.

"Degraded Piping Program - Phase II," Semiannual Report, NUREG/CR-4082, Vol. 3, March 1986.

"Degraded Piping Program - Phase II," Semiannual Report, NUREG/CR-4082, Vol. 4, July 1986.

"Degraded Piping Program - Phase II," Semiannual Report, NUREG/CR-4082, Vol. 5, December 1986.

"Degraded Piping Program - Phase II," Semiannual Report, NUREG/CR-4082, Vol. 6, April 1988.

"Degraded Piping Program - Phase II," Semiannual Report, NUREG/CR-4082, Vol. 7, March 1989.

"Degraded Piping Program - Phase II," Semiannual Report, NUREG/CR-4082, Vol. 8, March 1989.

"NRC Leak-Before-Break (LBB.NRC) Analysis Method for Circumferentially Through-Wall Cracked Pipes Under Axial Plus Bending Loads," Topical Report, NUREG/CR-4572, March 1986.

"Elastic-Plastic Finite Element Analysis of Crack Growth in Large Compact Tension and Circumferentially Through-Wall-Cracked Pipe Specimen--Results of the First Battelle/NRC Analysis Round Robin," Topical Report, NUREG/CR-4573 September 1986.

"An Experimental and Analytical Assessment of Circumferential Through-Wall Cracked Pipes Under Pure Bending," Topical Report, NUREG/CR-4574, June 1986.

"Predictions of J-R Curves With Large Crack Growth From Small Specimen Data," Topical Report, NUREG/CR-4575, August 1986.

"An Assessment of Circumferentially Complex-Cracked Pipe Subjected to Bending," Topical Report, NUREG/CR-4687, September 1986.

"Analysis of Cracks in Stainless Steel TIG Welds," Topical Report, NUREG/CR4806, November 1986.

"Approximate Methods for Fracture Analyses of Through-Wall Cracked Pipes," Topical Report, NUREG/CR-4853, January 1987.

"Assessment of Design Basis for Load-Carrying Capacity of Weld-Overlay Repair," Topical Report," NUREG/CR-4877, February 1987.

"Analysis of Experiments on Stainless Steel Flux Welds," Topical Report, NUREG/CR-4878, February 1987.

"Experimental and Analytical Assessment of Circumferentially Surface-Cracked Pipes Under Bending," Topical Report, NUREG/CR-4872, April 1987.

Previous Related Documents from NRC's International Piping Integrity Research Group (IPIRG) Program

"Evaluation and Refinement of Leak-Rate Estimation Models," NUREG/CR-5128, April 1991.

EXECUTIVE SUMMARY

The objective of the U.S. NRC's Short Cracks in Piping and Piping Welds Research Program, which began in March of 1990 and will extend for four years, is to verify and improve fracture analyses for circumferentially cracked large diameter nuclear piping using integrated results from analytical, material characterization, and full-scale pipe fracture efforts. Only quasi-static loading rates are evaluated, since the NRC's International Piping Integrity Research Group (IPIRG) Program evaluated the effects of seismic loading rates on cracked piping systems.

The term "short cracks" encompasses crack sizes typically considered in leak-before-break (LBB) or pragmatic in-service flaw evaluations. A typical LBB size crack for a large diameter pipe is 6 percent of the circumference, which is much less than the 20 to 40 percent ratios investigated in many past pipe fracture programs. Some key results from this reporting period are presented below.

Short-Through-Wall-Cracked Pipe

Several material characterization efforts were undertaken in this task. The first involved evaluation of the mechanical properties of a French wrought TP316 stainless steel pipe which, unlike other austenitic steels tested, displayed significant anisotropic strength. At this time, it is not known if such anisotropy may be important in analyzing pipe fracture behavior.

A metallographic investigation was conducted on a tested piece of a 28-inch-diameter TP316 stainless steel pipe that had a through-wall crack in the center of a girth weld. The most striking observation from the pipe test was the strong tendency for the crack to extend along the weld fusion line for a considerable distance. Crack growth along the fusion line of stainless steel submerged arc welds is consistent with Degraded Piping Program results indicating that the toughness of the fusion line may be lower than the toughness of the submerged arc weld. This lower toughness region could affect the NRC LBB procedures and the ASME IWB-3640 analysis where cracked pipe evaluations typically consider flux weld metals as having the lowest toughness.

Finite element analyses were conducted to evaluate the GE/EPRI J-estimation functions for short circumferential through-wall cracks in pipes subjected to bending loads. The new functions significantly improved the predicted rotation for the cracked pipe section. These new functions will be included in a future release of the NRCPIPE code.

Short-Surface-Cracked Pipe

An analysis of the earlier small-diameter surface-cracked pipe experiments on stainless steel pipe showed that there is a general correction factor on the Net-Section-Collapse analysis as a function of the pipe radius to thickness ratio. This correction appears to be independent of the crack size. The trend is that as the mean radius to thickness ratio increases, the maximum load decreases below the Net-Section-Collapse analysis predictions. This work points out a limitation of the ASME flaw evaluation criterion.

Crack Jumps and Dynamic Strain Aging

Dynamic strain aging (DSA) is being investigated because it is believed to be responsible for crack jumps in pipe fracture tests at 288 C. Work on this task included consideration of several new experiments and tests that gave further insight into the phenomenon of DSA. One evaluation was on a carbon steel Babcock & Wilcox (B&W) submerged arc weld that behaved differently from all the base metals tested. Strength and hardness peaks at elevated temperature indicated strong susceptibility to DSA, but at a significantly higher temperature than for base metal. This weld also had a higher toughness at seismic loading rates than at quasi-static rates, unlike base metals, which showed reduced toughness or no change in toughness at seismic rates. The reasons for the different DSA behaviors of the weld remain uncertain, but may be related to chemical composition.

Additional efforts involved examination of the fracture surfaces of areas where there was stable and unstable crack growth in a C(T) specimen test at 288 C. The two types of growth showed similarities in fracture profile, microstructure, and failure mode (ductile dimple rupture) but differences in dimple size (larger in the unstable fracture regions) and coloration (distinct color difference on the oxidized stable and unstable crack surfaces).

Finally, we conducted an examination of the number and magnitude of crack jumps that occurred in laboratory specimens and pipe tests on the same material. While a loose correlation appears to exist between laboratory tests and pipe tests, the crack jump phenomenon appears to be probabilistic and will require more test data if predictive techniques are to be improved. It was also found that crack jumps at LWR temperatures are more likely to occur in pipe fracture tests than in laboratory fracture tests, suggesting that the laboratory tests may not be reproducing full-scale fracture behavior.

Anisotropic Fracture Properties and Skewed Crack Growth in Circumferentially Cracked Pipes

Data from this program and results from the literature were examined to see if a screening criterion could be developed to estimate the likelihood of skewed crack growth in circumferentially cracked pipes. Anisotropic fracture properties are believed to be the cause of cracks turning away from the circumferential direction, even under pure longitudinal loading. This crack turning could be significant for LBB analyses where there are combined longitudinal, hoop, and torsional stresses. Frequently, only the longitudinal stresses are considered for circumferential cracks. However, if the low toughness direction and principal stresses are at an angle to the circumferential direction, the concern is whether the failure stresses could be lower than calculated in current LBB procedures.

Our findings indicated that toughness anisotropy, as determined from Charpy tests in several orientations, is more dependent on the shape of the nonmetallic inclusions than on their volume fracture or on any other metallurgical feature; stringer type inclusions cause far greater anisotropy than do globular inclusion. Anisotropy can best be minimized by sulfide shape control (via chemical additives) or by cross-rolling of plate for seam-welded pipe.

Attempts to correlate skewed crack growth in pipes to the degree of toughness anisotropy met with only limited success. Although there is a slight general trend toward less-angular crack growth with decreasing anisotropy, the results show a great deal of scatter. A closer evaluation of these data will be conducted.

Crack-Opening Area Analyses

The results in this reporting period are on a subtask to provide a technical basis for changes to NRC Regulatory Guide 1.45 on leakage detection systems. A probabilistic analysis is being conducted to assess changes to leakage detection system capabilities relative to conditional failure probabilities.

Initial efforts involved examination of some deterministic aspects. The first was to assess the accuracy of current J-estimation schemes to predict the maximum load and crack opening of complex-cracked pipe. Another deterministic evaluation was to assess the potential for restraint of crack opening when the crack is close to a terminal end. A fixed terminal end prevents ovalization and the induced rotation of the pipe due to the eccentricity of the crack and axial membrane stresses. This assessment showed that if the crack is far from the fixed end or short in length, there is no restraint of the axial membrane stress component of the crack opening. In these cases, the existing crack-opening-area analyses can be used. However, for longer cracks that are close to a fixed end, the crack opening due to the pressure loading can be reduced significantly (up to a factor of 2). It may be advisable to account for this crack-opening restraint in an LBB analysis. This is the first time such an effect has been considered.

NRCPIPE Code

Task 7 is the effort to formalize the fracture analyses into a computer code called NRCPIPE. The current NRCPIPE code was created during the Degraded Piping Program and contains only analyses for circumferential through-wall-cracked pipe. Some corrections to that code were made and released in Version 1.4e. An initial surface crack version called NRCPIPES has been created. It contains the SC.TNP and SC.TKP J-estimation analyses for finite-length circumferential surface cracks. These analyses were developed in the Degraded Piping Program.

Interprogram Program Cooperation and Program Management

Professor Jwo Pan at the University of Michigan is performing a numerical evaluation of weld residual stresses on the crack driving force for elastic-plastic analyses. These results will be compared with simple approximate methods to assess potential Code techniques.

Another activity within this task involves cooperation with the ASME Section XI pipe flaw evaluation task group. Several different efforts were undertaken in this reporting period. The first was to develop equations to allow Charpy energy values to be used in an elastic-plastic fracture mechanics analysis of an axial surface crack in ferritic pipe. The second was to develop a data base of past quasi-static pipe fracture data. Finally, an evaluation of the potential effect of proposed changes to the ASME Code Section III to eliminate inertial stresses from the design equations was made. It was agreed that if inertial stresses are eliminated in the design stress, then they should be explicitly included in the flaw evaluation criteria. The Battelle assessment included technical justification from the NRC's International Piping Integrity Research Group (IPIRG) program, where double-ended-guillotine break fracture occurred in pipes tested under inertial, seismic anchor motion, thermal expansion, pressure, and dead-weight loading.

Major Conclusions

Major conclusion to date is.

- Short circumferential through-wall flaws fail closer to limit-load (net-section-collapse) predictions than the longer flaws tested in past programs. The significance of this is that for LBB analyses, typically the circumferential flaw lengths in large diameter pipe (28 inches or larger) are quite short, approximately 6 percent of the circumference. This short length means that; (1) the failure loads are not as sensitive to toughness variations, and (2) if using a criterion such as the ASME Z-factor approach, which is based on long circumferential flaws, then there is an extra degree of conservatism. However, for small diameter pipe (i.e., 4 to 6 inches), the LBB through-wall-crack size may be up to 30-percent of the circumference, hence these pipes would be more sensitive to toughness variations, and the ASME Section XI Z-factor based criterion would be more appropriate. It is possible to develop engineering corrections to the Z-factor approach that would account for crack length, as well as diameter, to have a more consistent fracture analysis for LBB of any size pipe.

ACKNOWLEDGMENTS

This work is supported by the U.S. Nuclear Regulatory Commission through the Materials Engineering Branch of the Office of Nuclear Regulatory Research under Contract No. NRC-04-90-069. Mr. A. Hiser is the NRC program manager.

We would also like to thank others at Battelle who have helped in these efforts. Technicians who have contributed to the initial efforts are: Mr. R. Gertler, Mr. P. Held, Mr. J. Kramer, Mr. P. Mincer, Mr. D. Rider, Mr. J. Ryan, Mr. D. Shoemaker, and Mr. J. Woods. We thank Mrs. B. Blanton for typing this report, Dr. A. Hopper and Mr. M. Steve for editorial review comments, and Mr. D. Hayes for drafting assistance.

NOMENCLATURE

1. SYMBOLS

A_c	Charpy specimen cross-sectional area
a	Half the crack length
a_1	Power-law coefficient in stress-strain model
a_2	Power-law exponent in stress-strain model
a_e	Effective half crack length
c	Half the circumferential crack length
$\hat{C}$	Constraint factor for complex-cracked pipe, see Eq. 7-3
D	Nominal pipe diameter
D_m	Mean pipe diameter
d	Surface crack depth
E	Young's modulus
F	Function relating elastic stress intensity factor to stress in GE/EPRI estimation scheme
$F_B(x,y)$	Dimensionless geometry function
f_1,f_2,f_4	Function used in GE/EPRI estimates scheme
h_1,h_2,h_3,h_4	Functions tabulated in GE/EPRI method
I	Moment of inertia
J	J-integral fracture parameter
J_D	Deformation J
J_e	Elastic component of J-integral
J_i	J-integral at crack initiation but not necessarily a valid J_{Ic} by ASTM E813-81

J_{Ic}	Plane strain J at crack initiation by ASTM E813
J_M	Modified J
J_M^{cc}	Complex-crack J_M-resistance curve
J_M^{TWC}	Through-wall-crack J_M-resistance curve
J_p	Plastic component of J-integral
J-R	J-integral resistance (curve)
K	Elastic stress intensity factor
K_I	Mode I stress intensity factor
K_{Ic}	Linear-elastic fracture toughness
ℓ	Half axial crack length
L	Pipe length
L_R	Location of pipe restraint measured from crack plane
M	Moment
M_p	Bulging factor for surface crack
M_t	Folias through-wall flaw bulging factor
m	Slope of J_M-resistance curve
M_o	Limit moment at a nominal stress of σ_o
N	1/n, also used for number of cycles
n	Ramberg-Osgood strain-hardening exponent
P	Applied load
$P_{closure}$	Load required to close the crack
P_m	Membrane stress
R	Ratio of minimum load over maximum load

R^*	Adjusted mean radius of complex-cracked pipe
R_m	Mean pipe radius
r_y	Plastic-zone radius
S_m	ASME design stress
t	Thickness of pipe
t^*	Adjusted thickness of complex-cracked pipe, t-d
V_1, V_2, V_3	Displacement functions in GE/EPRI analysis
Z	A stress multiplier in ASME IWB-3640 and -3650 analyses
α	Ramberg-Osgood parameter
β	Dimensionless factor in expression for half the plastic rotation of a pipe with no crack
$\Gamma(x)$	Gamma function
Δ	Load-line displacement for axial tension
Δa	Increment of crack growth
Δ_e	Elastic axial displacement due to the presence of the crack
Δ_p	Plastic part of load-point displacement
δ	Displacement at center of crack
δ_e	Elastic displacement at center of crack
δ_i	Crack-opening displacement at crack initiation
δ_{nor}	Normalized crack-opening displacement
δ_p	Plastic displacement at center of crack
δ_s	Scaled center crack-opening displacement
δ_{uns}	Unscaled center crack-opening displacement
δ_∞	Crack-opening displacement due to axial tensile stress with no restraints

η	Eta factor, a geometric factor (η) times the energy = J
ϵ	Strain
ϵ_o	Ramberg-Osgood reference strain
θ	Half crack angle of through-wall crack in a pipe
ν	Poisson's ratio
ϕ	Half rotation angle of pipe
ϕ_e^c	Half the elastic rotation due to presence of crack
ϕ_e^{nc}	Half the elastic rotation if no crack is present
ϕ_p^c	Half the plastic rotation due to presence of crack
ϕ_p^{nc}	Half the plastic rotation if no crack is present
σ	Stress
σ_a	Axial stress
σ_{Code}	Bending stress calculated according to ASME Code Source equations
σ_{exp}	Experimentally determined bending stress
σ_f	Flow stress
σ_{nor}	Normalized crack-opening displacement
σ_{nsc}	Net-Section Collapse analysis predicted stress
σ_o	Ramberg-Osgood reference stress
σ_{ref}	Reference tensile stress
σ_{ten}	Tension stress
σ_u	Ultimate strength
σ_y	Yield strength
σ^∞	Far field applied stress

2. ACRONYMS AND INITIALISMS

AEC	Atomic Energy Commission
AISI	American Iron and Steel Institute
API	American Petroleum Institute
ASME	American Society of Mechanical Engineers
ASTM	American Society of Testing and Materials
B&W	Babcock and Wilcox
BHN	Brinell hardness number
BMI	Battelle Memorial Institute
CC	Complex crack
CEA	Commissariat a l'Energia Atomique
C-L	Circumferential-longitudinal orientation (axial through-wall crack growth direction)
COA_R	Crack-opening area
COD	Crack-opening displacement
CTOA	Crack tip opening angle
C(T)	Compact (tension) specimen
CVN	Charpy V-notch
CVP	Charpy V-notch plateau energy
d-c EP	Direct current electric potential
DEGB	Double-ended guillotine break
DPP	Degraded Piping Program
DP2.P	Dimensionless plastic-zone parameter
DS	Double shear

DSA	Dynamic strain aging
DTRC	David Taylor Research Center
EDF	Electricité de France
EDM	Electric-discharge machining
EP	Electric potential
EPFM	Elastic-plastic fracture mechanics
EPRI	Electric Power Research Institute
FEM	Finite element method
GE	General Electric
GR	Grade
IP	Internal pressure
IPIRG	International Piping Integrity Research Group
JAERI	Japanese Atomic Energy Research Institute
LBB	Leak-before-break
L-C	Longitudinal-circumferential orientation (direction of through-wall crack growth around pipe circumference)
L-R	Longitudinal-radial orientation
LWR	Light water reactor
ND	Not determined
NRC	Nuclear Regulatory Commission
NRC-NRR	Nuclear Regulatory Commission - Office of Nuclear Reactor Regulation
NSC	Net-Section Collapse analysis
NT	Not tested
OD	Outside diameter

PWR	Pressurized water reactor
R-C	Radial-circumferential orientation
R-L	Radial-longitudinal orientation
RT	Room temperature
SA	Shear area percent at the Charpy V-notch energy temperature
SAW	Submerged arc weld
SC	Surface crack
SEM	Scanning electron microscope
SG	Side groove
S-L	Short-longitudinal orientation
SMiRT	Structural Mechanics in Reactor Technology (Conference)
SS	Single shear
SSE	Safe shut-down earthquake
S-T	Short-transverse orientation
STA	Science and Technology Agency (of Japan)
TBD	To be determined
T-L	Transverse-longitudinal direction
T-S	Transverse-short direction
TWC	Through-wall crack, through-wall-cracked
UTS	Ultimate tensile strength
YS	Yield strength

1. INTRODUCTION

The "Short Cracks in Piping and Piping Welds" program was initiated to address Nuclear Regulatory Commission (NRC) licensing needs and to resolve some critical findings from the NRC's Degraded Piping Program. The term "short cracks" refers to the type of cracks assessed in leak-before-break (LBB) or pragmatic in-service flaw evaluations. A typical LBB-size crack for a large diameter pipe is 6 percent of the circumference, which is much less than the circumferential lengths of 20 to 40 percent investigated in other past pipe fracture programs. Hence, the term "short cracks" in this project does not refer to microscopic cracks in the sense of the technical interests of the aerospace industry.

This 4-year program started on March 23, 1990. This third semiannual report covers progress from March 1991 through September 1991, along with plans for the next 12 months.

The nine tasks addressed in this program are:

(1) Short through-wall cracked (TWC) pipe evaluations

(2) Short surface-cracked (SC) pipe evaluations

(3) Bi-metallic weld crack evaluations

(4) Dynamic strain aging and crack instabilities evaluations

(5) Fracture evaluations of anisotropic pipe

(6) Crack-opening-area evaluations

(7) NRCPIPE Code improvements

(8) Additional tasks, if needed

(9) Interprogram cooperation and program management.

Of these, significant work has started in Tasks 1, 2, 4, 5, and 6. No work has been identified under Task 8 at this time.

Most of the tasks in this program involve integrated analytical, material characterization, and full-scale pipe fracture experimental efforts. The specific efforts in this program are limited to circumferential cracks in straight pipe, and loads that are applied at quasi-static rates. A summary of all the pipe experiments is given in Table 1.1. Seismic loading rate behavior is being investigated in the NRC's International Piping Integrity Research Group program (IPIRG).

Table 1.1 Summary of proposed pipe experiments

Expt. No.[a]	Diameter	Schedule	Material	Temperature	Test[b] Date	Task No.
Unpressurized through-wall-cracked pipe experiments						
1.1.1.21	28 inch	60	A516 Gr70	288C (550F)	10/25/90	1
1.1.1.22	36 inch	160	A516 Gr70	288C (550F)	(5/93)	1
1.1.1.23	28 inch	80	TP316 SAW	288C (550F)	5/23/91	1
1.1.1.24	24 inch	100	A333 Gr6 SAW	288C (550F)	3/13/92	1
1.1.1.26	4 inch	80	TP316LN	20C (72F)	2/27/91	1
Unpressurized uncracked pipe experiment						
1.1.1.25	28 inch	60	A516 Gr70	288C (550F)	2/07/92	1
Bi-metallic weld fusion line experiments - TWC						
1.1.3.8	36 inch	160	A516/SS-SAW	288C (550F)	(1/94)	3
Unpressurized surface-cracked pipe experiments						
1.2.1.20	16 inch	30	TP316	100C (212F)	1/15/92	2
1.2.1.21	6 inch	XXS	TP304	288C (550F)	4/16/91	2
1.2.1.22	6 inch	40	TP304	288C (550F)	3/15/91	2
Pressurized surface-cracked pipe experiments						
1.2.3.15	28 inch	60	A516	288C (550F)	11/03/91	2
1.2.3.16	28 inch	80	TP316 SAW	288C (550F)	9/05/91	2
1.2.3.17	36 inch	160	A516 SAW	288C (550F)	(9/93)	2
Bi-metallic weld fusion line experiments - SC						
1.2.3.21	36 inch	160	A516/SS-SAW	288C (550F)	(7/94)	3

(a) Experiment numbers are consecutive with Degraded Piping Program Data Record Book entries.
(b) Anticipated test dates in parenthesis.

2. TASK 1 SHORT TWC PIPE EVALUATIONS

2.1 Task Objective

The objective of this task is to modify and verify analyses for short through-wall-cracked (TWC) pipe using existing and new data on large-diameter pipe.

2.2 Task Rationale

The results of this task will help to refine the fracture analyses in LBB procedures used to evaluate through-wall cracks in large-diameter pipes.

2.3 Task Approach

The five subtasks in this task are:

Subtask 1.1	Material characterization of pipes to be tested
Subtask 1.2	Facility modifications for large-diameter pipe experiments
Subtask 1.3	Conduct large-diameter pipe experiments
Subtask 1.4	Analysis modification and verifications
Subtask 1.5	Topical report.

During this reporting period progress was made in Subtasks 1.1, 1.3, and 1.4; hence, only these subtasks will be discussed.

2.3.1 Subtask 1.1 Material Characterization for Short TWC Pipe Experiments

2.3.1.1 Objective

The objective of this activity is to generate the data necessary to document the material strength and toughness for analysis in Subtask 1.4.

2.3.1.2 Rationale

The material property data needed for the analysis procedures in Subtask 1.4 will be determined from each pipe and weld to be tested. These data are also of value for the NRC PIFRAC database (Ref. 2.1).

... Charpy, chemical analysis, tensile, and J-R curves, need to be generated for the 28-inch-diameter stainless steel weld and the 24-inch-diameter carbon steel submerged-arc weld used in Subtask 1.3. Characterization of the stainless steel weld has been completed and the results were reported in Reference 2.2.

No characterization work is planned within Task 1 for the 24-inch-diameter carbon-steel submerged-arc weld because characterization work is planned within Task 2 for a nominally identical weld prepared in 25.4-mm (1-inch)-thick carbon-steel plate (see Section 3.3.1.3).

Characterization of the French TP316LN stainless steel pipe used in the new 4-inch-diameter TWC pipe experiment has been completed and was reported in Reference 2.2. Material property data for other materials to be subjected to pipe tests in Task 1 are available from the Degraded Piping Program (Ref. 2.3). All characterization data are recorded digitally and reduced to a format identical to that used in past Degraded Piping Program data record book entries. These data also are available for input into the NRC PIFRAC database.

In addition to the complete characterization activities described here, other activities in support of pipe fracture experiments are undertaken as needed. Several of these other activities are described in Section 2.3.1.4.

2.3.1.4 Progress

During the past reporting period, several activities were undertaken in support of pipe fracture experiments within Task 1. These activities included: (1) tensile tests on the base metal for pipe experiments in which the crack was located in weld metal, (2) visual and metallographic examination of the fracture in a welded TP304 stainless steel pipe (Experiment 1.1.1.23), and (3) examination of ovalization of tension and compression specimens in Pipe IP-A2 (TP316LN stainless steel).

Base Metal Tensile Tests

In Pipe Experiment 1.1.1.23, a through-wall crack was located in a submerged-arc girth weld in Pipe DP2-A51, a 28-inch-diameter TP316L stainless steel pipe that had been purchased from excess inventory of replacement pipe from the Nine Mile Point plant (Ref. 2.3). The chemical composition of the pipe is shown in Table 2.1. Longitudinal tensile specimens were machined from a section of the pipe that had already been subjected to the pipe experiment. They were tested to provide tensile data needed in the analysis of the pipe experiment. The specimens were located in close proximity to the through-wall machined notch so that the material from which they were machined would not have experienced plastic strain during the pipe test.

Quasi-static tensile tests were conducted at both room temperature and 288 C (550 F) at a strain rate of nominally 3×10^{-4}. Table 2.2 is a summary of the tensile properties of the pipe. Engineering stress-strain curves and true stress-strain curves are presented in Figures 2.1 and 2.2, respectively. As is commonly observed in austenitic stainless steels, both strength and ductility properties are lower at 288 C (550 F) than at room temperature.

Table 2.1 Chemical Composition of Pipe DP2-A51 (TP316L Stainless Steel)

Element	Percent by Weight of Indicated Element	
	Pipe DP2-A51	ASTM A240 Requirement for TP316L
C	0.021	0.030 max
Mn	1.8	2.00 max
P	0.031	0.045 max
S	0.018	0.030 max
Si	0.55	0.75 max
Cu	0.2	(a)
Sn	0.008	(a)
Ni	9.8[b]	10.00-14.00
Cr	17.3	16.00-18.00
Mo	2.1	2.00-3.00
Al	0.01	(a)
V	0.08	(a)
Nb	0.013	(a)
Zr	0.001	(a)
Ti	0.004	(a)
B	0.0002	(a)
Ca	0.0024	(a)
Co	0.12	(a)
W	0.0	(a)
Se	0.00	(a)
N	0.07	0.10 max

(a) Not specified.
(b) Nickel content does not meet specification.

Table 2.2 Tensile properties of Pipe DP2-A51 (TP316L stainless steel)

Specimen Number	Test Temperature C	Test Temperature F	0.2% Offset Yield Strength MPa	0.2% Offset Yield Strength ksi	Ultimate Tensile Strength MPa	Ultimate Tensile Strength ksi	Elongation, pct in 25.4 mm (1.0 in.)	Reduction of Area, pct
A51-1	20	68	254	36.9	N.D.	N.D.	79.0	82.8
A51-2	20	68	263	38.1	597	86.6	79.0	83.9
A51-4	288	550	143	20.8	427	62.0	38.4	70.8

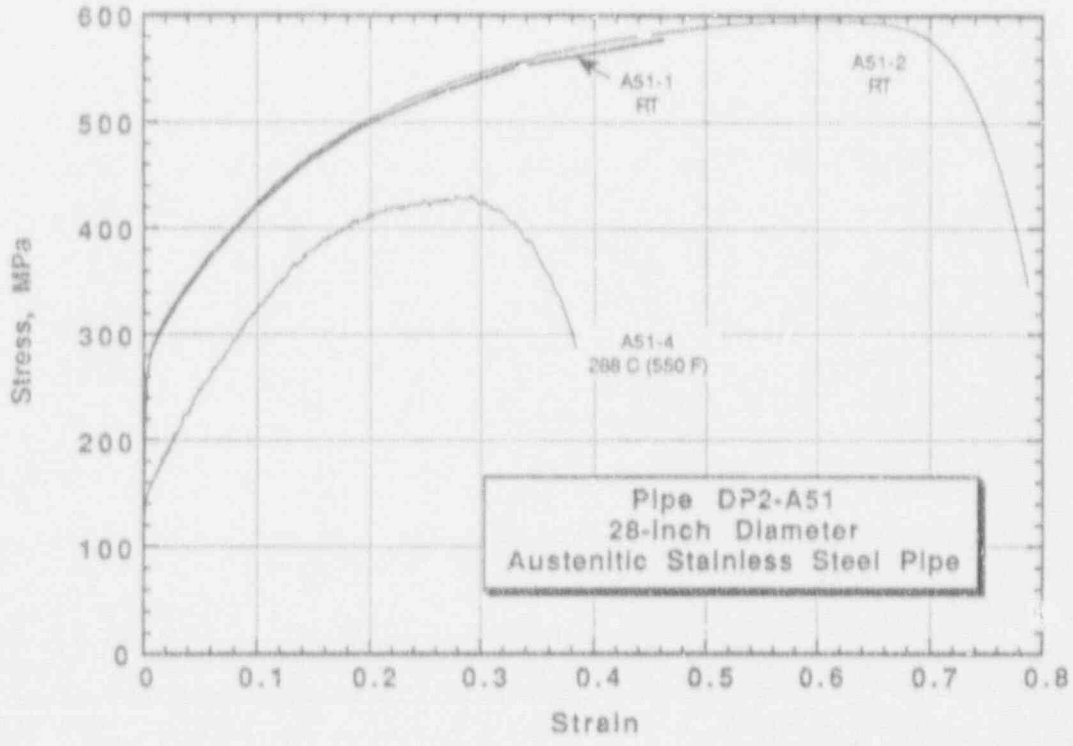

Figure 2.1 Engineering stress-strain curves for tensile specimens machined from Pipe DP2-A51 (TP316L stainless steel)

SC-SA-5/92-F2.1

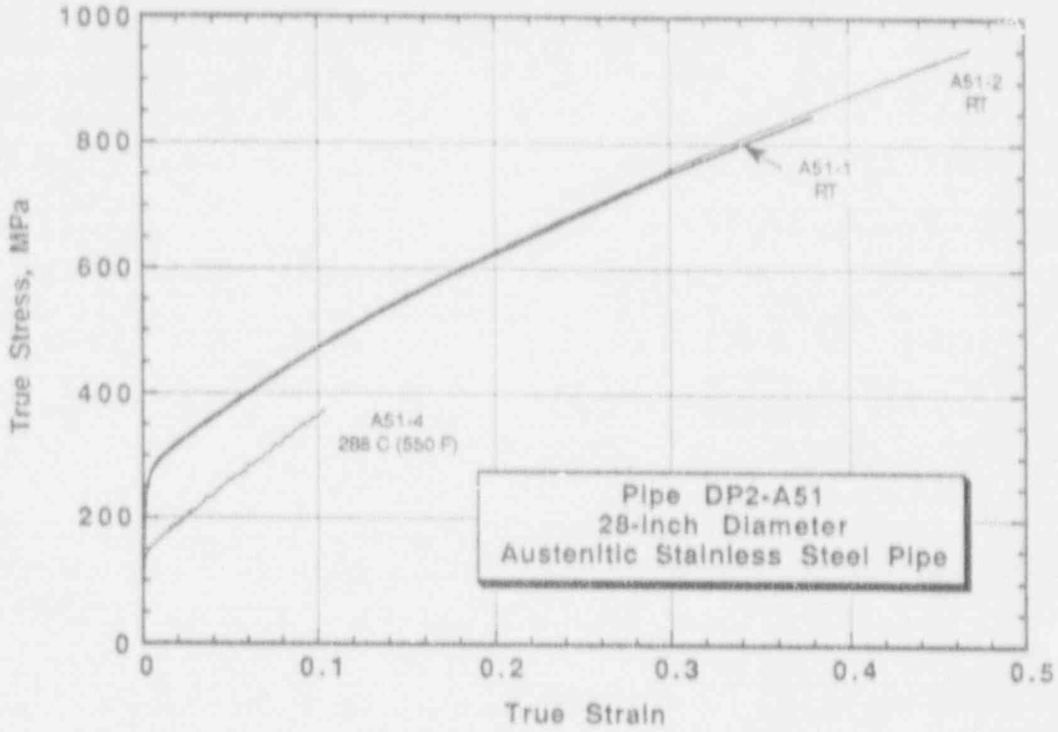

Figure 2.2 True stress-strain curves for tensile specimens machined from Pipe DP2-A51 (TP316L stainless steel)

SC-SA-5/92-F2.2

Examination of the Fracture from Welded Pipe Experiment 1.1.1.23

In Pipe Experiment 1.1.1.23, the crack-growth behavior at one end of the starting flaw was noticeably different from that at the other end (Ref. 2.2). A visual and a metallographic examination of the fracture were performed to aid in understanding the differences.

This test was conducted on Pipe DP2-A51, a 28-inch-diameter TP316L stainless steel pipe that had been purchased from excess inventory of replacement pipe from the Nine Mile Point plant. It contained a short through-wall crack centered in the submerged-arc girth weld. Side A of the crack was reported to have initiated at a later time and displayed significantly less crack extension than Side B. It also grew completely out of the weld zone and into the base metal after 100 to 125 mm (4 to 5 inches) of extension, whereas the Side B crack tended to remain, at least partially, in the weld metal. In addition, it was reported that several jewelers saw blades were required to cut the final slot in Side A, while only one blade was needed for Side B. The objective of the examination was to provide information that would help explain the differences in the nature of the crack extension on either side of the starter notch.

A sketch of the fracture path is shown in Figure 2.3. During the early stages of growth, the Side B fracture appeared to be less tilted than the Side A fracture. The fracture surfaces permit three additional observations: (1) the tilt of Side A and Side B fracture surfaces during the early stages of

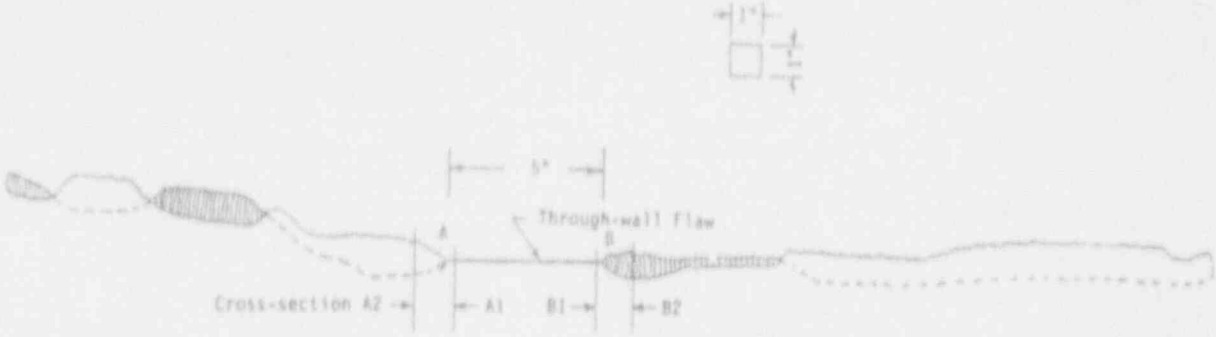

Figure 2.3 Sketch of fracture path in pipe test 1.1.23

Note: The view is from the outside of the pipe and assumes the pipe to be flattened. The shaded areas indicate fracture surfaces tilted toward the viewer.

SC-SA-5/92-F2.3

growth were in opposite directions, (2) the Side A fracture surface exhibited a bifurcation in the crack at the end of the saw-cut notch, and (3) the length of the crack front in the early stages of growth was larger on Side A than Side B of the crack due to the greater tilt angle.

Sections were taken from each side of the crack for metallographic examination. Sections A1 and B1 (see Figure 2.3) contained the jewelers-saw-cut portion of the through-wall flaw; Sections A2 and B2 were located approximately 25 mm (1 inch) from the original flaw tips. The arrows in Figure 2.3 indicate the viewing direction of each cross section. Each section was ground through 600 grit paper and etched to reveal the location of the weld. Figure 2.4 shows that the saw-cut starter notch was located very nearly in the center of the root pass of the weld zone at each end of the flaw. Figure 2.5 shows the crack location relative to the weld zone at Sections A2 and B2. Most of the fracture surfaces on both sides of the crack appear to be along, or very close to, the weld fusion line. The presence of the weld metal in Section A2 and the near absence of weld metal in Section B2 indicates that the crack on Side A extended along one fusion line and the crack from Side B extended along the other fusion line. Notice also that the tilt angle in Section B2 is substantially less than in Section A2.

Knoop microhardness and Rockwell B hardness profiles were determined in the weld in Sections A1 and B1. Figure 2.6 shows the approximate locations at which the hardness measurements were made and lists the corresponding hardness numbers. The results show very little difference between the two sides of the weld. The hardness of the weld varied from 85 to 97 Rockwell B (143 to 232 Knoop hardness number) on Side A and from 89 to 96 Rockwell B (190 to 263 Knoop) on Side B. The average Rockwell B hardness was 91.4 for Side A and 92.8 for Side B. The Knoop hardness numbers showed a higher variation than the Rockwell B numbers, which is typical for microhardness test results in weld metals. They also showed that, on average, Side B was slightly harder than Side A. Thus, the observation that cutting the final slot in Side A required more jewelers-saw blades than in Side B cannot be explained by greater average hardness at Side A. Rather, it is likely that the

Figure 2.4 Cross sections showing the location of the saw cut notch in the weld

SC-SA-5/92-F2.4

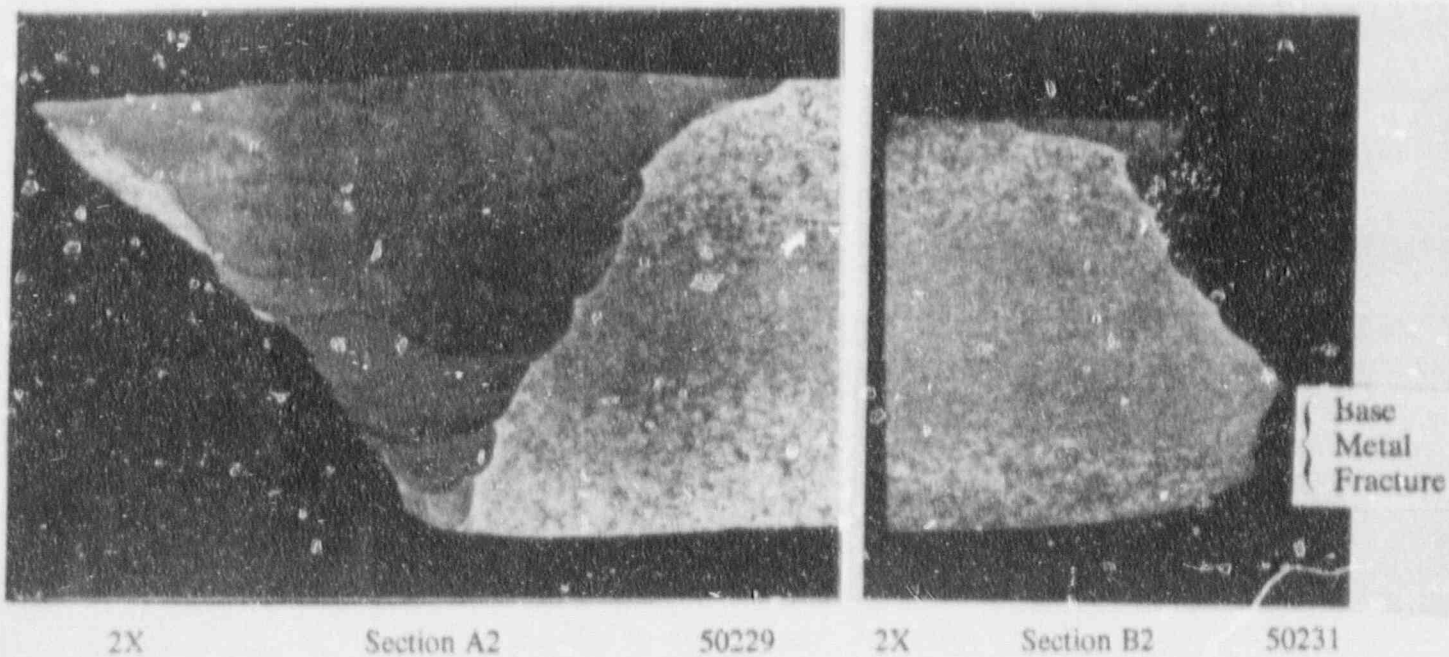

Figure 2.5 Cross sections showing the location of the crack with respect to the weld

SC-SA-5/92-F2.5

Figure 2.4 Cross sections showing the location of the saw cut notch in the weld

SC-SA-5/92-F2.4

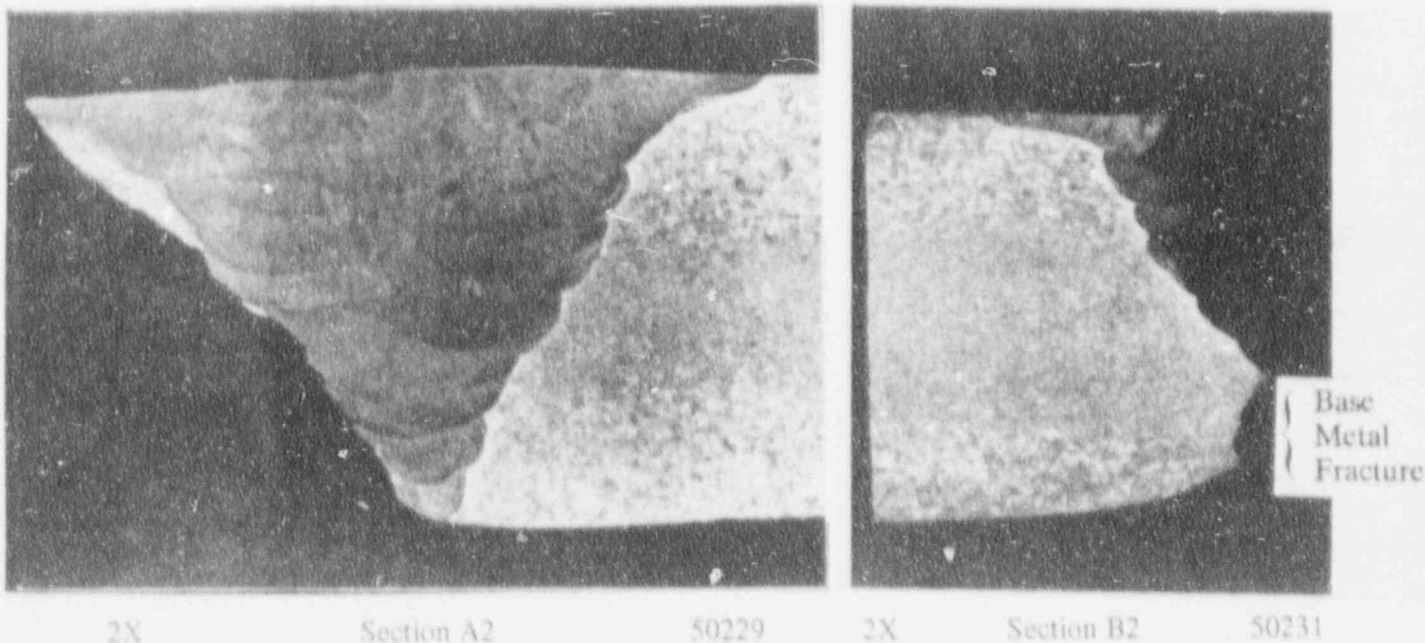

Figure 2.5 Cross sections showing the location of the crack with respect to the weld

SC-SA-5/92-F2.5

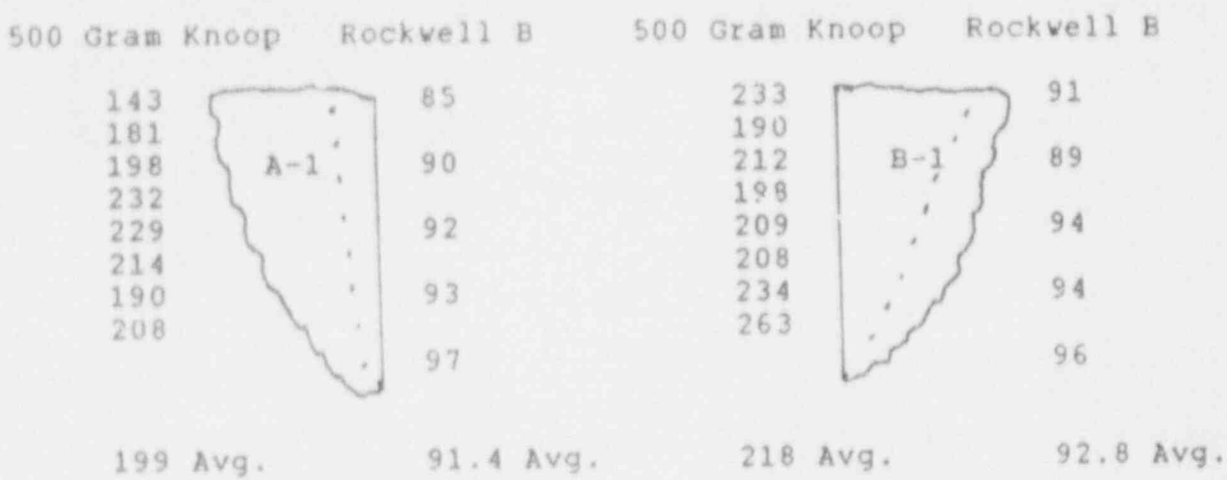

Figure 2.6 Locations and results of the hardness tests

SC-SA-5/92-F2.6

problem of excessive saw-blade wear at Side A may have been caused by small particles of entrapped slag from the welding process.

The precise reasons for the differences in crack extension between the two sides of this weld remain unknown. However, the crack bifurcation on Side A of the crack tends to be associated with higher energy for crack initiation, and the larger initial tilt of the crack on Side A in comparison to Side B (see Figure 2.5) would be expected to increase the energy necessary to extend a crack. In addition, each crack extended along a different fusion line, each with unknown J-R behavior. Each of these observations might help to explain the later onset and smaller amount of crack growth at Side A relative to Side B. However, they do not explain why the crack at Side A veered away from the weld after 100 to 125 mm (4 to 5 inches) of growth and, thereafter, grew in the base metal.

The most striking observation in this examination was the strong tendency for the crack to extend along or very close to the fusion line of the weld. Similar findings were reported in the Degraded Piping Program (Ref. 2.4) for submerged-arc welds in austenitic stainless steel, lending further credence to the suspicion that the fusion line region in the austenitic welds may possess lower toughness than the SAW or base metal.

Ovalization of Tension and Compression Specimens in Pipe IP-A2 (TP316LN Stainless Steel)

A limited metallographic investigation was undertaken to determine the orientation of both tension and compression specimens machined from Pipe IP-A2, a 4-inch-diameter Schedule 160 TP316LN stainless steel pipe that had been furnished to Battelle by Commissariat a l'Energie Atomique (CEA). The pipe originally was in the possession of Électricité de France (EDF) and carried the designation Z3 CND 18-12 (316L) stainless steel. It came from EDF Tube Experiment No. 24.

Both tension tests and compression tests at room temperature had led to ovalization of the originally circular cross sections of the test specimens as plastic strain occurred. In the necked region of the tension specimens, the ovalization was very pronounced; the ratio of the ellipse minor axis to the ellipse major axis was approximately 0.58. Ovalization was less pronounced in the compression specimens and depended on the amount of plastic strain imposed before the test was terminated. For a compressive strain of approximately 9 percent, the ratio of minor-to-major ellipse axis was approximately 0.96.

Metallographic examination of a cross section of one of the tension specimens, one of the compression specimens, and a piece of the pipe from which they were machined showed clearly the orientation of the ellipses relative to the pipe wall. As is shown schematically in Figure 2.7, the major axis of the elliptical cross section of the tension specimen was aligned with the circumferential direction in the pipe wall. In the compression specimen, on the other hand, the minor axis of the ellipse was aligned with the circumferential direction. These observations, along with the finding that the modulus of elasticity in the longitudinal direction of the pipe was unusually low for an austenitic stainless steel—157.5 GPa (22.84 x 10^6 psi), as determined by a resonant frequency method—suggest that the pipe has preferred orientation, or crystallographic texture, of the individual grains making up the pipe. The presence of preferred orientation could have important implications in interpreting finite element analyses of the pipe fracture experiment for this and other pipes, since FEM analyses typically assume isotropic strength properties.

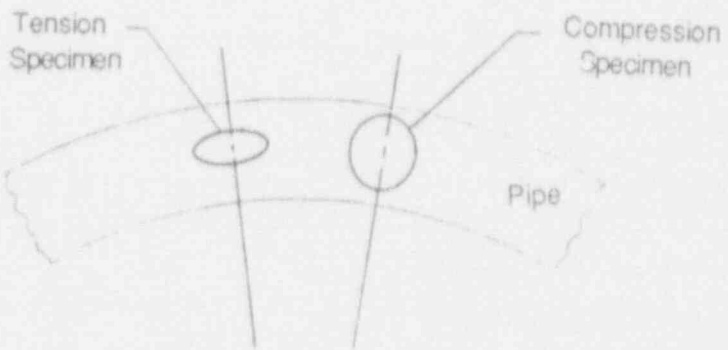

Figure 2.7 Schematic illustration of ovalization in tension and compression specimen cross sections from Pipe IP-A2 (TP316LN stainless steel)

Note: Drawing not to scale

SC-SA-5/92-F2.7

2.3.2 Subtask 1.3 Large-Diameter Pipe Fracture Experiments

2.3.2.1 Objective

The objective of this activity is to develop pipe fracture data for the verification of fracture analyses used in LBB evaluations of large-diameter pipe.

2.3.2.2 Rationale

Past work in the Degraded Piping Program (Ref. 2.3) on long circumferential through-wall cracks showed different results for thinner versus thicker large-diameter pipe. A relatively thin steam-line pipe had failure stresses well below those predicted by the net-section-collapse (NSC) analysis, but agreed well with predictions from various J-estimation scheme analyses. Conversely, a thicker cold-leg pipe reached the NSC stress, which is much higher than that predicted by the J-estimation scheme predictions. For all of these experiments, a long (37 percent of the pipe circumference) through-wall crack was evaluated. Additional large-diameter pipe experiments with shorter through-wall cracks in sufficiently low toughness pipe materials are needed to assess the various elastic-plastic fracture analyses.

2.3.2.3 Approach

Four through-wall-cracked pipe experiments and one uncracked pipe experiment on large-diameter pipe will be conducted as part of this subtask, see Table 2.3. The pipe diameters for these experiments are 24, 28, and 36 inches. Different mean radius to thickness, R_m/t, ratios will be considered.

In addition, the test matrix for this subtask also includes a 4-inch-diameter pipe experiment. The objective of this experiment (1.1.1.26), which was not included in the original test matrix, is to compare the French (EDF) pipe test system with the Battelle pipe test facilities, since discrepancies

Table 2.3 Test Matrix for Subtask 1.3 - Large-Diameter Through-Wall-Cracked Pipe Fracture Experiments

Expt. No.	Nominal Diameter	Schedule	Material	Test Temperature	Crack Length (2c/πD)
1.1.1.21	28 inches	[illegible]	A515 GR 60	288C (550 F)	0.0625
1.1.1.22	36 inches	160	A516 GR 70	288C (550 F)	0.0625
1.1.1.23	28 inches	80	TP316L SAW	288C (550 F)	0.0625
1.1.1.24	24 inches	80	A333 GR6 SAW	288C (550 F)	0.0625
1.1.1.25	28 inches	60	A515 GR 60	288C (550 F)	0.0
1.1.1.26	4 inches	80	TP316LN	22C (72 F)	0.244

were found in FEM analyses of one Battelle and one French pipe test on different size pipes. The section of French pipe used was from the moment arm of their Experiment No. 24. The test specimen was machined to reproduce nearly the same diameter, wall thickness, and crack size as used in the EDF experiment.

2.3.2.4 Progress

The results for the 28-inch-diameter carbon steel through-wall-cracked pipe experiment (1.1.1.21) were discussed in the first semiannual report for this program (Ref. 2.5). The results for the 28-inch-diameter stainless steel submerged-arc weld (SAW) through-wall-cracked pipe experiment (1.1.1.23) and the 4-inch-diameter stainless steel French pipe experiment (1.1.1.26) were discussed in the second semiannual report of this program (Ref. 2.2).

In this reporting period, work has focussed on preparing test specimens for the 24-inch-diameter carbon steel SAW through-wall crack experiment (1.1.1.24) and the 28-inch-diameter carbon steel uncracked pipe experiment (1.1.1.25). For the 24-inch-diameter carbon steel SAW experiment, a pipe material and weld procedure to be used for the experiment have been identified. The pipe material to be used is DP2-F4. This is a section of 24-inch-diameter Schedule 80 (30.96 mm [1.219 inch] wall thickness) SA-333 Grade 6 pipe obtained for the Degraded Piping Program. That pipe came from the excess pipe inventory of a nuclear power plant. The weld procedure for this experiment will be SAW. The weld wire will be a high manganese, high molybdenum wire carrying the designations EA3 and SFA 5.23. The flux will be Linde 80. This procedure was obtained from Babcock and Wilcox (B&W) as being typical of the procedures used by B&W in the construction of the Midland nuclear power plant, as well as most other carbon steel piping systems in their other PWR's. At this time quotes for fabricating this weld, along with a similar plate weld to be used for material characterization, have been obtained from a local ASME Nuclear Code-certified welding shop. The welds will be made in the near future.

For the 28-inch-diameter carbon steel uncracked pipe experiment, the test specimen has been cut to length and an instrumentation plan has been formulated. After consulting with the individuals conducting the finite element analyses for this experiment, it was decided to collect the data listed in Table 2.4. These are the data deemed necessary to verify the finite element analyses.

In addition to preparing the test specimens for Experiments 1.1.1.24 and 1.1.1.25, a number of calculations were made to compare the experimental results (i.e., maximum experimental moments) with predictions from various analyses. The analysis methods considered were the Net-Section-Collapse (NSC), Dimensionless Plastic Zone Parameter (DPZP), and ASME Section XI IWB-3640 (for austenitic steels) and IWB-3650 (for ferritic steels) analyses. The experimental results from Experiments 1.1.1.21, 1.1.1.23, and 1.1.1.26 as well as the experimental results from the companion long through-wall crack experiments from the Degraded Piping Program are compared with the various analysis methods in Table 2.5 and Figures 2.8 through 2.10.

In comparing the results from the short through-wall-cracked pipe experiments from this program with results from the long through-wall-cracked pipe experiments from the Degraded Piping Program, it can be seen that the NSC analysis overpredicts the experimental maximum load to a greater extent for the long cracks than it does for the short cracks. This observation also holds true for the DPZP

Table 2.4 Data to be collected on 28-inch-diameter carbon steel uncracked pipe experiment (1.1.1.25)

- Load
- Load-line displacement
- Pipe ovalization at one cross section inside center span
- Pipe rotation
- Strain data at one cross section inside center span:
  - Bi-axial gage at top outside surface
  - Uni-axial gage (longitudinal orientation) at top inside surface
  - Uni-axial gage (longitudinal orientation) at side of pipe on outside surface
  - Bi-axial gage at bottom outside surface
  - Bi-axial gage at bottom inside surface

and ASME analyses, since these analyses have their basis an EPFM correction based on long cracks. The reason for the greater overprediction of maximum loads for the long cracks is that the longer cracks are more sensitive to toughness effects than the short cracks. As Figure 2.11 shows, the longer the crack length the greater the difference between the elastic-plastic and limit-load solutions. Therefore, since the failure criterion for large-diameter, low-toughness pipes, such as evaluated herein, is governed more by elastic-plastic conditions than by limit-load conditions, it is not surprising that the NSC analysis overpredicts the experimental results more for the long crack length case than it does for the short crack length case. This observation will be further validated as the results from the remaining two large-diameter short through-wall-cracked pipe experiments become available.

The significance of this finding is that for leak-before-break (LBB) analyses, the margins associated with any limit-load based fracture/stability analyses for LBB size through-wall flaws will be greater than expected, based on the long through-wall crack data from the Degraded Piping Program, as well as the ASME Z-factor and DPZP analyses.

Also of note from Table 2.5 and Figure 2.10 is the fact that the ASME Section XI analyses typically underpredicted the experimental failure moments for the five experiments considered. The one exception was the 4-inch-diameter stainless steel pipe experiment (1.1.1.26). The degree of overprediction for this experiment was minor, less than 4 percent. For the two carbon steel experiments the extent of the underprediction was especially significant. The Section XI predicted moment for the long crack experiment (4111-2) was only 47 percent of the experimental maximum moment while the predicted moment for the short crack experiment (1.1.1.21) was only 39 percent of the experimental maximum moment. As noted in References 2.2 and 2.6, the IWB-3650 analysis tends to be more conservative than the IWB-3640 analysis.

Table 2.5 Comparison of maximum experimental moments from through-wall-cracked experiments with predicted moments from NSC, DPZP, and ASME analyses

Expt. No.	Material	OD, mm	t, mm	$2c/\pi D_m$	σ_y, MPa	σ_u, MPa	S_m, MPa	J_i, kJ/m^2	Maximum Moment, kN-m	Maximum Moment/Predicted Moment			
										(NSC)	(DPZP)	(IWB-3640)	(IWB-3650)
4111-2	A515 GR 60 Base Metal	711.2	23.6	0.37	231	544	114	216	1204	0.738	0.834	NA	2.131
1.1.1.21	A515 GR 60 Base Metal	711.2	22.7	0.0625	231	544	114	216	3246	0.868	0.980	NA	2.535
4111-5	TP316 SAW	719.6	30.2	0.37	229	501	121	109	1256	0.636	0.847	1.077	NA
1.1.1.23	TP316L SAW	711.2	30.2	0.0625	143	427	96	59.7	3062	0.853	1.172	1.417	NA
1.1.1.26	TP316LN Base Metal	106.2	8.31	0.244	254	532	138	879	17.1	0.942	0.942	0.962	NA

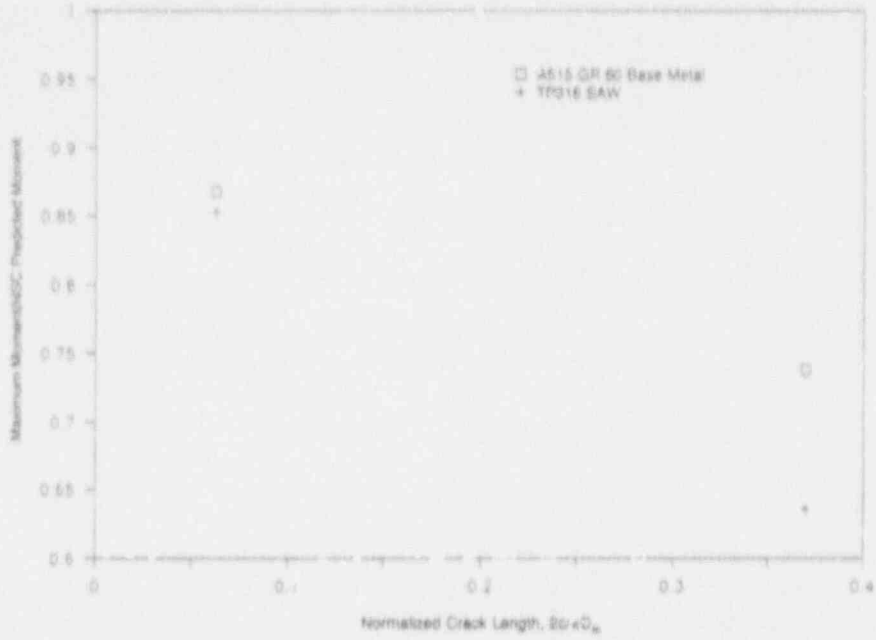

Figure 2.8 Plot of the ratio of the maximum experimental moment to the net-section-collapse predicted moment as a function of the normalized crack length ($2c/\pi D_m$)

SC-SA-5/92-F2.8

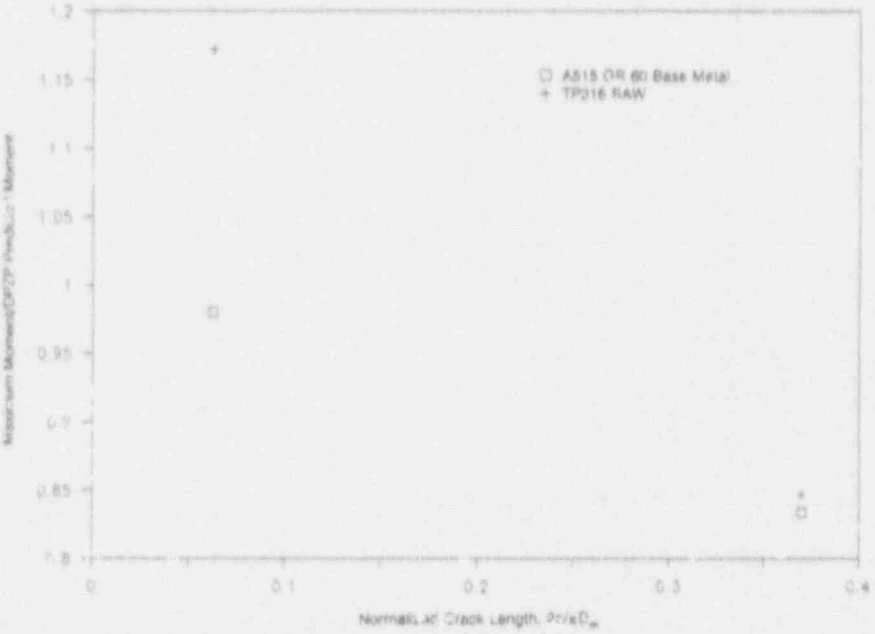

Figure 2.9 Plot of the ratio of the maximum experimental moment to the dimensionless-plastic-zone-parameter predicted moment as a function of the normalized crack length ($2c/\pi D_m$)

SC-SA-5/92-F2.9

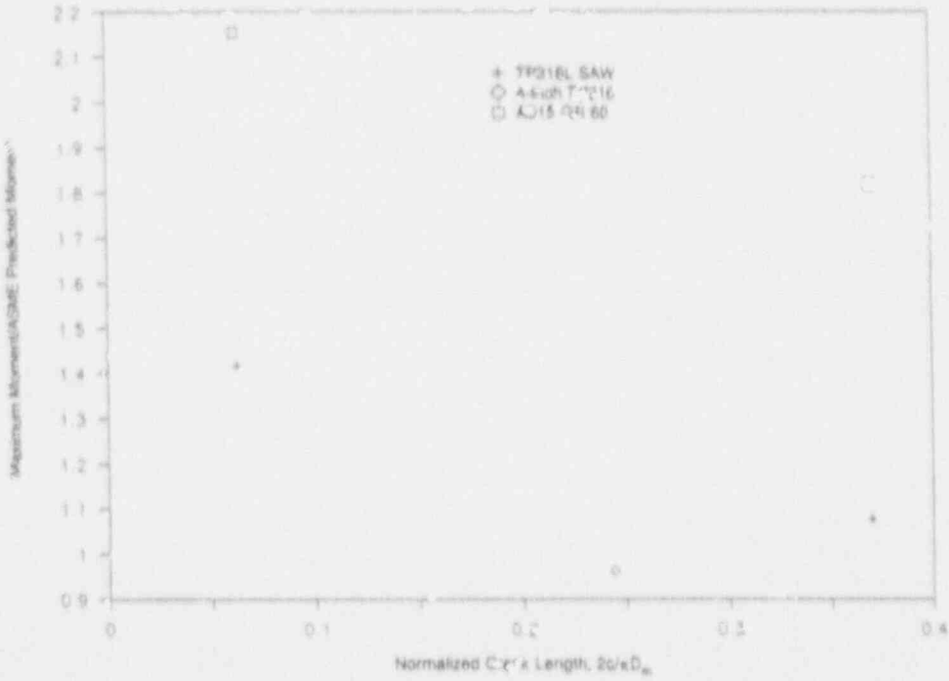

Figure 2.10 Plot of the ratio of the maximum experimental moment to the ASME IWB-3640 and IWB-3650 predicted moment as a function of the normalized crack length ($2c/\pi D_m$)

SC-SA-5/92-F2.10

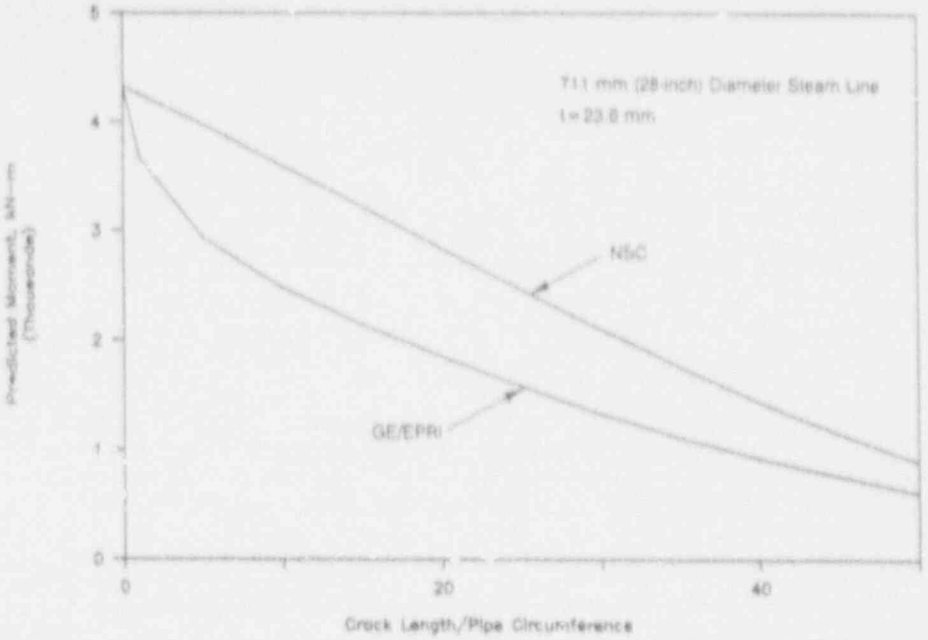

(a) Moment versus normalized circumferential TWC length

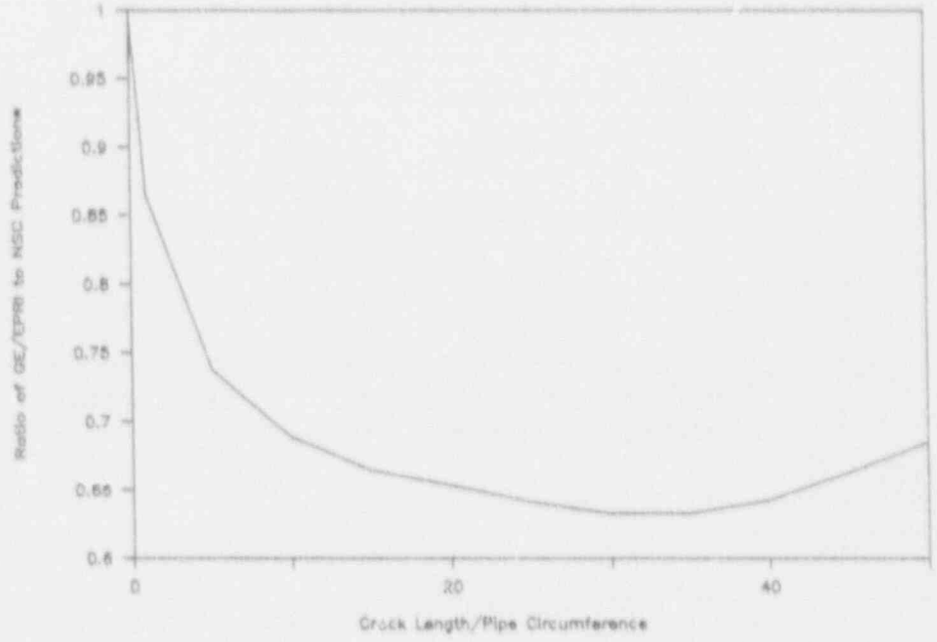

(b) Ratio of EPFM to NSC moment versus normalized circumferential TWC length

Figure 2.11 Typical plot of predicted failure stress versus crack length for limit-load (independent of toughness) and GE/EPRI elastic plastic (toughness dependent) analyses (Calculations for 711-mm (28-inch) diameter 23.6-mm (0.929-inch) thick A515 Gr 60 steam-line pipe)

SC-SA-5/92-F2.11

2.3.3 Subtask 1.4 Analyses for Short Through-Wall Cracks in Pipes

2.3.3.1 Objective

The objective of this subtask is to develop, improve, and verify the engineering analyses for short circumferential through-wall-cracked pipe.

2.3.3.2 Rationale

The short through-wall-cracked pipe analysis improvements are aimed at LBB fracture evaluations for larger diameter pipe.

2.3.3.3 Approach

The three activities in this subtask are:

Activity 1.4.1	Improve short through-wall-cracked pipe analysis and compare predictions with existing data
Activity 1.4.2	Analyze large-diameter pipe TWC test results
Activity 1.4.3	Analyze through-wall cracks in welds.

Activity 1.4.1 Improve Short Through-Wall-Cracked Pipe Analysis and Compare with Existing Data

Objective

This activity will involve several efforts to identify shortcomings in existing analyses and then to make and verify improvements. In general, the objective of this activity is to make needed improvements in the analyses for better prediction of circumferential short through-wall-cracked pipe.

Approach

The four separate efforts in this activity are:

(a) Numerically assess the effect of plastic ovalization on the validity of J
(b) Determine pipe ovalization effects on limit-load analysis
(c) Improve F-, V-, and h-functions
(d) Compare predictions from improved analyses with existing data.

Activities 1.4.1(a) and 1.4.1(c) were the only active efforts during this progress report.

Activity 1.4.1(a) Numerically Assess the Effect of Plastic Ovalization on the Validity of J

Experiment 1.1.1.21 was chosen to be modeled for this activity. This test was conducted on a 28-inch-diameter TWC pipe. A 3D finite element model was prepared for this case. The FE calculation

up to crack initiation has been performed using the incremental theory of plasticity law given in ABAQUS. A scheme to extend the analysis to incorporate crack growth has also been developed. The analysis beyond crack initiation has been put on hold until problems dealing with mesh refinement have been resolved.

tivity 1.4.1(c) Improve F-, V-, and h-functions

talytical methods for predicting the elastic or elastic-plastic behavior of large circumferential through-wall cracks in tubes subjected to bending, tension, or combined bending and tension are well developed. References 2.7 and 2.8 summarize five such methods and provide a number of comparisons between analytically predicted results and experimental data. These techniques consist of developing methods for estimating the value of the J-integral. Classical J-tearing theory is used for the analyses. A method has also been recently developed to estimate J for a through-wall crack in a pipe weld (Ref. 2.9).

Unfortunately, the ability of these J-estimation techniques to predict the crack growth behavior for small cracks ($\leq$ 12 percent of the circumference) has not been established, even though such small cracks are often of concern in practical structures. Indeed, the finite element solutions compiled in the GE/EPRI handbook (Ref. 2.10) appear quite inadequate for small-size cracks (see Refs. 2.7 and 2.8). This activity completes the results of a series of finite element solutions for small cracks tabulated in the spirit of the GE/EPRI handbook (Ref. 2.10). Specifically, the solutions of Reference 2.10 for θ/π = 1/8 and 1/16 are redone for Ramberg-Osgood coefficients n = 1, 3, 5, 7, 10 for bending, where θ is half the crack angle.

The theoretical background for the development and use of simplified elastic-plastic fracture methods is fully discussed in Reference 2.7. Here we provide solutions for the J-integral, the crack-opening displacements, and the rotation due to the crack for short crack problems under pure bending. Some of these results were presented in the second semiannual report (Ref. 2.2) with more detailed discussion. However, for completeness, the entire set of solutions is provided here.

The GE/EPRI Estimation Scheme—The GE/EPRI method takes advantage of the scaling properties in linear and nonlinear elasticity to interpolate over the range from small-scale yielding to large-scale yielding and to normalize fracture parameters such as J, crack-opening displacement (COD), and displacements. The elastic-plastic solution is obtained by superposition of a small-scale yielding solution and of the fully plastic solution. The stress-strain law is defined by a Ramberg-Osgood relation:

$$\frac{\varepsilon}{\varepsilon_o} = \frac{\sigma}{\sigma_o} + \alpha\left(\frac{\sigma}{\sigma_o}\right)^n \qquad (2\text{-}1)$$

where σ_o is an arbitrary reference stress (usually defined as the yield stress), α and n are curve fitting parameters, and $\varepsilon_o = \sigma_o/E$.

This normalization reduces the fracture parameter determination to the computation of coefficients depending, for given types of geometry and loading, only on the strain hardening coefficient n and a

few geometrical parameters. Tabulated values of these coefficients were computed (Ref. 2.10) using the finite element technique. J for a through-wall cracked pipe in bending is written in the following form:

$$J = J_e + J_p$$

$$J = f_1 \frac{M^2}{E} + \alpha\, \sigma_o\, \varepsilon_o\, a \left(1 - \frac{\theta}{\pi}\right) h_1 \left(\frac{M}{M_o}\right)^{n+1} \qquad (2\text{-}2a)$$

In Equation 2-2a, θ is the half-crack angle, a is the half-crack length ($a = R_m\theta$), R_m is the mean radius of the pipe, and M_o is the limit moment, defined in Reference 2.10 (see Figure 2.12). Also

$$f_1 = \text{fcn}\left(a_e\,,\ \frac{R_m}{t}\right) \qquad (2\text{-}2b)$$

$$h_1 = \text{fcn}\left(\frac{\theta}{\pi}\,,\ \frac{R_m}{t}\,,\ n\right) \qquad (2\text{-}2c)$$

and are tabulated (where t is the pipe wall thickness). In the pipe bending case, M = the moment and the effective crack size, a_e, based on an Irwin plastic zone correction, is written as:

$$a_e = a + \frac{r_y}{1 + \left(\frac{M}{M_o}\right)^2} \qquad (2\text{-}3a)$$

$$a = R_m\theta \qquad (2\text{-}3b)$$

$$r_y = \frac{1}{2\pi}\left[\frac{n-1}{n+1}\right]\left(\frac{K}{\sigma_o}\right)^2 \qquad (2\text{-}3c)$$

where K, the stress intensity factor, is a function of a and not of a_e. Other parameters such as crack-opening displacement and load-point rotations were also evaluated in Reference 2.10.

The GE/EPRI method, as developed for TWC pipe, appears to be too conservative, i.e., the compiled values of h_1 and, hence, J are too large. In fact, for the smaller crack sizes, the results appear quite inadequate. Indeed, the pipe rotations due to the crack are negative for $\theta/\pi = 1/16$, as compiled in Reference 2.10 for both elastic and plastic solutions. As discussed in References 2.7, 2.8, and 2.11,

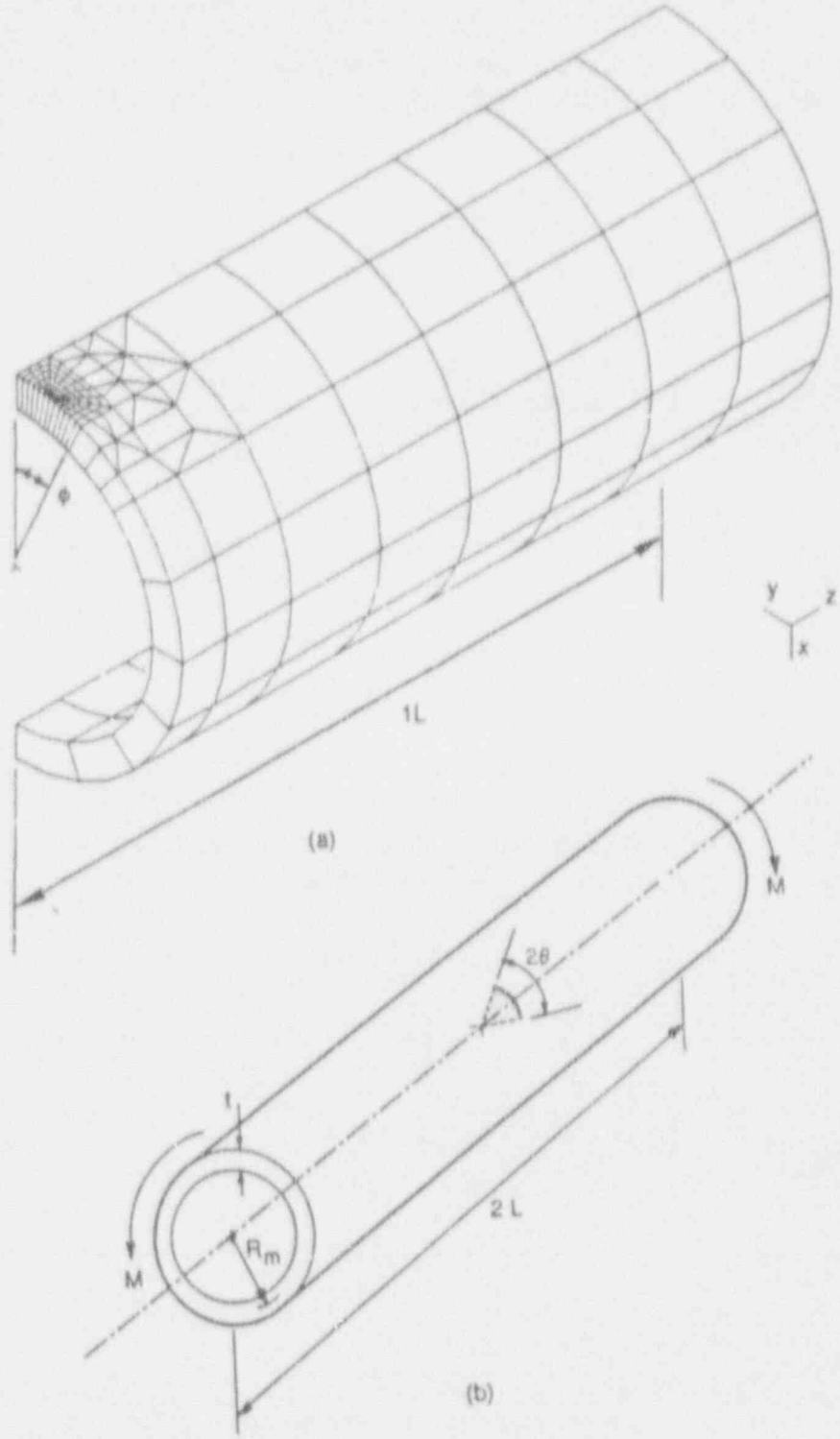

Figure 2.12 Typical finite element (a) mesh used for analysis (1/4 model), and (b) circumferential cracked pipe geometry

SC-SA-5/92-F2.12

this problem may be due to the use of the 9-node shell element in Reference 2.10 to produce the solutions, and overly stiff results occurred. Here we recompute the solutions of Reference 2.10 for $\theta/\pi = 1/8$ and $\theta/\pi = 1/16$. In this fashion, more reliable predictions of crack instability for the smaller crack sizes using the GE/EPRI scheme are expected by using brick instead of shell elements.

Finite Element Model and Analysis Matrix—Six finite element meshes have been developed, one for each case listed in Table 2.6. A typical finite element mesh and geometric definitions are illustrated in Figure 2.12(a). A quarter model is used by taking advantage of symmetry. Twenty node isoparametric brick elements are being used with focused elements at the crack tip. Only one element through the pipe wall is used, and, as such, the tabulated results should be considered as average values through the pipe wall. Elastic results for tension loading are also compiled here.

The elastic solutions are developed using elastic properties. A deformation theory plasticity algorithm in the ABAQUS finite element code is used to generate the plastic solution. Because a through-wall-cracked pipe subjected to bending is a plane stress problem, the special (hybrid) elements in the ABAQUS library which adequately handle plastic incompressibility are not necessary. A reduced (2 x 2) Gaussian quadrature integration rule is utilized.

The GE/EPRI handbook (Ref. 2.10) compiled tables whereby J and the crack-mouth-opening displacement (at the center of the crack), δ, are tabulated for specific geometric and material parameters. The parameters include R_m/t, θ, and the Ramberg-Osgood power-law exponent, n. For a uniaxial tensile bar, the Ramberg-Osgood relation is as written in Equation 2-1.

Table 2.6 Matrix of finite element calculations (total of 30 analyses for bending)

Model No.	Model Name[a]	R_m/t	n[b]	θ/π	Remarks	Loading
1	CASE1A	5	1,3,5,7,10	0.0625	5 Runs	Bending
2	CASE2A	10	1,3,5,7,10	0.0625	5 Runs	Bending
3	CASE3A	20	1,3,5,7,10	0.0625	5 Runs	Bending
4	CASE1B	5	1,3,5,7,10	0.1250	5 Runs	Bending
5	CASE2B	10	1,3,5,7,10	0.1250	5 Runs	Bending
6	CASE3B	20	1,3,5,7,10	0.1250	5 Runs	Bending

(a) "A" refers to $\theta/\pi = 0.0625$. "B" refers to $\theta/\pi = 0.125$.
(b) n = 1 is elastic.

Here we follow the convention of Reference 2.10 and compile values for J (see Eq. 2-2a) and the center crack-mouth-opening displacement, δ:

$$\delta = \delta_e + \delta_p$$
$$\delta = f_2 \frac{M}{E} + \alpha \varepsilon_o a\, h_2 \left(\frac{M}{M_o}\right)^n \tag{2-4a}$$

where δ_e and δ_p are elastic and plastic contributions of the center crack-mouth-opening displacement, respectively.

We also compile the rotations due to the presence of the crack:

$$\phi^c = \phi_e^c + \phi_p^c$$

$$\phi^c = f_4 \frac{M}{E} + \alpha \varepsilon_o\, h_4 \left(\frac{M}{M_o}\right)^n \tag{2-4b}$$

In Equation 2-4b, $\phi_e{}^c$ and $\phi_p{}^c$ represent the additional elastic and plastic rotations due to the presence of the crack.

For the elastic contribution, using the GE/EPRI convention (Eq. 2-2), we write:

$$f_1\left(\frac{\theta}{\pi}, \frac{R_m}{t}\right) = \pi a \left(\frac{R_m}{I}\right)^2 F^2\left(\frac{\theta}{\pi}, \frac{R_m}{t}\right) \tag{2-5}$$

Also, from Equations 2-4a and 2-4b:

$$f_2\left(\frac{\theta}{\pi}, \frac{R_m}{t}\right) = 4a \frac{R_m}{I} V_1\left(\frac{\theta}{\pi}, \frac{R_m}{t}\right) \tag{2-6}$$

$$f_4\left(\frac{\theta}{\pi}, \frac{R_m}{t}\right) = 4 \frac{R_m}{I} V_3\left(\frac{\theta}{\pi}, \frac{R_m}{t}\right) \tag{2-7}$$

In Equations 2-5 to 2-7, I is the moment of inertia of the uncracked section, which for large R_m/t is written as:

$$I = \pi R_m^3 t \tag{2-7a}$$

and F, V_1, and V_3 are compiled from the finite element solutions. Note that F is the function conventionally defined in the stress intensity factor definition as:

$$K_I = \sigma\sqrt{\pi a}\, F\left(\theta, \frac{R_m}{t}\right) \tag{2-8}$$

The plastic functions h_1, h_2, and h_4 are also compiled. The ABAQUS deformation theory routine uses a constitutive law that includes the elastic term (Eq. 2-1), i.e., it is not truly a fully plastic solution. The analyses are performed to a load level in which plastic strains greatly dominate elastic strains everywhere in the body, which effectively results in a nearly fully plastic solution. However, for completeness, we obtain the fully plastic solution by subtracting out the (separately calculated) elastic results. Hence, from Equations 2-2 and 2-4 to 2-7, the functions h_1, h_2, and h_4 are evaluated using:

$$h_1 = \frac{J - J_e}{\alpha\, \sigma_o\, \varepsilon_o\, a \left(1 - \frac{\theta}{\pi}\right)\left(\frac{M}{M_o}\right)^{n+1}} \tag{2-9}$$

$$h_2 = \frac{\delta - \delta_e}{\alpha\, \varepsilon_o\, a \left(\frac{M}{M_o}\right)^{n}} \tag{2-10}$$

$$h_4 = \frac{\phi - \phi_e^c - \phi_e^{nc} - \phi_p^{nc}}{\alpha\, \varepsilon_o \left(\frac{M}{M_o}\right)^{n}} \tag{2-11}$$

The dimensionless elastic functions (F and V_1) are compiled first to determine J_e, δ_e, and ϕ_e^c. Then the results of the ABAQUS solution provide J, δ, and ϕ from which Equations 2-9 to 2-11 provide

h_1, h_2, and h_4. In Equation 2-11, ϕ_e^{nc} and ϕ_p^{nc} represent the elastic and plastic rotations which would exist if no crack were present. These were defined in Reference 2-10, but for completeness, we provide them here.

$$\phi_e^{nc} = 2\frac{ML}{EI} \tag{2-12}$$

$$\phi_p^{nc} = \frac{2L\alpha\varepsilon_o}{R_m}\left[\frac{M}{4\sigma_o R_m^2 t\beta}\right]^n \tag{2-13}$$

where

$$\beta = \frac{\sqrt{\pi}}{2}\,\frac{\Gamma\left(1+\frac{1}{2n}\right)}{\Gamma\left(\frac{3}{2}+\frac{1}{2n}\right)} \tag{2-14}$$

For our purposes, the gamma function can be approximated in the range of interest here with:

$$\Gamma(x+1) = x! = 1 + b_1x + b_2x^2 + \ldots + b_8x^8$$

b_1 =	.577191652	b_5 =	-.756704078
b_2 =	.988205891	b_6 =	.482199394
b_3 =	-.897056937	b_7 =	-.193527818
b_4 =	.918206857	b_8 =	.035868343

This form was used accurately in Reference 2.9, where in that reference the symbol $\hat{K}$ was used rather than β.

Results—A complete set of analyses was performed for the matrix of cases shown in Table 2.6 using ABAQUS on Battelle's Vax Computer for Model 2 (n = 1, 3, 5, 7, 10). Both elastic and fully plastic (deformation theory) computations were made for bending loads.

The GE/EPRI compilations appear to be more accurate for the large crack sizes. Hence, a comparison for the case of $R_m/t = 10$ was made here to verify the accuracy of the approach taken. For this case, $\theta/\pi = 0.5$ and n = 3 was chosen. Table 2.7 lists results. The comparison for the value of the J-integral is very good. However, the difference in h_4 is not insignificant.

Table 2.7 Check case for $R_m/t = 10$, $\theta/\pi = 1/2$, $n = 3$

Functions[a]	GE/EPRI	3D-Solid ABAQUS
h_1	2.105	2.105
h_2	3.331	3.195
h_4	3.232	4.635

(a) h_1 relates fully plastic J to moment.
h_2 relates fully plastic center crack-mouth-opening displacement to moment.
h_4 relates fully plastic pipe rotation to moment.

Tables 2.8 through 2.11 provide the solutions compiled for all of the cases listed in Table 2.6. Table 2.8 is the elastic solution, while Tables 2.9 through 2.11 provide solutions for $R_m/t = 5$, 10, and 20, respectively. Note that GE/EPRI did not provide solutions for $n = 10$ and some of the $n = 7$ cases due to numerical difficulties.

In order to obtain the h-functions, the ABAQUS calculation involved elastic and plastic analysis (deformation theory) for a series of bending moment loads until a fully plastic criterion was met. One check on the fully-plastic h-functions reported in Tables 2.9 through 2.11 was to calculate these functions at all load levels and verify that h-functions do not vary once certain load levels (plasticity dominates) are reached. A typical plot of the h_1 function with bending moment is shown in Figure 2.13 and it shows that the h_1 function levels off after some load value. This technique was used to produce all of the h-functions. It was also necessary to ensure that the rotations were not large in evaluating h_4.

Elastic Tension Solutions—In a manner completely analogous to that described for bending, the elastic functions were compiled for a tensile-loaded cracked pipe. Here:

$$K_I = \sigma^{\infty}\sqrt{\pi a}\, F\left(\frac{\theta}{\pi}, \frac{R_m}{t}\right) \tag{2-15}$$

$$\delta_e = \frac{4\sigma^{\infty} a}{E}\, V_1\left(\frac{\theta}{\pi}, \frac{R_m}{t}\right) \tag{2-16}$$

Table 2.8 F, V_1, for bending with $R_m/t = 5, 10, 20$. (ABAQUS 3D-Solid Solution for the n=1 case of Table 2.6

	Function[a]	$R_m/t = 5$	$R_m/t = 10$	$R_m/t = 20$
$\theta/\pi = 1/16$	F	1.022	1.049	1.097
	V_1	1.234	1.206	1.111
	V_3	0.028	0.035	0.098
$\theta/\pi = 1/8$	F	1.103	1.208	1.418
	V_1	1.388	1.480	1.482
	V_3	0.126	0.160	0.231

(a) F relates elastic stress intensity factor to stress.
V_1 relates elastic center-crack-opening displacement to moment.
V_3 relates elastic pipe rotation to moment.

Table 2.9 h-functions for through-cracks in bending for $R_m/t = 5$ (ABAQUS - 3D Solid Solution)

	Function[a]	n = 3	n = 5	n = 7	n = 10
$\theta/\pi = 1/16$	h_1	5.451	5.766	5.681	5.263
	h_2	6.896	7.003	6.715	6.087
	h_4	0.826	1.452	1.879	2.371
$\theta/\pi = 1/8$	h_1	4.484	3.976	3.372	2.464
	h_2	5.820	4.999	4.165	2.959
	h_4	1.194	1.454	1.461	1.291

(a) F relates elastic stress intensity factor to stress.
V_1 relates elastic center-crack-opening displacement to moment.
V_3 relates elastic pipe rotation to moment.

Table 2.10 h-functions for through-cracks in bending for $R_m/t = 10$ (ABAQUS - 3D Solid Solution)

	Function[a]	n = 3	n = 5	n = 7	n = 10
$\theta/\pi = 1/16$	h_1	6.225	6.701	6.784	6.749
	h_2	7.422	7.739	7.632	7.527
	h_4	1.156	1.802	2.220	2.826
$\theta/\pi = 1/8$	h_1	5.791	5.512	4.770	3.825
	h_2	6.693	6.319	5.329	4.221
	h_4	1.550	1.886	1.864	1.713

(a) F relates elastic stress intensity factor to stress.
V_1 relates elastic center-crack-opening displacement to moment.
V_3 relates elastic pipe rotation to moment.

Table 2.11 h-functions for through-cracks in bending for $R_m/t = 20$ (ABAQUS - 3D Solid Solution)

	Function[a]	n = 3	n = 5	n = 7	n = 10
$\theta/\pi = 1/16$	h_1	7.044	8.022	8.756	8.815
	h_2	7.073	8.050	8.787	8.812
	h_4	1.505	2.348	3.087	3.770
$\theta/\pi = 1/8$	h_1	8.448	8.281	7.748	6.524
	h_2	7.498	7.491	7.160	5.890
	h_4	2.216	2.738	2.963	2.728

(a) F relates elastic stress intensity factor to stress.
V_1 relates elastic center-crack-opening displacement to moment.
V_3 relates elastic pipe rotation to moment.

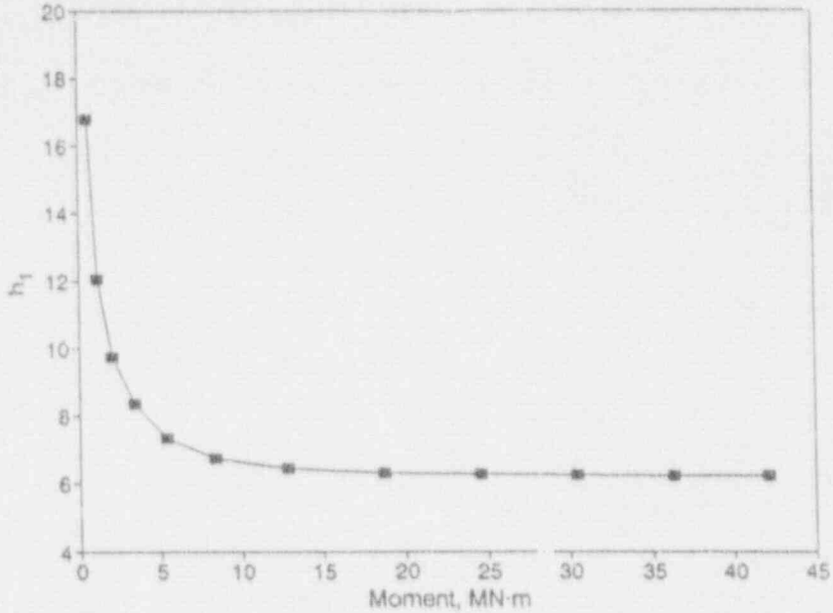

Figure 2.13 Plasticity function h_1 (ABAQUS - Solid Element Results) for pipe under bending, $R_m/t = 10$, $n = 3$, and $\theta/\pi = 0.0625$

SC-SA-5/92-F2.13

$$\Delta_e = \frac{4\sigma^{\infty}a}{E} V_2\left(\frac{\theta}{\pi}, \frac{R_m}{t}\right) \tag{2-17}$$

In Equations 2-15 to 2-17, σ^{∞} is the far field applied tensile stress and Δ_e is the elastic displacement at the uncracked pipe neutral axis due to the crack. The other parameters were defined earlier.

The results are presented in Table 2.12 and compared with the GE/EPRI results from Reference 2.10. The differences are not insignificant, especially for the axial displacement due to the crack.

Discussion—The differences between the previously developed solutions (Ref. 2.10) and the present results appear to be most important for small crack sizes (θ/π = 1/8, 1/16), although results for large cracks (especially for rotations) appear to be suspect. The present solutions were developed using the three-dimensional solid elements (20-node brick) and the deformation theory algorithm of ABAQUS. The solutions presented here are believed to be the more accurate of the two solutions. However, the results of Reference 2.10 predict lower loads which are conservative. For crack-opening displacements, the new results predict a higher crack opening for typical PWR and BWR piping.

Table 2.12 F_1, V_1, V_2 for tension[a] (Elastic Analysis, ABAQUS Results)

Case		Function[b]	θ/π = 1/16	θ/π = 1/8	θ/π = 1/2
1	R_m/t = 5	F	1.027 (1.049)	1.139 (1.176)	(c)
		V_1	1.178 (1.050)	1.359 (1.202)	(c)
		V_2	0.042 (0.044)	0.096 (0.114)	(c)
2	R_m/t = 10	F	1.049 (1.077)	1.250 (1.259)	(c)
		V_1	1.179 (1.082)	1.481 (1.319)	(c)
		V_2	0.054 (0.052)	0.437 (0.127)	(c)
3	R_m/t = 20	F	1.107 (1.127)	1.469(1.387)	(c)
		V_1	1.258 (1.144)	1.719 (1.530)	(c)
		V_2	0.230 (0.059)	0.591 (0.138)	(c)
4	R_m/t = 10	F	(c)	(c)	4.401 (4.208)
		V_1	(c)	(c)	9.280 (8.323)
		V_2	(c)	(c)	3.140 (2.807)

(a) The numbers in parentheses represent the GE/EPRI original solutions.
(b) F relates elastic stress intensity factor to stress.
V_1 relates elastic center crack-opening displacement to load.
V_2 relates elastic axial displacements due to the crack to load.
(c) These runs were not part of the current program. For checking purposes, one run for θ/π = 1/2 and R_m/t = 10 (Case 4) was made.

From an LBB viewpoint, this means that the GE/EPRI functions may be nonconservative. Solutions for large n were not possible as convergence problems occurred in Reference 2.10. Here, no convergence problems were experienced. The problems with the small crack solutions of Reference 2.10 are discussed in much more detail in References 2.7, 2.8, and 2.11.

Figure 2.14(a) presents a plot of the F-function results (Eq. 2-8) and the GE/EPRI solution as a function of R_m/t for θ/π = a/b = 1/16, where a is the crack length and b is the uncracked ligament. The differences are about three percent. Figure 2.14(b) shows a comparison of V_1 values (Eq. 2-6), which are related to the crack-opening displacement. The differences are about 20 percent for R_m/t = 5. Comparisons of h_1 (J-integral) and h_2 (crack-opening displacement) are presented in Figures

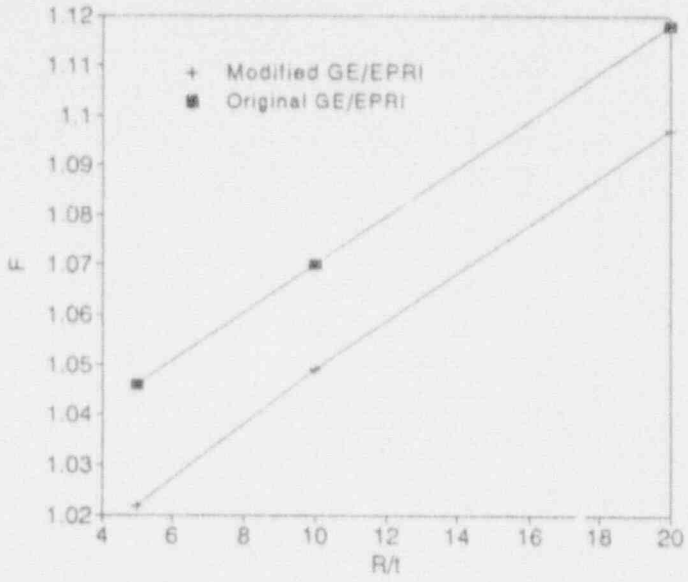

(a) F-function comparison, $\theta/\pi = 1/16$ (F relates elastic stress intensity factor to stress)

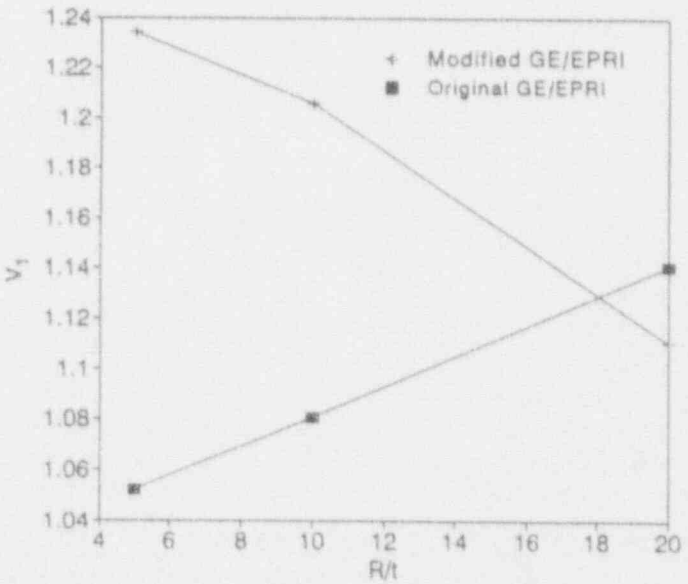

(b) Comparison of V_1 values for $\theta/\pi = 1/16$ (V_1 relates elastic center-crack-mouth-opening displacement to moment)

Figure 2.14 Comparison of ABAQUS FEM results to past GE/EPRI solutions for elastic functions

SC-SA-5/92-F2.14a/b

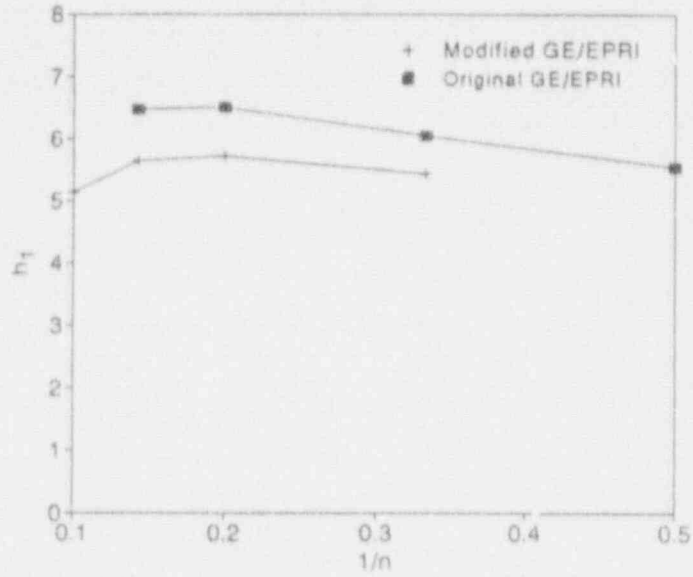

(a) $R_m/t = 5$, $\theta/\pi = 1/16$

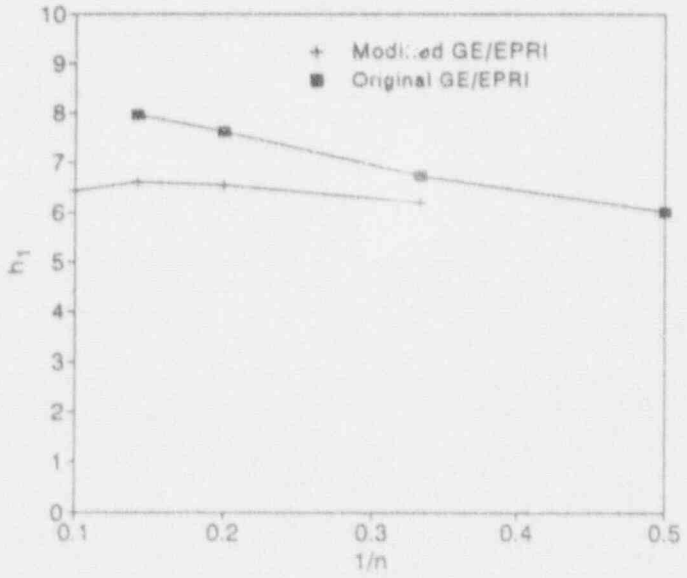

(b) $R_m/t = 10$, $\theta/\pi = 1/16$

Figure 2.15 Comparison of ABAQUS FEM results to past GE/EPRI solutions for h_1 fully plastic functions (h_1 relates fully plastic J to moment)

SC-SA-5/92-F2.15a/b

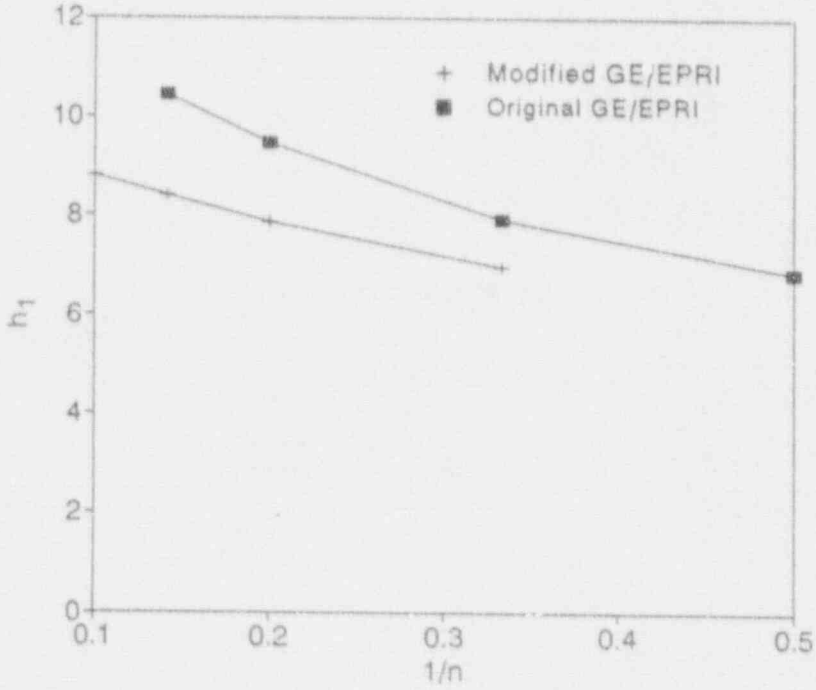

(c) $R_m/t = 20$, $\theta/\pi = 1/16$

Figure 2.15 (Continued)

SC-SA-5/92-F2.15c

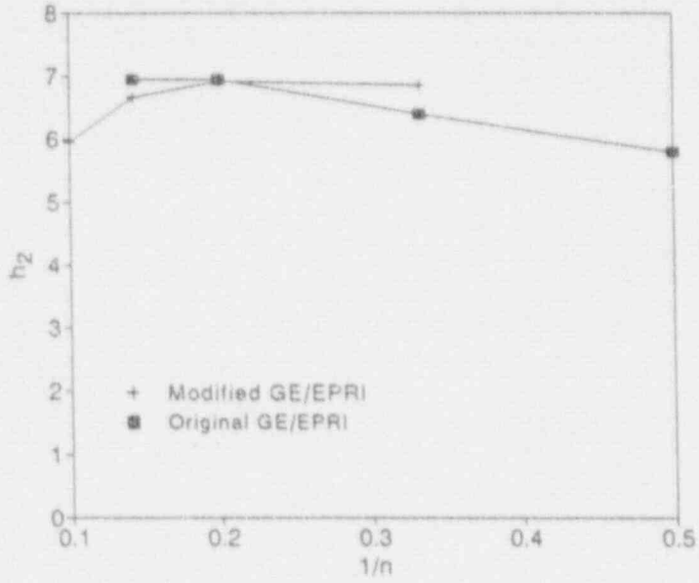

(a) $R_m/t = 5, \theta/\pi = 1/16$

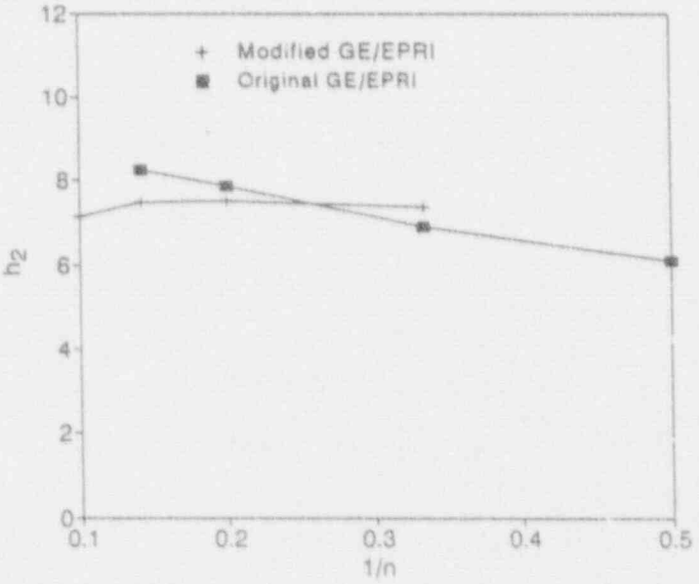

(b) $R_m/t = 10, \theta/\pi = 1/16$

Figure 2.16 Comparison of ABAQUS FEM results to past GE/EPRI solutions for h_2 fully plastic functions (h_2 relates fully plastic center-crack-opening displacement to moment)

SC-SA-5/92-F2.16a/b

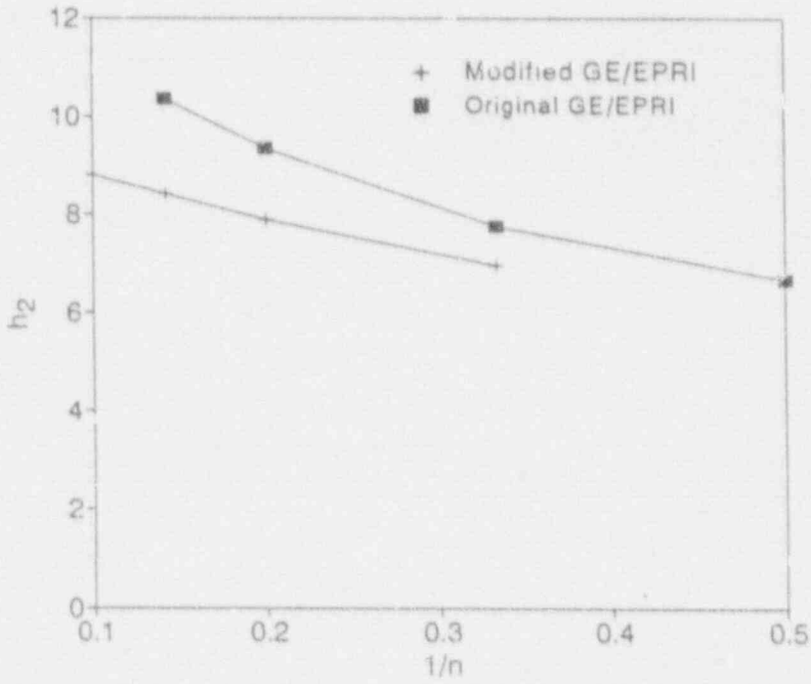

(c) $R_m/t = 20$, $\theta/\pi = 1/16$

Figure 2.16 (Continued)

SC-SA-5/92-F2.16c

2.15 and 2.16, respectively. In these figures, note that the present solutions were not compiled for n = 2 (1/n = 0.5), while the GE/EPRI solutions were not compiled for n = 10 (1/n = 0.1). The h_1 and h_2 values differ by as much as 25 percent between the two solutions.

A comparison of J as a function of moment is given in Figure 2.17 for θ/π = 1/8, R_m/t = 5, and n = 3, 7 and in Figure 2.18 for θ/π = 1/16, R_m/t = 20, and n = 3, 7. These figures show that the differences between the original and modified solutions can be significant at higher loads.

Finally, Figures 2.19(a) through 2.19(d) provide comparisons between the presently produced rotation results and those of Reference 2.10. These are presented last because it will be seen that some major differences between the results are realized. All of these comparisons are for θ/π = 1/16.

Figure 2.19(a) compares the two calculations of the elastic function, V_3. Of particular note are the negative values of V_3 from the GE/EPRI results. Of course, it is physically impossible to obtain negative rotations due to the crack. Similar observations for the plastic (h_4) solutions can be made, as seen in Figures 2.19(b) through 2.19(d), for R_m/t = 5, 10, and 20, respectively, and θ/π = 1/16. The original GE/EPRI solutions are either negative or far too small.

Conclusion—Solutions for the small circumferential crack under elastic-plastic conditions have been compiled for the case of pure bending. These are compiled in a format identical to that of Reference 2.10. Solutions for the tension case and combined tension-bending may be compiled in the future. Work is also continuing on the development of alternative improved estimation schemes for small cracks in pipe (Refs. 2.7 and 2.8) and a crack in a pipe weld (Ref. 2.9). Results will be published in the next semiannual report.

Activity 1.4.2 Analyze Large-Diameter Pipe TWC Test Results

Objective

The objective in this activity is to analyze the large-diameter, short through-wall-cracked pipe fracture experiments.

Rationale

These pipe fracture data were developed to assess the J-estimation schemes to be used in LBB analyses for typical fracture behavior.

Approach

The pipe fracture data will be used to assess the accuracy of J-estimation schemes in the current version of NRCPIPE and the improved versions from the analysis improvements developed in

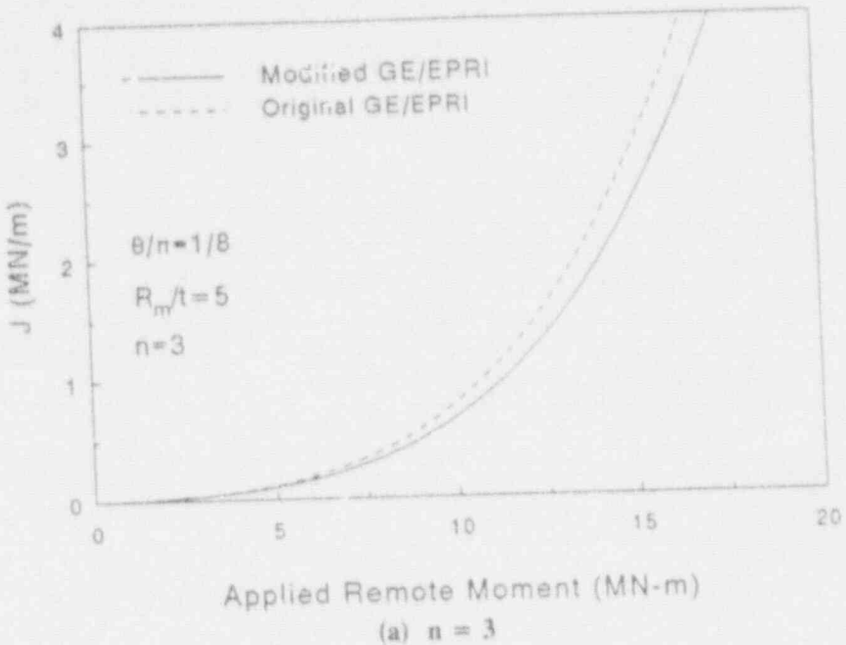

(a) n = 3

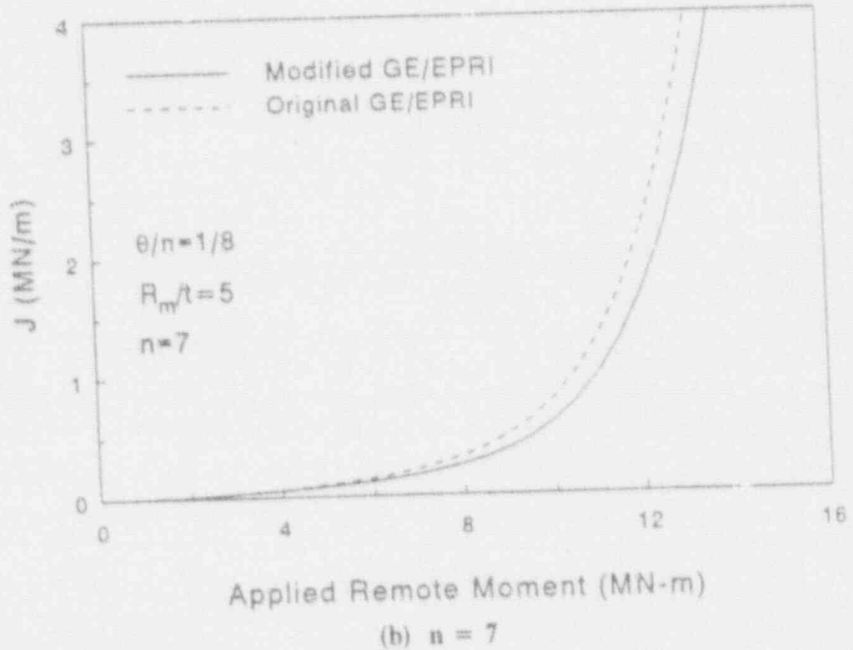

(b) n = 7

Figure 2.17 Comparison of J versus moment for $R_m/t = 5$, $\theta/\pi = 1/8$

SC-SA-5/92-F2.17a/b

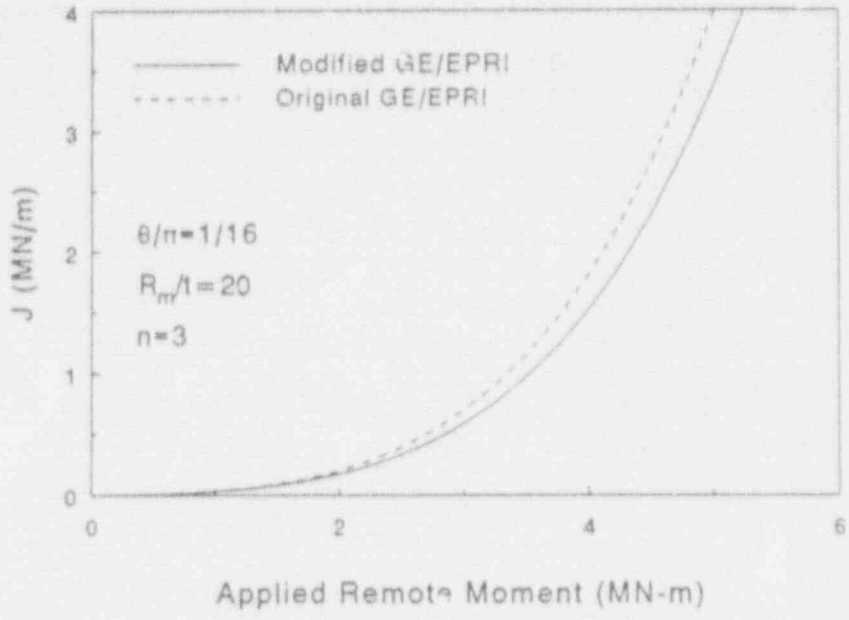

(a) n = 3

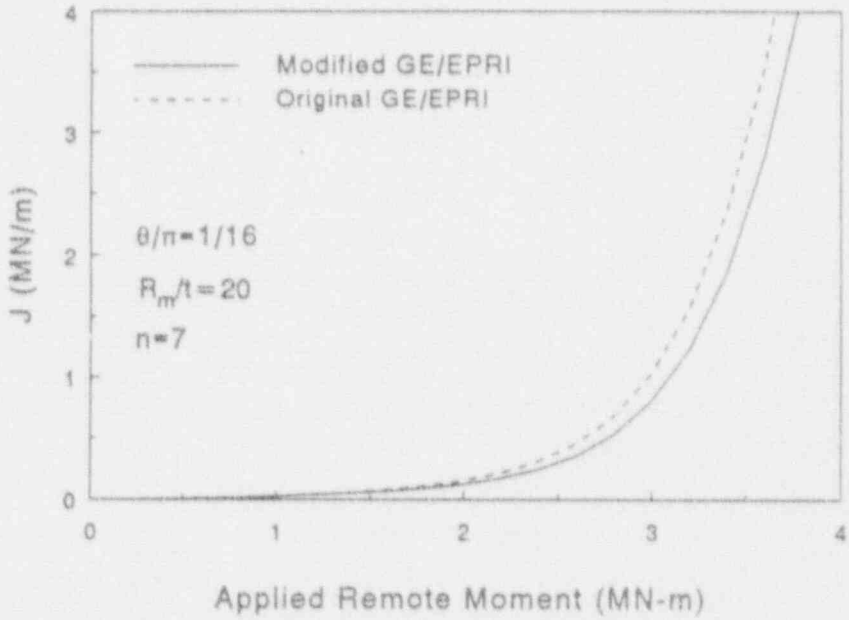

(b) n = 7

Figure 2.18 Comparison of J versus moment for $R_m/t = 20$, $\theta/\pi = 1/16$

SC-SA-5/92-F2.18a/b

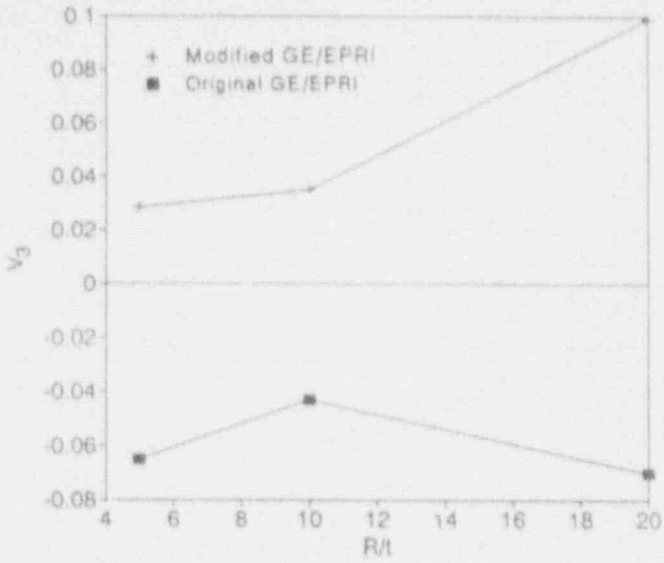

(a) V_3 function comparisons, $\theta/\pi = 1/16$ (V_3 relates elastic rotation due to crack to moment)

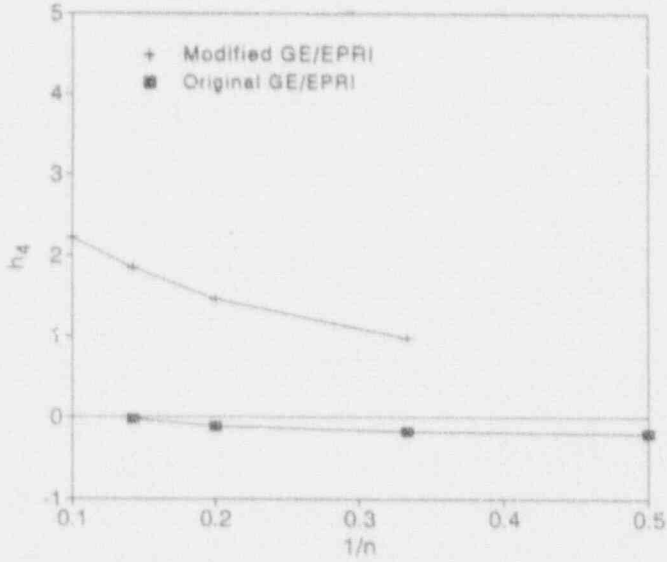

(b) Comparison of h_4-functions, $R_m/t = 5$, $\theta/\pi = 1/16$ (h_4 relates fully plastic rotation to moment)

Figure 2.19 Comparison of ABAQUS FEM results to past GE/EPRI solutions for elastic and fully plastic rotation functions

SC-SA-5/92-F2.19a/b

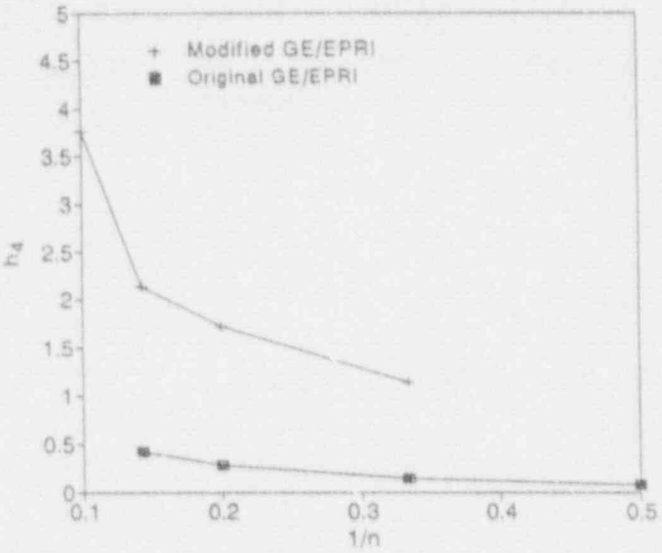

(c) Comparison of h_4-functions, $R_m/t = 10$, $\theta/\pi = 1/16$ (h_4 relates fully plastic rotation to moment)

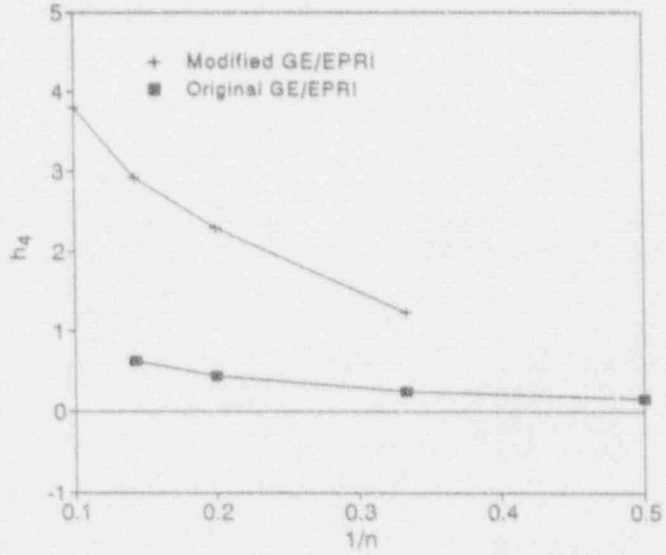

(d) Comparison of h_4-functions, $R_m/t = 20$, $\theta/\pi = 1/16$ (h_4 relates fully plastic rotation to moment)

Figure 2.19 (Continued)

SC-SA-5/92-F2.19c/d

Activity 1.4.1. This effort will consider accuracy of the Ramberg-Osgood fit, different fits of the J-R curve, as well as the other improvements made in the J-estimation schemes.

Progress

Progress in this activity during this reporting period was presented in the second semiannual report. This was done for the sake of completeness; most of the work conducted in this activity had been performed in the previous reporting period.

Activity 1.4.3 Analyze Through-Wall Crack in Welds

Objective

This activity involves developing a methodology to accurately assess the fracture behavior of pipe with a crack in the center of the weld.

Rationale

The current practice is to use the toughness of the weld and the strength of the base metal. Limited data from the Degraded Piping Program on as-welded and solution-annealed welds suggest that the strength of the weld metal should also be included.

Progress

Progress in this activity during this reporting period was presented in the second semiannual report. This was done for the sake of completeness as most of the work conducted in this activity had been performed in the previous reporting period.

2.4 Plans for Next Year of the Program

Work expected to be completed during the next year of the program is described below.

2.4.1 Subtask 1.1 Material Characterization for Short TWC Pipe Experiments

As was noted in Section 2.3.1.3, fabrication and characterization of a weld in a carbon-steel plate, nominally identical to a weld in a carbon steel pipe which is to be tested in Task 1, will be carried out within Task 2. Fabrication of the welded plate is expected to be completed in the first half of

1992; material characterization efforts probably will start in the second half of the next year of the program.

2.4.2 Subtask 1.2 Upgrading of the Large-Pipe Test Facility

The load capacity of the large-pipe test facility used for this program is scheduled at the end of the next year to be upgraded by replacing the existing actuators with new, larger actuators and by increasing the local reinforcement around the actuator and the end restraint locations.

2.4.3 Subtask 1.3 Large-Diameter Pipe Fracture Experiments

The 28-inch-diameter carbon steel uncracked pipe experiment (1.1.1.25) and the 24-inch-diameter carbon steel SAW through-wall-cracked pipe experiment (1.1.1.24) will be conducted in the next year of the program.

2.4.4 Subtask 1.4 Analyses for Short Through-Wall Cracks in Pipes

The following activities will continue in the next year of the program.

Activity 1.4.1(a) - Numerically Assess the Effect of Plastic Ovalization on the Validity of J. Once the mesh refinement problems have been resolved this activity will be renewed and the analysis including crack growth completed. The results from this activity will determine the severity of the effect of pipe ovalization on the validity of J.

Activity 1.4.1(c) - Improve F, V, and h-Functions. During the next year the GE/EPRI functions developed here will be incorporated into the NRCPIPE code used to analyze TWC pipes.

Activity 1.4.2 - Analyze Large-Diameter Pipe TWC Test Results. Experiment 1.1.1.24 is scheduled to be conducted in the next reporting period. This experiment will be analyzed after the data have been reduced.

Activity 1.4.3 - Analyze Through-Wall Cracks in Welds. Efforts will involve analyzing pipe weld crack experiments from the Degraded Piping Program and Experiment 1.1.1.23. This work planned for the last reporting period has been postponed in order to complete other activities in Subtask 6.6.

2.5 References

2.1 Hiser, A. L. and Callahan, G. M., "A User's Guide to the NRC's Piping Fracture Mechanics Database (PIFRAC)," NUREG/CR-4894, May 1987.

2.2 Wilkowski, G. M. and others, "Short Cracks in Piping and Piping Welds," Battelle, NUREG/CR-4599, Vol. 1, No. 2, April 1992.

2.3 Wilkowski, G. M. and others, "Degraded Piping Program - Phase II," Summary of Technical Results and Their Significance to Leak-Before-Break and In-Service Flaw Acceptance Criteria, March 1984 - January 1989, Battelle, NUREG/CR-4082, Vol. 8, March 1989.

2.4 Wilkowski, G. M. and others, "Analysis of Experiments on Stainless Steel Flux Welds," NUREG/CR-4878, April 1987.

2.5 Wilkowski, G. M. and others, "Short Cracks in Piping and Piping Welds," by Battelle, NUREG/CR-4599, Vol. 1, No. 1, May 1991.

2.6 Schmidt, R. and others, "International Piping Integrity Research Group Program - Final Report," by Battelle, July 1991.

2.7 Gilles, P. and Brust, F. W., "Approximate Methods for Fracture Analyses of Through-Wall Cracked Pipes, Part I, Theory," Nuclear Engineering and Design, Vol. 127, pp 1-17, 1991.

2.8 Gilles, P., Chao, K. S., and Brust, F. W., "Approximate Methods for Fracture Analyses of Through-Wall Cracked Pipes, Part II, Applications," Nuclear Engineering and Design, Vol. 127, pp 19-31, 1991.

2.9 Rahman, S., Brust, F. W., Nakagaki, M., and Gilles, P., "An Approximate Method for Estimating Energy Release Rates of Through-Wall Cracked Pipe Weldments," ASME PVP publication PVP-Vol. 215, pp. 87-92, June 1991.

2.10 Kumar, V. and others, "Advances in Elastic-Plastic Fracture Analysis," EPRI Final Report NP-3607, August, 1984.

2.11 F. W. Brust, "Approximate Methods for Fracture Analysis of Through-Wall Cracked Pipes," NUREG/CR-4853, February 1987.

3. TASK 2 SHORT SC PIPE EVALUATIONS

3.1 Task Objective

The objectives of this task are to modify and verify analyses for short surface-cracked (SC) pipe using existing and new data on large-diameter pipe.

3.2 Task Rationale

Many of the past programs used large surface cracks for the purpose of having failure loads close to the yield strength of the pipe. Typical flaws in service are much smaller than the flaws from these past programs. These results will verify and may refine analyses that have been used for pragmatic in-service flaw evaluations such as those in ASME Section XI.

3.3 Task Approach

This task has been divided into five subtasks:

Subtask 2.1 Material characterization for surface-cracked pipe experiments
Subtask 2.2 Small-diameter pipe fracture experiments in pure bending for limit-load ovalization correction
Subtask 2.3 Large-diameter surface-cracked pipe fracture experiment in combined bending and tension (pressure)
Subtask 2.4 Analysis of short surface cracks in pipes
Subtask 2.5 Topical report.

Details of each of these subtasks are presented in the following paragraphs.

3.3.1 Subtask 2.1 Material Characterization for Surface-Cracked Pipe Experiments

3.3.1.1 Objective

The objective of this activity is to generate the data necessary to document the material strength and toughness for analysis in Subtask 2.4.

3.3.1.2 Rationale

The material property data needed for the analysis procedures in Subtask 2.4 will be determined for each pipe and weld to be tested. These data are also of value for the NRC PIFRAC database (Ref. 3.1).

3.3.1.3 Approach

With two exceptions, material property data, i.e., Charpy, chemical analysis, tensile, and J-R curves, are already available from the Degraded Piping Program (Ref. 3.2) for pipes to be tested within Task 2. One exception is a 16-inch-diameter austenitic stainless steel pipe to replace one damaged in the accident associated with IPIRG Experiment 1.3-7. The pipe that was damaged had previously been characterized in the Degraded Piping Program. Since that pipe is not available for testing in Task 2, a replacement will have to be procured and characterized. The other exception is a 36-inch-diameter carbon-steel pipe weld which is to be fabricated and tested in Subtask 2.3. Rather than conduct tests on specimens machined from the welded pipe, material characterization tests will be performed on a weld in a 25.4-mm (1-inch)-thick carbon steel plate, prepared in a manner nominally identical to that used in welding the pipe.

The data will be recorded digitally and reduced to a format identical to that used in past Degraded Piping Program data record book entries. These data would also be available for input into the NRC PIFRAC database.

3.3.1.4 Progress

A 16-inch-diameter austenitic stainless steel pipe was obtained from Savannah River to replace the pipe that was damaged in an accident associated with an IPIRG pipe experiment.

Discussions were held with Babcock & Wilcox personnel relative to procuring welded carbon-steel pipes from the Midland plant for testing in Task 2, or procuring filler metal used in the construction of the piping system in that plant. That filler metal then would be used in preparing weldments for Task 2 tests. At the end of the reporting period, it appeared unlikely that either welded pipes or leftover filler metal would be available to this program. In that event, Babcock & Wilcox would provide recommendations regarding typical welding procedures, filler metal, and flux for fabricating the weldments to be tested in Task 2.

3.3.2 Subtask 2.2 Smaller Diameter Pipe Fracture Experiments in Pure Bending for Limit-Load Ovalization Correction

3.3.2.1 Objective

The objective of this effort is to develop experimental data for internally surface-cracked pipe under four-point bending that can be used to assess the empirical ovalization correction for limit-load failures.

3.3.2.2 Rationale

In the Degraded Piping Program, an empirical correction for the Net-Section-Collapse analysis of circumferentially surface-cracked pipe in pure bending was developed (Ref. 3.3). It was found that the correction was a function of the pipe R_m/t ratio, see Figure 3.1. The data represented in Figure 3.1 are for experiments with relatively large surface cracks, typically 50 percent of the pipe circumference and 66 percent of the thickness in depth. Data on smaller crack sizes are needed to

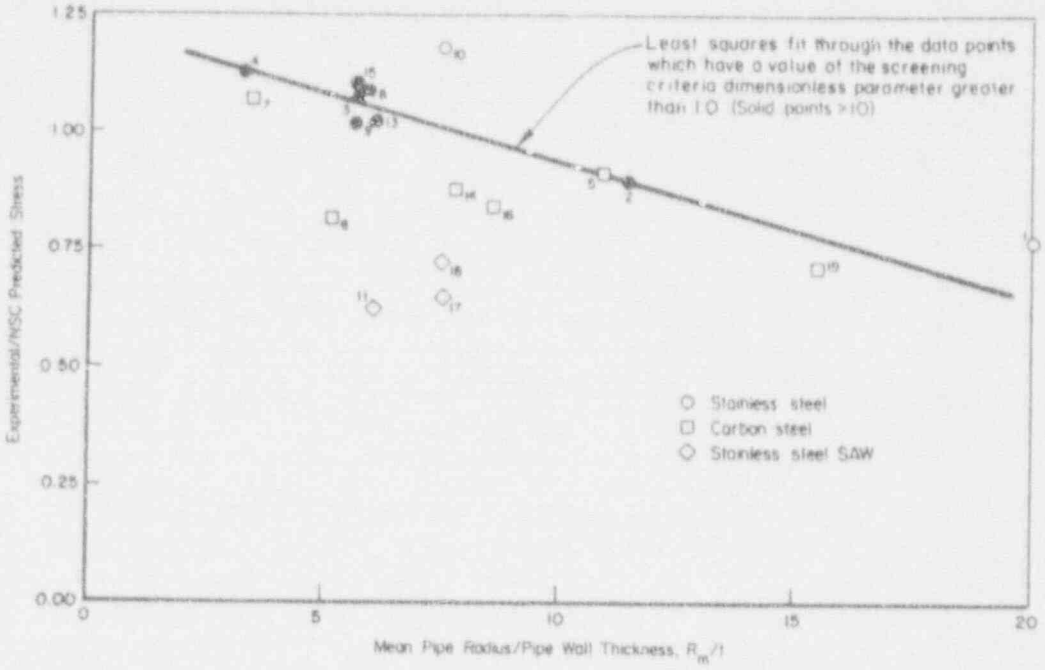

Figure 3.1 Empirical ovalization correction factor for circumferentially surface-cracked ($d/t = 0.66$ and $2c/\pi D_m = 0.5$) pipe in bending

SC-SA-5/92-F3.1

generalize such a correction. The correction for the limit-load case is necessary since many of the elastic-plastic fracture analyses and code flaw assessment criteria (i.e., IWB-3640 and IWB-3650 from Section XI of the ASME Code) have as their basis limit-load solutions.

3.3.2.3 Approach

To satisfy the need for data to verify the analyses, three smaller diameter pipe fracture experiments will be conducted, see Table 3.1. The pipe material for each experiment will be a high toughness stainless steel. Therefore, for the pipe diameters under consideration in this subtask, fully plastic conditions should exist. This will facilitate the analysis of the data in that any lowering of the failure moments with respect to the net-section-collapse predicted moments can be attributed to ovalization effects and not contained plasticity (elastic-plastic) conditions.

Note that the three pipe materials evaluated in this study are pipes obtained from canceled nuclear power plants. The pipe geometries represent the range of R_m/t ratios that may be used in nuclear piping; the largest radius-to-thickness (R_m/t) ratio is 21.3 and the smallest is 3.8.

The surface flaw size used in this subtask was established through parametric analysis. The flaw size chosen, 25 percent of the pipe circumference in length and 50 percent of the pipe wall thickness in

Table 3.1 Smaller diameter pipe experiments with short cracks under bending for Subtask 2.2

Test No.[a]	Nominal Diameter	Schedule	R_m/t	Material	Temperature	$2c/\pi D_m$[b]	d/t[b]
1.2.1.20	16-inch	30	21.3	TP316	288 C (550 F)	0.25	0.5
1.2.1.21	6-inch	XXS	3.8	TP304	288 C (550 F)	0.25	0.5
1.2.1.22	6-inch	40	11.8	TP304	288 C (550 F)	0.25	0.5

(a) Test numbers are consecutive with those in the Degraded Piping Data Record Books.
(b) $2c/\pi D_m$ = circumferential crack length/mean pipe circumference, d/t = surface crack depth/pipe thickness.

depth, was the smallest flaw (established through analysis) that would fracture prior to the onset of pipe buckling.

3.3.2.4 Progress

The results for the two nominal 6-inch-diameter surface-cracked pipe experiments were discussed in detail in the second semiannual report from this program (Ref. 3.4).

During this reporting period efforts for this subtask have focussed on preparing the test specimen for the 16-inch-diameter Schedule 30 stainless steel pipe experiment. This experiment has the highest R_m/t ratio to be evaluated. Consequently, the degradation in load-carrying capacity due to ovalization effects should be the most severe. As a result, the outcome of this experiment will be an important test case for the analysis. The pipe originally scheduled for this experiment was destroyed during the IPIRG Subtask 1.3 accident, and it was necessary to obtain a suitable replacement pipe. During this reporting period, negotiations were completed whereby a 5.5-meter (18-foot) section of 16-inch-diameter Schedule 30 Type 316L stainless steel pipe was donated to this program by the operators of the Savannah River facility. At this time the test specimen for this experiment has been cut off this joint of pipe and the initial surface crack machined into the inside pipe surface. The surface flaw has been instrumented and the test specimen is ready to be welded onto the appropriate moment arm pipes.

One additional comment concerning this experiment is warranted. The test specimen for this experiment will be pressurized, whereas the test specimens for the other two small-diameter surface crack experiments were unpressurized. The fact that this experiment will be pressurized is not ideal, since the internal pipe pressure will stiffen the pipe and influence the amount of ovalization and, thus, the empirical ovalization correction factor associated with this experiment. However, it was deemed necessary to pressurize this pipe because the 6-inch-diameter Schedule 40 pipe sample buckled prior to attaining maximum load. Consequently, this 16-inch-diameter pipe, with a larger R_m/t ratio (21.3

versus 11.8 for the 6-inch Schedule 40 pipe experiment) would probably buckle prior to maximum load if it were not pressurized.

3.3.3 Subtask 2.3 Large-Diameter Surface-Cracked Pipe Fracture Experiments Under Combined Bending and Tension (Pressure)

3.3.3.1 Objective

The objective of this subtask is to develop experimental data for internally surface-cracked large-diameter pipe under more typical combined pressure and bending loading conditions for the purpose of making a critical assessment of the ASME Section XI and J-estimation scheme predictive analyses.

3.3.3.2 Rationale

With one exception, the largest pipes evaluated in the surface-cracked pipe experiments conducted as part of the Degraded Piping (Ref. 3.2), the IPIRG (Ref. 3.5), and the EPRI NP-2347 (Ref. 3.6) programs were 16 inches in diameter. The one exception was a 30-inch-diameter carbon steel surface-cracked pipe experiment conducted as part of the IPIRG program, Ref. 3.7. Consequently, a definite void exists in the pipe fracture experimental database. Since pipe diameter is an important governing parameter in assessing the failure mode, i.e., limit-load or elastic-plastic, it seems prudent to fill this void. The effects of larger diameter pipe on the fracture behavior of surface-cracked pipe need to be evaluated in order to make a critical evaluation of the ASME Section XI and J-estimation scheme predictive analyses.

3.3.3.3 Approach

To satisfy the data requirement for verifying the analysis methods, three large-diameter surface-cracked pipe fracture experiments will be conducted, see Table 3.2.

Table 3.2 Test matrix for large-diameter surface-cracked pipe experiments

Expt. No.	Nominal Diameter	Schedule	Material	Test Temp.	Test Pressure	$2c/\pi D_m$	d/t
1.2.3.15	28-inch	60	A515 GR60	288 C (550 F)	9.56 MPa (1387 psi)	0.25	0.5
1.2.3.16	28-inch	80	TP316L SAW	288 C (550 F)	10.14 MPa (1470 psi)	0.25	0.5
1.2.3.17	36-inch	160	A516 GR70 SAW	288 C (550 F)	TBD	TBD	TBD

TBD = To be determined.

3.3.3.4 Progress

During the last reporting period, two of the three large-diameter surface-cracked pipe fracture experiments from Table 3.2 were conducted, i.e., the 28-inch-diameter carbon steel base metal experiment (1.2.3.15) and the 28-inch-diameter stainless steel SAW experiment (1.2.3.16). The final large-diameter surface-cracked pipe fracture experiment, the 36-inch-diameter carbon steel SAW cold-leg experiment (1.2.3.17), will be conducted after the large-pipe test facility is upgraded in Subtask 1.2.

Experiment 1.2.3.15 28-inch-Diameter Carbon Steel Base Metal Experiment

The 28-inch-diameter A515 Grade 60 carbon steel base metal experiment was conducted at Battelle's large-pipe test facility at West Jefferson, Ohio. A schematic of the test specimen for this experiment is shown in Figure 3.2. The initial flaw size was 50 percent of the pipe wall thickness in depth and 25 percent of the pipe circumference in length. The flaw was introduced into the inside pipe surface using electric-discharge-machining (EDM) techniques to give a sharp notch with a radius of 0.127 mm (0.005 inch). The machined flaw was not fatigue precracked. The test temperature was 288 C (550 F). The loading conditions were quasi-static, monotonically increasing 4-point bending with a constant internal pipe pressure of 9.56 MPa (1.39 ksi). This internal pipe pressure resulted in an axial membrane stress (P_m) of 75.0 MPa (10.9 ksi), which is 65.6 percent of the design stress (S_m) for this material at 288 C (550 F). The pressurizing medium was subcooled water.

Figure 3.3 is a plot of the total applied load versus load-line displacement for this experiment. The total applied load values include the dead-weight load contribution of 62.2 kN (13,915 pounds) due to the weight of the pipe, water, and end restraints. From Figure 3.3 it can be seen that the maximum applied load for this experiment was 1064 kN (239,300 pounds).

Figure 3.4 is a plot of the crack section moment versus the crack section rotation data from this experiment. The rotation data represent the half rotation (ϕ) of the crack section, see Figure 3.4, and are the data from the inclinometers that were mounted to the side of the pipe, 559 mm (22 inches) either side of the crack plane. From Figure 3.4 it can be seen that the maximum moment for this experiment was 2189 kN-m (19,380,000 in-lbs).

Experiment 1.2.3.16 28-inch-Diameter Stainless Steel SAW Surface Crack Experiment

The 28-inch-diameter stainless steel SAW surface-cracked pipe experiment was conducted at Battelle's large-pipe test facility at West Jefferson, Ohio. The test pipe was a section of the same pipe used in the 28-inch-diameter stainless steel SAW through-wall crack experiment (1.1.1.23). The pipe material identification number is DP2-A51. The pipe base material is TP316L stainless steel. The test weld was fabricated at a local ASME Nuclear Code-certified welding shop using the same procedures, wire, and flux as used for the test weld for Experiment 1.1.1.23. The welding procedures for these welds are given in Appendix A, as obtained from General Electric. The material properties for the pipe material and weld metal are given in Table 3.3. The results of the chemical analyses of the stainless steel base metal and weld materials are given in Table 3.4. In this experiment it was decided to leave the weld crown on the outside surface in place, whereas for the stainless steel SAW through-wall crack experiment the weld crown was ground off.

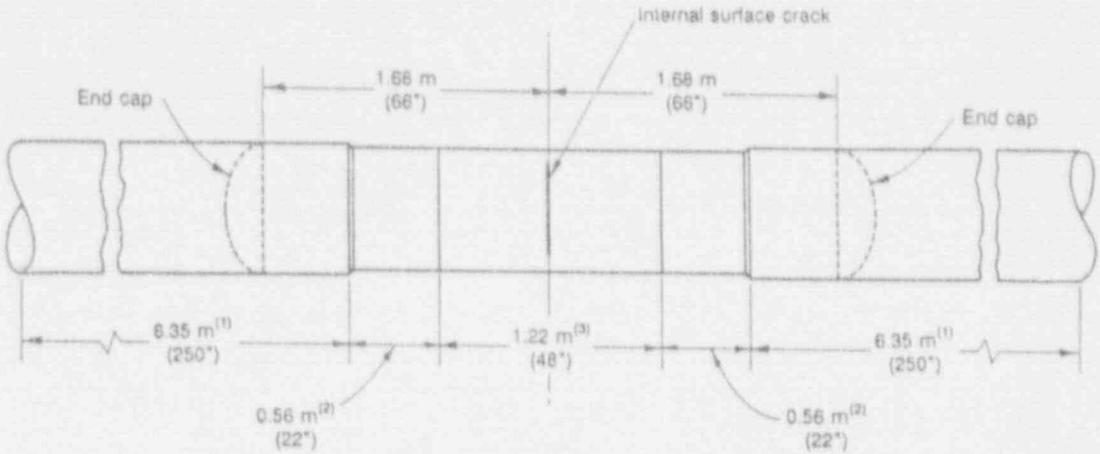

	[1]	[2]	[3]
Outside Diameter	762 mm (30")	711 mm (28")	711 mm (28")
Wall Thickness	38.1 mm (1.5")	25.3 mm (0.995")	24.0 mm (0.945")
Ident. No.	IP-F5	DP2-F91	DP2-F26

(a) Details of test specimen

DRB/1.2.3.15/F2

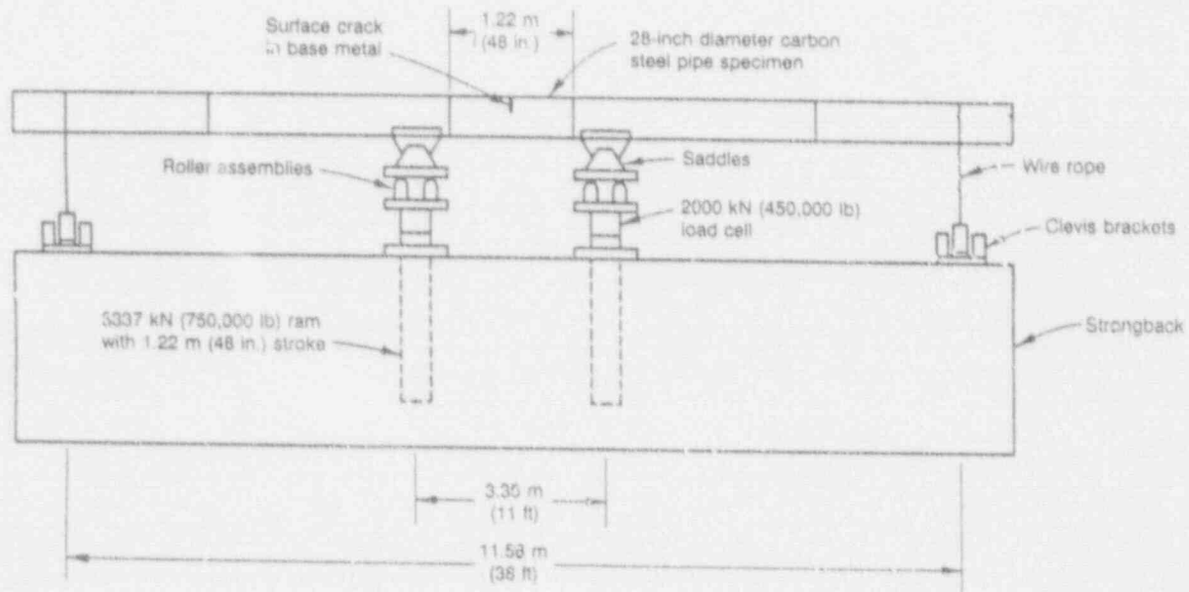

(b) Schematic of test apparatus

SC-SA-5/92-F3.2

Figure 3.2 Schematic and dimensions of Experiment 1.2.3.15

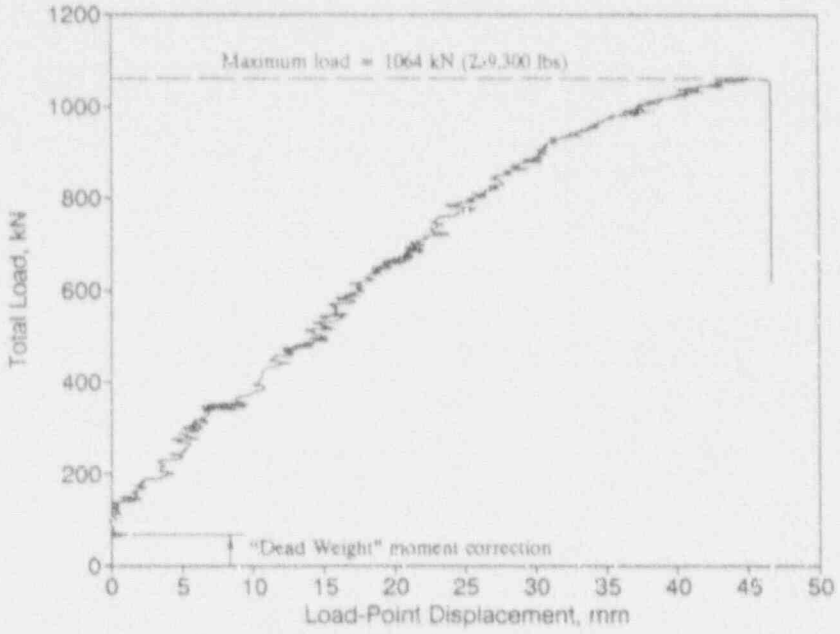

Figure 3.3 Total applied load versus load-line displacement for Experiment 1.2.3.15

SC-SA-5/92-F3.3

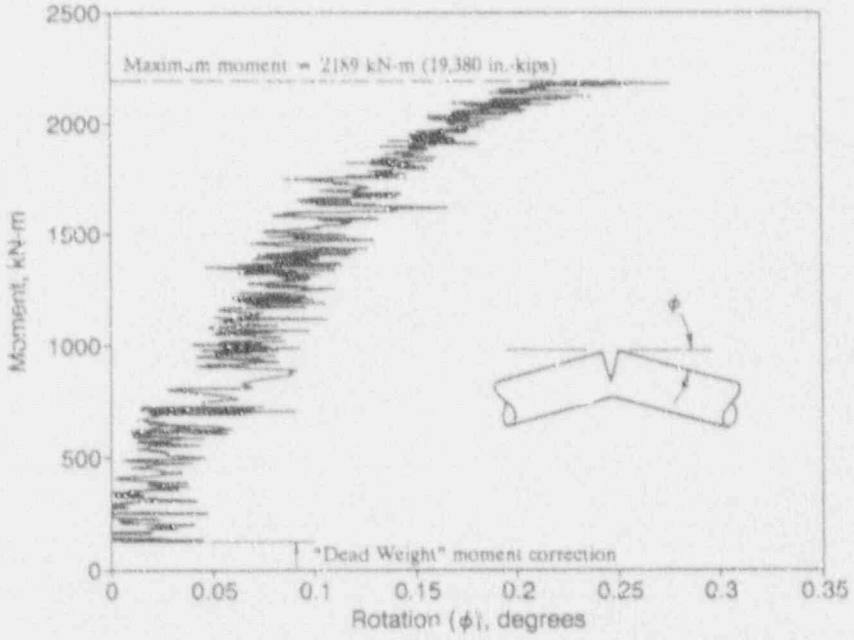

Figure 3.4 Moment versus half rotation (ϕ) based on the inclinometers for Experiment 1.2.3.15

SC-SA-5/92-F3.4

Table 3.3 Material property data for 28-inch-diameter stainless steel base metal and SAW materials at 288 C (550 F)

	Base Metal (DP2-A51)	Weld Metal (DP2-A45W2)
Yield Strength, MPa (ksi)	143 (20.8)	366 (53.0)
Ultimate Strength, MPa (ksi)	427 (62.0)	503 (72.9)
Reduction of Area, percent	70.8	58.5
J_i, kJ/m^2 (in-lb/in^2)	NA[a]	59.5 (341)[b]
dJ/da, MJ/m^3 (in-lb/in^3)	NA[a]	160 (23,250)[b]

(a) NA - Not available.
(b) Average of two 20 percent side-groove specimens.

Table 3.4 Chemical composition of stainless steel submerged-arc weld (DP2-A45W2) and pipe (DP2-A51) materials

	Percent by Weight of Indicated Element		
Element	Weld Metal (DP2-A45W2)	Base Metal (DP2-A51)	ASTM A240 Specification for TP316L
C	0.03	0.021	0.030 max
Mn	2.26	1.8	2.00 max
P	0.032	0.031	0.045 max
S	0.010	0.018	0.030 max
Si	0.89	0.55	0.75 max
Cu	0.26	0.2	(a)
Sn	0.010	0.008	(a)
Ni	9.6	9.8[b]	10.00-14.00
Cr	19.7	17.3	16.00-18.00
Mo	0.10	2.1	2.00-3.00
Al	0.015	0.01	(a)
V	0.070	0.08	(a)
Nb	0.012	0.013	(a)
Zr	0.015	0.001	(a)
Ti	0.006	0.004	(a)
B	0.0008	0.0002	(a)
Ca	0.0008	0.0024	(a)
Co	0.13	0.12	(a)
W	0.0	0.0	(a)
Se	0.00	0.00	(a)
N	N.D.[c]	0.076	0.10 max

(a) Not specified.
(b) Did not meet specification.
(c) N.D. - Not determined.

The initial flaw size was 50 percent of the pipe wall thickness in depth and 25 percent of the pipe circumference in length. The flaw was introduced into the inside pipe surface using electric-discharge-machining (EDM) techniques. The machined flaw was not fatigue precracked. The test temperature was 288 C (550 F). The loading conditions were quasi-static, monotonically increasing 4-point bending with a constant internal pipe pressure of 10.14 MPa (1.47 ksi). This internal pipe pressure resulted in an axial membrane stress (P_m) of 59.6 MPa (8.65 ksi), which is 62.0 percent of the design stress (S_m) for this material at 288 C (550 F). The pressurizing medium was subcooled water.

Figure 3.5 is a plot of the total applied load versus load-line displacement for this experiment. The total applied load values in Figure 3.5 include the equivalent applied load at the actuator of 62.2 kN (13,975 pounds) from the distributed dead-weight load contribution due to the weight of the pipe, water, and wire ropes at the end restraints. From this figure it can be seen that the maximum applied load for this experiment was 1018 kN (228,900 pounds).

Figure 3.6 is a plot of the crack section moment versus the crack section rotation data from this experiment. The rotation data represent the half rotation (ϕ) of the crack section, see Figure 3.6, and are the data from the inclinometers that were mounted to the side of the pipe, 559 mm (22 inches) either side of the crack plane. From Figure 3.6 it can be seen that the maximum moment for this experiment was 2094 kN-m (18,530,000 in-lbs).

Comparison of Experimental Results with IWB-3640 and IWB-3650 Predictions for Large-Diameter Surface-Cracked Pipe Experiments

Table 3.5 shows a comparison of the experimental maximum load values from the 28-inch-diameter A515 Grade 60 carbon steel base metal (1.2.3.15) and 28-inch-diameter TP316L stainless steel SAW (1.2.3.16) surface-cracked pipe experiments with predictions from the in-service flaw assessment criteria in Section XI of the ASME Code, i.e., IWB-3640 and IWB-3650. From Table 3.5 it can be seen that both assessment criteria underpredicted the experimental maximum moments. The IWB-3640 predicted or "allowable" stress for the stainless steel SAW experiment (1.2.3.16) was 75 percent of the maximum experimental stress, while the IWB-3650 predicted stress for the carbon steel base metal experiment (1.2.3.15) was only 40 percent of the maximum experimental stress. The extreme underprediction of the carbon steel results is consistent with past findings (Refs. 3.2 and 3.5).

3.3.4 Subtask 2.4 Analysis of Short Surface Cracks in Pipes

3.3.4.1 Objective

The objective of this subtask is to develop, improve, and verify the engineering analyses for short circumferential surface-cracked large-diameter pipe where elastic-plastic fracture is expected.

3.3.4.2 Rationale

The short surface-cracked (SC) pipe analysis improvements are aimed at assessing and improving the ASME Section XI flaw evaluation criteria (Refs. 3.8 and 3.9).

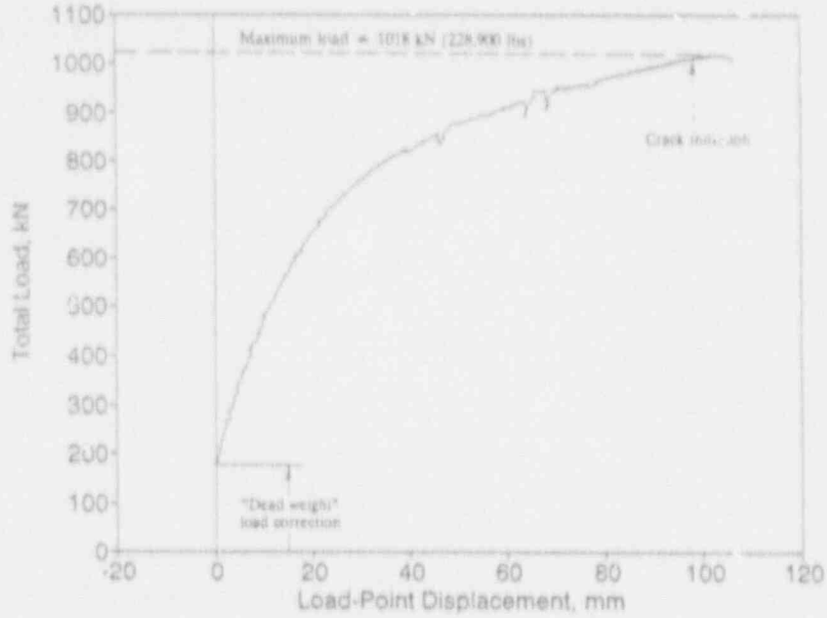

Figure 3.5 Total load versus load-line displacement for Experiment 1.2.3.16 28-inch-diameter stainless steel TP316L SAW experiment with crack parameters (d/t = 0.5, θ/π = 0.25)

SC-SA-5/92-F3.5

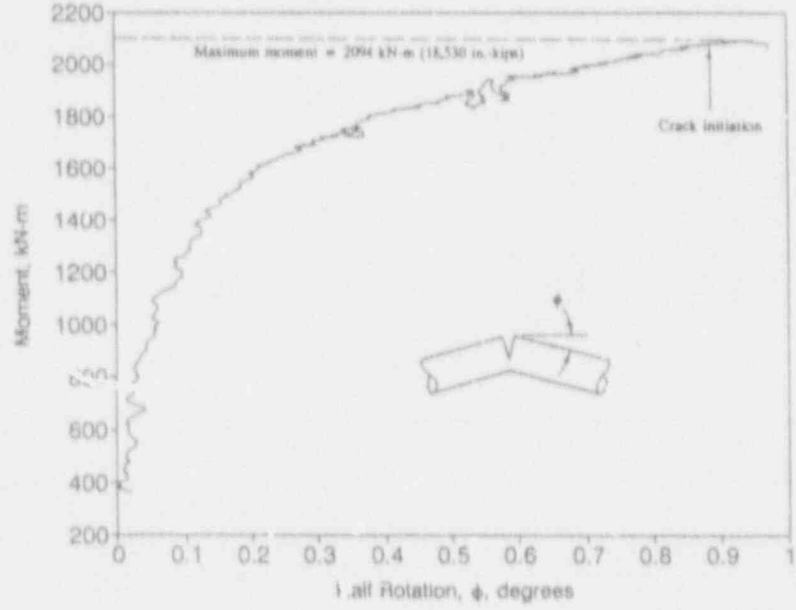

Figure 3.6 Moment versus half rotation (ϕ) based on the inclinometers for Experiment 1.2.3.16

SC-SA-5/92-F3.6

Table 3.5 Comparison of experimental results from 28-inch-diameter carbon steel base metal (1.2.3.15) and 28-inch-diameter stainless steel SAW (1.2.3.16) surface-cracked pipe experiments with predictions from in-service flaw assessment criteria in Section XI of the ASME Code

Expt. No.	Material	OD, mm	t, mm	$2c/\pi D_m$	d/t	S_m, MPa	σ_f,[a] MPa	Maximum Moment, kN-m	Pressure, MPa	$(\sigma_{exp}+\sigma_a)/(\sigma_{Code}+\sigma_a)$
1.2.3.15	A515 Grade 60	711	22.7	0.25	0.5	114	274	2189	9.56	2.476
1.2.3.16	TP316L SAW	711	30.2	0.25	0.5	96.2	289	2094	10.14	1.326

(a) $\sigma_f = 2.4\ S_m$ for ferritic steels and $3\ S_m$ for austenitic steels.

3.3.4.3 Approach

The five activities in this subtask are:

Activity 2.4.1	Uncracked pipe analysis
Activity 2.4.2	Improve SC.TNP and SC.TKP analyses
Activity 2.4.3	Compare improved limit-load solutions with short surface-cracked small-diameter pipe data
Activity 2.4.4	Analyze large-diameter surface-cracked pipe test data
Activity 2.4.5	Evaluate procedures in J-estimation schemes for surface cracks in welds.
Activity 2.4.6	Extend SC.TNP and SC.TKP for external surface-crack geometries under combined loading.

Only Activities 2.4.1, 2.4.3, and 2.4.6 were active during this reporting period.

Activity 2.4.1 Uncracked Pipe Analysis

During May, 1991, we met with Dr. Brickstad of Sweden while he attended the IPIRG meeting. Dr. Brickstad brought copies of a Swedish report by Dr. H. Oberg showing that for a stainless steel uncracked bend-bar specimen, the analytical method underpredicted the experimental results by more than the investigators thought possible. This is consistent with our uncracked pipe analyses of the JAERI stainless steel uncracked pipe experiments, as well as many of the stainless steel through-wall-cracked pipe analyses. We therefore conducted an FEM analysis of this simple uncracked bend-bar specimen for comparison with the Swedish analytical result.

Two sets of analyses were completed. The first involved an in-house research code (FLIP) used at Battelle that allows a power-law representation of the stress strain behavior. The constitutive model was described by

$$\varepsilon = \alpha (\sigma)^N \qquad (3\text{-}1)$$

where

$\alpha = 4.65 \times 10^{-6}$ for $0 < \sigma \leq 242.5$ MPa
$\alpha = 7.14 \times 10^{-15}$ for $\sigma > 242.5$ MPa

and

$N = 1.019$ for $0 < \sigma \leq 242.5$ MPa
$n = 4.715$ for $\sigma > 242.5$ MPa

The data and the power-law fit are shown in Figure 3.7. As seen, this representation for the stress-strain behavior is excellent. The FEM results using this representation under plane stress assumptions were identical to the analytical predictions using elastic-plastic beam theory (Figure 3.8) of Dr. H. Oberg in Sweden.

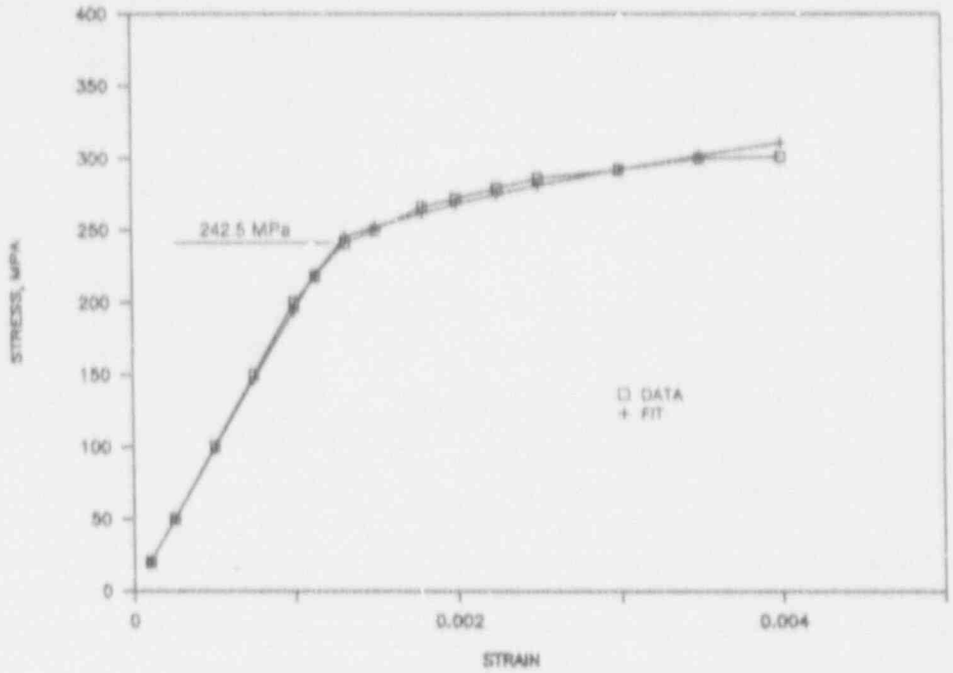

Figure 3.7 Stress-strain data for the Swedish uncracked stainless steel four-point bend-bar with a power-law fit

SC-SA-5/92-F3.7

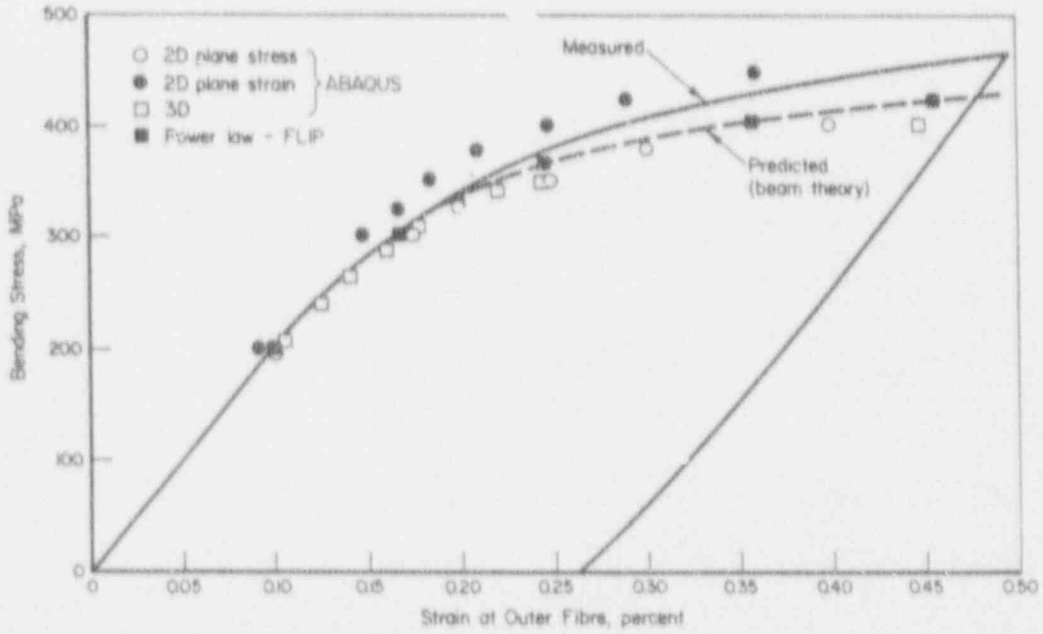

Figure 3.8 Comparison of experimental data and beam theory results with FEM prediction using ABAQUS (2D plane stress/strain 3D) and FLIP (power law) Code

SC-SA-5/92-F3.8

The second set of FEM calculations was conducted using incremental theory of plasticity in ABAQUS. Three cases were used: (1) 2D plane stress, (2) 2D plane strain, and (3) complete 3D models. These results are also shown in Figure 3.8. As expected, the experimentally measured values fall between the predictions of plane stress and plane strain. The results using the 3D model were expected to be in direct agreement with experimental observations, but were found to be almost identical to those for the plane stress model.

This discrepancy between experimental results and analytical/GE predictions on uncracked stainless steel specimens has not been resolved. A more detailed study of this problem and its implications in predicting the behavior of uncracked pipe (and hence cracked pipe) will be undertaken in the IPIRG-2 Program.

Activity 2.4.3 Compare improved limit-load solutions with short surface-cracked small-diameter pipe data

The maximum moment for the 6-inch-diameter Schedule XXS pipe Experiment 1.2.1.21 was 1.1×10^6 in-lbs. This value of the moment includes kinematic correction. Figure 3.9 shows a plot of the maximum moment predicted for this pipe geometry and material properties using the Net-Section-Collapse analysis for various flaw geometries. Also indicated are buckling loads calculated by ABAQUS and by Battelle's (Mesloh's) closed form buckling analysis, Ref. 3.10. The experimental value for the maximum moment is about 22 percent less than that predicted by the Net-

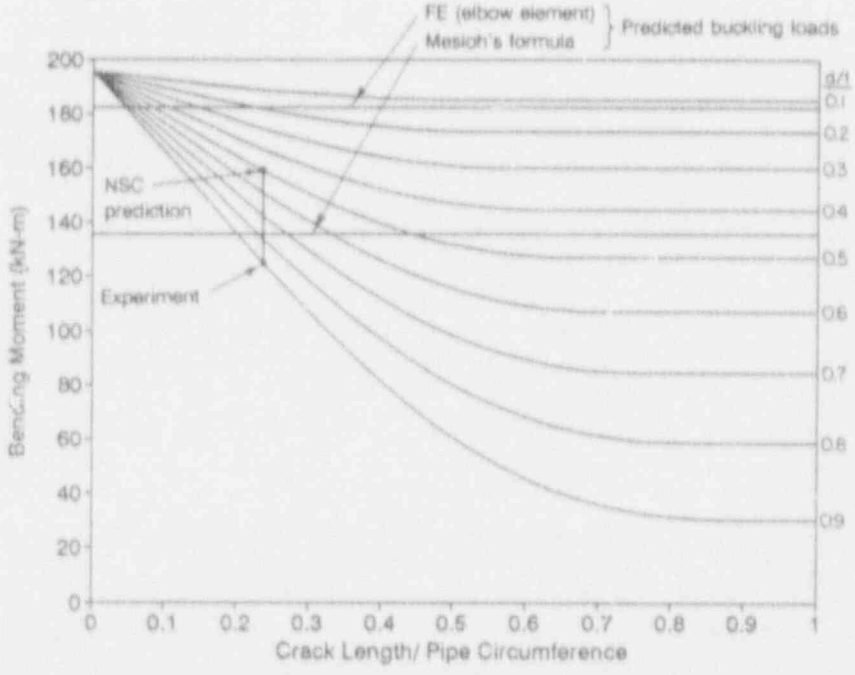

Figure 3.9 Comparison of experimental data with Net-Section-Collapse predictions for 6-inch XXS pipe (Experiment No. 1.2.1.21) [$\sigma_f = (\sigma_f + \sigma_u)/2$]

SC-SA-5/92-F3.9

Section-Collapse analysis. Interestingly in the 6-inch-diameter Schedule 40, the pipe started to buckle and a maximum load was achieved prior to the crack initiation, but the Schedule XXS pipe's maximum load corresponded to the start of crack growth.

To assess the differences observed between the experimental and Net-Section-Collapse analysis, a comparison of the ratio of the maximum experimental stress to the predicted Net-Section-Collapse analysis stress as a function of the pipe R_m/t ratio for a number of surface-cracked pipe experiments was made. This was done to also determine the effects of short versus long surface cracks on the net-section-collapse analysis, see Figure 3.10. Most of the data points in Figure 3.10 are for experiments from the Degraded Piping Program, Ref. 3.11. Figure 3.10 only includes the data from those surface-crack pipe experiments for which limit-load failure was expected rather than EPFM failure. This occurs when the dimensionless plastic-zone parameter (DPZP) is greater than 0.2. As can be seen in Figure 3.11, if the DPZP is greater than 0.2 for surface-cracked pipe, then fully plastic conditions should be expected. The line drawn in Figure 3.10 represents a least squares fit of the data. Also included in Figure 3.10 are the data points for the two 6-inch-nominal-diameter stainless steel short surface-cracked pipe experiments conducted as part of this program (1.2.1.21 and 1.2.1.22) and two 4-inch-nominal-diameter stainless steel pipe experiments with relatively short surface cracks conducted as part of a previous Battelle/EPRI program, Experiments 5S and 6S (Ref. 3.6). In examining Figure 3.10 it can be seen that the data from these four relatively small surface-cracked pipe experiments agree fairly well with the data from the larger surface-cracked pipe experiments from the Degraded Piping Program. From these data, it appears that the effect of crack size on the ovalization correction factor for limit-load failures for surface-cracked pipe is minor.

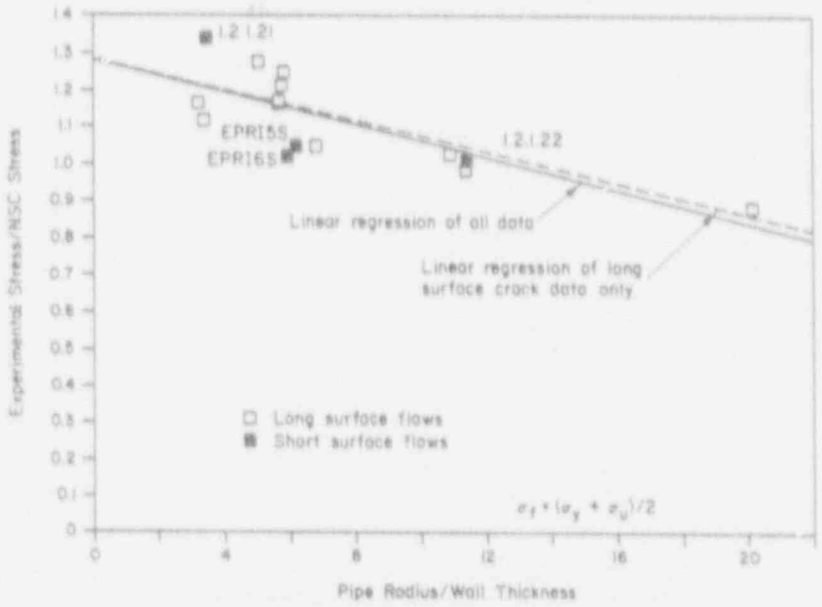

Figure 3.10 Plot of the ratio of the maximum experimental stress to the predicted net-section-collapse stress as a function of the pipe R/t ratio for a series of surface-cracked pipe experiments for which the dimensionless plastic zone parameter is greater than 0.2

SC-SA-7/91-F3.9

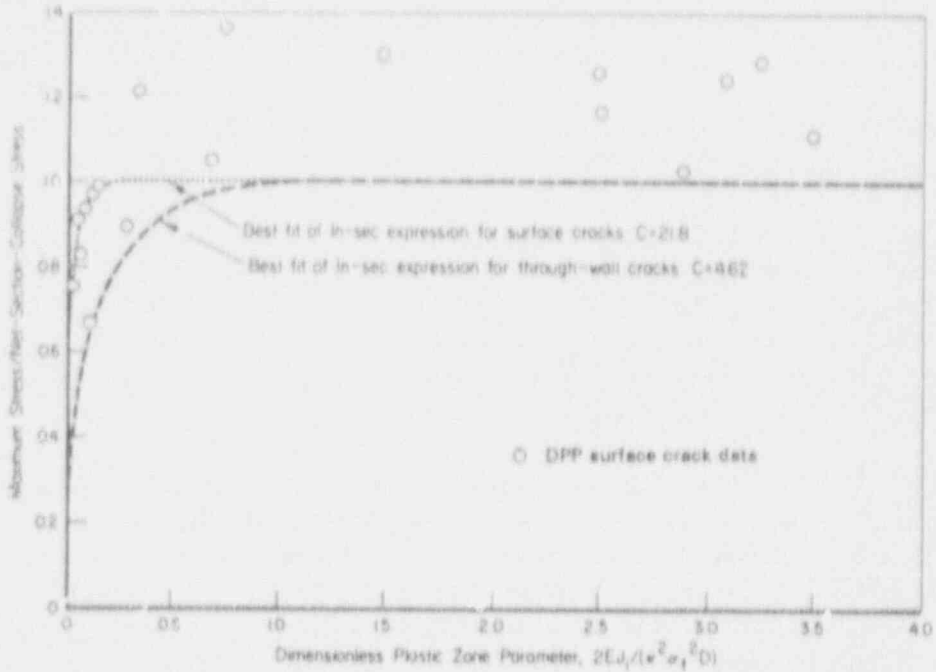

Figure 3.11 Analysis showing that if dimensionless plastic zone parameter is greater than 0.2 then fully plastic conditions should exist for surface-cracked pipe

SC-SA-5/92-F3.11

Consequently, if deemed appropriate, one generalized ovalization correction factor for limit-load failures for all crack sizes could be incorporated into a code in-service flaw-assessment criterion such as found in Section XI of the ASME Code, or limits on the applicability of the net-section-collapse analysis as of function of κ_m/t can be established.

Activity 2.4.6 Extend SC.TNP and SC.TKP for External Surface-Crack Geometries under Combined Loading

A copy of the DTRC report (Ref. 3.12) on J versus crack growth per cycle, da/dN, for low cycle fatigue was reviewed with the application to low cycle fatigue predictions in mind. The main concern is the compatibility of the Dowling operational definition of J with the J values in the SC.TNP and SC.TKP solutions.

The DTRC report uses an operational definition of J developed by Dowling. This methodology makes laboratory specimen low cycle fatigue crack growth data consistent with high cycle fatigue data. The difficulty comes when one wants to use this relationship in a structural application where there are negative load ratios. In this case, the Dowling definition of J is inconsistent with the deformation or incremental plasticity definition of J used in structural analysis.

Dowling's definition of J integrates the area under the load-displacement curve, but for negative loading the area includes loads corresponding to crack closure. In the DTRC report, the crack closure load was found to occur at negative loads that were about 30 percent of the applied positive load. This additional area increases the Dowling operational definition of J relative to a deformation plasticity J. The difficulty is that the J calculated from elastic-plastic fracture mechanics analyses (deformation J) for the structure, such as the SC.TNP analysis (Ref. 3.11) developed by Battelle for the NRC for circumferentially surface-cracked piping, does not recognize the negative loading contributions to J. Here the applied J is proportional to the applied load, P, i.e.,

$$J = J_e + J_p \tag{3-2}$$

$$J_e \propto P^2 \tag{3-3}$$

$$J_p \propto P^{n+1} \tag{3-4}$$

To integrate the Dowling approach for determining low cycle fatigue crack growth in laboratory specimens with structural predictions requires modification of the J-estimation scheme analysis. Two possible methods were considered: the SC.TNP and η-factor approach, and a simplified modification to the SC.TNP analysis.

Combined SC.TNP and η-factor Approach

This approach can be divided into six steps.

Step 1 is to obtain the laboratory specimen operational J versus da/dN results, as DTRC has done.

Step 2 involves having an estimation scheme to predict the moment-rotation or load-displacement relation for the cracked structure. The SC.TNP analysis is such an analysis for circumferentially surface-cracked pipe. Several analyses exist for circumferential through-wall-cracked pipe, e.g., GE/EPRI, LBB.NRC, LBB.ENG, etc. in Reference 3.13.

Step 3 involves making an assumption about when crack closure may occur in the structure (cracked pipe). As a first approximation, assume it occurs at 30 percent of the applied tension load, although some percentage of the maximum load for that size crack may be more appropriate. The IPIRG R=-1 TWC pipe test data (Ref. 3.14) may be useful in defining the closure loads for through-wall-cracked pipe in reverse loading. It is anticipated that the crack closure behavior may be different for a through-wall crack than a surface crack.

Step 4 involves calculation of the operational J from the closure load to the peak load, see Figure 3.12. For a cracked pipe, an η-factor analysis is now needed. Pan (Ref. 3.15) developed such an analysis for circumferentially surface-cracked pipe, and there are other such analyses for circumferentially through-wall-cracked pipe, Ref. 3.13.

Step 5 involves incrementing the crack using the pipe operational J value and the da/dN value from the specimen operational J data from Step 1.

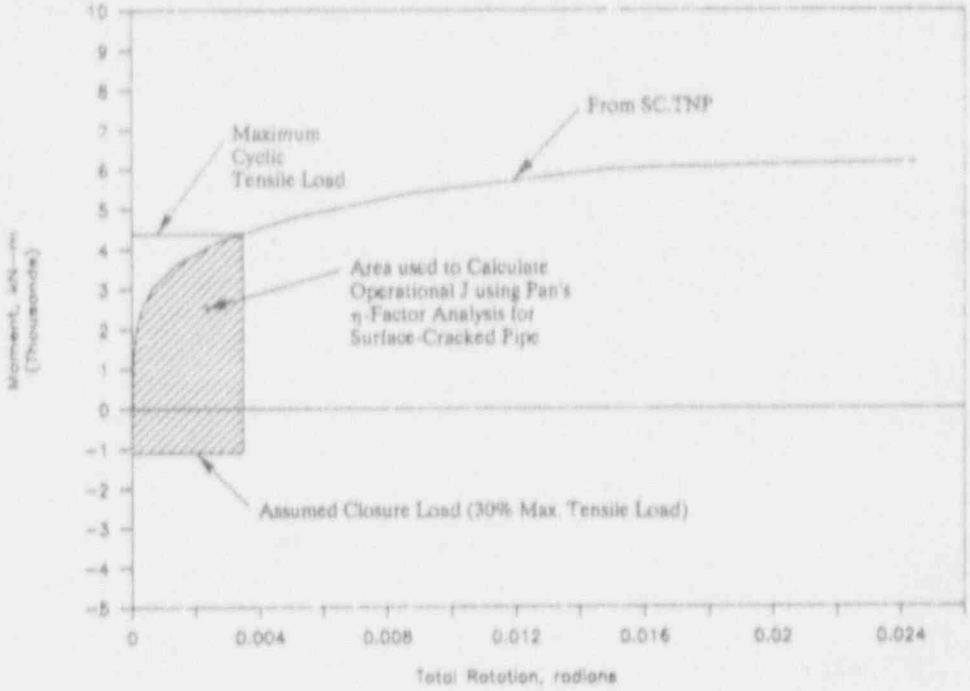

Figure 3.12 Schematic of moment-rotation relation for a surface-cracked pipe. Shaded area used for determination of Dowling operational J for low cycle fatigue analysis. Combined SC.TNP and η-factor analyses

SC-M-4/91-F7

Step 6 involves a recalculation of the moment-rotation or load-displacement response for the incremented crack using the methods in Step 2. A potential problem is in accounting for any cyclic hardening or softening in predicting the moment-rotation response of the structure for subsequent cycles beyond crack initiation. This is a difficult problem even in a full blown finite element analysis.

Simplified Modification to SC.TNP Analysis

Another approach would be to simply add the closure load ($P_{closure}$) to the applied load (P) directly in the SC.TNP analysis, i.e.,

$$J = J_e + J_p \tag{3-5}$$

$$J_e \propto (P + P_{closure})^2 \tag{3-6}$$

$$J_p \propto (P + P_{closure})^{n+1} \tag{3-7}$$

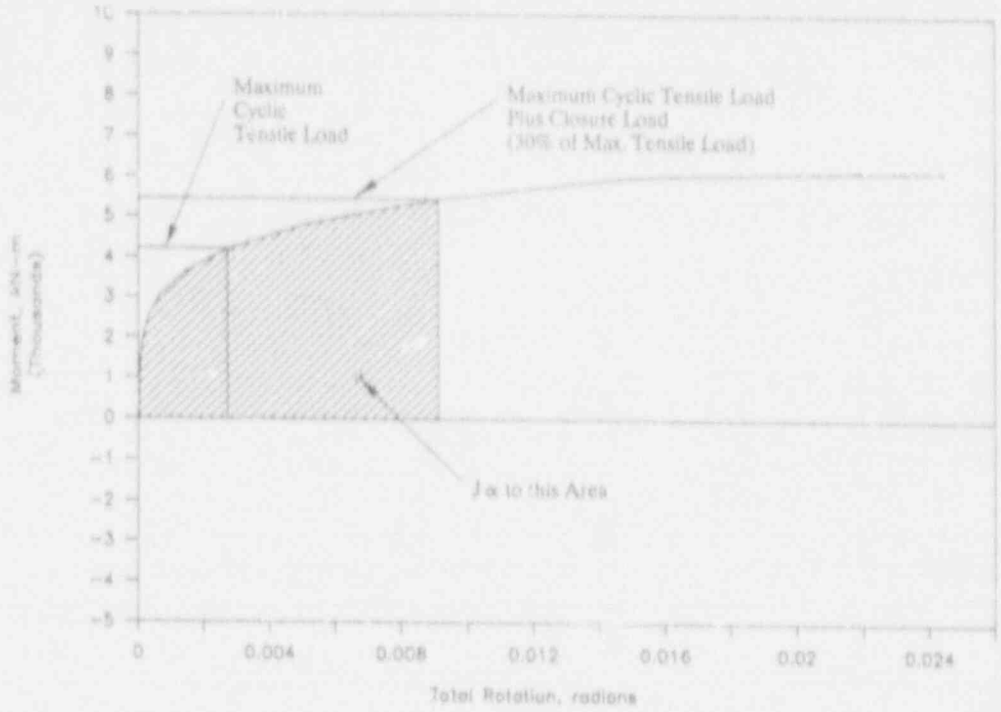

Figure 3.13 Schematic of moment-rotation relation for a surface-cracked pipe. Shaded area used for determination of Dowling operational J for low cycle fatigue analysis. SC.TNP analyses using closure loads as an additive load

SC-SA-5/92-F3.13

Although this is a simpler method, the addition of the closure load to the tension load may give significantly different results. This is illustrated in Figure 3.13, where the same tension and closure loads as in Figure 3.12 are used. In comparing the two figures, one can see that the area (and hence, J) in Figure 3.13 is almost twice as large in Figure 3.12. Hence, adding the closure load as a tension load in the SC.TNP analysis to calculate an operational J would be inconsistent with the Dowling general procedures and would be very conservative.

We believe that, in the future, it may be desirable to include the potential low cycle fatigue crack growth from a seismic event in either LBB or in-service inspection criteria, i.e., ASME Section XI IWB-3640 and IWB-3650. It is suspected that, for a through-wall crack used in LBB analyses, the low cycle fatigue growth is not very significant in affecting the final failure loads. The crack growth for a surface crack, however, may have greater effect on the final failure loads. Past EPRI/GE (Ref. 3.16), JAERI (Ref. 3.17), and STA (Ref. 3.18) cyclic pipe experiments show that the cyclic loads caused failures well below net-section-collapse loads using the initial flaw size.

3.4 Plans for Next Year of the Program

The efforts described below will be undertaken during the next year of the program.

3.4.1 Subtask 2.1 Material Characterization for Surface-Cracked Pipe Experiments

During the next year, it is expected that characterization of the replacement 16-inch-diameter austenitic stainless steel pipe from Savannah River will be completed. In addition, the carbon steel submerged-arc weld in 25.4-mm (1-inch)-thick plate will be fabricated and material characterization tests completed.

3.4.2 Subtask 2.2 Smaller Diameter Pipe Fracture Experiments in Pure Bending for Limit-Load Ovalization Correction

The 16-inch-diameter Schedule 30 stainless steel surface-cracked pipe experiment will be conducted in the next year.

3.4.3 Subtask 2.3 Large-Diameter Surface-Cracked Pipe Fracture Experiments Under Combined Bending and Tension (Pressure)

Specimen preparation for the 36-inch-diameter carbon steel (cold-leg pipe) SAW surface-cracked pipe experiment (1.2.3.17) will begin. The test weld for this experiment will be fabricated at the same time as the test weld for the 24-inch-diameter carbon steel SAW through-wall crack experiment (1.1.1.24). The weld procedures for both experiments will be the same. Experiment 1.2.3.17 cannot be conducted until the upgrade of the large-pipe test facility is completed in Subtask 1.2.

3.4.4 Subtask 2.4 Analysis of Short Surface Cracks in Pipes

For Activity 2.4.1, it has been proposed that the discrepancy between the experimental data and finite element predictions for the uncracked pipe will be studied as part of IPIRG-2. These results will be incorporated into the conclusions of this activity. This subtask will be put on hold during the next reporting period. Some literature survey for the LBB.ENG2 method for the surface crack analysis may be conducted. Once the TWC analyses work in Subtask 1.4 is completed this subtask will be resumed.

3.5 References

3.1 Hiser, A. L. and Callahan, G. M., "A User's Guide to the NRC's Piping Fracture Mechanics Database (PIFRAC)," NUREG/CR-4894, May 1987.

3.2 Wilkowski, G. M. and others, "Degraded Piping Program - Phase II," Summary of Technical Results and Their Significance to Leak-Before-Break and In-Service Flaw Acceptance Criteria, March 1984-January 1989, by Battelle Columbus Division, NUREG/CR-4082, Vol. 8, March 1989.

3.3 Wilkowski, G. M. and others, "Degraded Piping Program - Phase II," Semiannual Report, April 1985-September 1985, by Battelle Columbus Division, NUREG/CR-4082, Vol. 3, March 1986.

3.4 Wilkowski, G. M. and others, "Short Cracks in Piping and Pipe Welds," by Battelle, NUREG/CR-4599, Vol. 1, No. 2, March 1992.

3.5 Schmiot, R. A., Wilkowski, G. M., and Mayfield, M. E., "The International Piping Integrity Research Group (IPIRG) Program - An Overview," SMiRT-11, Paper G12/1, August 1991.

3.6 Kanninen, M. F. and others, "Instability Predictions for Circumferentially Cracked Type 304 Stainless Steel Pipes under Dynamic Loadings," EPRI Report NP-2347, April 1982.

3.7 Noda, H., Kashima, K., Gotoh, N., Hata, H., Yamamoto, Y., and Kashida, K., "Fracture Criterion of Japanese Large-Diameter Carbon Steel Cracked Pipe," SMiRT-11, Paper SDO-04(FG)/1, pp. 383-394, August 1991.

3.8 Case N-436, "Alternative Methods for Evaluation of Flaws in Austenitic Piping," ASME Boiler and Pressure Vessel Code, Section XI, Division 1, pp. 763-765, May 14, 1986.

3.9 American Society of Mechanical Engineers Boiler and Pressure Vessel Code, Edition July 1989, see Code Case N-463.

3.10 Mesloh, R. E., Sorenson, J. E., and Atterbury, T. J., "Buckling Offshore Pipelines," Gas Magazine, pp. 40-43, July 1973.

3.11 Scott, P. M. and Ahmad, J., "Experimental and Analytical Assessment of Circumferentially Surface-Cracked Pipes under Bending," NUREG/CR-4877, April 1987.

3.12 Joyce, J. A. and Hackett, E. M., "Elastic-Plastic Characterization of a Cast Stainless Steel Pipe Elbow Material," NUREG/CR-5774, January 1992.

3.13 Brust, F. W., "Approximate Methods for Fracture Analyses of Through-Wall-Cracked Pipes," NUREG/CR-4853, February 1987.

3.14 Wilkowski, G. M., Vieth, P., Kramer, G., Marschall, C., and Landow, M., "Results of Separate-Effects Pipe Fracture Experiment," Post SMiRT-11 Conference #2, Paper 4.2, August 1991.

3.15 Pan, J., "Some Considerations on Estimation of Energy Release Rates for Circumferentially Cracked Pipe," Journal of Pressure Vessel Technology, Vol. 106, pp. 391-398, November 1984.

3.16 Hale, D. A. and others, "The Growth and Stability of Stress Corrosion Cracked in Large-Diameter BWR Piping," EPRI Report NP-2472 Volume 2, see Appendices B and C, July 1982.

3.17 Murakami, E. and others, "Crack Growth of Nuclear Piping under Dynamic Loading," ASME PVP special publication PVP 167, pp. 115-120, July 1989.

3.18 Ogawa, N., "Experimental Study of Piping Stability under Strong Earthquake," ASME PVP special publication PVP 150, pp. 69-80, July 1988.

4. TASK 3 BIMETALLIC WELD CRACK EVALUATIONS

This task was not active this fiscal year; hence there is no progress to report.

5. TASK 4 DYNAMIC STRAIN AGING

5.1 Task Objective

The objective of this task is to evaluate and predict the effects of crack instabilities, believed to be due to dynamic strain aging (DSA), on the fracture behavior of pipe. Specific objectives are to establish a simple screening criterion to predict which ferritic steels may be susceptible to unstable crack jumps, and to evaluate the ability of current J-based analysis methodologies to assess the effect of unstable crack jumps on the fracture behavior of ferritic steel pipe. If necessary, alternative procedures for predicting pipe behavior in the presence of crack jumps will be derived.

5.2 Task Rationale

The methodology developed here will be applicable to both LBB and in-service flaw evaluations. It will also be valuable for selection of materials for future advanced reactor designs.

5.3 Task Approach

The four subtasks and two optional subtasks in this task are:

Subtask 4.1	Establish a screening criterion to predict unstable crack jumps in ferritic steels
Subtask 4.2	Evaluate procedures for characterizing fracture resistance during crack jumps in laboratory specimens
Subtask 4.3	Assess current procedures for predicting crack jump magnitude in pipes
Subtask 4.4	Prepare interim and topical reports on dynamic-strain-aging induced crack instabilities in ferritic nuclear piping steels at LWR temperatures
Subtask 4.5	(Optional Subtask) Refine procedures for characterizing fracture resistance during crack jumps in laboratory specimens
Subtask 4.6	(Optional Subtask) Refine procedures for predicting crack jump magnitude in pipes.

Significant efforts were made only in Subtask 4.1 during the past reporting period.

5.3.1 Background

The approach in Task 4 is based on experimental data obtained in the Degraded Piping Program (Ref. 5.1). In several pipe steels tested at 288 C (550 F), both in laboratory and pipe specimens, crack instabilities were observed, interspersed between periods of stable, ductile tearing. These instabilities have been assumed to be related to a steel's susceptibility to DSA (Ref. 5.2). DSA is a pinning of dislocation movement by free nitrogen or carbon atoms in the crystallographic structure. This increases the flow properties and reduces the ductility. However, no firm proof of that tie-in between

DSA and crack instabilities presently exists. Information about crack instabilities is lacking in other areas as well. Some questions include:

(1) How large must a crack instability be to significantly affect flawed-pipe safety analyses?
(2) Are J-based analysis procedures valid when crack instabilities occur?
(3) Are there simple ways to predict the occurrence and severity of crack instabilities in a particular steel?
(4) Is there a correlation between crack jumps in C(T) specimens and pipe specimens?
(5) How reproducible is the phenomenon?
(6) Do the fracture surfaces or microstructures associated with crack instabilities have any unusual features?

The significance of crack instabilities in flawed-pipe safety analyses has already been demonstrated in at least one 288 C (550 F) pipe test conducted at David Taylor Research Center. In this experiment, a crack jump of approximately one-fourth of the pipe circumference was observed for a through-wall circumferential crack. Such an instability in a nuclear plant could lead to a large loss of cooling water. Therefore, it is important in this program to determine how to predict the occurrence and magnitude of crack instabilities. Subtask 4.3 represents an attempt to address these issues in a logical manner.

A limited number of laboratory experiments are being conducted in Subtask 4.1. The results of those experiments, when combined with existing data, will be used to establish a direct link between crack instabilities and DSA. If that link can be established, then it should be possible to assess a steel's propensity for crack jumps by conducting a few tensile tests or, even better, a few hardness tests. Hardness tests would be especially attractive in nondestructive, in-plant testing of pipes for which no archival material exists. Within Subtask 4.1, data also are being obtained on correlating crack jumps in C(T) and pipe specimens, on determining the reproducibility of crack jumps in replicate tests, and on determining the presence of any unusual fractographic or microstructural features in specimens that display crack instabilities.

The activities involved in developing the screening criteria for dynamic strain aging in Subtask 4.1 will also determine what triggers dynamic crack jumps. From a global sense, the dynamic crack jumps could be triggered by being at the proper temperature and strain rate and by having a material sufficiently susceptible to dynamic strain aging. The latter can be determined by the screening criteria, ideally with a simple test such as the hardness ratio at high temperature to room temperature. From a microstructural viewpoint, metallographic investigations of past fracture surfaces from Degraded Piping Program test specimens at the points of initiation and arrest of the crack jumps may shed further light on how to predict the start of an instability, or better yet, how to manufacture steels that would not produce instabilities for future plant construction.

In addition to the work in Subtask 4.1, efforts will be undertaken in Subtask 4.2 to modify analytical procedures for calculating fracture resistance in laboratory specimens during a crack instability. Included in this activity will be an evaluation of a J-resistance curve approach, an evaluation of alternate measures of fracture resistance (CTOA, for example), and an assessment of plausible

analysis methods to account for crack jumps. The results of Subtask 4.2 will provide information on the variability of the toughness during the instability event and at the end of the crack jump.

The results of Subtask 4.2 will then be used in Subtask 4.3 to make engineering predictions of the length of crack jumps in pipe, using several approaches. One approach will apply the NRCPIPE code (see Task) and another will use an energy balance method (Ref. 5.3). The success of these engineering approaches will be evaluated and a determination will be made as to whether improved methods should be recommended for study in optional activities. The first optional subtask is aimed at improving the analytical procedures for calculating fracture resistance during unstable cracking in laboratory specimens. The second seeks to improve the ability to analyze crack jumps in pipes.

The details of the steps to be undertaken in each of the activities are given in the following sections.

5.3.2 Subtask 4.1 Establish a Screening Criterion to Predict Unstable Crack Jumps in Ferritic Steels

The establishment of a screening criterion will involve the following efforts:

Activity 4.1.1 Conduct laboratory tests to determine correlations among tensile properties, hardness, DSA, and the occurrence of crack instabilities in both C(T) specimens and pipes, and

Activity 4.1.2 Using the results of Activity 4.1.1, formulate a practical screening criterion for predicting crack instabilities in pipes.

The details of these activities are given below.

5.3.2.1 Activity 4.1.1 Conduct Laboratory Tests to Determine Correlations Among Tensile Properties, Hardness, DSA, and the Occurrence of Crack Instabilities in Both C(T) Specimens and Pipes

The objectives of this activity are to: (1) establish a direct link between crack instabilities and dynamic strain aging (DSA), thus making it possible to use tests that reveal susceptibility to DSA as screening tests for indicating susceptibility to crack instabilities, (2) examine test data and fracture specimens to correlate crack jumps in C(T) and pipe specimens, (3) investigate reproducibility of crack jumps, and (4) discern any unusual fractographic and/or microstructural features associated with crack instabilities.

Work during the last six months included the following items:

- Conduct additional elevated-temperature Brinell hardness tests on carbon-steel weld metal to determine the temperature of peak hardness
- Conduct additional compact-specimen tests at 288 C (550 F) on a carbon steel which is known to exhibit crack jumps to obtain data on the reproducibility of crack jumps in a given material; in those tests, instrumentation was employed that permitted gathering load, displacement, and crack growth data during the crack jump event

- Conduct fractographic and metallographic examinations of compact specimens to reveal possible differences in fracture mode or microstructure between slow, stable tearing and crack jumps
- Examine load-displacement records to obtain quantitative data on crack jump magnitude and frequency for both pipe tests and compact-specimen tests of carbon steels.

Conduct Additional Elevated-Temperature Brinell Hardness Tests

Earlier work (Ref. 5.4) had shown that carbon steel base metals susceptible to dynamic strain aging exhibited a peak in ultimate tensile strength at temperatures in the range of approximately 200 to 250 C (392 to 482 F). The single submerged-arc weld metal examined in that study (identified as DP2-F29W, an SAW girth weld in a 16-inch-diameter A106 Grade B carbon steel pipe) also exhibited a strength peak, but at a higher temperature of approximately 350 C (662 F). Each of the base metals also displayed a hardness peak, but at a temperature somewhat higher than that of the strength peak. The reason for the higher temperature of the hardness peak was assumed to be the result of a higher strain rate in the hardness tests compared with the tensile tests. The hardness tests on the submerged-arc weld metal also showed indications of a peak value but the range of test temperatures was not sufficiently great to reveal the temperature at which the peak occurred. Accordingly, additional hardness tests were performed on the same weld metal specimen tested previously, but nearer the bottom of the weld, to encompass a wider range of temperatures. The procedures employed for conducting the elevated-temperature Brinell hardness tests were the same as those described in our last semiannual report, Ref. 5.4.

The results of those additional hardness tests are shown in Figure 5.1, along with the earlier hardness and tensile strength results. Notice that a hardness peak was observed at a temperature of approximately 500 C (932 F), which is more than 150 degrees C (270 degrees F) higher than the ultimate-tensile-strength peak. Notice also that the two series of hardness tests did not superpose, presumably because the tests were conducted in two different regions of the weld where the chemical composition and/or the microstructure may have been slightly different.

The reasons for the higher peak-temperature for the ultimate tensile strength and hardness in the weld metal as compared with base metal are not known at this time. Part of the difference might be related to the higher silicon content (approximately 0.6 versus 0.2 percent) and higher molybdenum content (approximately 0.4 versus 0.04 percent) in the weld metal compared with the various base metals studied (Ref. 5.4). Whatever the source of the different behavior between the weld metal and the base metals, it is interesting to note that the J-R curve for the weld metal was raised significantly by increasing the loading rate in the compact-specimen tests by a factor of several thousand, whereas that for a carbon steel base metal (DP2-F30, A106 Grade B) was lowered substantially (Ref. 5.5). These limited data indicate that the effect of strain rate on the crack-growth resistance of carbon steels depends on the temperature range of the dynamic strain aging phenomenon, which itself is strain-rate dependent.

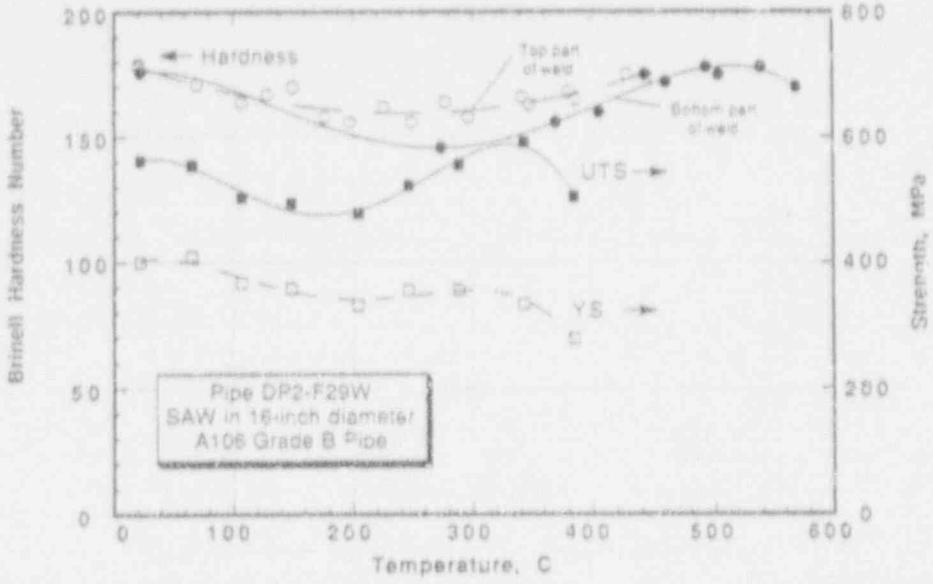

Figure 5.1 Brinell hardness and tensile strength versus test temperature for a submerged-arc weld in A106 Grade B pipe (DP2-F29W)

SC-SA-5/92-F5.1

Conduct Additional Compact-Specimen Tests at 288 C (550 F)

The steel selected for further study of the crack-jump phenomenon at 288 C (550 F) was A515 Grade 60 (Pipe DP2-F26) because earlier tests indicated that side-grooved compact specimens machined from this pipe consistently exhibited crack jumps of sufficient magnitude to permit gathering of data during one or more of the crack jump events. The two principal purposes of conducting additional tests on this steel were to: (1) determine the reproducibility of the crack jump behavior in one steel, and (2) obtain load, displacement, and crack extension data during one or more of the crack jump events.

Each of the compact specimens machined from Pipe DP2-F26 was 1T planform size and had a thickness of 20.8 mm (0.82 inch); side grooves had a depth of 10 percent per side. Each was tested at 288 C (550 F) because previous experiments had shown that this was the temperature at which crack jumps were most likely to occur. The experimental approach in conducting these additional tests was to use a conventional load cell and conventional clip gage in conjunction with rapid-response amplifiers, remove all filtering of the electronic signals, and record via a high-speed tape recorder only that portion of the test beyond maximum load, i.e. that portion in which crack jumps were more likely to occur. Additionally, a transient recorder was used in an attempt to capture data at very high rates during actual crack jump events. Conventional recording devices also were used to obtain data at slow rates during the entire test.

Of the four tests conducted at 288 C (550 F) on compact specimens machined from Pipe DP2-F26, three were instrumented to provide data during crack jumps. Each of the four specimens exhibited at

least two significant crack jumps, as indicated by the sharp load drops in the load-displacement curves shown in Figure 5.2. Useful data were obtained during each of the crack jump events in the three tests that were designed to obtain such data. Preliminary analysis of the three crack jumps in Specimen No. F26-108 indicates that the crack velocity during a crack jump was orders of magnitude slower than a cleavage crack, probably no greater than approximately 0.5 m/s. Nonetheless, that velocity is approximately 40,000 times greater than the value of 1.25×10^{-5} m/s estimated for the slow, stable crack extension during the remainder of the compact-specimen test.

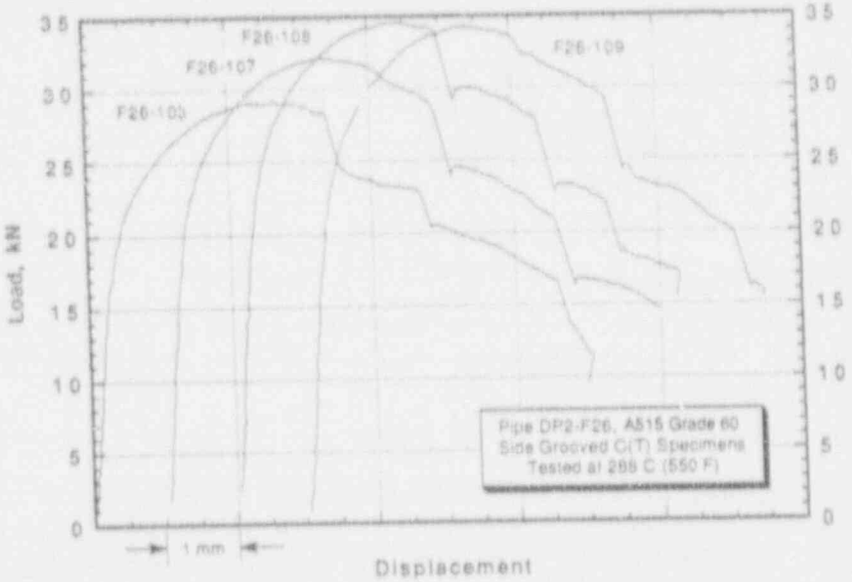

Figure 5.2 Load-displacement curves for four C(T) specimens from Pipe DP2-F26 (A515 Grade 60)

Specimens were tested at 288 C (550 F) and displayed crack jumps as indicated by load drops

SC-SA-5/92-F5.2

With respect to the reproducibility of crack jumps in this material (Pipe DP2-F26, A515 Grade 60), Table 5.1 summarizes the data for a total of six fatigue-precracked and side-grooved compact specimens tested at Battelle in the Degraded Piping Program and Short Crack Program. The results in Table 5.1 indicate good reproducibility; each of the six specimens exhibited two to four significant load drops ($\geq$ 10 percent of the existing load) during the course of a J-R curve test.

Conduct Fractographic and Metallographic Examinations

In conducting the above tests at 288 C (550 F) on compact specimens machined from Pipe DP2-F26, it was noted that the fracture surfaces of specimens that exhibited crack jumps had both dark and light bands, indicative of different degrees of oxidation on the fracture surfaces. The dark bands

Table 5.1 Reproducibility of crack jumps in compact specimens machined from Pipe DP2-F26 (A515 Gr 60, 28-inch diameter)

(Note: Specimens were 1T x 21 mm (0.82 in.) thick, L-C orientation, fatigue precracked, 20 percent side grooved, tested at 288 C (550 F)

Specimen Identification No.	Total Number of Sudden Load Drops Observed	Number of Load Drops ≥ 10% of Existing Load
F26-19	4	3
F26-22	6	4
F26-103	7	3
F26-107	2	2
F26-108	3	3
F26-109	3	2

appeared to be associated with slow, stable crack growth and the light bands with rapid crack jumps. The dark/light sequence seemed contrary to intuition, which might have supposed that there would be a more gradual gradation in fracture-surface color from dark to light as the crack progressed from its origin to its final position at the end of the test, although the region associated with a crack jump might have been expected to show a fairly uniform color.

Figure 5.3 is an enlarged photograph of a portion of the fracture surface of Specimen No. F26-107, which displayed two significant crack jumps when tested at 288 C (550 F). The boundaries between the light regions (Regions B and D) and dark regions (Regions A, C, and E) have been highlighted with a dark ink line; these ink lines were used in making nine-point-average crack-length determinations directly from the photographs. Also shown on the photograph is the crack length at the dark/light interface, relative to the fatigue-precrack tip, along the mid-thickness line. These dimensions were useful in positioning the specimen in subsequent examinations in a scanning electron microscope (SEM).

To test whether the boundaries between the dark and light regions were truly indicative of transitions between slow and fast crack growth, the nine-point-average crack lengths at the boundaries, measured from the photograph in Figure 5.3, were compared with the crack lengths at the start and end of crack jumps, as determined from the direct-current electrical potential (d-c EP) data obtained during the test. Similar measurements were made on Specimen No. F26-108, which exhibited three distinct crack jumps in a 288 C (550 F) test. The results, shown in Table 5.2, indicate that the magnitude of the crack jumps measured from the dark/light boundaries overestimated the crack jumps calculated from the change in d-c EP by an average of approximately 55 percent for the five crack jumps observed in the two tests. Individual overestimates ranged from approximately 15 to 90 percent. Figure 5.4 is a comparison of crack lengths as determined by the two different measurement methods

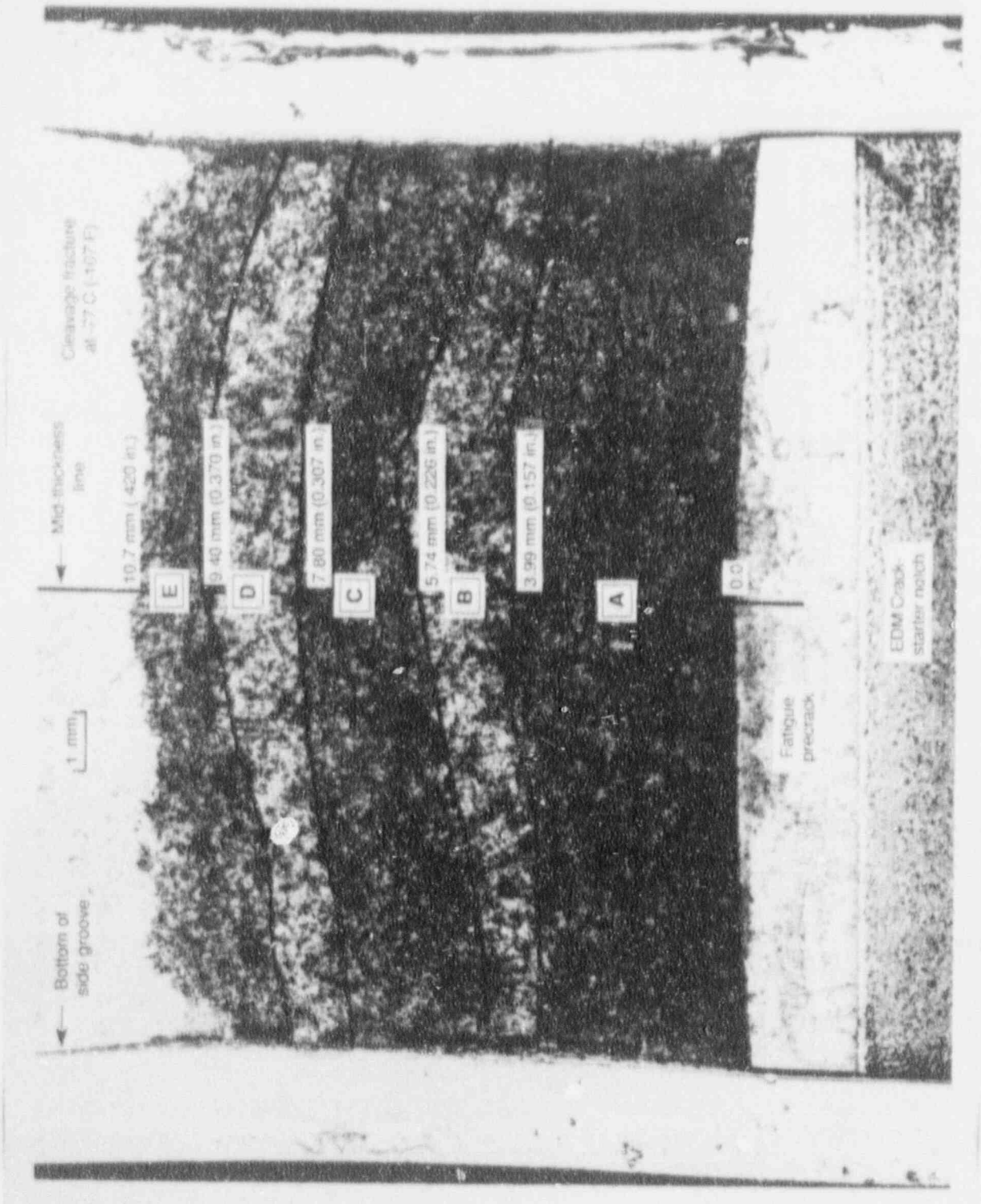

Figure 5.3 Photograph of a portion of the fracture surface of Compact Specimen F26-107 (A515 Grade 60 steel); specimen was tested at 288 C (550 F) and displayed two significant crack jumps in Areas B and D

SC-SA-5/92-F5.3

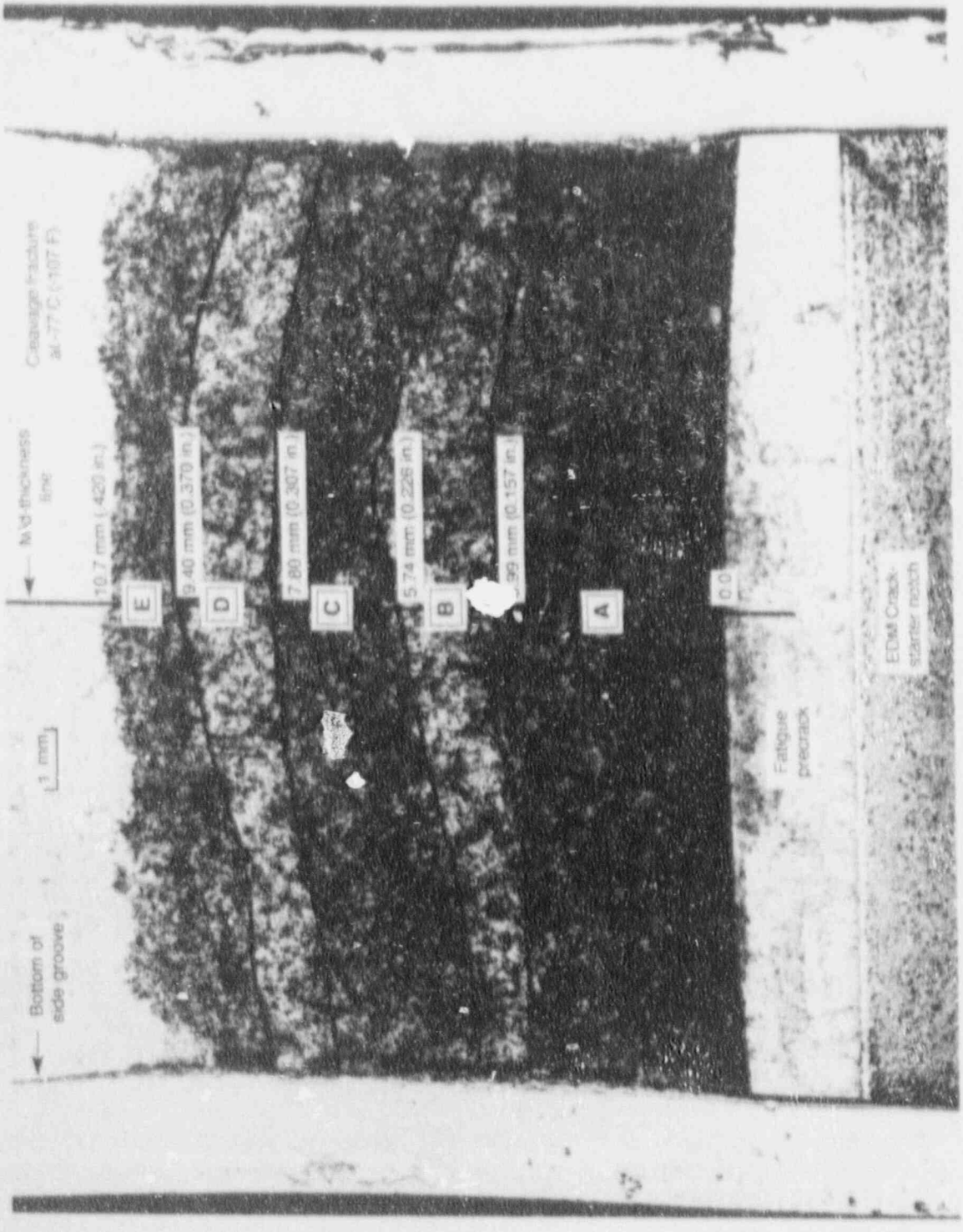

Figure 5.3 Photograph of a portion of the fracture surface of Compact Specimen F26-107 (A515 Grade 60 steel); specimen was tested at 288 C (550 F) and displayed two significant crack jumps in Areas B and D

SC-SA-5/92-F5.3

Table 5.2 Comparison of crack jump lengths based on fracture surface appearance [Δa (appearance)] with those based on change in d-c EP [Δa (EP)]

	Δa(Appearance)		Δa(EP)		Δa(Appearance) / Δa(EP)
	mm	inch	mm	inch	
Spec. F26-107					
Crack jump No. 1	1.47	0.058	0.99	0.039	1.49
Crack jump No. 2	1.52	0.060	0.8.	0.035	1.71
Spec. F26-108					
Crack jump No. 1	1.07	0.042	0.91	0.036	1.17
Crack jump No. 2	1.35	0.053	0.91	0.036	1.47
Crack jump No. 3	1.47	0.058	0.79	0.031	1.87
				Avg.	1.54

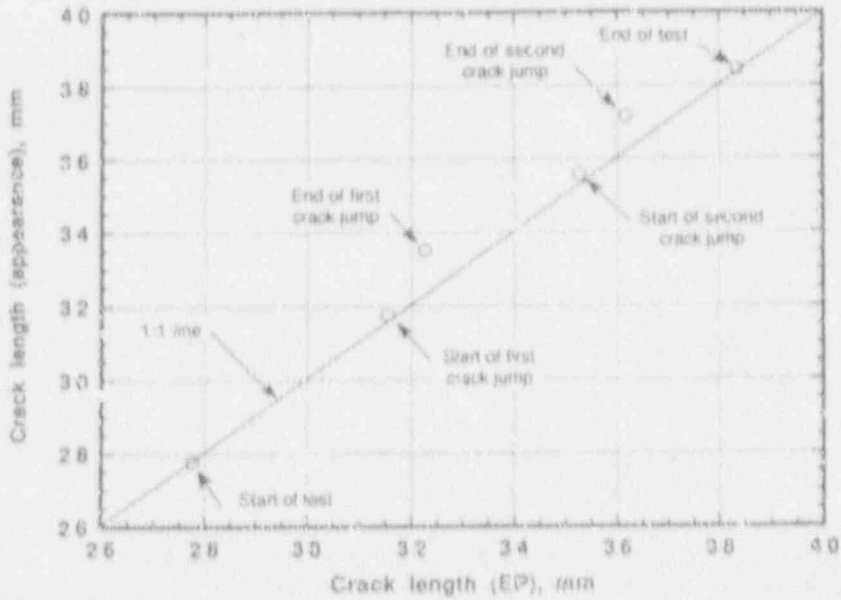

Figure 5.4 Comparison of crack length measurements by d-c EP with those from fracture-surface appearance for Specimen F26-107 (A515 Grade 60 steel)

SC-SA-5/92-F5.4

for Specimen No. F26-107. Notice in the figure that there is good agreement between the two different methods at the onset of both crack jumps and at the end of the test. One possible explanation of this difference in the arrested crack length is that the region of light-colored fracture extends beyond the arrest of the crack jump and into the region of slow, stable tearing. Therefore, while the alternating light and dark colors on the fracture surface are indicative of alternating fast and slow fracture, respectively, the amount of light-colored fracture appears to significantly overestimate the amount of rapid fracture.

Specimen No. F26-107 also was subjected to examination in a scanning electron microscope in an attempt to discern fractographic differences between the slow-crack-growth and the fast-fracture areas. Areas along the specimen mid-thickness line were examined, both within the dark regions and the light regions and at the boundaries between the two regions. Figure 5.5 shows SEM fractographs taken in Areas A, B, C, D, and E (refer to Figure 5.3). Each region consisted entirely of ductile dimpled rupture. No features were evident that clearly distinguished one region from another, although there were indications that the dimples in the dark regions of the fracture surface may have been slightly coarser than those in the light regions. Likewise, the transition from slow-to-fast fracture, while evident to the naked eye from color differences on the fracture surface, was not readily discernible in the scanning electron microscope.

Although it was not considered likely that possible microstructural differences along the fracture path in the compact specimens were responsible for the occurrence of the crack jumps, Specimen No. F26-107 was sectioned along its mid-thickness plane and that section was prepared for metallographic examination. As expected, there were no discernible differences between the microstructure associated with the slow fracture and that associated with the crack jumps. Likewise, no significant difference in fracture profile was evident for slow versus fast fracture. Figure 5.6 is a photomacrograph at 9X magnification of the polished and etched cross section to illustrate this conclusion. The regions labeled A, C, and E, which can be matched with those in Figure 5.3, are regions of slow, stable crack growth that were easily identifiable on the fracture surface by a dark oxide. The regions labeled B and D were characterized by a light oxide on the fracture surface. As was noted previously, the major portion, but not all, of those two light-colored regions was associated with rapid crack jumps.

Based on the evidence reported here, the crack jumps observed in compact-specimen tests (and pipe tests as well) of carbon steel at 288 C (550 F) appear nominally identical to slow crack growth under SEM examination, have similar fracture profiles when compared with slow-growing cracks, and are not the result of variations of the steel's microstructure. Despite these findings, the occurrence of crack jumps is readily apparent to the naked eye as light-colored regions on the fracture surface alternating with dark-colored regions. Limited evidence suggests strongly that the extent of the light-colored region significantly overestimates the extent of rapid crack growth.

Examine Load-Displacement Records of Compact Specimen and Pipe Tests

Load-displacement records from both compact-specimen tests and full-scale pipe tests conducted at 288 C (550 F) were examined for evidence of sudden load drops which are always associated with the occurrence of crack jumps. Each load drop was tabulated along with the magnitude of the load drop, expressed as a percentage of the load that existed at the onset of the load drop. The results of that

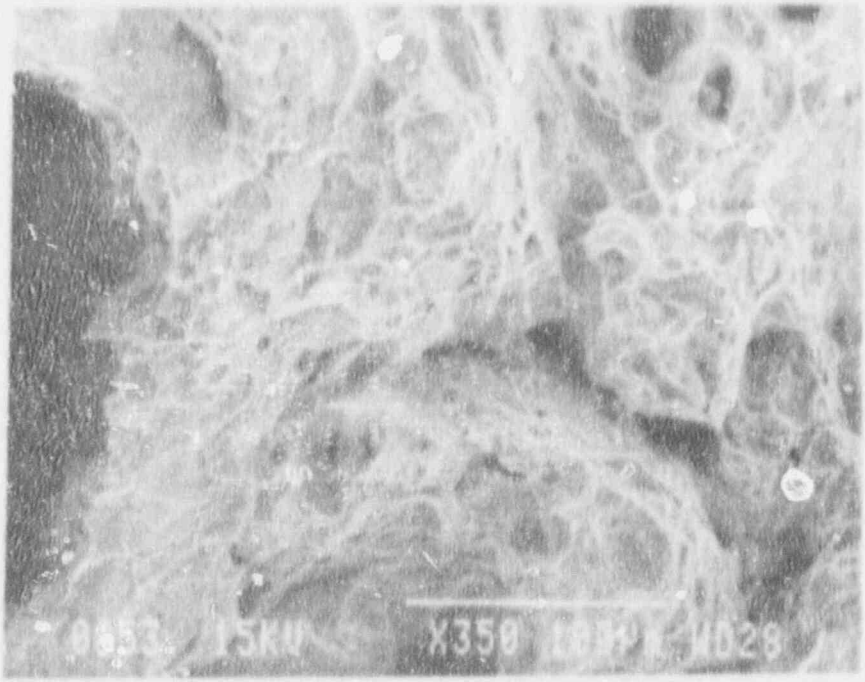

350X (a) Area A in Figure 5.3 (stable growth) 0853

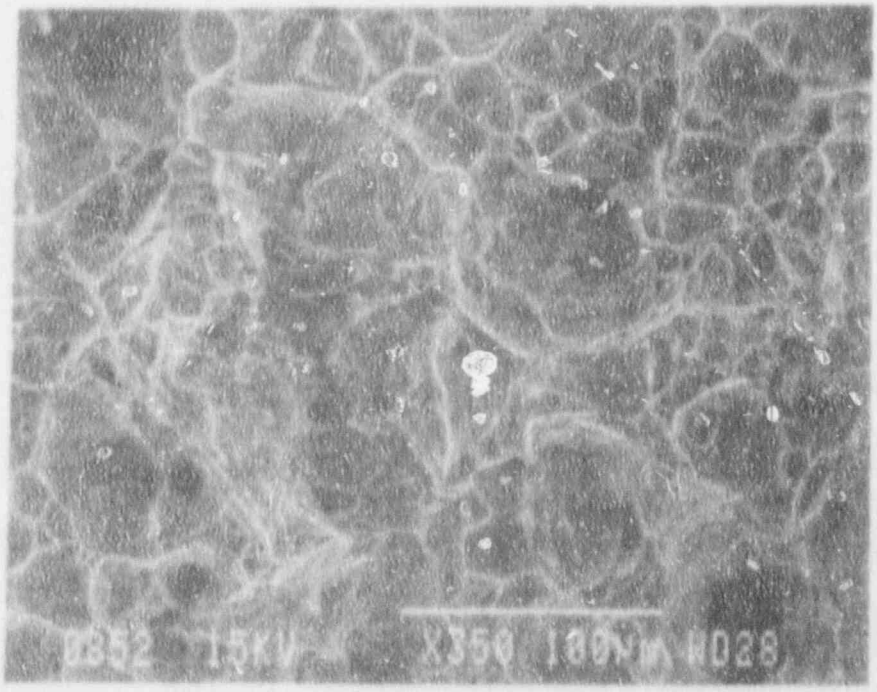

350X (b) Area B in Figure 5.3 (unstable growth) 0852

Figure 5.5 SEM fractographs of Compact Specimen F26-107 (A515 Gr 60 steel) from dark and light regions in Figure 5.3: (a) Area A, (b) Area B, (c) Area C, (d) Area D, and (e) Area E

SC-SA-5/92-F5.5a/b

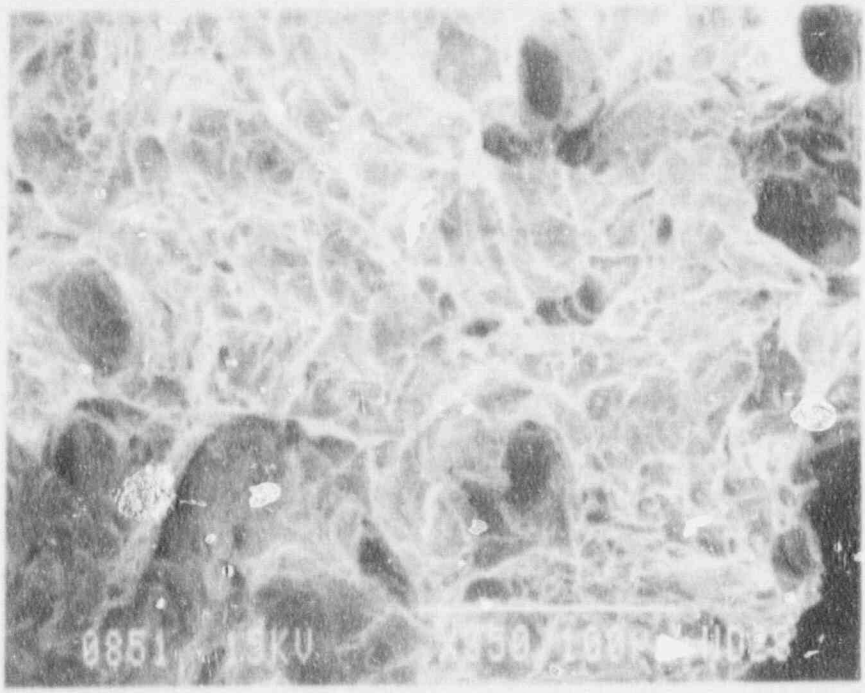

350X (c) Area C in Figure 5.3 (stable growth) 0851

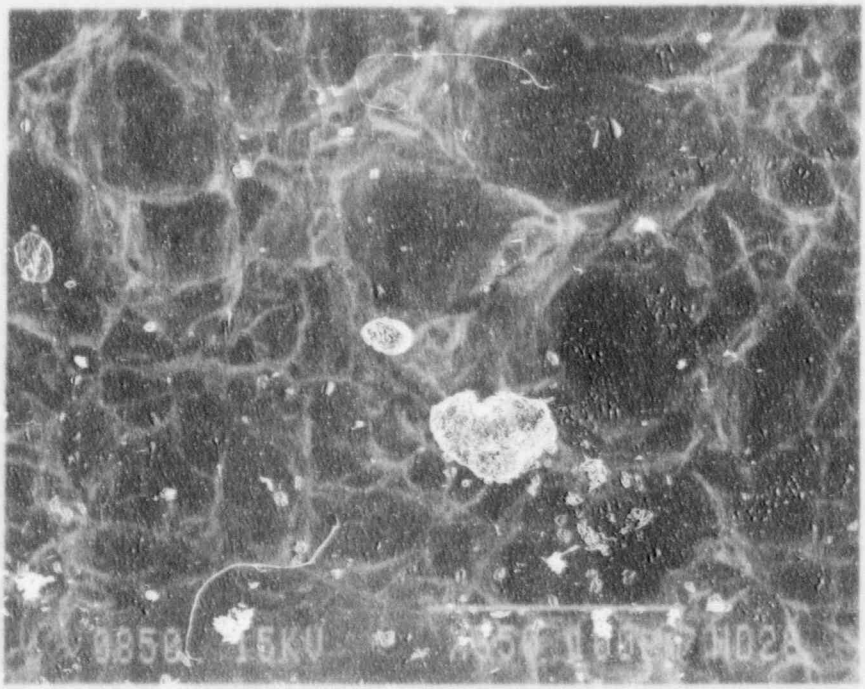

350X (d) Area D in Figure 5.3 (unstable growth) 0850

Figure 5.5 (Continued)

SC-SA-5/92-F5.5c/d

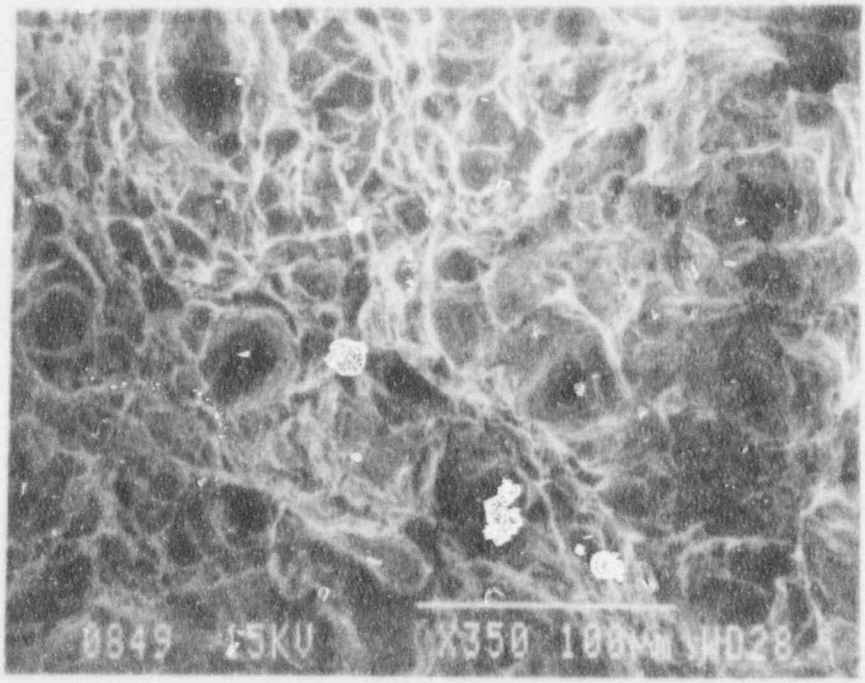

350X (e) Area E in Figure 5.3 (stable growth) 0849

Figure 5.5 (Continued) SC-SA-5/92-F5.5e

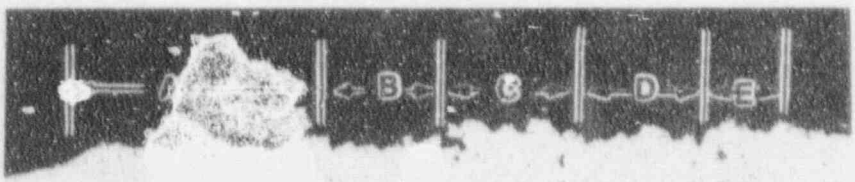

9X Etchant: 2% Nital 50495

Figure 5.6 Photomacrograph of midthickness plane to reveal crack profile of Compact Specimen No. F26-107 tested at 288 C (550 F)

A, C, and E: dark-colored fracture surface having stable crack growth (see Figure 5.3).

B and D: light-colored fracture surface having unstable crack growth (see Figure 5.3)

SC-SA-5/92-F5.6

examination are presented in Table 5.3, which provides information on both the total number of load drops and the magnitude of the load drops for a particular test. Notice in Table 5.3 that there is no close correlation between the number of crack jumps or their magnitudes when comparing compact specimens and pipes.

Table 5.4 compares the crack-jump behavior of pipes and compact specimens for each of thirteen carbon steels investigated (ten base metals and three weld metals). Further, Table 5.4 indicates that there is no overall correlation between the occurrence of crack jumps in compact specimens and their occurrence in pipes. In only eight of the thirteen steels was such a correlation observed. In two of the steels (Pipe DP2-F1 and DP2-F86W), a total of only one crack jump was observed in four compact-specimen tests. In two other steels (DP2-F2 and DP2-F26), crack jumps were observed in side-grooved compact specimens but not in plane-sided specimens. In one steel (DP2-F29W), compact-specimen tests showed only numerous tiny jumps, while in another steel (DP2-F9), through-wall-cracked pipes exhibited crack jumps while surface-cracked pipes did not. In general, unstable crack jumps did not occur for surface-cracked pipe prior to the maximum load, but occurred after the surface crack became a TWC. A possible reason for this is that there is very little crack growth for a surface crack from initiation to maximum load, hence the likelihood of an instability occurring probabilistically is small.

Two conclusions may be drawn from the results presented in Tables 5.3 and 5.4: (1) the fact that eight of thirteen steels studied (62 percent) showed agreement between through-wall-cracked pipes and compact specimens in whether or not crack jumps occurred suggests that a loose, but not a perfect, correlation exists between pipe behavior and compact-specimen behavior in this regard, and (2) the occurrence of crack jumps is a probabilistic phenomenon and requires considerably more data than are now available to establish the nature of the correlations between compact-specimen tests and pipe tests. It may be that the crack growth in the pipe tests is much larger than in C(T) tests, hence probabilistically there is a more significant likelihood of a crack jump in TWC pipe than C(T) specimens. This will be examined further in this program.

5.3.2.2 Activity 4.1.2 Using the Results of Activity 4.1.1, Formulate a Practical Screening Criterion for Predicting Crack Instabilities in Pipes

The objective of this activity is to formulate a practical screening criterion, based on the results of Activity 4.1.1, that will permit prediction of crack instabilities in specific pipes.

In Reference 5.4, it was concluded that hardness data at 288 C (550 F) and at room temperature would be sufficient to assess a particular steel's propensity for crack jumps at 288 C (550 F). If the hardness ratio at those two temperatures, BHN (288)/BHN (RT), equals or exceeds 1.02, crack jumps should be anticipated in compact-specimen tests at 288 C (550 F). The additional elevated-temperature hardness results obtained during the current reporting period on a submerged-arc weld in A106 Grade B steel (DP2-F29W) do not alter that conclusion.

Several other questions were addressed during the current reporting period. They pertained to the reproducibility of crack jumps in C(T) tests, the presence of unusual fractographic or metallographic features associated with crack jumps, and the ability of C(T) tests to predict crack jumps in pipe tests.

Table 5.3 Summary of crack jump events in ferritic pipe steels tested quasi-statically at 288 C (550 F) in L-C orientation

Test Ident. No.	Type of Test[a]	Total Number of Crack Jumps	Number of Crack Jumps in Which the Load Dropped by the Indicated Percentage of the Existing Load					Remarks
			0-5%	5-10%	10-20%	20-40%	>40%	
		Pipe DP2-F1 (A106 Gr B): 6-inch-dia. x 0.280-inch wall						
4112-5	Pipe test; 4 pt. bend; SC	0	0	0	0	0	0	
ZP13-3LC[b]	Compact tension; 0.4T x 0.23 in.; 0% SG	0	0	0	0	0	0	
ZP13-4LC[b]	Compact tension; 0.4T x 0.23 in.; 0% SG	1	0	0	0	0	1	
ZP13-7LC[b]	Compact tension; 0.4T x 0.23 in.; 20% SG	0	0	0	0	0	0	
ZP13-8LC[b]	Compact tension; 0.4T x 0.23 in.; 20% SG	0	0	0	0	0	0	
		Pipe DP2-F2 (A106 Gr B): 6-inch dia. x 0.864-inch wall						
4112-7	Pipe test; 4 pt. bend; SC	1	0	0	1	0	0	Crack jump occurred after the SC became a TWC
ZP14-13LC[b]	Compact tension; 0.8T x 0.7 in.; 20% SG	4	2	1	1	0	0	
ZP14-4LC[b]	Compact tension; 0.8T x 0.7 IN.; 20% SG	4	1	0	3	0	0	
ZP14-3LC[b]	Compact tension; 0.8T x 0.7 in.; 0% SG	0	0	0	0	0	0	
ZP14-5LC[b]	Compact tension; 0.8T x 0.7 in.; 0% SG	0	0	0	0	0	0	
		Pipe DP2-P9 (SA333 Gr 6): 10-inch dia. x 0.719-inch wall						
4115-1	Pipe test; 4 pt. bend; SC	0	0	0	0	0	0	
4115-2	Pipe test; 4 pt. bend; SC	0	0	0	0	0	0	
4121-6	Pipe test; internal pressure; SC	0	0	0	0	0	0	
4131-3	Pipe test; 4 pt. bend + press; TWC	10	1	5	3	1	0	Two of the crack jumps occurred before max. load
4131-4	Pipe test; 4 pt. bend + press; SC	0	0	0	0	0	0	
4131-7	Pipe test; 4 pt. bend; TWC	7	0	6	1	0	0	
4131-8	Pipe test; 4 pt. bend; SC	0	0	0	0	0	0	
F9-17	Compact tension; 1T x 0.55 in.; 0% SG	0	0	0	0	0	0	
F9-25	Compact tension; 1T x 0.55 in.; 0% SG	6	4	2	0	0	0	
F9-19	Compact tension; 1T x 0.55 in.; 20% SG	8	3	5	0	0	0	
F9-26	Compact tension; 1T x 0.55 in.; 20% SG	25	16	6	3	0	0	

Table 5.3 (Continued)

Test Ident. No.	Type of Test[a]	Total Number of Crack Jumps	Number of Crack Jumps in Which the Load Dropped by the Indicated Percentage of the Existing Load					Remarks
			0-5%	5-10%	10-20%	20-40%	>40%	
		Pipe DP2-F11 (SA 333 Gr 6): 4-inch dia. x 0.337-inch wall						
4111-1	Pipe test; 4 pt. bend; TWC	0	0	0	0	0	0	
F11-15	Compact tension; 0.4T x 0.21 in.; 0% SG	0	0	0	0	0	0	
F11-16	Compact tension; 0.4T x 0.21 in.; 20% SG	0	0	0	0	0	0	
F11-103	Compact tension; 0.4T x 0.21 in.; 20% SG	0	0	0	0	0	0	
F11-107	Compact tension; 0.4T x 0.21 in.; 20% SG	0	0	0	0	0	0	
		Pipe DP2-F13 (A106 Gr B): 16-inch-dia. x 0.5-inch wall						
4112-9	Pipe test; 4 pt. bend; SC	2	0	0	2	0	0	Crack jumps occurred after SC became TWC
F13-19	Compact tension; 1T x 0.37 in.; 0% SG	0	0	0	0	0	0	
F13-20	Compact tension; 1T x 0.37 in.; 20% SG	0	0	0	0	0	0	
		Pipe DP2-F26 (A515 Gr 60): 28-inch-dia. x 0.875-inch wall						
4111-2	Pipe test; 4 pt. bend; TWC	15	5	5	5	0	0	
F26-17	Compact tension; 1T x 0.82 in.; 0% SG	0	0	0	0	0	0	
F26-21	Compact tension; 1T x 0.82 in.; 0% SG	0	0	0	0	0	0	
F26-19	Compact tension; 1T x 0.82 in.; 20% SG	4	0	1	2	1	0	
F26-72	Compact tension; 1T x 0.82 in.; 20% SG	6	2	0	1	3	0	
F26-103	Compact tension; 1T x 0.82 in.; 20% SG	7	4	0	3	0	0	
F26-107	Compact tension; 1T x 0.82 in.; 20% SG	2	0	0	1	1	0	
F26-108	Compact tension; 1T x 0.82 in.; 20% SG	3	0	6	3	0	0	
F26-109	Compact tension; 1T x 0.82 in.; 20% SG	3	1	0	2	0	0	

Table 5.3 (Continued)

Test Ident. No.	Type of Test[a]	Total Number of Crack Jumps	Number of Crack Jumps in Which the Load Dropped by the Indicated Percentage of the Existing Load					Remarks
			0-5%	5-10%	10-20%	20-40%	>40%	
		Pipe DP2-F29 (A106 Gr B): 6-inch-dia. x 1.03-inch wall						
4112-8	Pipe test; 4 pt. bend; SC	0	0	0	0	0	0	
F29-11	Compact tension; 1T x 0.85 in.; 20% SG	5	0	4	1	0	0	
F29-13	Compact tension; 1T x 0.85 in.; 20% SG	5	0	4	1	0	0	
F29-17	Compact tension; 1T x 0.85 in.; 0% SG	4	0	1	3	0	0	
F29-18	Compact tension; 1T x 0.85 in.; 20% SG	5	0	0	5	0	0	
		Submerged-arc weld in Pipe DP2-F29 (A106 Gr B): 16-inch dia. x 1.03-inch wall						
4141-8	Pipe test; 4 pt. bend; SC	1	1	0	0	0	0	Crack jump occurred prior to breakthrough of the SC.
4141-9	Pipe test; 4 pt. bend + press; TWC	3	0	3	0	0	0	Each of the indicated crack jumps was uncertain on the basis of the load-displacement record.
F29W-12	Compact tension; 1T x 0.85 in.; 20% SG	11	11	0	0	0	0	
		Pipe DP2-F30 (A106 Gr B): 6-inch dia. x 0.562-inch wall						
4112-6	Pipe test; 4 pt. bend; SC	4	3	1	0	0	0	Crack jumps occurred after SC became TWC.
4113-5	Pipe test; 4 pt. bend; CC	21	9	11	1	0	0	Three of the crack jumps occurred prior to max. load.
4113-6	Pipe test; 4 pt. bend; CC	6	4	0	1	1	0	Two of the crack jumps occurred prior to max. load; the largest crack jump was uncertain on the basis of the load-displacement record.
4114-1	Pipe test; 4 pt. bend; CC	1	0	0	0	0	1	One major instability at max. load produced a double-ended-guillotine break.
1.2-7	Pipe test; 4 pt. bend; TWC	0	0	0	0	0	0	
ZP15-3LC[b]	Compact tension; 1/2T x 0.36 in.; 0% SG	6	6	0	0	0	0	
ZP14-4LC[b]	Compact tension; 1/2T x 0.36 in.; 0% SG	15	15	0	0	0	0	
ZP15-5LC[b]	Compact tension; 1/2T x 0.36 in.; 20% SG	15	15	0	0	0	0	
ZP15-6LC[b]	Compact tension; 1/2T x 0.36 in.; 20% SG	14	14	0	0	0	0	
F30-108	Compact tension; 1/2T x 0.36 in.; 20% SG	24	19	5	0	0	0	
F30-112	Compact tension; 1/2T x 0.36 in.; 20% SG	3	0	0	0	1	2	
F30-113	Compact tension; 1/2T x 0.36 in.; 20% SG	6	1	1	0	3	1	
F30-114	Compact tension; 1/2T X 0.36 in.; 20% SG	2	0	0	0	0	2	
F30-115	Compact tension; 1/2T x 0.36 in.; 20% SG	20	17	1	0	1	1	

Table 5.3 (Continued)

Test Ident. No.	Type of Test[a]	Total Number of Crack Jumps	Number of Crack Jumps in Which the Load Dropped by the Indicated Percentage of the Existing Load					Remarks
			0-5%	5-10%	10-20%	20-40%	>40%	
		Pipe DP2-F34 (A516 Gr 70); 36-inch-dia. x 3.0-inch wall						
4111-6	Pipe test; 4 pt. bend; TWC	1	0	0	1	0	0	Crack jump occurred at max. load.
F34-19	Compact tension; 1T; 20% SG	4	4	0	0	0	0	
F34-20	Compact tension; 1T; 20% SG	3	3	0	0	0	0	
F34-B1[b]	Compact tension; 4T x 2.6 in.; 20% SG	0	0	0	0	0	0	
F34-B2[b]	Compact tension; 4T x 2.6 in.; 0% SG	0	0	0	0	0	0	
F34-17	Compact tension; 1T; 20% SG	1	0	0	1	0	0	L-R, rather than L-C, orientation.
F34-18	Compact tension; 1T; 20% SG	1	0	1	0	0	0	L-R, rather than L-C, orientation.
		Shop weld in Pipe DP2-F34 (A516 Gr 70); 36-inch dia. x 3.4 in. wall						
4141-7	Pipe test; 4 pt. bend; TWC	6	0	2	3	1	0	
F34W-29	Compact tension; 1-3/8T x 1.25 in.; 20% SG	0	0	0	0	0	0	
F34W-30	Compact tension; 1-3/8T x 1.25 in.; 20% SG	0	0	0	0	0	0	
F34W-31	Compact tension; 1-3/8T x 1.25 in.; 20% SG	0	0	0	0	0	0	
F34W-32	Compact tension; 1-3/8T x 1.25 in.; 20% SG	0	0	0	0	0	0	
F34W-W1[b]	Compact tension; 4T x 2.6 in.; 20% SG	1	0	0	1	0	0	Crack jump was uncertain on the basis of the load-displacement record.
F34W-W2[b]	Compact tension; 4T x 2.6 in.; 0% SG	0	0	0	0	0	0	

Table 5.3 (Continued)

Test Ident. No.	Type of Test[a]	Total Number of Crack Jumps	Number of Crack Jumps in Which the Load Dropped by the Indicated Percentage of the Existing Load					Remarks
			0-5%	5-10%	10-20%	20-40%	>40%	
	E7018 Submerged-Arc Weld in Pipe F86 (A106 Gr B); 6.6-inch dia. x 0.5 in. wall							
BCD/WJ-1	Pipe test; 4 pt. bend; TWC	18	7	8	3	0	0	One crack jump occurred prior to max. load.
F86W-13	Compact tension; 1/2T x 0.38 in.; 0% SG	0	0	0	0	0	0	
F86W-14	Compact tension; 1/2T x 0.38 in.; 0% SG	0	0	0	0	0	0	
F86W-15	Compact tension; 1/2T x 0.38 in.; 20% SG	1	0	1	0	0	0	
F86W-16	Compact tension; 1/2T x 0.38 in.; 20% SG	0	0	0	0	0	0	
	Pipe IP-F1 (similar to SA333 Gr 6); 30-inch dia. x 1.54-inch wall							
IPIRG 4.3-1	Pipe test; 4 pt. bend + press.; TWC	1	0	0	0	1	0	Tested at 300 C (572 F); both ends of the crack experienced a jump, but the end that had the smaller amount of static growth had the larger crack jump.
IPIRG 4.3-2	Pipe test; 4 pt. bend + press.; SC	0	0	0	0	0	0	
IP-F1-4	Compact tension; 3T x 1 in.; 0% SG	0	0	0	0	0	0	
IP-F1-5	Compact tension; 3T x 1 in.; 20% SG	0	0	0	0	0	0	
IP-F1-6	Compact tension; 3T x 1 in.; 0% SG	0	0	0	0	0	0	
IP-F1-7	Compact tension; 1.5T x 1.4 in.; 0% SG	0	0	0	0	0	0	
IP-F1-8	Compact tension; 1.5T x 1.4 in.; 20% SG	0	0	0	0	0	0	

(a) SC = surface crack.
SG = side groove.
TWC = through-wall crack.
CC = complex crack (360 degree SC with TWC in same plane).

(b) Tested at Materials Engineering Associates (Ref. 5.6).

Table 5.4 Observations of crack jumps in compact specimen tests and full-scale pipe tests of carbon steels at 288 C (550 F)

Pipe Ident. No.	Material	Crack Jumps Observed		
		In Pipe Tests		In C(T) Tests
		TWC	SC	
DP2-F1	A106 Gr B, 6-in. dia., Sch. 40	No[a]	No[b]	Yes[c,d]
DP2-F2	A106 Gr B, 6-in. dia., Sch. XXS	Yes[e]	No[b]	Yes[e,d]
DP2-F13	A106 Gr B, 16-in. dia., Sch. 40	Yes[e]	No[b]	No
DP2-F29	A106 Gr B, 16-in. dia., Sch. 100	No[a]	No[b]	Yes
DP2-F30	A106 Gr B, 6-in. dia., Sch. 120	Yes[f]	No[b]	Yes
DP2-F29W	SA weld in Pipe DP2-F29 (A106 Gr B)	Yes	Yes[b,g]	Yes[h]
DP2-F86W	SA weld in A106 Gr B, 6-in. dia., 0.5-in. wall	Yes	NT[i]	Yes[e]
DP2-F9	A333 Gr 6, 10-in. dia., Sch. 100	Yes	No	Yes
DP2-F11	A333 Gr 6, 4-in. dia., Sch. 80	No	NT[i]	No
IP-F1	Japanese STS49, 30-in. dia., 1.54-in. wall (Similar to A333 Gr 6)	Yes	No[b]	No
DP2-F26	A515 Gr 60. 28-in. dia., 0.875-in. wall	Yes	NT[i]	Yes[e]
DP2-F34	A516 Gr 70, 36-in. dia., 3.5-in. wall	Yes	NT[i]	Yes
DP2-F34W	Shop weld in Pipe DP2-F34 (A516 Gr 70)	Yes	NT[i]	No

(a) No crack jumps after cracks in SC test became a TWC.
(b) A single surface-cracked pipe test was conducted.
(c) A total of one crack jump was observed in four pipe tests.
(d) C(T) tests were conducted at Materials Engineering Associates using the unloading compliance method, Ref. 5.6.
(e) Crack jumps were observed only in side-grooved C(T) specimens.
(f) Crack jumps were observed in each of three complex-cracked pipe tests; a single TWC pipe test exhibited no crack jumps; in an SC test there were unstable crack jumps after the crack became a TWC.
(g) Crack jump prior to surface crack penetration.
(h) Crack jumps were numerous but of small magnitude.
(i) Not tested.

In the single steel selected for crack-jump reproducibility studies (DP2-F26, A515 Grade 60), a total of six nominally identical tests at 288 C (550 F) on side-grooved specimens demonstrated good reproducibility. As was noted in Section 5.3.2.1, each specimen exhibited two to four significant load drops (≥ 10 percent of the existing load) during the course of a J-R curve test. On the other hand, the reproducibility among nominally identical specimens was not as good in several other materials. For example, in Pipe DP2-F1 (A106 Grade B) and in a submerged-arc girth weld in Pipe DP2-F86W (A106 Grade B), four compact specimens were tested for each pipe; three of those displayed no crack jumps, but the fourth showed one crack jump.

Additional examination of the compact specimens from the steel used in the crack-jump reproducibility studies revealed no unusual fractographic or metallographic features associated with the crack jumps. As expected, the jumps do not appear to be associated with microstructural variations. Also, the appearance of the fracture surfaces in the SEM is nominally the same for rapid crack jumps as for slow, stable crack growth.

Probably the most significant finding within Task 4 during the current reporting period is the failure to find an overall correlation between crack jumps in pipe tests and crack jumps in compact specimens machined from those pipes (see Table 5.4). Of thirteen pipes tested, eight showed agreement between pipes and C(T) specimens with respect to the occurrence, or lack of occurrence, of crack jumps. The remaining five pipes did not show agreement between the two types of tests. From these findings, it appears that the occurrence of crack jumps is a probabilistic phenomenon and will require the accumulation of more extensive data than are now available to establish the nature of the correlations between compact-specimen tests and pipe tests. The source of greatest concern is the fact that, of four pipes that showed no crack jumps in C(T) tests, three showed crack jumps in pipe tests.

5.4 Plans for Next Year of the Program

The efforts described below will be undertaken during the next year.

5.4.1 Subtask 4.1 Establish a Screening Criterion to Predict Unstable Crack Jumps in Ferritic Steels

There are two specific activities in this subtask. Plans for these activities are:

Activity 4.1.1—Conduct Laboratory Tests to Determine Correlations Among Tensile Properties, Hardness, DSA, and the Occurrence of Crack Instabilities in Both C(T) Specimens and Pipes. All the experimental efforts have been completed. Data reduction on the dynamic crack growth measurements will be completed this year.

Activity 4.1.2—Using the Results of Activity 4.1.1, Formulate a Practical Screening Criterion for Predicting Crack Instabilities in Pipes. All of these efforts will be completed next year.

5.4.2 Subtask 4.2 Evaluate Procedures for Assessing Fracture Resistance During Crack Jumps in Laboratory Specimens

There are three specific activities in this subtask. The plans for next year for these activities are:

Activity 4.2.1—Evaluate J-resistance Curve Approach. These efforts will be completed next year.

Activity 4.2.2—Evaluate Alternative Material Resistance Measures. These efforts will start next year but will not be completed until the following year.

Activity 4.2.3—Assess Plausible Analysis Methods to Account for Crack Jumps. These efforts will start next year but will not be completed until the following year.

5.4.3 Subtask 4.3 Assess Current Procedures for Predicting Crack Jump Magnitude in Pipes

There are two specific activities in this subtask. The plans for next year are:

Activity 4.3.1—Predict the Magnitude of Crack Jumps in Pipes Using Current Analysis Methods. These efforts will start in the next year.

Activity 4.3.2—Assess the Success of the Current Approximate Approaches and Identify if Optional Efforts are Warranted. These efforts will start in the next year.

5.4.4 Subtask 4.4 Prepare Interim and Topical Reports on Dynamic Strain Aging Induced Crack Instabilities in Ferritic Nuclear Piping Steels at LWR Temperatures

These reports will be written in the next year.

5.4.5 Optional Subtask 4.5 Refine Procedures for Assessing Fracture Resistance During Crack Jumps in Laboratory Specimens

If this subtask is undertaken, it will start in the next year.

5.4.6 Optional Subtask 4.6 Refine Procedures for Predicting Crack Jump Magnitude in Pipes

If this subtask is undertaken, it will start in the next year.

5.5 References

5.1 Wilkowski, G. M. and others, "Degraded Piping Program - Phase II," Summary of Technical Results and Their Significance to Leak-Before-Break and In-Service Flaw Acceptance Criteria, March 1984 - January 1989, Battelle, NUREG/CR-4082, Vol.8, March 1989.

5.2 Marschall, C. W., Landow, M. P., and Wilkowski, G. M., "Effect of Dynamic Strain Aging on Fracture Resistance of Carbon Steels Operating at Light-Water-Reactor Temperatures," in ASTM STP 1074, pp 339-360, 1990.

5.3 Wilkowski, G. M. and Kramer, G., "An Energy Balance Approach to Estimate the Initiation and Arrest of Ductile Fracture Instability in Circumferentially Cracked Pipe," ASME Special Technical Publication PVP Vol. 167, pp 103-114, July 1989.

5.4 Wilkowski, G. M. and others, "Short Cracks in Piping and Welds," Battelle, NUREG/CR-4599, BMI-2173, Vol. 1., No. 2, December 1991.

5.5 Schmidt, R. A., Wilkowski, G. M., and Mayfield, M. E., "The International Piping Integrity Research Group (IPIRG) Program: An Overview," SMiRT-11, Paper G23/1, August 1991.

5.6 Hiser, A. L., "Fracture Toughness Characterization of Nuclear Piping Steels," NUREG/CR-5188, November 1989.

6. TASK 5 FRACTURE EVALUATIONS OF PIPE ANISOTROPY

6.1 Task Objective

The objective of this subtask is to assess whether anisotropic fracture properties (where the toughness is typically lower in a helical direction or the axial direction for ferritic seamless pipe) together with the occurrence of high principal stresses in a helical direction can cause a lower failure stress than calculated using the toughness in the L-C orientation and using only the longitudinal stresses.

6.2 Task Rationale

The rationale for this task is to assess if margins in current LBB and ASME flaw evaluation procedures could be significantly eroded for out-of-plane crack growth under certain service loading conditions. If margins in current procedures are found to be significantly eroded, modifications to existing fracture analysis methods will be made.

6.3 Task Approach

Five subtasks will be conducted in this task. Two of them are optional subtasks that would be started only with NRC approval after an interim report is completed. The subtasks are:

Subtask 5.1	Assess effect of toughness anisotropy on pipe fracture under combined loads
Subtask 5.2	Determine magnitude of toughness anisotropy and establish a screening criterion to predict out-of-plane crack growth
Subtask 5.3	Prepare interim and topical reports on anisotropy and mixed-mode studies
Subtask 5.4	Establish ductile crack growth resistance under mixed-mode loading (optional subtask)
Subtask 5.5	Refine J-estimation scheme analyses for pipes (optional subtask).

6.3.1 Background

The approach is based on the following two facts: (a) out-of-plane (angled) crack growth under nominally Mode I loading has been observed in both laboratory and pipe specimens of ferritic pipe materials (Refs. 6.1 and 6.2) and (b) the data and observations have not yet been adequately analyzed to assess the ramifications of the phenomenon under realistic loading conditions and for large diameter pipes.

Existing data suggest that the out-of-plane crack growth observed in the Degraded Piping Program experiments was due to toughness (or, more precisely, crack growth resistance) anisotropy (Ref. 6.2). The toughness anisotropy arises from nonmetallic inclusions, which tend to be aligned parallel to the principal working direction. In the Degraded Piping Program, an ad hoc modification to existing J-estimation analysis methods was made by using projected rather than actual crack length in J-R curve

calculations for pipe experiment data. It is not known if this procedure would be sufficiently accurate for larger-diameter pipes under combined bending, internal pressure, and torsional loads.

A prudent overall approach is to first assess the ramifications of toughness anisotropy on the behavior of pipes under a sufficiently broad range of service loading conditions. This assessment will be accomplished using parametric analyses (Subtask 5.1). The analyses will be performed using the finite element method on a pipe involving bending, internal pressure, torsion, and combined loadings. The crack driving force will be computed under each loading type as a function of angle from the crack plane. Using existing data and engineering judgment, the results will be used to identify realistic service loading conditions, which may require modifications to existing analysis methods to avoid nonconservative predictions. So that the assessment is realistic, Subtask 5.2 is focusing on determining the realistic magnitude of anisotropy in representative ferritic piping materials. This determination will be made mostly by using available data. A minimum number of laboratory specimens are being tested to generate quantitative information for analysis. In Subtask 5.2 we are also attempting to develop a screening test that would make it possible to predict the occurrence of toughness anisotropy or out-of-plane crack growth in pipes.

An interim report will be prepared (Subtask 5.3) using the findings in Subtasks 5.1 and 5.2. The report will provide the technical bases for a decision by the NRC as to the subsequent course of action. For example, the findings may indicate that there is no practical need for modifying existing analysis methods. But assuming that, for certain realistic situations, modifications in analysis methods are called for, our approach contains Optional Subtasks 5.4 and 5.5. These activities are aimed at providing the NRC with a validated analysis procedure for predicting crack growth behavior in nuclear power plant piping of materials with significant material anisotropy.

Progress is reported for Subtasks 5.1 and 5.2 only, because the other subtasks are inactive.

6.3.2 Subtask 5.1 Assess Effect of Toughness Anisotropy on Pipe Fracture Under Combined Loads

The general objective of this subtask is to conduct a parametric analysis to determine if there is significant nonconservatism in current LBB analyses for service loading conditions of circumferentially through-wall cracked pipe with anisotropic fracture toughness. There are six activities within this subtask.

Activity 5.1.1	Determine driving force for angled stationary crack
Activity 5.1.2	Conduct tensile tests at different orientations, and on additional skewed orientation C(T) specimens on a 4-inch-diameter pipe to assess strength and toughness variations
Activity 5.1.3	Determine driving force for angled growing crack
Activity 5.1.4	Determine angled crack principal stresses
Activity 5.1.5	Formulate approximate corrections
Activity 5.1.6	Assess if optional efforts are necessary.

Analysis methods that are currently used to assess crack growth and fracture in nuclear piping assume Mode I (opening mode) conditions. Mode I crack growth requires symmetry of the field variables about a plane through the crack. However, load conditions exist in nuclear piping systems that may violate the Mode I symmetry assumptions upon which J-integral analysis methods are based. Two basic conditions exist in nuclear piping that may lead to a violation of the Mode I crack growth assumption:

(1) out-of-plane (angled) crack growth, and
(2) mixed-mode loading (bending and torsion).

Most ferritic nuclear piping exhibits out-of-plane ductile crack growth from a circumferential through-wall crack. J-estimation scheme analyses of experiments from the Degraded Piping Program in which the crack grew at an angle assumed straight crack growth but gave reasonable predictions of maximum load. However, the reasons for this success were never adequately explained. Moreover, the effect of angular crack growth under mixed-mode conditions (bending, torsion, tension) was never established.

Three important aspects of the angle-crack problem are addressed in this task:

(1) initiation under bending only and combined pressure and bending — a Mode I problem but with anisotropic toughness,
(2) initiation under bending, pressure, and torsion — a mixed-mode problem with anisotropic and isotropic toughness, and
(3) angled crack growth under mixed-mode conditions.

In addition, the effectiveness of current simplified J-estimation analysis procedures in predicting this type of crack growth is considered. This effort also includes finding the proper characterizations of both angled crack growth and crack growth perpendicular to the pipe axis under mixed-mode loading caused by bending and torsion. If significantly lower failure loads are predicted for loading of anisotropic toughness pipe (including combined loading) relative to analyses considering only longitudinal stresses, then optional activities, also provided here, are suggested to enable the development of a simplified procedure for mixed-mode, ductile fracture.

Work within Activity 5.1.2 was completed during the previous reporting period and the results were reported in Reference 6.3. The other activities were inactive during the current reporting period.

6.3.3 Subtask 5.2 Determine Magnitude of Toughness Anisotropy and Establish a Screening Criterion to Predict Out-of-Plane Crack Growth

The establishment of a screening criterion is necessary to determine which materials are susceptible to out-of-plane crack growth. Ideally, such a criterion will enable an evaluation of anisotropic fracture to be made on piping in a plant without archival material. This activity requires a small amount of material property testing. The actual magnitude of this activity is much smaller than the other activities, but it has a high significance. We have divided this subtask into three activities.

Activity 5.2.1	Document inclusion size, shape, distribution, and orientation in carbon-steel pipes
Activity 5.2.2	Examine the literature and conduct tests to determine toughness anisotropy as a function of inclusion characteristics
Activity 5.2.3	Assess usefulness of screening tests to predict out-of-plane crack growth

Progress during the past six-month period has been confined primarily to examination of the literature pertaining to toughness anisotropy within Activity 5.2.2. Attention was also given to assessing the usefulness of screening tests to predict out-of-plane crack growth in Activity 5.2.3.

6.3.3.1 Activity 5.2.2 Examine literature and conduct tests to determine toughness anisotropy as a function of inclusion characteristics

The objective of this activity is to determine the relation between inclusions, or other microstructural features, and toughness anisotropy in carbon steels, based on a review of data from the technical literature and on the results of Charpy V-notch impact tests on specimens machined from pipes at several different orientations.

During the last six months, pertinent references from a limited review of the literature were obtained and carefully examined. Extended abstracts of selected references are presented in Appendix B. Charpy V-notch impact tests at several different orientations for four different carbon steel pipes that exhibited skewed crack growth in pipe fracture experiments were completed during the previous reporting period and the results were reported in Reference 6.3.

The limited review of the literature conducted within this activity has led to no new information on skewed crack growth in carbon-steel pipes containing circumferential flaws, or on the explanation for the skewed growth. It has been assumed by Battelle investigators that the skewed crack growth arises from anisotropy of the toughness properties; that is, the crack-growth resistance is much lower in the axial direction than in the circumferential direction. Thus, a crack that originally is growing circumferentially will have a tendency to deviate from that direction if the toughness in the axial direction is substantially lower. On a microscopic scale, it may be that the crack is extending by a combination of circumferential and axial growth, and that the crack-growth angle depends on the relative amount of the axial growth component which, in turn, depends on the degree of anisotropy. In addition to the anticipated effect of toughness anisotropy on crack-growth angle, it might be anticipated also that the method of loading would have an effect. For example, bending, which produces axial tensile stresses, might be expected to favor circumferential growth while internal pressure, for which hoop tensile stresses predominate, might be expected to favor axial growth. Each of these possibilities is considered in Section 6.3.3.2 of this report. The remainder of this section reviews information from the technical literature which deals with sources of toughness anisotropy in carbon steels.

From information found in the review, there are three main contributors to toughness anisotropy in carbon steels: (1) elongated inclusions, (2) banded microstructures, and (3) crystallographic texture. By far the most important contributor is elongated nonmetallic inclusions, predominantly manganese sulfides, which become elongated during the metalworking operations by virtue of their high ductility.

When highly elongated sulfide inclusions are present, the ratio of the Charpy upper plateau energy in the minimum-toughness direction to that in the maximum-toughness direction (termed the anisotropy coefficient in Reference 6.4) can reach values as low as approximately 0.25 to 0.35 (References 6.3, 6.5-6.11).

Several methods have been advanced for minimizing or overcoming the toughness anisotropy due to the manganese sulfide inclusions. An obvious method would be to reduce the sulfur content of the steel. However, according to Matrosov and Polyakov (Ref. 6.4), significant reductions in toughness anisotropy occur only when the sulfur content is below approximately 0.01 percent. Reducing the sulfur from 0.04 to 0.02 percent has relatively little effect. Sharp improvements can be realized when the sulfur level is maintained at 0.004 percent or below. Nonetheless, two of the references examined (References 6.10 and 6.12), in which steels containing 0.005 percent sulfur were tested, indicated that even low-sulfur steels can exhibit significant toughness anisotropy. For example, in Reference 6.10, the anisotropy coefficient was 0.50 as determined from Charpy tests on a heat treated, low-alloy steel plate. In Reference 6.12, the anisotropy coefficient for A533, Grade B, Class 1 steel plate was 0.63 to 0.74, as determined from compact-specimen tests. Although at one time the attainment of low sulfur levels was difficult and expensive, economical industrial methods are currently available for accomplishing this result.

Similarly, anisotropy due to manganese sulfide inclusions could be minimized by reducing the manganese content. However, because of its many useful alloying characteristics in carbon steels, elimination of manganese is not recommended (Ref. 6.4).

A second way to minimize anisotropy due to manganese sulfide inclusions is to employ cross rolling in the fabrication of plate and sheet. Hodge, Frazier, and Boulger (Ref. 6.10) demonstrated that planar anisotropy could be eliminated in a steel that contained as much as 0.06 percent sulfur by cross rolling it 46 percent. However, cross rolling is not always practical; in any event, it cannot be employed in the manufacture of seamless pipes.

A third method for minimizing toughness anisotropy is to reduce the ductility of the sulfur-bearing inclusions and, therefore, their ability to form highly elongated stringers. As pointed out by Matrosov and Polyakov (Ref. 6.4), the most effective way to form low-plasticity sulfides is to add titanium, zirconium, calcium, or rare-earth metals, especially cerium. Each of these elements has a higher affinity for sulfur than does manganese. Those authors cited an investigation in which the anisotropy coefficient was approximately 0.4 when the cerium/sulfur ratio in the steel was zero. However, when cerium was added to bring the cerium/sulfur ratio to 1.5 to 2.0, the anisotropy coefficient was raised to a value of approximately 0.85. Park and others (Ref. 6.13) also reported benefits, albeit smaller than those in Ref. 6.4, of adding an unspecified rare earth to steels containing approximately 0.02 percent sulfur. Such means for achieving sulfide-shape control have been adequately investigated and developed for use in tonnage production of weldable structural steels.

For steels tested at Battelle within Activity 5.2.2 (Ref. 6.3), the shape of the sulfur-bearing inclusions was found, as expected, to have an important effect on the anisotropy coefficient. For two pipes that contained stringer-type inclusions [Pipe DP2-F11 (A333 Grade 6) and Pipe DP2-F30 (A106 Grade B)], the anisotropy coefficient was approximately 0.3, whereas for two other pipes that contained elliptical inclusions [Pipe DP2-F26 (A515 Grade 60 and Pipe DP2-F29 (A106 Grade B)], the

anisotropy coefficient was 0.51 to 0.55. In the examples cited, it is interesting to note that the inclusion shape was much more important than the volume fraction of inclusions present -- the two steels which exhibited the lowest coefficients (greatest anisotropy) had sulfur contents from 0.014 to 0.015 percent, while those showing the highest coefficients (least anisotropy) had sulfur contents from 0.023 to 0.027 percent.

The reasons for the different shapes of the inclusions in the steels discussed in the preceding paragraphs are uncertain, based on the chemical compositions reported in Table 6.2 of Reference 6.3. The two steels which contained stringer-type inclusions had higher aluminum contents (0.01 and 0.05 percent) than did the two which contained elliptical inclusions (0.000 and 0.003 percent), indicating that they may have been killed, or semi-killed steels, thereby improving the plasticity of the sulfides, as is discussed more fully in the next paragraph. There is no indication from the chemical composition that there was a deliberate attempt to control inclusion shape in the two steels which had elliptical inclusions; both titanium and zirconium were absent and the chemical analysis did not attempt to determine rare earth or calcium levels.

Matrosov and Polyakov (Ref. 6.4) also discussed the role of oxygen in controlling the shape of sulfur-bearing inclusions. Although the role of oxygen is relatively modest, the authors state that, in balanced or rimmed steels, the sulfides contain significant amounts of oxygen, which considerably reduces their plasticity and their ability to form stringers. Therefore, rimmed steels are likely to show less toughness anisotropy than fully killed steels, in which most of the oxygen is present in the form of oxide inclusions and the sulfides are nearly pure manganese sulfide.

In addition to elongated inclusions, a second contributor to toughness anisotropy is banded microstructures resulting from chemical inhomogeneities. For example, in a steel made up of ferrite and pearlite, a banded microstructure would appear in the microscope as alternating bands of ferrite (light etching) and pearlite (dark etching), aligned in the principal working direction. According to Matrosov and Polyakov (Ref. 6.4) banding alone can produce an anisotropy coefficient as low as approximately 0.8. Several references were reviewed in which elevated-temperature homogenization treatments were employed to reduce the degree of banding. In Reference 6.12, hot-rolled carbon-manganese steel plates containing approximately 0.02 percent sulfur were homogenized at unspecified temperatures for unspecified times. For a steel that had been rare-earth treated to control sulfide shape, homogenization increased the anisotropy coefficient from 0.67 to 0.85. The effect of homogenization was much less pronounced for a steel without rare earth additions; the anisotropy coefficient increased only from 0.54 to 0.58. In Reference 6.8, a ferritic steel plate of unspecified type and unspecified sulfur content showed an increase in anisotropy coefficient from 0.35 to 0.45 after a homogenization treatment. However, in Reference 6.10, relatively little effect on the anisotropy coefficient was noted, regardless of sulfur content from 0.005 to 0.179 percent, from a homogenization treatment of 10 hours at 1290 C (2350 F), even though Charpy values were increased.

The degree of banding can also be reduced by decreasing the carbon content of the steel (Ref. 6.4). In order for the effect of lower carbon to be significant in reducing anisotropy due to banding, it is necessary to go to reduced-pearlite steels (up to 0.08 percent carbon) or even to pearlite-free steels (up to 0.03 percent carbon). Of course, reducing the carbon to those levels causes a substantial loss

of strength, which can be overcome by microalloying with elements such as niobium, vanadium, and titanium. The authors of Reference 6.4 point out that, even at the time of preparation of their paper (1976), the beneficial effect of a reduction in carbon was being widely used in the development of a group of reduced-pearlite and pearlite-free precipitation hardening steels.

A third contributor to toughness anisotropy is known variously as crystallographic texture or preferred orientation. This condition exists in a plate or a pipe when the individual grains (crystals) are not randomly oriented, but have a preferred orientation dictated by the details of the thermomechanical treatments to which the component has been subjected. Little information is available on the quantitative effect of crystallographic texture on toughness anisotropy. Fegredo, Faucher, and Shehata (Ref. 6.14) investigated the effect of texture by rolling low-carbon steels containing two levels of sulfur (0.007 and 0.02 percent) at a number of different temperatures, ranging from 680 to 1200 C (1255 to 2190 F). However, they did not make any toughness measurements in the orientations of highest toughness. Hence, it is not possible to determine anisotropy coefficients from their data. In spite of the lack of data regarding texture effects on toughness anisotropy, it is believed that the magnitude of the texture effect is comparable with that of banding and much less important than sulfide shape.

To summarize briefly, the major contributor to toughness anisotropy is highly elongated, stringer-type, sulfur-bearing inclusions. When they are present, anisotropy coefficients as low as 0.25 to 0.35 are commonly observed. Reducing sulfur levels below approximately 0.005 percent and achieving sulfide shape control by addition of elements that reduce the plasticity of the inclusions are effective in achieving greatly improved anisotropy coefficients. Nonetheless, significant anisotropy may remain even after those procedures are adopted. The most certain way to achieve an anisotropy coefficient of 1.0 is to employ cross rolling. Unfortunately, that procedure is not always practical and can be employed only in the manufacture of seam welded pipe but not seamless pipe. Much less is known about two other sources of toughness anisotropy—banded microstructures and crystallographic texture—but each is believed to be much less important than inclusion shape. Some researchers report that modest reductions in anisotropy due to banding can be achieved by thermal homogenization treatments.

6.3.3.2 Activity 5.2.3 Assess Usefulness of Screening Tests to Predict Out-of-Plane Crack Growth

The objective of this activity is to assess the usefulness of screening tests, namely, microscopic examination of nonmetallic inclusions or Charpy V-notch tests at several different orientations, to predict the occurrence and severity of out-of-plane crack growth in pipe experiments.

As was noted in Battelle's Second Semiannual Report (Ref. 6.3), it appears that microscopic examination of inclusions may provide a promising approach to predicting the relative degree of anisotropy in carbon steel pipes. Specifically, it was found that pipes having elliptical-type inclusions displayed significantly less Charpy V-notch toughness anisotropy than did pipes having stringer-type inclusions. A question that was not answered, however, was whether a correlation exists between the anisotropy coefficient and the tendency for out-of-plane crack growth. An attempt was made to answer that question during this reporting period by examining the fracture paths in carbon steel pipes that have been subjected to Charpy tests to determine anisotropy coefficients.

Fracture paths were examined and documented in a total of 23 pipe fracture experiments representing 10 different carbon steel pipes tested at Battelle. Sketches of the fracture paths are shown in Appendix C. Information from those experiments is summarized in Table 6.1, where the approximate crack-growth angles were measured from the illustrations in Appendix C. Also shown in Table 6.1 are the toughness anisotropy coefficients that were determined from Charpy tests or C(T) tests in several orientations.

Figure 6.1 is a graph of crack-growth angle versus the anisotropy coefficient of the pipe, in which the data have been differentiated according to the type of crack and the type of loading. Clearly, the data shown do not reveal a distinct relation between crack-growth angle and anisotropy coefficient. A high degree of scatter in crack growth angle is evident over the entire range of anisotropy coefficients examined. Notice particularly the data for through-wall-cracked pipes tested in four-point bending at an anisotropy coefficient of 0.35; one pipe displayed a crack-growth angle as great as 59 degrees, while in another pipe, both the crack tips grew at zero degrees. Although it may be possible that pipes free of anisotropy (coefficient of 1.0) would consistently display circumferential crack growth (zero degrees), that result is not suggested by the data in Figure 6.1.

In addition to the unexpected lack of correlation between crack-growth angle and anisotropy coefficient in Figure 6.1, two other puzzling features are evident. First, the addition of internal pressure loading to the four-point bend loading, depicted by filled circles and filled squares in Figure 6.1, did not significantly change the crack-growth angle at a given value of anisotropy coefficient, even though an increase in angle might have been anticipated. Second, the lone test in which loading was accomplished entirely by internal pressure (no bending) and in which it might have been expected that an unusually large crack-growth angle would occur, exhibited circumferential crack growth.

The results shown in Figure 6.1 suggest that development of a simple screening criterion, involving microstructural examination of inclusions or Charpy testing in several directions, to predict the tendency for skewed crack growth in pipe tests is not feasible at this time. Other factors, as yet unknown, apparently have a greater effect on skewed crack growth than does the anisotropy coefficient.

6.4 Plans for Next Year of the Program

During the next year the following efforts are scheduled.

6.4.1 Subtask 5.1 Assess Effect of Toughness Anisotropy on Pipe Fracture Under Combined Loads

There are six activities in this subtask. The plans for each of these are given below.

Activity 5.1.1—Determine Driving Force for Angled Stationary Crack. These finite element analyses will be completed for stationary cracks of different orientations.

Table 6.1 Skewed crack growth in circumferentially cracked carbon steel pipes tested at Battelle

Pipe Ident. No.	Steel Type	Pipe Test No.	Type of Crack[a]	Type of Loading[b]	Approx. Crack Growth Angle, degree[c]	Anisotropy Coefficient[d]
DP2-F1	A106 Gr B	4112-5	SC (int)	4 pt. bend	17; 24	N.D.[e]
DP2-F2	A106 Gr B	4112-7	SC (int)	4 pt. bend	47, 72; 48, 48	N.D.
DP2-F9	A333 Gr 6	4115-1	SC (int)	4 pt. bend	52; 35	0.40[f]
		4121-6	SC (ext)	IP only	0; 0	0.40
		4131-3	TWC	4 pt. bend + IP	45; 19	0.40
		4131-4	SC (int)	4 pt. bend + IP	28; 35	0.40
		4131-7	TWC	4 pt. bend	18; 25	0.40
		4131-8	SC (int)	4 pt. bend	31; 32	0.40
DP2-F11	A333 Gr 6	4111-1	TWC	4 pt. bend	59; 37	0.35[g]
DP2-F13	A106 Gr B	4112-9	SC (int)	4 pt. bend	25, 31, 39, 25, 25; 40, 48, 36, 27, 18, 27	N.D.
DP2-F26	A515 Gr 60	4111-2	TWC	4 pt. bend	15, 34; 27, 32	0.51[f]
DP2-F29	A106 Gr B	4112-8	SC (int)	4 pt. bend	29; 38	0.55[f]
DP2-F29W	SAW in A106 Gr B	4141-9	TWC	4 pt. bend + IP	30, 13; 52[h]	0.55
DP2-F30	A106 Gr B	4112-6	SC (int)	4 pt. bend	30; 42	0.28[f]
		IPIRG 1.2-2	TWC	4 pt. bend[i]	63; 63	0.28
		IPIRG 1.2-4	TWC	4 pt. bend[j]	57; 56	0.28
		IPIRG 1.2-6	TWC	4 pt. bend[k]	27; 29	0.28
		IPIRG 1.2-6A	TWC	4 pt. bend[l]	36; 38	0.28
		IPIRG 1.2-7	TWC	4 pt. bend	51; 34	0.28
		IPIRG 1.2-8	TWC	4 pt. bend[l]	12; 32	0.28
		IPIRG 1.2-10	TWC	4 pt. bend[m]	27; 28	0.28
		IPIRG 1.2-11	TWC	4 pt. bend[l]	29; 30	0.28
DP2-F32	API 5LX65	4111-4	TWC	4 pt. bend	0; 0	0.35[f]

(a) SC (int) = internal surface crack.
SC (ext) = external surface crack.
TWC = through-wall crack.

(b) IP = internal pressure.

(c) Where more than two angles are listed, the crack changed direction; sometimes the new growth angle returned the crack toward the plane of the original circumferential crack. For SC pipe, the angle is after the crack grows beyond the initial notch.

(d) Ratio of minimum to maximum toughness.

(e) Not determined.

(f) Determined from Charpy V-notch impact tests in two, or more, directions.

(g) Determined from compact-specimen tests in two directions. Note that the minimum-toughness direction was at angle of approximately 66 degrees to the circumferential direction in this seamless pipe.

(h) Cracks grew out of weld metal into base metal.

(i) Cyclic loading; R ratio (i.e., min. load/max. load) = 0.

(j) Cyclic loading; R = -1.

(k) Cyclic loading at high rate; R = -1.

(l) Monotonic loading at high loading rate.

(m) Cyclic loading at high rate; R = 0.

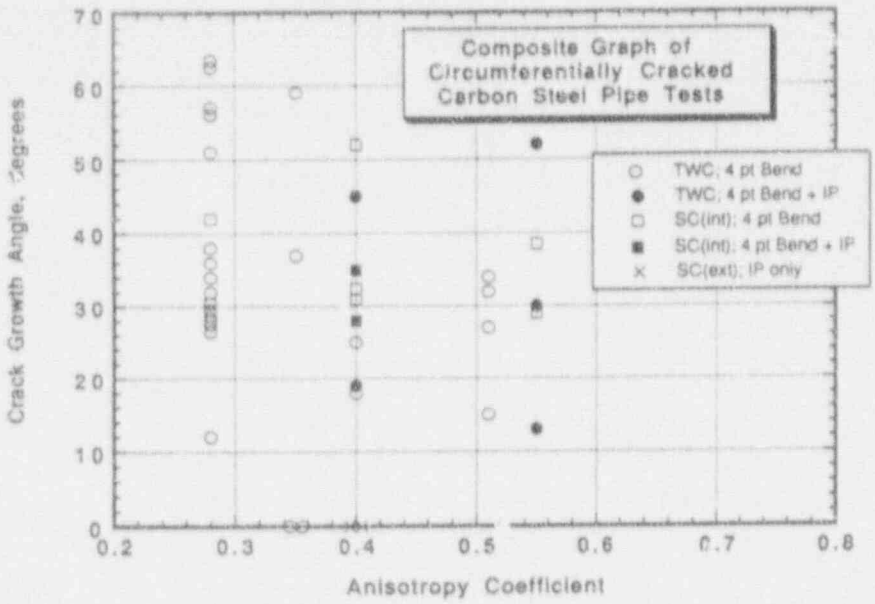

Figure 6.1 Crack-growth angle versus anisotropy coefficient for circumferentially cracked carbon steel pipes tested at Battelle (see Table 6.1 for key to abbreviations)

SC-SA-5/92-F6.1

Activity 5.1.2—Conduct Tensile tests at Different Orientations. This activity has been completed. The data will be put into a digital format for future incorporation to the PIFRAC data base.

Activity 5.1.3—Determine Driving Force for Angled Growing Crack. No efforts are planned for next year.

Activity 5.1.4—Determine Angled Crack Principal Stresses. No efforts are planned for next year.

Activity 5.1.5—Formulate Approximate Corrections. No efforts are planned for next year.

Activity 5.1.6—Assess if Optional Efforts are Necessary. No efforts are planned for next year.

6.4.2 Subtask 5.2 Determine Magnitude of Toughness Anisotropy and Establish a Screening Criterion to Predict Out-of-Plane Crack Growth

There are three activities in this subtask. The plans for each of these are given below.

Activity 5.2.1—Document Inclusion Size, Shape, Distribution, and Orientation in Carbon-Steel Pipes. These efforts have been completed.

Activity 5.2.2—Examine Literature and Conduct Tests to Determine Toughness Anisotropy as a Function of Inclusion Characteristics. These efforts have been completed.

Activity 5.2.3—Assess Usefulness of Screening Tests to Predict Out-of-Plane Crack Growth. These efforts were initiated during the current reporting period and will be completed during the next year.

6.4.3 Subtask 5.3 Prepare Interim and Topical Reports on Anisotropy and Mixed-Mode Studies

No efforts are planned for this subtask next year.

6.4.4 Optional Subtask 5.4 Establish Ductile Crack Growth Resistance Under Mixed-Mode Loading

No efforts are planned for this optional subtask next year.

6.4.5 Optional Subtask 5.5 Refine J-Estimation Scheme Analyses for Pipes

No efforts are planned for this optional subtask next year.

6.5 References

6.1 Wilkowski, G. M. and others, "Degraded Piping Program - Phase II," Summary of Technical Results and Their Significance to Leak-Before-Break and In-Service Flaw Acceptance Criteria, March 1984 - January 1989, Battelle, NUREG/CR-4082, Vol. 8, March 1989.

6.2 Scott, P. and Brust, F., "An Experimental and Analytical Assessment of Circumferential Through-Wall-Cracked Pipes under Pure Bending," Battelle Topical Report from NRC Degraded Piping Program, NUREG/CR-4574, September 1986.

6.3 Wilkowski, G. M. and others, "Short Cracks in Piping and Piping Welds," Battelle, NUREG/CR-4599, BMI-2173, Vol. 1, No. 2, December 1991.

6.4 Matrosov, Yu. I. and Polyakov, I. E., "Improving Toughness and Ductility and Reducing Property Anisotropy in Low Alloy Steels," BISI Translation 14384, Stal', 1976 (2), pp.162-167.

6.5 Burnos, V. A., Vaschilo, T. P., and Balandina, L. E., "Evaluation of the Quality of the Metal of Pipes According to Impact Toughness with Anisotropy Taken into Account," Industrial

Laboratory (USSR); English Translation of Zavodskaya Laboratoriya, Vol. 54, No. 5, May 1988, pp. 548-550.

6.6 Harada, S., Endo, T., and Kaseda, M., "Effects of Forging Ratio and Specimen Orientation on Elastic-Plastic Fracture Toughness of Thick Forged Steel Plates," Role of Fracture Mechanics in Modern Technology, G. C. Sih, H. Nisitani, and T. Ishihara Eds., Elsevier Science Publishers, 1987, pp. 485-496.

6.7 Kramer, G. S., Wilkowski, G. M., and Maxey, W. A., "Flaw Tolerance of Spiral Welded Line Pipe," Battelle Report to American Gas Association, American Gas Association Catalog No. L51514, January 1987.

6.8 Rosenfield, A. R. and Hahn, G. T., "Metallurgical Origins of Fracture Toughness," in 5th Symposium on Line Pipe Research, American Gas Association Catalog No. L30174, November 20, 1974.

6.9 Williams, D. N., "Metallurgical Factors," in 6th Symposium on Line Pipe Research, American Gas Association Catalog No. L30175, October 29, 1979.

6.10 Hodge, J. M., Frazier, R. H., and Boulger, F. W., "The Effect of Sulfur on the Notch Toughness of Heat-Treated Steels," Transactions of the Metallurgical Society of AIME, Volume 215, October 1959, pp. 745-753.

6.11 Tomita, Y., "Effect of Decreased Hot-Rolling Reduction Treatment on Fracture Toughness of Low-Alloy Structural Steels," Metallurgical Transactions A, Vol. 21A, September 1990, pp. 2555-2563.

6.12 Garwood, S. J., "The Effect of Temperature, Orientation, and Constraint on the Toughness of A533 Class 1 Steel," Application of Fracture Mechanics to Materials and Structures, Martinus Nijhoff Publishers, 1984, pp. 939-950.

6.13 Park, J. W., Kim, J. S., and Moon, I. G., "The Effect of Banded Structure and Sulfide Morphology on the Anisotropy of Tensile Ductility and Impact Toughness," Journal of the Korean Institute of Metals, Vol. 22, No. 7, July 1984, pp. 588-595 (in Korean).

6.14 Fegredo, D. M., Faucher, B., and Shehata, M. T., "Influence of Inclusion Content, Texture and Microstructure on the Toughness Anisotropy of Low Carbon Steels," Strength of Metals and Alloys, Vol. 2, Pergamon Press, Ltd., Oxford, 1985, pp. 1127-1132.

7. TASK 6 CRACK-OPENING AREA EVALUATIONS

7.1 Task Objective

The objective of this subtask is to make improvements in the crack-opening area predictions for circumferentially cracked pipe, with particular attention to cracks in welds. The crack-opening area (COA_R) analyses will be incorporated into the SQUIRT code.

7.2 Task Rationale

From past efforts in the Degraded Piping Program, IPIRG, and ASME Section XI round-robin efforts, it has been found that the leakage area predictions are reasonably consistent for circumferential through-wall-cracked pipe in bending (with the cracks in the base metal). For the case of a crack in the center of the weld, the predictions showed more scatter in the intermediate to higher bending load levels. For the case of a crack in the base metal, but with the pipe in combined bending and tension, the scatter in the results was significantly greater. If the crack had been in a weld under combined loading, the scatter probably would have increased even more. The accuracy of the solutions for a crack in a weld and for cracked pipe under combined loading needs verification and improvement for LBB analyses.

7.3 Task Approach

The five specific subtasks in this task are:

Subtask 6.1	Create combined loading improvements
Subtask 6.2	Implement short TWC crack-opening improvements
Subtask 6.3	Improve weld crack evaluations
Subtask 6.4	Modify SQUIRT Code
Subtask 6.5	Prepare topical report on crack-opening area improvements
Subtask 6.6	Leak rate quantification.

Work was conducted only in Subtask 6.6 during this reporting period.

7.3.1 Subtask 6.6 Leak Rate Quantification

This is a new subtask created during the course of this program. Its objective, rationale, and approach are given below.

7.3.1.1 Objective

The objective of this effort is to perform analyses to support changes to the NRC's current Regulatory Guide 1.45, "Reactor Coolant Pressure Boundary Leakage Detection Systems."

7.3.1.2 Rationale

Regulatory Guide 1.45 was published in May 1973 and is now considered outdated. The NRC currently wants to update this procedure, taking into account the current leak-detection instrumentation capabilities, experience from the accuracy of leak detection systems in the past, and current analysis methods to assess the significance of detectable leakage relative to the structural integrity of the plant. Leak-detection capabilities at normal operating conditions are used in current leak-before-break (LBB) analyses. The consistency of the LBB procedures needs to be considered in any changes to Regulatory Guide 1.45, and the impact of such changes on structural integrity of piping not approved for LBB needs to be considered.

7.3.1.3 Approach

The analyses to be performed shall build on other work being done in Task 6. The specific work to be performed shall include the following activities.

Activity 6.6.1	Develop the technical background information for verification of analyses to be used
Activity 6.6.2	Develop SQUIRT4 and SQUIRT5 Codes
Activity 6.6.3	Evaluate the proposed changes in leak detection requirements in terms of the potential impact on LBB analyses
Activity 6.6.4	Evaluation of the proposed changes on leak rate for "non-LBB" piping systems
Activity 6.6.5	Coordination with NRC-RES and NRC-NRR staff
Activity 6.6.6	NUREG report.

Detailed approaches for some of the above activities (Activities 6.6.1, 6.6.3, and 6.6.4) are described in the second semiannual report (Ref. 7.1) and will not be repeated here. Activity 6.6.2 is a new activity created since the last semiannual report. The effort under this activity involves modification of a computer code SQUIRT, which was previously developed at Battelle in conjunction with the IPIRG program (Ref. 7.2). The modified versions (SQUIRT4 and SQUIRT5) will allow the determination of circumferential crack size for a specified leak rate and load condition with known geometric and material properties of the pipe.

Progress to be reported is limited to several efforts under Activities 6.6.1 and 6.6.2. The details of these efforts are reported below.

Activity 6.6.1 Develop the Technical Background Information for Verification of Analyses

The efforts involved in this activity include:

(1) Obtaining typical system normal plus safe shut-down earthquake (SSE) stresses. This shall be done by reviewing information in technical reports and through guidance from NRC-NRR staff.

Material property data to be used shall come from the NRC's PIFRAC database (Ref. 7.3), the Degraded Piping Program (Ref. 7.4), and the IPIRG program (Ref. 7.2) as applicable.

(2) Verification analyses shall be conducted to define the areas of uncertainty in the analyses prior to conducting the necessary sensitivity studies. Such verification analyses shall include:

(a) Comparisons of predictions and experimental data for center-crack-opening displacement and failure loads for complex-cracked pipe.

(b) Evaluation of crack morphology effects on the leak-rate analyses. This shall involve examining photographs of fracture surfaces from various reports and actual surfaces where obtainable, to assess the different parameters necessary in the leak-rate analyses.

(c) Evaluation of the effect of restraint of induced bending for pressure/tension loads for TWC pipe. The effect could be to lower the crack-opening displacement from that calculated in typical LBB analyses.

(3) To establish confidence in the analysis procedures, benchmark leak-rate and failure load predictions shall be conducted for cracks that have been found by leakage in service.

Progress to date is limited to Items 2(a) and 2(c).

Activity 6.6.1(2a) Comparisons of predictions and experimental data for center-crack-opening displacement and failure load for complex-cracked pipe

The effort on Activity 6.6.1(2a) involves background and verification calculations for various complex-cracked pipes. The study focuses on the calculation of maximum loads and crack-opening displacements (COD) by estimation methods for various complex-cracked pipes subjected to remote bending loads. These theoretical predictions are then compared with existing experimental data from the Degraded Piping Program (DPP) (Ref. 7.4).

Elastic-Plastic Fracture

A complex crack is a very long, internal surface crack in a pipe, which may penetrate the wall thickness, thereby creating a short through-wall crack in the same plane as the surface crack. Figures 7.1(a) and 7.1(b) show an idealized through-wall crack and internal surface crack. When the surface crack encompasses the entire pipe circumference, under external load it may penetrate the pipe thickness and hence may become a complex crack as exhibited in Figure 7.1(c). When subjected to further loading, the likelihood of pipe instability and/or arrest then requires understanding the structural behavior of complex-cracked pipe. Understanding the behavior of complex cracks, therefore, aids in performing leak-before-break analysis.

For accurately predicting the load-carrying capacity of complex-cracked pipes, an analysis based on fracture mechanics methodologies is necessary. Since nuclear power-plant piping materials are

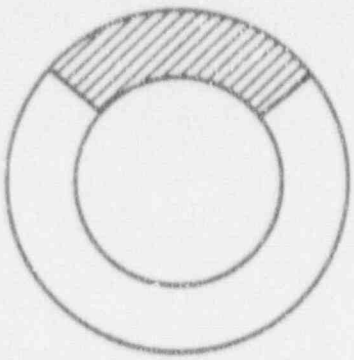

(a) Simple Through-Wall Crack

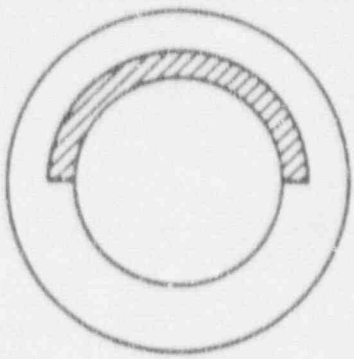

(b) Internal Surface Crack

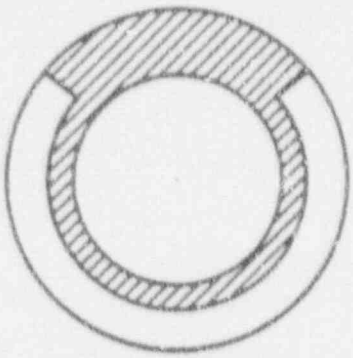

(c) Complex Crack

Figure 7.1 Typical crack geometries in piping and piping welds

SC-SA-5/92-F7.1

generally tough and ductile, the fracture mechanics approach should include elastic-plastic considerations. However, elastic-plastic fracture mechanics analysis of a complex-cracked pipe in bending poses a formidable problem even with three-dimensional finite element analysis. The main difficulty is in determining the crack driving force, since attention must be given to both radial and circumferential crack-growth directions. Another complicating factor is that the surface crack may close in the compressively stressed region of the pipe. This would necessitate the use of special techniques to model the resulting load transfer across the cracked surfaces.

A detailed numerical investigation of the complex-cracked pipe problem using three-dimensional finite element nonlinear analysis would be prohibitively expensive and is considered beyond the scope of the current effort. Instead, simple engineering estimation techniques will be used. In general, the estimation schemes may be classified as either predictive or generative. Predictive schemes usually require knowledge of the crack-growth resistance and plastic-flow behavior of the material. This information is used to predict the load-displacement behavior of the structure, including loads and displacements at crack initiation and at crack-growth instability. Generative schemes require knowledge of the experimentally applied load (or displacement) versus crack-growth data, and are used to calculate crack-growth resistance as a function of crack extension.

In the engineering elastic-plastic fracture mechanics approach, the crack driving force is commonly expressed in terms of J, which represents the energy release rate of a cracked body. The corresponding crack growth resistance is the J-resistance curve of the material. Typically, a generative J-estimation method is used in analyzing small-scale bend or compact tension [C(T)] specimen data to calculate the J-resistance curve. These data consist of load and load-line displacement as functions of crack extension. Next, a predictive J-estimation method is used to determine the loads and displacements at crack initiation, during stable growth, and at crack-growth instability in pipes. Part of the input to the predictive analysis is the J-resistance curve. Typically, a lower bound J-resistance curve is used in the interest of conservative prediction.

Strictly speaking, precise formulas to calculate J for a complex-cracked pipe in bending have not yet been developed, primarily because the problem is too complicated to allow using the usual strength-of-material analyses employed in estimating J for simpler problems. Here, it is assumed that the available generative and predictive J-estimation formulas for simple through-wall circumferentially cracked pipes in bending can be applied to analyze complex-cracked pipes. This is done by adjusting the pipe radius and the thickness in the crack plane to account for the presence of the surface crack. Thus, any radial crack-driving force contribution is ignored. Only growth of the through-wall crack in the circumferential direction is considered. Also, possible closure of the surface crack in the compressively stressed region of the crack plane is frequently not included in the analysis, which is believed to cause the loads to be underpredicted and the crack opening to be overpredicted.

η-factor Analysis of Complex-Cracked Pipe

J-resistance curves for the complex-cracked pipes are obtained using what is known as an η-factor approach (Ref. 7.5). In essence, this involves calculating the elastic component J_e and the plastic component J_p of the total energy release rate J. Consider a through-wall-cracked (TWC) pipe with adjusted mean radius R^*, adjusted thickness t^*, and an initial crack angle 2θ which is subjected to a remote bending moment M. The elastic and plastic components of the total energy release rate are given by

$$J_e = \frac{1}{E}\left[\sigma\sqrt{\pi R^*\theta}\; F_B\left(\frac{\theta}{\pi}, \frac{R^*}{t^*}\right)\right]^2 \tag{7-1}$$

$$J_p = -\frac{F'(\theta)}{2\,R^*t^*F(\theta)}\int^P P\, d\Delta_p \tag{7-2}$$

in which $\sigma = M/\pi R^{*2}t^*$ is the far-field uniaxial tensile stress, $F(\theta) = \cos(\frac{1}{2}\theta) - \frac{1}{2}\sin(\theta)$, E is the modulus of elasticity, P is the concentrated load in the four-point bending, and Δ_p is the plastic part of the load-point displacement, and F_B is a dimensionless geometry function of θ/π and R^*/t^* which is tabulated in Reference 7.6. The prime in Equation 7-2 denotes the symbol for ordinary differentiation with respect to the argument. Also in Equation 7-2, the plastic component of the J-resistance curve is based on Ernst's J_M (modified J) parameter (Ref. 7.7) for analyzing data beyond J-controlled growth. No correction was made to account for crack growth as required in obtaining J_D (deformation J). In

this study, the J-resistance curve will be represented by the J_M-resistance curve defined above. On the basis of Equations 7-1 and 7-2, the J_M-resistance curves can be determined from a single pipe experiment once the simultaneous measurement of load, load-point displacement, and crack extension are provided.

J-Resistance Curves

In common elastic-plastic fracture mechanics applications, J_M-resistance curves are obtained from small-specimen data. To determine whether these can be used to reliably and accurately predict the elastic-plastic crack growth behavior in nuclear power-plant pipes, it is worthwhile to assess how these J_M-resistance curves compare with those obtained from the complex-cracked pipes.

In Reference 7.8, a detailed study comparing the J_M-resistance curves from the C(T) specimens and pipe test data was carried out. For example, Figure 7.2 shows a plot of J_M versus crack extension Δa obtained from both η-factor analysis (generative J-estimation) and C(T) specimen data for two Type 304 stainless steel complex-cracked pipe experiments (Experiment 4113-1 and 4113-2) conducted in Reference 7.8. Results from these experiments along with others performed in the same reference and elsewhere consistently show that the complex-cracked pipe resistance curves are significantly lower than the side-grooved C(T) specimen resistance curves. The quantitative aspects of the study in Reference 7.8 also indicate that the ratio of J_M-resistance obtained from complex-cracked pipe tests and C(T) specimens is strongly correlated with the pipe geometric parameter d/t, where d and t represent the depth of the surface crack and the thickness of the pipe, respectively. This ratio is also found to be invariant with respect to crack length increment Δa at which it is evaluated.

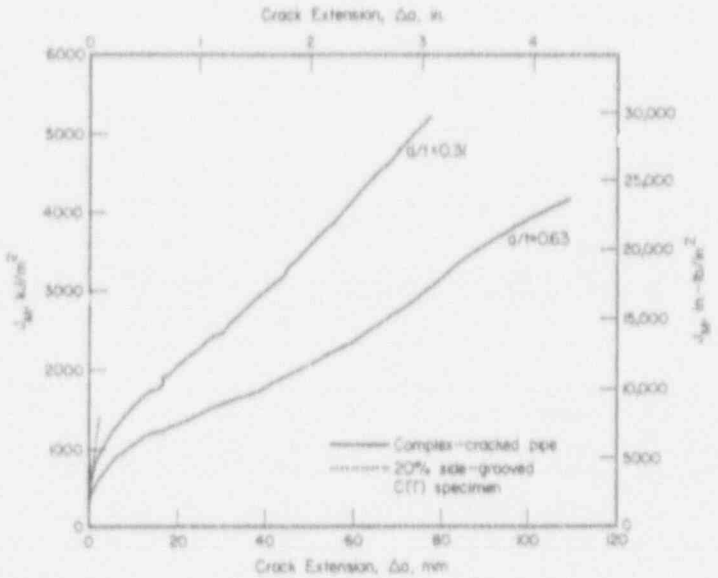

Figure 7.2 Comparison of J_M-resistance curves from pipe experiments and C(T) specimen data

SC-SA-5/92-F7.2

The above observations on J_M-resistance curves from the experiments performed in References 7.8, 7.9, and 7.10 suggest that it may be useful to establish a constraint factor $\hat{C}$ as a function of d/t. Consequently, simple through-wall-cracked pipe resistance curves which are adequately represented by compact tension specimen data may then be used to predict complex-cracked pipe resistance curves. For example, using the currently available data, one can find the points on a complex-crack J_M-resistance curve (J_M^{CC}) knowing the points on the corresponding through wall-crack J_M-resistance (J_M^{TWC}) by using the following relation:

$$J_M^{CC} = \hat{C}\, J_M^{TWC} \tag{7-3}$$

where the value of $\hat{C}$ as a function of d/t can be found from an available data base generated from available pipe experiments. Figure 7.3 shows the plot of $\hat{C}$ versus d/t created from various pipe tests performed by DTRC (Ref. 7.10) and Battelle (Refs. 7.8 and 7.11).

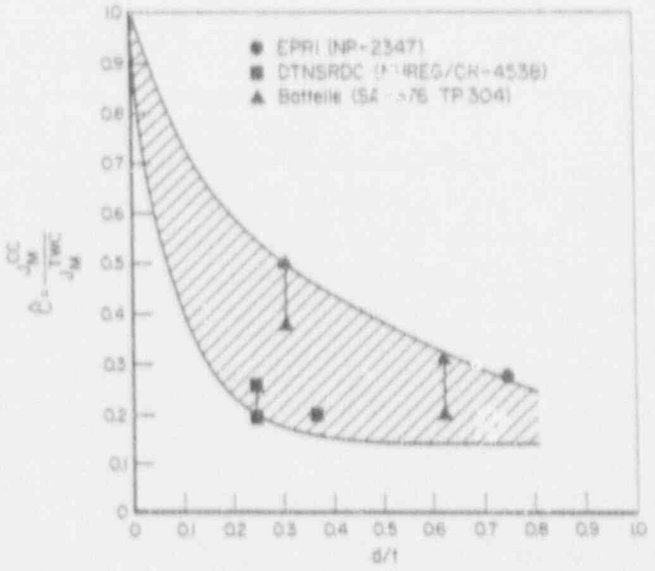

Figure 7.3 Complex-cracked pipe constraint factor as a function of d/t ($\hat{C}$ values from upper bound curve)

SC-SA-5/92-F7.3

Predictive J-Estimation Method

As discussed earlier, the two different types of J-estimation schemes are the generative and the predictive. While generative schemes are used for determining the fracture resistance of the material, the predictive schemes are needed to obtain predictions of loads and displacements at crack initiation,

during stable crack growth, and at instability, provided the fracture resistance of the material is known. Currently, available predictive J-estimation schemes applicable to cracked-pipe geometries include the GE/EPRI method (Ref. 7.12), the Paris method (Ref. 7.13), the LBB.NRC technique (Ref. 7.14), the LBB.ENG1 and LBB.ENG2 methods (Refs. 7.15 and 7.16), among others. These estimation schemes are, however, mainly developed for simple TWC pipes. To date, no estimation method exists for evaluating the performance of complex-cracked pipes subjected to external loads.

In this study, the LBB.ENG2 method will be used to determine various fracture parameters of interest. Details of this method can be obtained from the original references (Refs. 7.15 and 7.16) In performing analytical calculations, it is assumed that the J-estimation formulas (LBB.ENG2) for simple through-wall-cracked pipes can be applied to analyze complex-cracked pipes. This is accomplished by adjusting the pipe radius and the thickness in the cracked plane to account for the presence of the internal surface crack. Thus, any radial crack-driving force contribution is ignored. Only growth of the through-wall crack in the circumferential direction is considered. In addition, possible closure of the surface crack in the compressive region of the crack plane is not included in the analysis.

Numerical Results

In order to meet the objectives of this study, results of ten complex-cracked pipe experiments conducted under the Degraded Piping Program (DPP) (Ref. 7.4) are considered. These are Experiments 4113-1, 4113-2, 4113-3, 4113-4, 4113-5, 4113-6, and 4114-1, 4114-2, 4114-3, 4114-4. Table 7.1 shows the test matrix of complex-cracked pipe tests considered in this study. Background and verification calculations are carried out by (1) analytically (theoretically) predicting maximum loads and center-crack-opening displacements of various complex-cracked pipes from these tests, and (2) comparing the theoretical results with those obtained from the aforementioned experimental data. In the predictive estimation method, two cases based on the selection of J_M-resistance curves are investigated. One corresponds to using a constraint factor of 1, implying the use of the J_M-resistance curve for C(T) specimen data without any reduction (J_M^{TWC}). The other is based on a J_M-resistance curve of C(T) specimens multiplied by the relevant reduction factor $\hat{C} < 1$ as a function of d/t (J_M^{CC}). Table 7.2 shows the numerical values of the $\hat{C}$ factors corresponding to each of the experiments considered in this study. The $\hat{C}$ values are obtained from the upper curve in Figure 7.

In conducting the predictive calculations, various analytic idealizations are considered. For example, it is assumed that the constitutive law characterizing a material's stress-strain response can be represented by the Ramberg-Osgood model

$$\frac{\epsilon}{\epsilon_0} = \frac{\sigma}{\sigma_0} + \alpha \left(\frac{\sigma}{\sigma_0}\right)^n \tag{7-4}$$

in which σ_0 is a reference stress, E is the modulus of elasticity, $\epsilon_0 = \sigma_0/E$ is the reference strain, and α and n are model parameters usually chosen from a best fit of laboratory data. Also, the J_M-

Table 7.1 Test matrix of complex-cracked pipe experiments

Expt. No.	Battelle Pipe Material Number	Pipe Material	Outside Pipe Diameter, mm (inches)	Wall Thickness, mm (inches)	$2a/\pi D_m$ [(a)]	$2c/\pi D_m$ [(b)]	d/t[(c)]	Test Temp., C (F)
4113-	DP2-A23	SA-376 TP304 Stainless Steel	168 (6.625)	14.5 (0.570)	0.37	1.0	0.31	288 (550)
4113-2	DP2-A23	SA-376 TP304 Stainless Steel	168 (6.625)	14.5 (0.570)	0.37	1.0	0.63	288 (550)
4113-3	DP2-I1	Inconel 600	168 (6.625)	11.0 (0.435)	0.37	1.0	0.34	288 (550)
4113-4	DP2-I1	Inconel 600	168 (6.625)	11.0 (0.435)	0.37	1.0	0.61	288 (550)
4113-5	DP2-F30	A106 Grade B	168 (6.625)	14.2 (0.560)	0.37	1.0	0.31	288 (550)
4113-6	DP2-F30	A106 Grade B	168 (6.625)	14.2 (0.560)	0.37	1.0	0.64	288 (550)
4114-1	DP2-F31A	A106 Grade B	165 (6.50)	12.7 (0.501)	0.37	1.0	0.47	288 (550)
4114-2	DP2-A23G	SA-376 TP304	167 (6.56)	13.5 (0.530)	0.37	1.0	0.32	288 (550)
4114-3	DP2-A8	SA-358 TP304	414 (16.3)	26.2 (1.03)	0.37	1.0	0.33	288 (550)
4114-4	DP2-A8	SA-358 TP304	414 (16.3)	26.2 (1.03)	0.37	1.0	0.33	288 (550)

(a) 2a is length of through-wall crack.
(b) 2c is length of internal surface crack.
(c) d is depth of internal surface crack; t is thickness of pipe.

Table 7.2 Comparisons of maximum loads for various complex-cracked pipes

Experiment No.	d/t	Constraint Factor, $\hat{C}$	Maximum Load, kN (predicted)		Maximum Load, kN (experiment)	Maximum Load, Exp/Pred	
			C(T) J-R	Using $\hat{C}$		C(T) J-R	Using $\hat{C}$
4113-1	0.31	0.50	115.44	99.59	124.10	1.08	1.24
4113-2	0.63	0.32	61.22	47.92	80.95	1.32	1.68
4113-3	0.34	0.50	115.88	100.21	117.87	1.02	1.16
4113-4[a]	0.61	0.32	66.85	52.52	86.74	1.30	1.65
4113-5	0.31	0.50	169.20	148.93	147.23	0.87	0.99
4113-6	0.64	0.32	88.14	69.94	[illegible]	1.00	1.26
4114-1	0.47	0.40	92.87	77.81	[illegible]	0.89	1.06
4114-2	0.32	0.50	32.18	27.76	[illegible]	0.99	1.04
4114-3	0.33	0.50	150.94	134.87	[illegible]	1.05	1.17
4114-4	0.33	0.50	150.94	134.87	[illegible]	1.01	1.13
					[illegible]age	1.04	1.24
					Std. Dev.	0.16	0.24

(a) Shim used in crack to allow for crack closure on compression side, but closure not accounted for in analysis.

resistance from the C(T) specimen is deemed to be adequately characterized by a linear equation of the form

$$J_M = J_i + m\,\Delta a \qquad (7\text{-}5)$$

in which $\Delta a = R\,\Delta\theta$ is the crack length extension (independent variable), J_i is the resistance threshold of crack initiation, and $m = dJ_M/d(\Delta a) = dJ_M/da$ is the slope of the J_M-resistance curve. Table 7.3 provides the numerical values of various input parameters mentioned earlier that are required to completely define Equations 7-4 and 7-5. These are obtained following an analysis of available test data from the Degraded Piping Program (Refs. 7.4 and 7.8).

Maximum Load Predictions

Table 7.2 gives the maximum loads for the above complex-cracked pipes subject to four-point bending that are obtained from both predictive estimation formulas and experimental data. In the estimation method, the maximum load is obtained based on J-tearing theory. Results suggest that:

(1) The predicted maximum loads for the pipes in Test Series 4113, with shallow surface crack ($d/t \approx 0.3$), compare well with those obtained from experimental observations. They also indicate that the use of J_M^{TWC} for the Experiments 4113-1 and 4113-3 resulted in better predictions than those based on the use of J_M^{CC} while the reverse is true for Experiment 4113-5.

(2) The predicted maximum loads for the pipes in Test Series 4114, estimated with reduced J_M-resistance curve (J_M^{CC}), are closer to experimentally observed values for the smaller pipe diameters (e.g., Experiment 4114-1 and 4114-2). They also indicate, however, that the use of J_M^{TWC} for the larger pipe diameters (e.g., Experiments 4114-3 and 4114-4) resulted in better predictions than those based on the use of J_M^{CC}.

Results from Table 7.2 also indicate that the estimation method underpredict maximum loads for the pipes with deeper surface cracks ($d/t \approx 0.6$), irrespective of the use of any J_M-resistance curves, with the exception of Experiment 4113-6 with J_M^{TWC}. One plausible reason for the general loss of accuracy in the case of deeper surface cracks may be attributed to the oversimplification in the J-estimation formulas for through-wall-cracked pipes.

Center-Crack-Opening Displacement

Figures 7.4 through 7.12 show the plots of applied load versus center-crack-opening displacement up to maximum load for various complex-cracked pipes from Experiments 4113-1, 4113-2, 4113-3, 4113-4, 4113-5, 4113-6 and 4114-1, 4114-2, 4114-3, 4114-4, all under four-point bending. They are obtained from both predictive estimation formulas (LBB.ENG2) and experimental data mentioned previously. Results suggest that in most cases, the exceptions being Experiments 4113-5 and 4114-1 and 4114-2, the predictive estimation model, with either case of J_M-resistance curves, overestimates the COD at all load levels. This can be qualitatively explained by noting that for complex-cracked

Table 7.3 Parameters of Ramberg-Osgood model and J_M-resistance [C(T) specimen] curves for the materials in various pipe experiments

Expt. No.	Material	n	α	ϵ_o	σ_o, MPa (ksi)	J_i, MN/m (klb/in)	m, MN/m^2 (klb/in^2)
4113-1	SA-376 TP304 Stainless Steel	3.8	43.6	0.00160	294.4 (42.7)	1.21 (6.90)	328.2 (47.60)
4113-2	SA-376 TP304 Stainless Steel	3.8	43.6	0.00160	294.4 (42.7)	1.21 (6.90)	328.2 (47.60)
4113-3	Inconel 600	3.9	42.5	0.00182	402.6 (58.4)	1.82 (10.39)	505.3 (73.29)
4113-4	Inconel 600	3.9	42.5	0.00182	402.6 (58.4)	1.82 (10.39)	505.3 (73.29)
4113-5	A106 Grade B Carbon	5.9	7.9	0.00237	470.2 (68.2)	0.10 (0.588)	107.2 (15.55)
4113-6	A106 Grade B Carbon	5.9	7.9	0.00237	470.2 (68.2)	0.10 (0.588)	107.2 (15.55)
4114-1	A106 Grade B	5.9	7.9	0.00237	470.2 (68.2)	0.10 (0.588)	107.2 (15.55)
4114-2	SA-376 TP304	3.8	43.6	0.00160	294.4 (42.7)	1.21 (6.90)	328.2 (47.60)
4114-3	SA-358 TP304	5.5	34.1	0.00180	323.3 (46.9)	0.31 (1.78)	166.9 (24.21)
4114-4	SA-358 TP304	5.5	34.1	0.00180	323.3 (46.9)	0.31 (1.78)	166.9 (24.21)

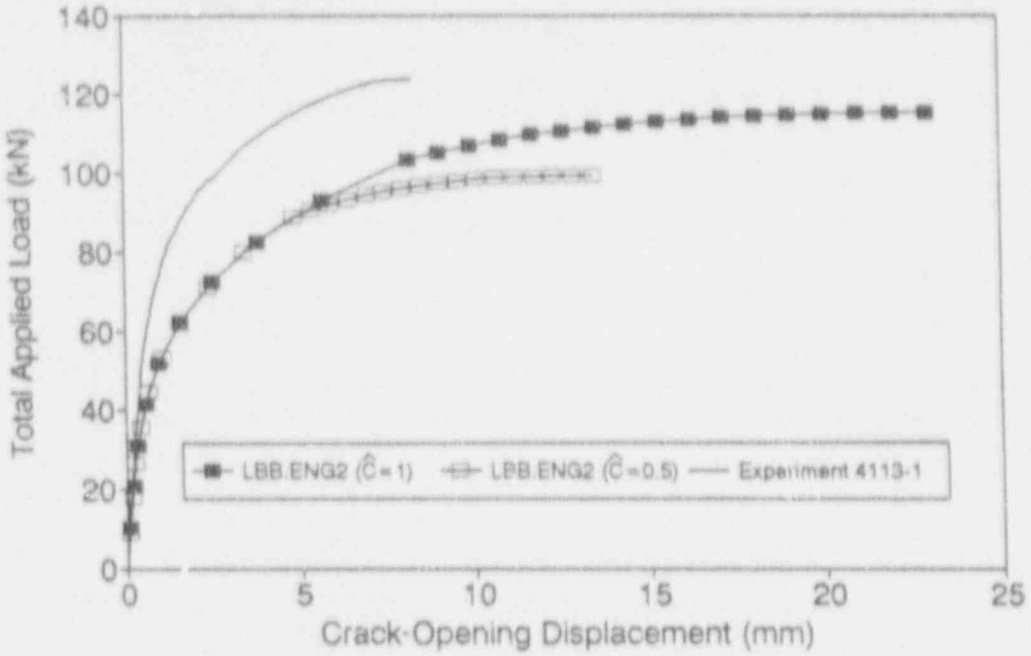

Figure 7.4 Load versus center-crack-opening displacement in Experiment 4113-1

SC-SA-5/92-F7.4

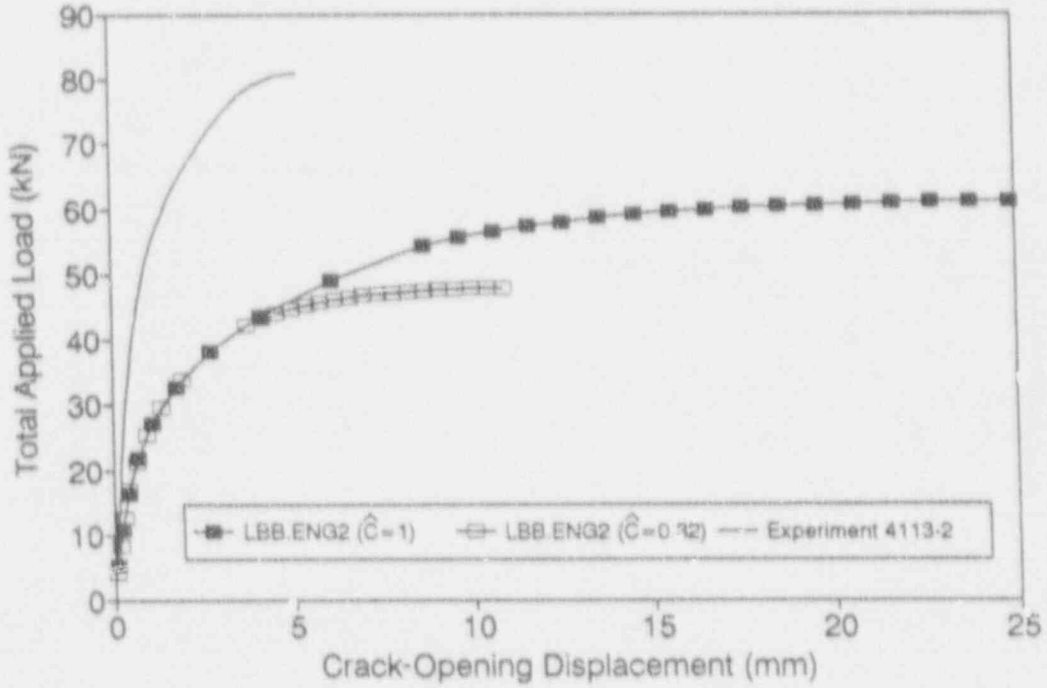

Figure 7.5 Load versus center-crack-opening displacement in Experiment 4113-2

SC-SA-5/92-F7.5

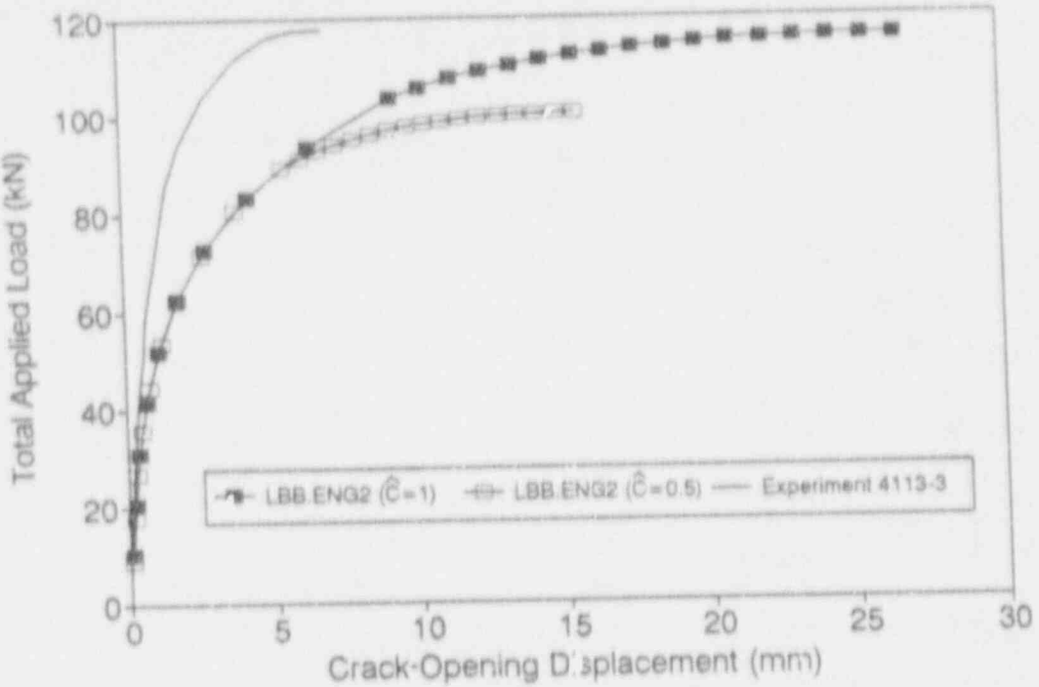

Figure 7.6 Load versus center-crack-opening displacement in Experiment 4113-3

SC-SA-5/92-F7.6

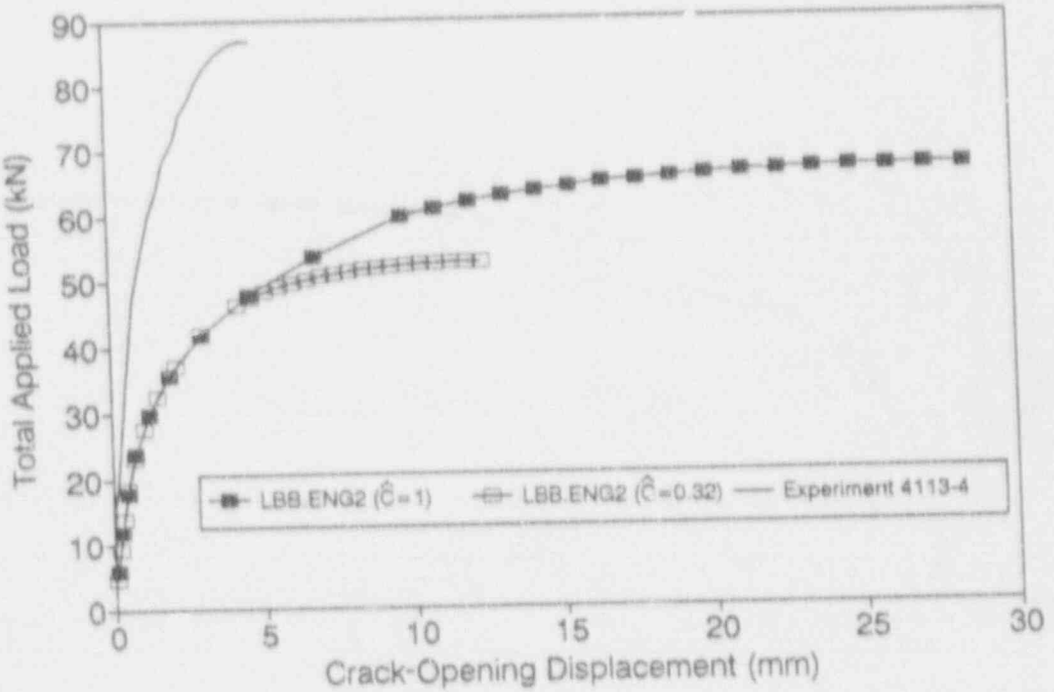

Figure 7.7 Load versus center-crack-opening displacement in Experiment 4113-4

SC-SA-5/92-F7.7

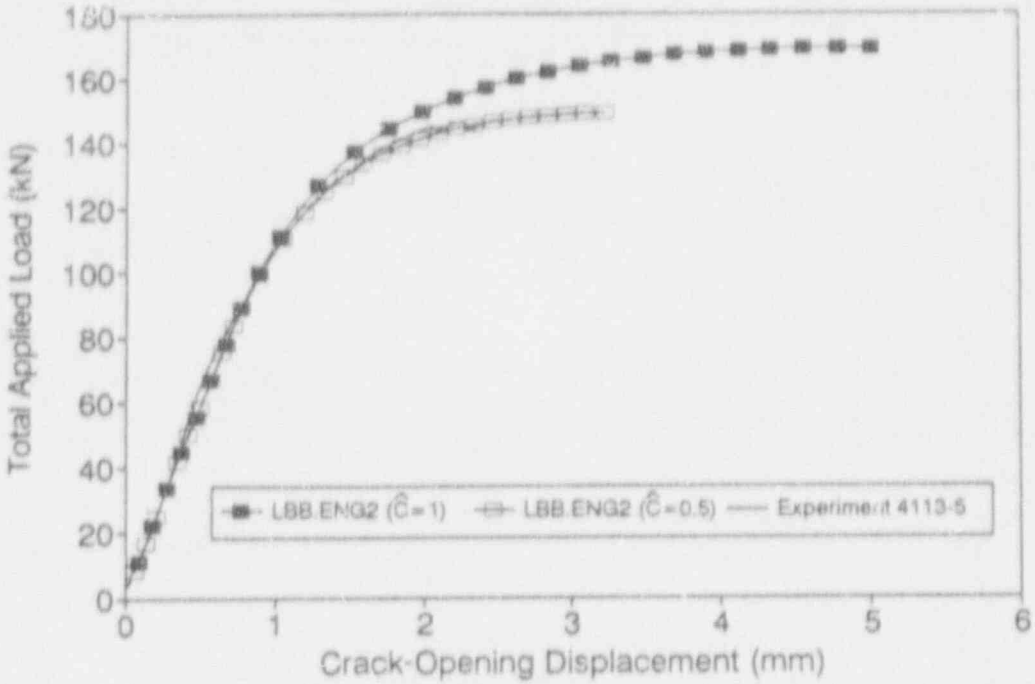

Figure 7.8 Load versus center-crack-opening displacement in Experiment 4113-5

SC-SA-5/92-F7.8

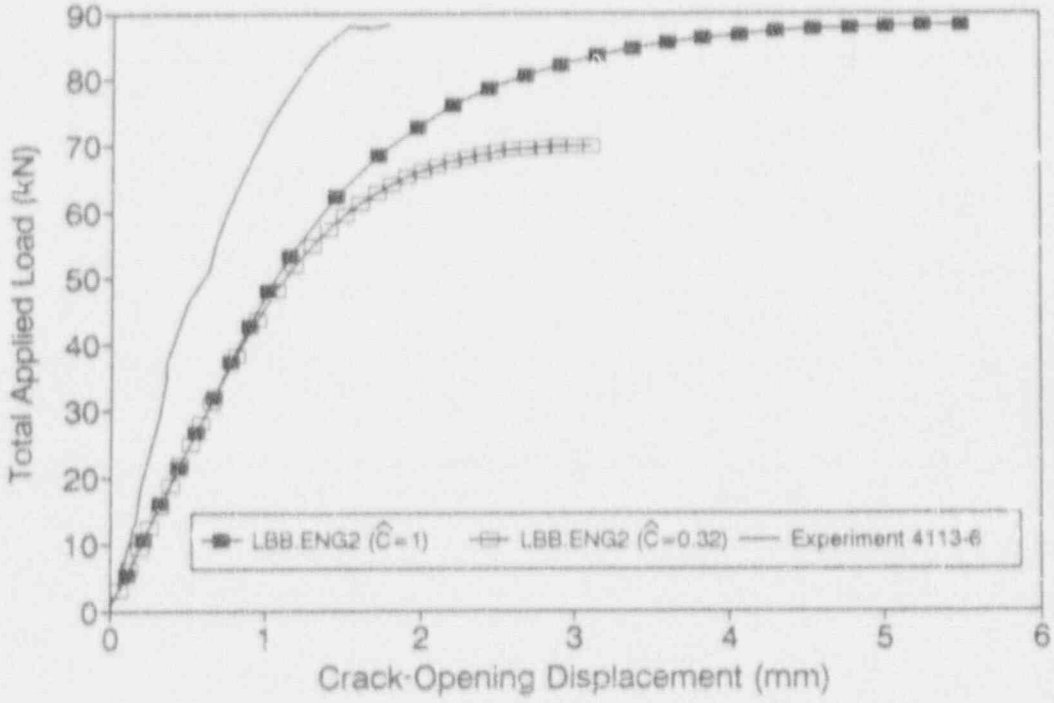

Figure 7.9 Load versus center-crack-opening displacement in Experiment 4113-6

SC-SA-5/92-F7.9

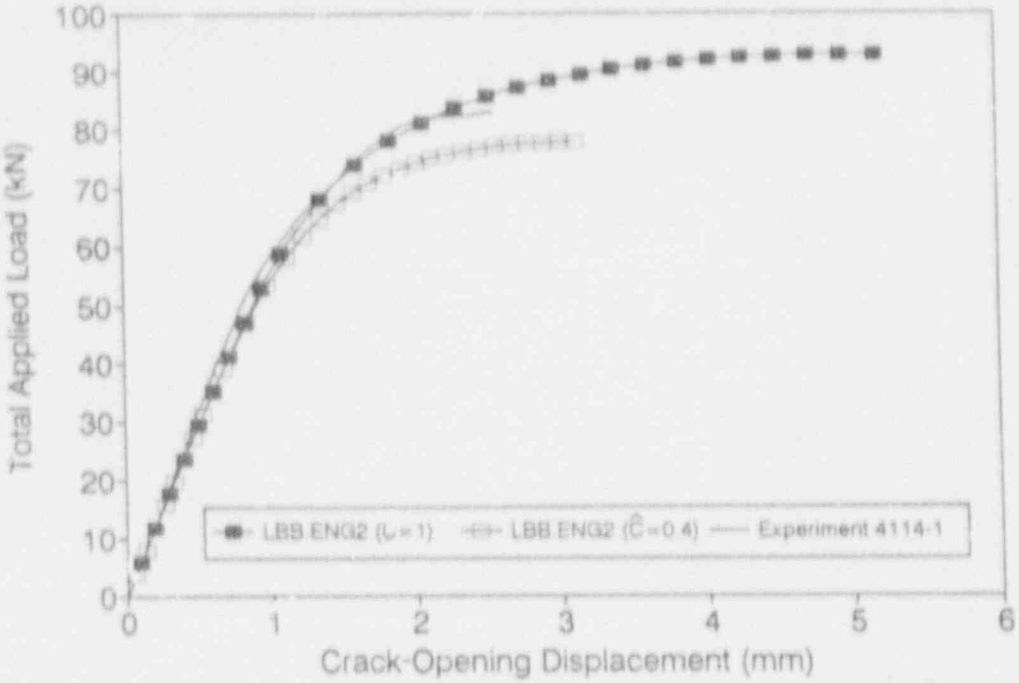

Figure 7.10 Load versus center-crack-opening displacement in Experiment 4114-1

SC-SA-5/92-F7.10

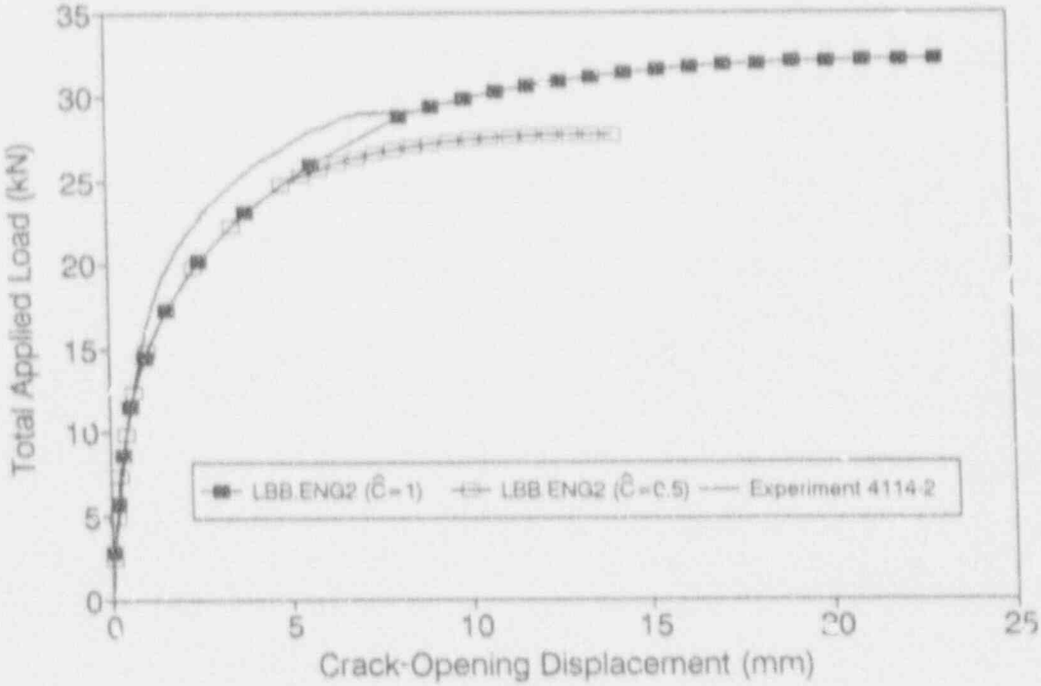

Figure 7.11 Load versus center-crack-opening displacement in Experiment 4114-1

SC-SA-5/92-F7.11

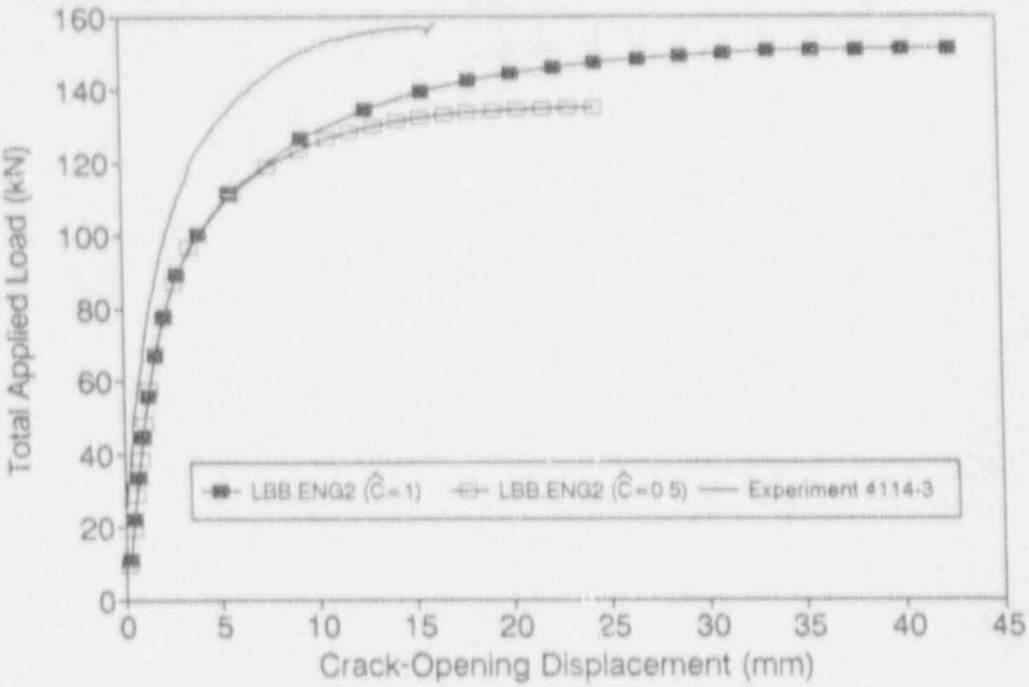

Figure 7.12 Load versus center-crack-opening displacement in Experiment 4114-3

SC-SA-5/92-F7.12

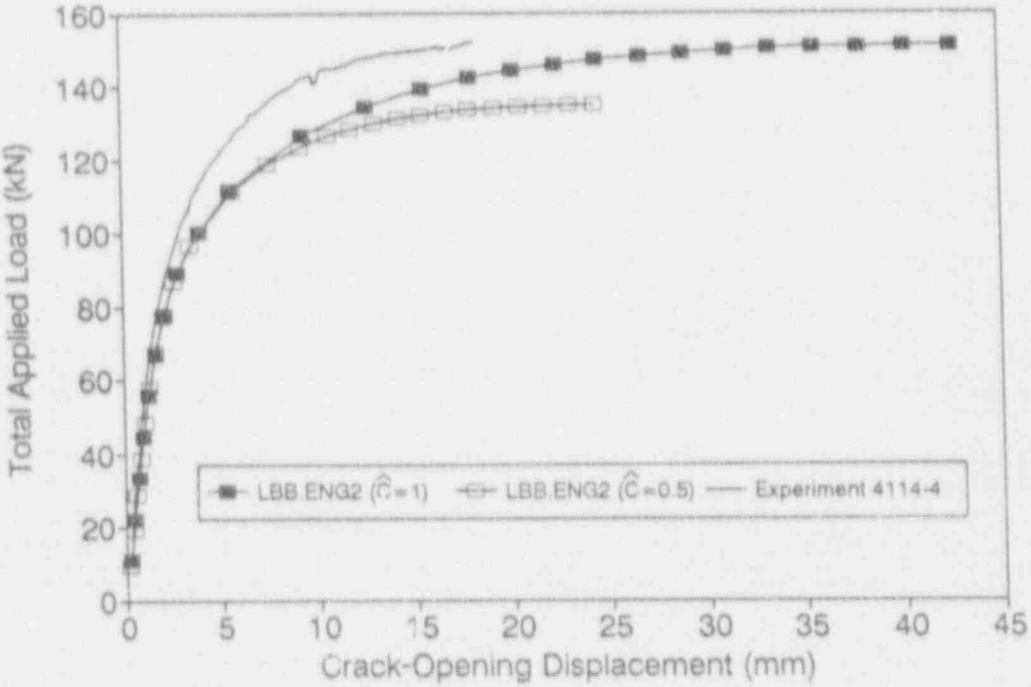

Figure 7.13 Load versus center-crack-opening displacement in Experiment 4114-4

SC-SA-5/92-F7.13

pipes, an effective through-wall cracked pipe thickness $t^* = t - d$ is used in the J-estimation formulas for through-wall cracked pipes. Consequently, the "equivalent" TWC pipe assumed in estimation models will have lower stiffness than actual complex-cracked pipe and, hence, the predicted COD becomes larger when compared with experimental results. Obviously, when the surface crack becomes deeper (e.g., Experiments 4113-2, 4113-4, and 4113-6), the magnitudes of these over-estimates of the COD will also become larger and can be significantly different from the experimental results, as exhibited in Figures 7.5, 7.7, and 7.9. Again, this general loss of accuracy can be attributed to the over-simplification in the J-estimation formulas for TWC pipes used for predicting COD of complex-cracked pipes.

Figures 7.8, 7.10, and 7.11 also indicate that the predicted COD for pipes in Experiments 4113-5, 4114-1, and 4114-2 obtained from both cases of J_M-resistance curves compare reasonably well with the experimentally observed COD values. However, the analytical prediction becomes superior when J_M^{CC} is used as the J_M-resistance curve instead of J_M^{TWC}.

Finally, Figure 7.14 exhibits several plots of COD at maximum load for various experiments considered in this study. As before, results of both predictive estimation model and experimental data are compared. They all consistently show that the use of the J_M-resistance curve from C(T) specimens multiplied by a relevant correction (constraint) factor $C < 1$ (i.e., J_M^{CC}) in Table 7.2 results in better prediction than that based on the use of J_M^{TWC}.

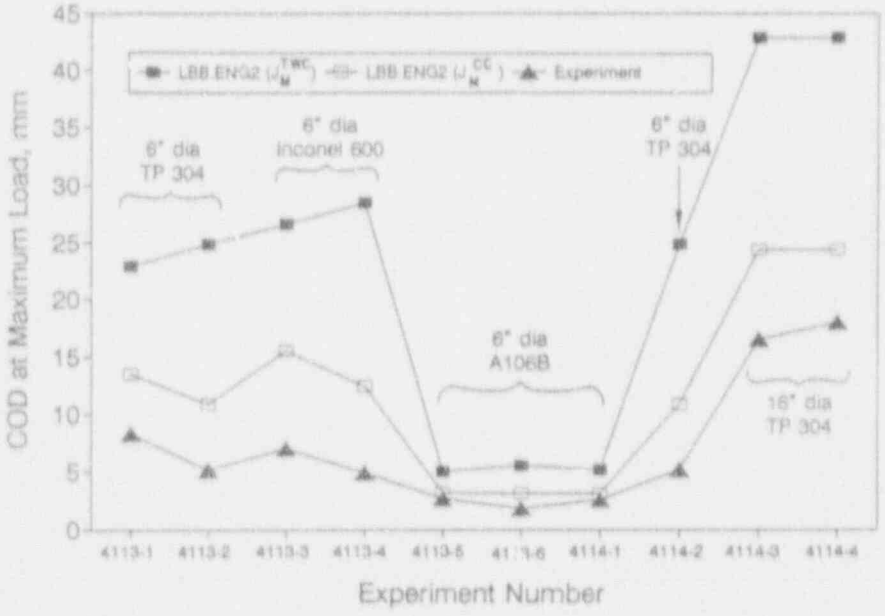

Figure 7.14 COD at maximum load for various complex-cracked pipe experiments

SC-SA-5/92-F7.14

Activity 6.6.1(2c) Evaluation of the effect of restraint of induced bending for pressure/tension loads for TWC pipe

The effort on the Activity 6.6.1(2c) involves evaluation of the effect of induced bending restraint for axial tension loads for circumferential through-wall cracked (TWC) pipe. A linear-elastic finite element analysis is carried out to determine these effects.

Overview

Current structural analyses of TWC pipes subjected to axial tension loads (generally pressure induced) assume that the pipe is free to rotate. The restraint of the rotation increases the failure stresses (Ref. 7.17), but can decrease the crack opening at a given load. If the pipe system restrains the bending (i.e., from cracks being close to a nozzle or restraint from the rest of the piping system) then the leak rate will be less than that calculated by using analyses that assume that the pipe is free to rotate. This will cause the actual crack to be larger than that calculated by the current analyses methods for the same leak rate. Since normal operating stresses have the pressure stress as a large component of the total stress, this can have a significant effect on LBB analyses. Figure 7.15 shows a TWC pipe with mean radius R_m, thickness t, and initial crack angle 2θ which is subjected to an axial tension load with complete restraint of bending at a distance L_R from the crack plane.

Analysis Procedure

Linear elastic analyses by the finite element method (FEM) have been performed to examine the effects of restraint due to induced bending in a piping system when the pressure load is applied. Figure 7.16 shows a typical mesh representing the finite element discretization. Results of crack-opening displacements as a function of "restraint length" are investigated. The restraint length (L_R) referred to here is simply the location of the restrained pipe cross sections relative to the crack plane and is shown in Figure 7.15.

The following are the procedural steps which are undertaken in this study to determine effects of restraint on induced bending:

Step 1: Pick a structural model (finite element model) of a cracked pipe with pipe thickness t, mean pipe diameter D_m, initial crack angle 2θ, and total length $2L_R$ where L_R is the restraint length discussed previously.

Step 2: Apply an arbitrary positive (tensile) displacement loading, Δ, to all the nodes in the cross sections located at a distance L_R from the cracked plane (i.e., the pipe ends in this case) in the longitudinal direction of the pipe. In this way the complete restraint of induced bending is simulated.

Step 3: Conduct the FEM analysis and obtain the COD and the corresponding tension and bending stresses at the cross sections L_R distance away from the cracked plane. Note, the above stresses are determined following additive decomposition of computed

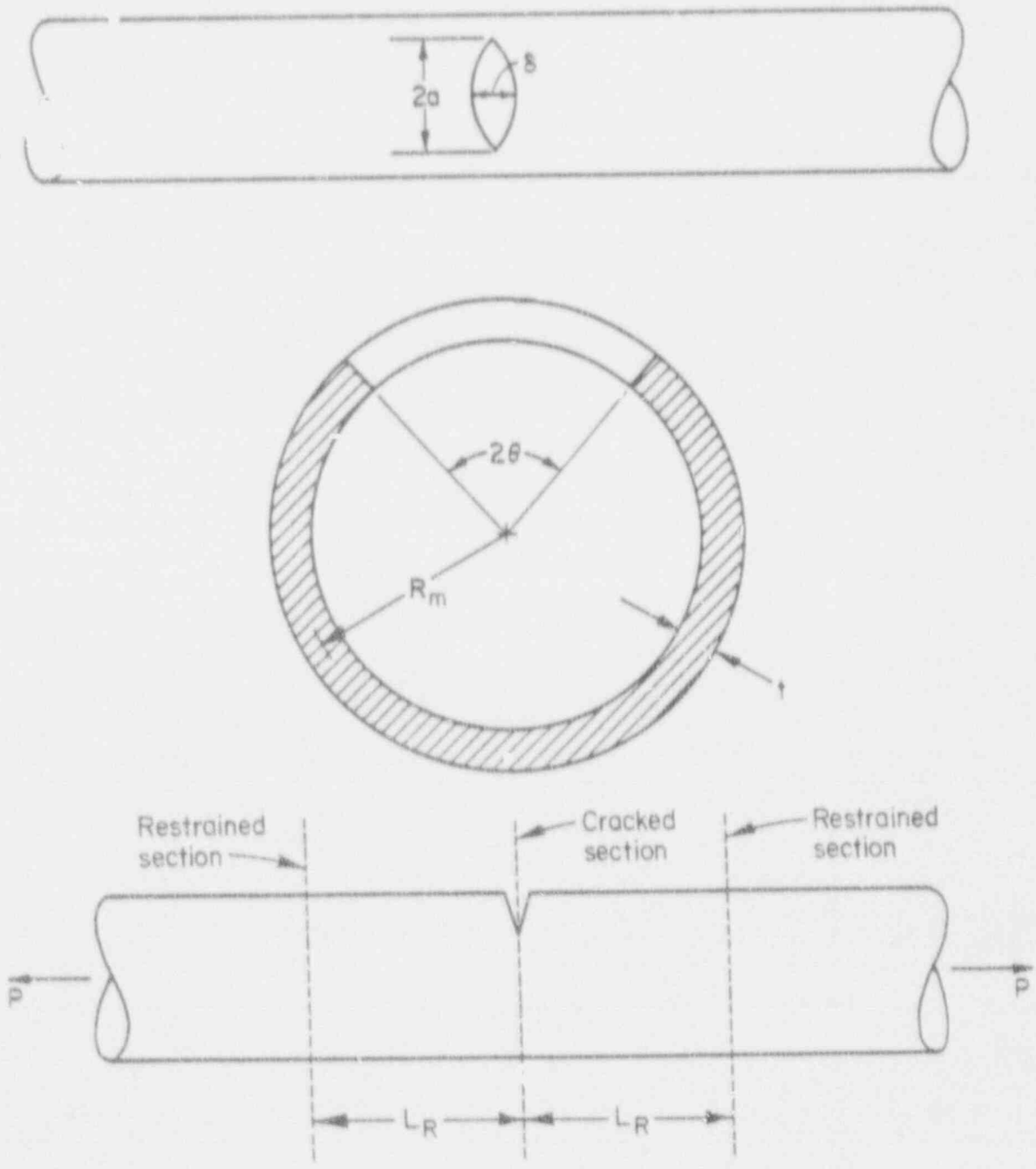

Figure 7.15 Schematics of through-wall-cracked pipe under pure tension (Restrained location prevents rotation and ovalization)

SC-SA-5/92-F7.15

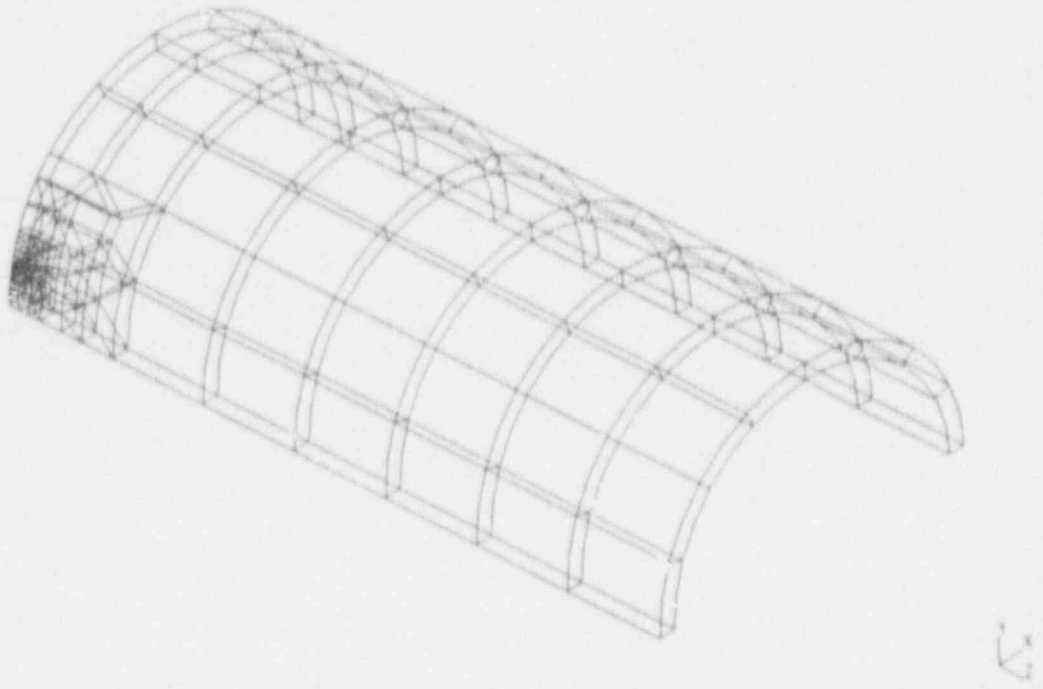

Figure 7.16 *Finite element mesh for linear elastic restraint of crack-opening displacement*

SCM-5/91-F5

reactive stresses at these cross sections. Denote the unscaled COD and the tension stress by δ_{uns} and σ_{ten}, respectively.

Step 4: Compute the scaled COD, $\delta_s = \delta_{uns} \times (\sigma_{ref}/\sigma_{ten})$, where σ_{ref} is any arbitrarily defined reference tensile stress. δ_s now represents the COD due to the reactive tensile stress σ_{ref} with complete restraint of bending at cross sections a distance L_R away from the cracked plane. This scaling is permissible since the analysis is linear elastic.

Step 5: Pick again a structural model (finite element model) and apply a tension stress loading of magnitude σ_{ref} (any value will do) but allowing free rotation. Denote the resultant COD by δ_∞ which now represents the reference crack-opening displacement due to axial tensile stress σ_{ref} when there are no external bending restraints present in the pipe, i.e., when the restraint length L_R approaches infinity.

Step 6: Divide the scaled COD, δ_s, by the reference COD, δ_∞, to get the normalized COD, $\delta_{nor} = \delta_s/\delta_\infty$. δ_{nor} now represents the restrained COD normalized by the unrestrained COD.

Step 7: For a given crack geometry, repeat Steps 1-6 for several values of L_R. Hence, determine the effects of restraint length L_R or normalized restrairt length L_R/D_m on the crack-opening displacement.

Numerical Results

As a numerical example, consider a TWC pipe with R_m = 355.6 mm (14 inches), t = 35.56 mm (1.4 inch), R_m/t = 10, and two distinct cases of initial crack angle 2θ with θ/π = 1/8 and θ/π = 1/4 ("small" and "large" cracks). For material properties, it is assumed that the modulus of elasticity E = 200 GPa (29,000 ksi) and the Poisson's ratio ν = 0.3. The pipe is subjected to remote pressure with the resultant force applied at the centroid of the uncracked pipe cross section. Linear elastic analyses using the finite element method (FEM) were performed using the code ABAQUS (Ref. 7.18). Three-dimensional solid brick elements were used in the FEM.

Tables 7.4 and 7.5 show the calculated values of various crack-opening displacements for both "small" (θ/π = 1/8) and "large" (θ/π = 1/4) cracks. These are obtained following the steps described earlier. Several values of restraint length L_R are considered and are also tabulated. It is assumed here that the arbitrary applied displacement Δ = 2.54 mm (0.1 inch) (Step 2), and L_R/D_m = 10 for both crack angles (Step 5). The arbitrary reference tensile stresses δ_{ref} are assumed to be 650.97 MPa and 849.12 MPa (94.4 ksi and 123 ksi) for θ/π = 1/8 and θ/π = 1/4, respectively (Steps 4 and 5). Following the FEM analysis, the corresponding values of reference COD, δ_{∞}, are computed to be 2.569 mm and 8.692 mm (0.101 inch and 0.342 inch), respectively (Step 5).

Figure 7.17 presents the results of normalized crack-opening displacement (δ_{nor}) as a function of normalized restraint length L_R/D_m in which $D_m = 2R_m$ represents the mean pipe diameter. As mentioned before, the COD values are normalized with reference to the crack-opening displacement when there are no external constraints present in the pipe (i.e., when the restraint length becomes infinity), allowing free rotation and ovalization. Results suggest that when the crack angle is small

Table 7.4 Elastic crack-opening displacements for TWC Pipe (θ/π = 1/8)

L_R/D	Unscaled COD, mm (δ_{uns})	Tensile Stress, MPa (σ_{ten})	Scaled COD, mm (δ_s)	Normalized COD, mm (δ_{nor})
1	2.460	849.12	2.460	0.9573
5	0.547	182.47	2.546	0.9909
10	0.290	95.83	2.569	1.000

Table 7.5 Elastic crack-opening displacements for TWC Pipe (θ/π = 1/4)

L_R/D	Unscaled COD, mm (δ_{unS})	Tensile Stress, MPa (σ_{ten})	Scaled COD, mm (δ_s)	Normalized COD, mm (δ_{nor})
1	4.873	650.97	4.873	0.5606
5	1.624	174.35	6.065	0.6977
10	0.870	75.84	7.469	0.8593
20	0.474	36.54	8.445	0.9716

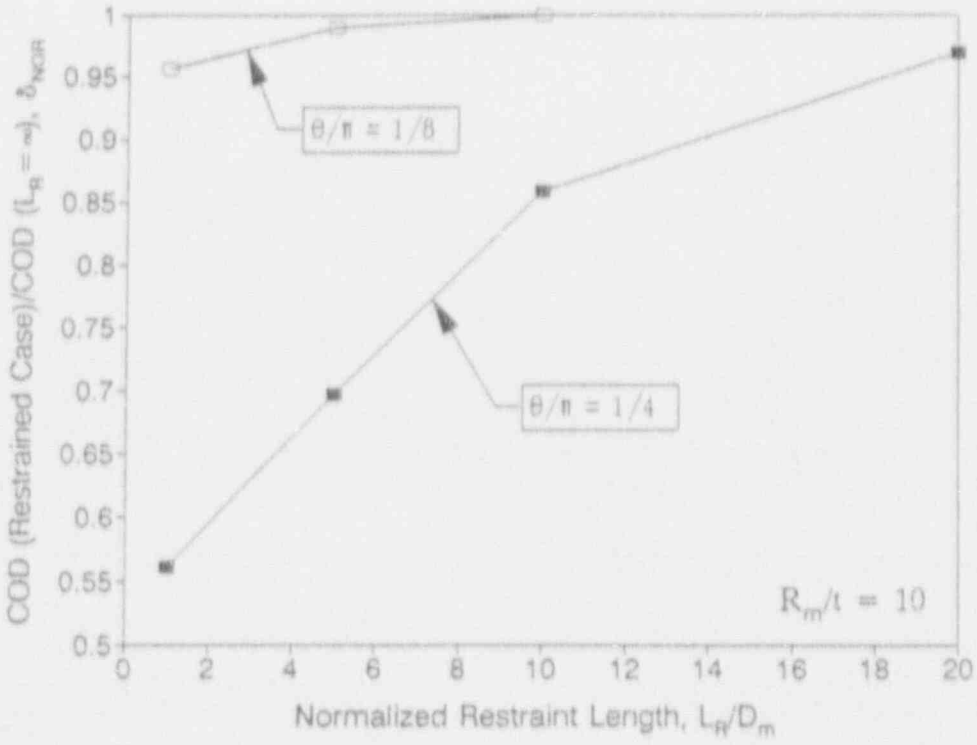

Figure 7.17 Effect of fully restrained bending conditions from crack location on COD normalized by unrestrained COD

SC-SA-5/92-F7.17

($\theta/\pi = 1/8$), the restraint effects are also small and may be neglected. However, for larger crack angles ($\theta/\pi = 1/4$), the restrained COD can be significantly different from the unrestrained COD, and hence, cannot be ignored in the crack-opening-area analysis for leak-rate quantification. It is interesting to note that a significant input parameter like the "restraint length" is not considered in either of the thermohydraulic codes SQUIRT (Ref. 7.19) or PICEP (Ref. 7.20) or in any other leak-rate analyses.

Activity 6.6.2 Develop SQUIRT4 and SQUIRT5 Codes

An initial modified version of the original SQUIRT code was developed. This version performs an iterative calculation to obtain a crack size for a given load and allowable leak rate for a piping system. This version is given an acronym SQUIRT4.

7.4 Plans for Next Year of the Program

The plans for efforts in the next year are summarized below.

7.4.1 Subtask 6.1 Create Combined Loading Improvements

There are three activities in this subtask. Activities 6.1.1 and 6.1.3 have been completed. The remaining Activity 6.1.2 (Account for Pressure on the Crack Face) will be started in the next year of the program.

7.4.2 Subtask 6.2 Implement Short TWC Crack-Opening Improvements

There are two activities in this subtask. No work was scheduled for this year. The activities will be started in the next year of the program.

7.4.3 Subtask 6.3 Improve Weld Crack Evaluations

There are two activities in this subtask. Activity 6.3.1 was completed. Activity 6.3.2 (Compare with Recent DPP and Task 1 Data) has started and will continue as data become available. It will be completed in the next year of the program.

7.4.4 Subtask 6.4 Modify SQUIRT Code

This subtask was not scheduled to start in this year. Work will begin in the next year of the program.

7.4.5 Subtask 6.5 Prepare Topical Report on Crack-Opening-Area Improvements

This subtask was not scheduled to start in this year. Work will begin in the next year of the program.

7.4.6 Subtask 6.6 Leak Rate Quantification

There are six activities in this subtask. Items 2(a) and 2(b) of Activity 6.6.1 have been completed. The future plan for the activities are given below.

Activity 6.6.1	Items 1, 2(c), and 3 under this activity will be completed in the next year.
Activity 6.6.2	The development of the SQUIRT4 program will be completed. In order to facilitate large number of repeated calculations to be made in the Activity 6.6.3, another version named SQUIRT5 will also be developed to automate the calculations.
Activity 6.6.3	Novel probabilistic methods will be developed to obtain a conditional failure probability based on LBB criteria. This will allow an evaluation of proposed changes in leak detection requirements in terms of potential impact on LBB analyses. Following development of SQUIRT4 and SQUIRT5 from Activity 6.6.2, calculations will be started to determine conditional probability of failure for various PWR and BWR nuclear piping systems. All these efforts will be completed in the next year of the program.
Activity 6.6.4	Evaluation of the proposed changes on leak rate for "non-LBB" piping systems will be started and completed during the next year.
Activity 6.6.5	Coordination with NRC-RES and NRC-NRR will be initiated for guidance on the selection of typical piping systems for the calculations to be made in the Activities 6.6.3 and 6.6.4.
Activity 6.6.6	Following completion of the technical work on the previous activities, a topical report will be prepared. This will be completed in the next year of the program.

7.5 References

7.1 Wilkowski, G. M. and others, "Short Cracks in Piping and Piping Welds," Second semiannual report by Battelle, NUREG/CR-4599, Vol. 1, No. 2, August 1991.

7.2 Schmidt, R. A., Wilkowski, G. M., and Mayfield, M. E., "The International Piping Integrity Research Group (IPIRG) Program - An Overview," SMiRT-11, Paper G12/1, August 1991.

7.3 Hiser, A. L. and Callahan, G. M., "A User's Guide to the NRC's Piping Fracture Mechanics Database (PIFRAC)," NUREG/CR-4894, May 1987.

7.4 Wilkowski, G. M. and others, "Degraded Piping Program, Phase II," Summary of Technical Results and Their Significance to Leak-Before-Break and In-Service Flaw Acceptance Criteria, March 1984 - January 1989, Battelle, NUREG/CR-4082, Vol. 8, March 1989.

7.5 "The Development of a Plan for the Assessment of Degraded Nuclear Piping by Experimentation and Tearing Instability Analysis," Prepared for NRC by Battelle, Final Report, NUREG/CR-3142, June 1983.

7.6 Kumar, V. and others, "An Engineering Approach for Elastic-Plastic Fracture Analysis," EPRI Topical Report, NP-1931, July 1981.

7.7 Ernst, H. A., "Material Resistance and Instability Beyond J-Controlled Crack Growth," Elastic-Plastic Fracture Second Symposium, Vol. I - Inelastic Crack Analysis, ASTM STP 803, pp. I-191 through I-213, November 1983.

7.8 Kramer, G. and Papaspyropoulos, V., "An Assessment of Circumferentially Complex-Cracked Pipe Subjected to Bending," NUREG/CR-4687, October 1986.

7.9 Wilkowski, G. M., Pan, J., and Kanninen, K. F., "Effect of Flaw Shape on J-Resistance Curve of a Circumferentially Cracked Pipe," Proceedings of the 4th ASME National Congress on Pressure Vessel and Piping Technology, Portland, Oregon, June 1983.

7.10 Hays, R. A., Vassilaros, M. G., and Gudas, J. P., "Fracture Analysis of Welded Type 304 Stainless Steel Pipe," Prepared by David Taylor Naval Ship R&D Center (DTNSRDC) for NRC, NUREG/CR-4538 Vol. 1, May 1986.

7.11 Kanninen, M. F. and others, "Instability Predictions for Circumferentially Cracked Type 304 Stainless Steel Pipes Under Dynamic Loading," EPRI Report, NP-2347, April 1982.

7.12 Kumar, V. and others, "Advances in Elastic-Plastic Fracture Analysis," EPRI Final Report, NP-3607, August 1984.

7.13 Paris, P. C. and Tada, H., "The Application of Fracture Proof Design Methods Using Tearing Instability Theory to Nuclear Piping Postulating Circumferential Through Wall Cracks," NUREG/CR-3464, September 1983.

7.14 "Report to the U.S. Nuclear Regulatory Commission Piping Review Committee," Prepared by the Pipe Break Task Group, NUREG/CR-1061, Vol. 3., November 1984.

7.15 Brust, F. W., "Approximate Methods for Fracture Analysis of Through-Wall Cracked Pipes," NUREG/CR-4853, February 1987.

7.16 Gilles, P. and Brust, F. W., "Approximate Fracture Methods for Pipes, Part I, Theory," Nuclear Engineering and Design, Vol. 127, pp. 1-17, 1991.

7.17 Wilkowski, G. M. and others, "Degraded Piping Program - Phase II," Semiannual Report, October 1984-March 1985, NUREG/CR-4082, Vol. 2., July 1985.

7.18 ABAQUS, User's Guide and Manual, Version 4.8, Hibbitt, Karlsson, & Sorensen, Inc., 1989.

7.19 Paul, D. D. and others, "Evaluation and Refinement of Leak-Rate Estimation Models," NUREG/CR-5128, April 1991.

7.20 Norris, D. and others, "PICEP: Pipe Crack Evaluation Program," EPRI Report, NP-3596-SR, 1984.

8. TASK 7 NRCPIPE IMPROVEMENTS

8.1 Task Objective

The main objective of this task is to incorporate the analysis improvements from Subtasks 1.4 and 2.4 into the NRCPIPE code. A secondary objective is to make the NRCPIPE code more efficient and also to restructure the code to allow for ease of implementation of the activities described below.

8.2 Task Rationale

In the Degraded Piping Program, the computer code NRCPIPE was developed for circumferential through-wall-cracked pipe fracture analyses. A VAX version of the code also contained the circumferential internal surface-wall-cracked pipe algorithms. The PC version was made specifically for the through-wall-cracked analyses. Numerous J-estimation schemes were developed or modified. The improvements developed in the current program need to be incorporated into this code to take advantage of technology developments, as well as to facilitate comparisons with the experimental results.

8.3 Task Approach

To accomplish the objectives of this task, four subtasks are to be undertaken:

Subtask 7.1	Improve efficiency of current version of NRCPIPE
Subtask 7.2	Incorporate TWC improvements in NRCPIPE
Subtask 7.3	Make surface crack version of NRCPIPE
Subtask 7.4	Provide new user's manual.

The crack-opening-area analysis improvements will be incorporated into the SQUIRT code in Subtask 6.4.

Before and after each of the changes described in the following activities, quality assurance calculations will be made. These will involve cases for which experimental data exist or data are being generated in Tasks 1 and 2 and hypothetical cases that check critical parameters of interest.

Although some progress was made, the results are not significant yet. These will be reported in the next program report.

8.3.1 Subtask 7.1 Improve Efficiency of Current Version of NRCPIPE

Efforts to improve the efficiency of the current version of NRCPIPE continued during this reporting period. Minor bugs relating to the COD values and output parameters in the LBB.ENG2 method were fixed and incorporated into Version 1.4e.

8.3.2 Subtask 7.2 Incorporate TWC Improvements in NRCPIPE

There are four activities in this subtask. These are:

Activity 7.2.1	Incorporate F-, V_3, and h_4-function improvements
Activity 7.2.2	Incorporate ovalization for short cracks
Activity 7.2.3	Incorporate bending and tension improvements
Activity 7.2.4	Incorporate improved analyses for weld and fusion line cracks.

In Activity 7.2.4 preliminary implementation of the cracked-pipe weldments algorithm that is being developed in Subtask 1403 for inclusion into NRCPIPE was begun. These are to be in Version 2.0. There was no effort in the other activities in this subtask.

8.3.3 Subtask 7.3 Make Surface Crack Version of NRCPIPE

There are six activities in this subtask. These are:

Activity 7.3.1	Make circumferentially surface-cracked pipe PC code of NRCPIPE
Activity 7.3.2	Incorporate ASME Section XI criteria in NRCPIPE (SC version)
Activity 7.3.3	Add J_e to SC.TNP and SC.TKP
Activity 7.3.4	Add ovalization
Activity 7.3.5	Incorporate new LBB.ENG surface-cracked pipe solution
Activity 7.3.6	Add pressure and bending solutions
Activity 7.3.7	Add surface-cracked pipe weld criteria.

In Activity 7.3.1 a PC based version of NRCPIPE (internal surface crack version) was developed from the VAX source code. This program was developed along the same lines as the TWC version discussed above and uses the SC.TNP and SC.TKP algorithms developed previously for the case of pure bending. The acronym for this program is NRCPIPES.

In Activity 7.3.6 improved algorithms for the case of combined pressure and bending loads developed in Subtask 2.4 were reviewed and evaluated for implementing into NRCPIPES.

8.3.4 Subtask 7.4 Provide New User's Manual

A User's Manual for the NRCPIPES code was written.

8.4 Plans for Next Year of the Program

Efforts scheduled for the next year are discussed below.

8.4.1 Subtask 7.1 Improve Efficiency of Current Version

Efficiency improvements to the existing NRCPIPE code continue on an ongoing basis. A revised version of this code will be delivered to the NRC.

8.4.2 Subtask 7.2 Incorporate TWC Improvements in NRCPIPE

Once all of the GE/EPRI functions are computed they will be implemented into NRCPIPE in Activity 7.2.1. Efforts will also involve incorporating bending and tension improvements. The development and implementation of the weld and fusion line cracks algorithm will continue in Activity 7.2.4.

8.4.3 Subtask 7.3 Make Surface Crack Version of NRCPIPE

Version 1.0 of the PC code NRCPIPES will be completed and sent to the NRC for review. Development and implementation of combined bending and pressure algorithm will continue in the next reporting period.

8.4.4 Subtask 7.4 Provide New User's Manual

A user's manual for the Version 1.0 of the surface crack code NRCPIPES will also be sent to the NRC along with the code.

9. TASK 8 ADDITIONAL EFFORTS

This task was not active this fiscal year; hence there is no progress to report. An initial sub-task on assessment of J-R curve validity limits to be conducted by Prof. F. Shih at Brown University is scheduled to start during the next reporting period.

10. TASK 9 INTERPROGRAM COOPERATION AND PROGRAM MANAGEMENT

10.1 Task Objective

The objective of this task is to develop and maintain national and international cooperation in sharing data and analysis procedures and to maintain program administration.

10.2 Task Rationale

In the Degraded Piping Program, a series of analytical round-robin efforts was organized. These efforts provided verification of procedures used in the Degraded Piping Program and helped develop a consensus on how to handle difficult analytical problems. This effort will build on that tradition thereby enhancing the quality of the work done in this program. The results of this program will be presented to ASTM E-24 and the ASME Section XI Flaw Evaluation Working Group. This will help implement the results into U.S. Codes and Standards.

In addition, it is efficient from a cost viewpoint to have the international cooperation and program administration efforts consolidated within a single task.

10.3 Task Approach

There are two specific subtasks in this task:

Subtask 9.1 Technical exchange and information meetings
Subtask 9.2 Program administration.

Only the technical efforts that are in Subtask 9.1 will be reviewed.

10.3.1 Subtask 9.1 Technical Exchange and Information Meetings

10.3.1.1 Objective

The objective of this subtask is to enhance the program's technical efforts by developing a forum to exchange technical information both nationally and internationally.

10.3.1.2 Rationale

The timely exchange of technical developments adds credibility to the results of this program, may result in cost savings to the NRC, and enhances implementation of the results into regulatory or code criteria.

10.3.1.3 Approach

There are four activities within this subtask:

Activity 9.1.1	ASME Section XI meetings
Activity 9.1.2	ASTM meetings
Activity 9.1.3	Other technical meeting coordination
Activity 9.1.4	Coordination with Japanese Elastic-Plastic Fracture in Inhomogeneous Materials program.

Reportable progress is given for Activities 9.1.1 and 9.1.4.

Activity 9.1.1 ASME Section XI Meetings

Three different efforts were undertaken in this reporting period relative to the ASME Section XI pipe flaw evaluation criteria.

Axial Flaw EPFM—Charpy Criteria Development

The first effort involved developing equations to allow for Charpy energy to be used in an elastic-plastic fracture mechanics analysis of an axial surface crack in ferritic pipe for fully ductile fracture. This development involved using the equations established by Maxey et al. at Battelle, on ferritic natural gas line-pipe steel, Ref. 10.1, given in Equation 10-1 for U.S. customary units used in the Code.

$$[(12CVP/A_c)E\pi]/(8\ell\sigma_f^2) = \ln\{\sec[(\pi/2)(M_p\sigma/\sigma_f)]\} \qquad (10\text{-}1)$$

where

CVP	=	Charpy V-notch plateau energy, ft-lb
A_c	=	Cross-sectional area of Charpy specimen, in^2 ($0.124\ in^2$ for a full-size specimen)
E	=	Elastic modulus, psi (28,000,000 psi for carbon steel)
ℓ	=	Half of the axial crack length, inches
σ_f	=	Flow stress, psi
M_p	=	Bulging factor for surface crack, see Eq. 10-2
σ	=	Hoop stress at failure, psi

$$M_p = (t/d\text{-}1)/(t/d - 1/M_t) \qquad (10\text{-}2)$$

and where

t	=	Pipe thickness, inch
d	=	depth of surface crack, inch
M_t	=	Folias through-wall flaw bulging factor, see Eq. 10-3.

$$M_t = [1 + 1.61/(4R_m t)\ell^2]^{0.5} \quad (10\text{-}3)$$

R_m = Mean radius, inch.

Figure 10.1 shows Maxey's results using his definition of flow stress: yield plus 68.95 MPa (10 ksi). Included in this figure are data from the AEC pipe fracture program conducted at Battelle, Ref. 10.2.

In the work by Maxey, Ret. 10.1, experiments were conducted on line-pipe steels that are not used in nuclear piping construction. To make this criterion applicable to nuclear steels, it was necessary to assess the ASME flow stress definition. The ASME Section XI Article IWB-3650 ferritic pipe flaw evaluation criteria defines flow stress as 2.4 times the design stress, S_m. There are no tabulated values of S_m for line-pipe steel in Section III of the ASME Boiler and Pressure Vessel Code. Instead, the actual properties were used with the general ASME criteria to define the S_m value as the lowest of:

(1) One-third of actual room temperature ultimate tensile strength,

(2) One-third of actual ultimate strength at the pipe test temperature,

(3) Two-thirds of actual yield at room temperature, or

(4) Two-thirds of actual yield strength at the pipe test temperature.

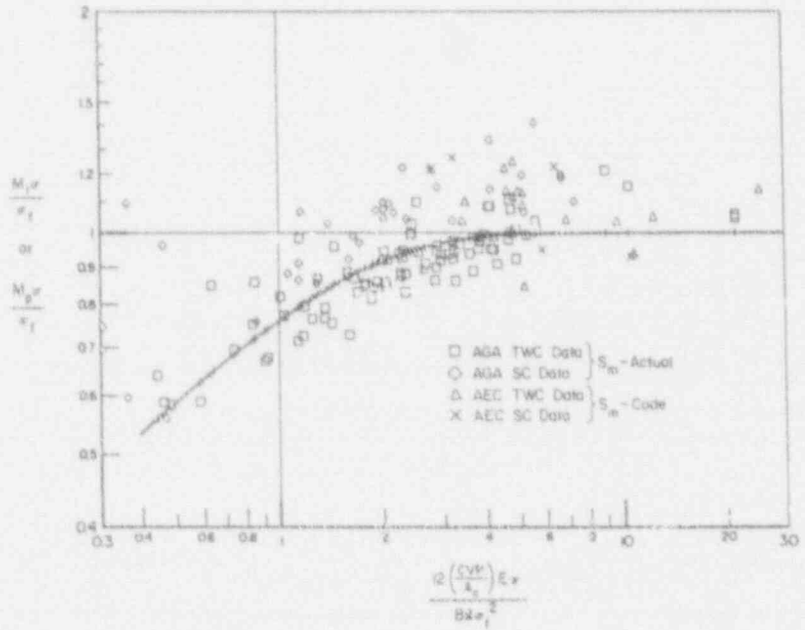

Figure 10.1 Axially cracked-pipe burst data and predictions using Maxey analysis with $\sigma_f = \sigma_y + 10$ ksi using actual properties

SC-SA-5/92-F10.1

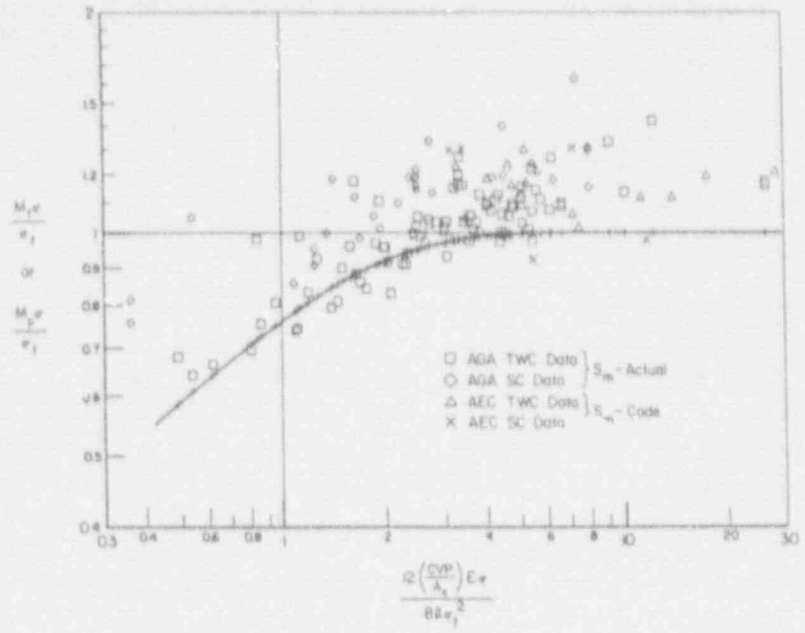

Figure 10.2 Comparison of axially cracked-pipe burst data to Maxey analysis with $\sigma_f = 2.4\ S_m$

SC-SA-5/92-F10.2

Since all these pipe experiments were conducted near room temperature and the yield to ultimate ratios are high, Criterion (1) defined the S_m values. For these values the term "S_m - Actual" was used, whereas for the AEC experiments the ASME Section III values were available and the term "S_m - Code" was used. Defining flow stress as $2.4S_m$ as per ASME Section XI IWB-3650, these data were replotted as shown in Figure 10.2. This results in the simple modification of Equation 10-1 to be.

$$[(12CVP/A_c)E\pi]/[8\ell(2.4S_m)^2] = \ln\{\sec[(\pi/2)(M_p\sigma/(2.4S_m))]\} \qquad (10\text{-}4)$$

As can be seen in Figure 10.2, this Equation 10-4 gives a reasonable lower bound to the pipe fracture data in that the data below this equation are one standard deviation below the average of the data.

To be in a form consistent with Article IWB-3650, a Z factor can be established by rearranging the terms in Equation 10-4, where

$$Z = (2/\pi)(\text{arcsec}\{\exp[369.5*CVP/(\ell S_m{}^2)]\})^{-1} \qquad (10\text{-}5)$$

The Z-factor can be used as a stress multiplier on the applied stress. Additionally, if the Charpy upper shelf energy is not known, then two options are available. The first is to use the Charpy energy from the mill certification, which is typically at room temperature or lower. This would be

conservative, but perhaps too conservative. The second option is to use a statistical correlation as defined in Equation 10-6 for the Charpy V-notch plateau energy, CVP.

$$CVP = (CVN * 100)/(SA + 25) \quad (10\text{-}6)$$

Here,

CVP = Charpy V-notch energy,
CVN = Charpy V-notch energy at any temperature,
SA = Shear area percent at the CVN temperature.

This correlation is a reasonable lower bound to Charpy data found for line-pipe (Ref. 10.1) and nuclear pipe steels tested in the Degraded Piping Program (Ref. 10.3). These data are shown in Figure 10.3 with average and ± standard deviation linear regression fits to the data. Table 10.1 shows a comparison of calculated Charpy plateau energy values, using Equation 10-6, to the actual Charpy energy value for Charpy data from an A515 Grade 60 pipe. Note that at low shear area percents, the calculated values are relatively low because the confidence in the data in that region is not good; also see Figure 10.3. When the data are actually at 100 percent shear area, then Equation 10-6 is also inherently conservative.

Since these data and analyses seemed to be close to average values and slightly conservative, they were proposed to be included in Appendix H of Section XI.

Pipe Fracture Data Bases

The second effort in the ASME Code activities was the start of a database for the committee to use that contains past quasi-static pipe fracture data. This effort was started, but additions are needed before a version is ready for release. This database will contain, at the least, data from:

- past EPRI/Battelle stainless steel pipe fracture programs (EPRI NP-192 and EPRI NP-2347),
- the NRC's Degraded Piping Program (NUREG/CR-4082),
- some of the past DTRC pipe fracture data (NUREG/4538 and NUREG/CR-3740),
- the IPIRG program, and
- results from this program.

Evaluation of ASME Section III Redefinition of the Design Stress Equation

As part of this effort, Dr. Wilkowski served on a special panel to evaluate the potential effect of changes proposed in Section III to eliminate inertial stresses from the design equations. Although the panelists had different reasons for reaching a consensus, the panel agreed that if inertial stresses are eliminated in the design stress, then in the flaw evaluation criteria they should be explicitly included. Battelle's assessment included technical justification from the NRC's International Piping Integrity

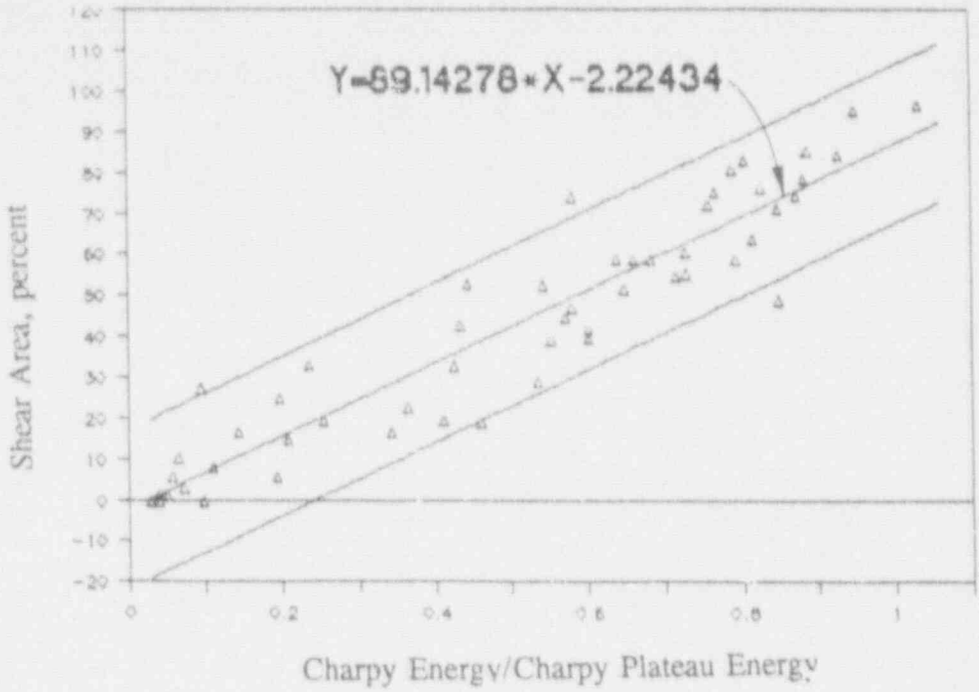

(a) Nuclear piping materials from the Degraded Piping Program

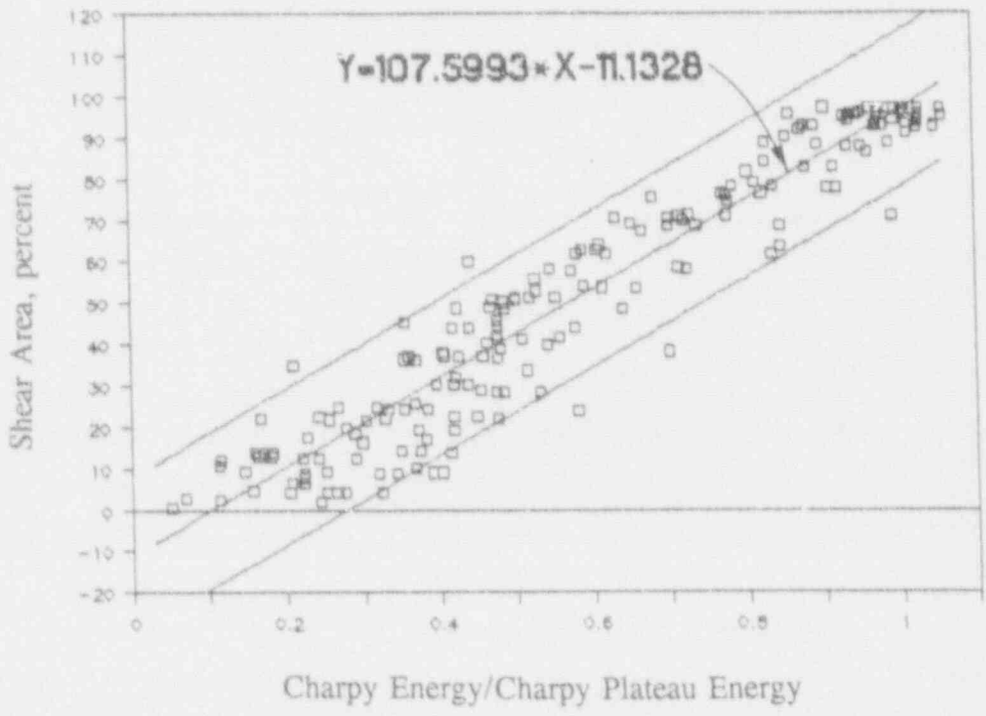

(b) Natural gas line-pipe steels

Figure 10.3 Correlation to predict Charpy plateau energy from Charpy energy and shear area percent at any temperature

SC-SA-5/92-F10.3a/b

Table 10.1 Sample calculations of Charpy upper plateau energy using Equation 10-6 for an A515 Gr 60 pipe (Pipe number DP2-F26)

Temperature, F	Charpy Energy, ft-lb	Shear Area, percent	Calculated Charpy Plateau Energy, ft-lb	Calc./Actual Charpy Plateau Energy[a]
-15	5	2	19	0.15
15	8	10	23	0.18
32	32	20	71	0.56
32	70	40	108	0.85
54	76	40	117	0.92
55	90	55	113	0.89
75	100	60	118	0.93
115	116	85	105	0.83
150	127	100	102	0.80
212	126	100	101	0.80

(a) 126.5 ft-lb used as actual Charpy plateau energy value.

Research Group (IPIRG) program, where DEGB fracture occurred in pipes tested under inertial loading, Ref. 10.4.

Activity 9.1.4 Coordination with Japanese Elastic-Plastic Fracture in Inhomogeneous Materials (EPI) program

As part of this effort, we are conducting some research investigations that are compatible with the Japanese Elastic-Plastic Fracture of Inhomogeneous Materials program. One of these is an analysis that is being conducted by Professor Jwo Pan at the University of Michigan. This involves a numerical evaluation of weld residual stresses on the crack driving force. The ASME Section XI pipe flaw evaluation criteria say to consider the residual stresses, but there are no guidelines. The numerical analysis from this program will involve thermal plastic analysis to numerically create the residual stress field, then create the crack by node release and evaluate the J values as the welded structure is loaded. These results will be compared with simple approximate methods to assess potential Code techniques.

10.4 Plans for Next Year of the Program

10.4.1 Subtask 9.1 Technical Exchange and Information Meetings

During the next year, efforts to coordinate with the ASME Section XI Code will continue. This will involve:

- Continuing to work on implementing the axial crack EPFM analysis into the ASME Section XI code for ferritic pipe.
- Continuing to develop the quasi-static pipe fracture data base for use in the ASME Section XI Code committees.
- Relating the results in this program, such as the effects of R_m/t ratio on the applicability of the Net-Section-Collapse analysis.
- Presenting the IPIRG program results, and drawing implications of that work on the ASME pipe flaw evaluation criteria.

The work at the University of Michigan on the effects of weld induced residual stresses and their effect on EPFM analyses will continue.

Additionally, Dr. C. Marschall will attend the ASTM E24 fracture mechanics meetings to keep abreast of any changes and to share relevant results from this program if they may affect the toughness testing standards.

10.5 References

10.1 Maxey, W. A., Kiefner, J. F., Eiber, R. J., and Duffey, A. R., "Ductile Fracture Initiation, Propagation, and Arrest in Cylindrical Vessels," ASTM STP 514, 1972, pp. 70-81.

10.2 Eiber, R. J., Maxey, W. A., and Duffey, A. R., "Investigation of the Initiation and Extent of Ductile Pipe Rupture," Battelle Memorial Institute Report, BMI-1908, 1971.

10.3 Wilkowski, G. M. and others, "Degraded Piping Program - Phase II," Summary of Technical Results and Their Significance to Leak-Before-Break and In-Service Flaw Acceptance Criteria," March 1984-January 1989, by Battelle Columbus Division, NUREG/CR-4082, Vol. 8, March 1989.

10.4 Schmidt, R. A., Wilkowski, G. M., and Mayfield, M. E., "The International Piping Integrity Research Group (IPIRG) Program: An Overview," SMiRT-11, Paper G23/1, August 1991.

11. SUMMARY

The major accomplishments of the program during this reporting period are summarized by Task.

11.1 Task 1 Through-Wall-Cracked Pipe Evaluations

Several material characterization efforts were undertaken in this task. The first involved evaluation of the properties of a French wrought TP316 stainless steel pipe. This pipe was found to have anisotropic material properties. The elastic modulus was very low in the axial direction, 140 GPa (20,000,000 psi), and the fracture surface of the longitudinal tensile specimen was elliptical in shape, showing significant anisotropic strain hardening. This is the first time we have seen significant anisotropy in a wrought austenitic steel base metal.

A metallographic investigation was conducted on a pipe test that had a through-wall crack in the center of a girth weld in a 28-inch-diameter TP316 stainless steel pipe. The crack grew along the fusion line in one growth direction and in the base metal in the other. The amount of crack growth along the fusion line was significantly greater than in the base metal. Crack growth along the fusion line of stainless steel submerged arc welds is consistent with past observations made in the Degraded Piping Program, Ref. 11.1. It appears that the toughness of the fusion line may be lower than the toughness of the submerged arc weld. This lower toughness region can affect the NRC LBB procedures and the ASME IWB-3640 analysis for cases where cracked pipe evaluations have typically considered the SAW metal as having the lowest toughness; the fusion line toughness has not been considered. This suggests that the toughness of weld fusion lines with the initial crack tip in the fusion line would be worthwhile investigating. This crack-tip location would be representative of an intergranular stress corrosion crack or a lack-of-side-wall-fusion weld defect.

As part of Task 1, FEM analyses were conducted to evaluate the GE/EPRI J-estimation functions for short circumferential through-wall cracks in pipes subjected to bending loads. A few cases involving pure tension load were also evaluated. ABAQUS 3D 20-node brick elements were used in the analysis. These elements provide more accurate results than the shell elements used in the original GE/EPRI solutions, Ref. 11.2. The new functions (V_3 and h_4) significantly improved the predicted rotation for the cracked pipe section. The predicted crack-opening displacement and crack driving force (J) was in better agreement with the experimental data than those from the GE/EPRI analysis. These new functions will be included in a future release of the NRCPIPE code.

11.2 Task 2 Surface-Cracked Pipe Evaluations

In this task, two large-diameter surface-cracked pipe experiments were conducted in which the pipes were loaded by internal pressure and four-point bending. The two pipes, an A515 Grade 60 Schedule 60 steam-line pipe and a TP316 stainless steel Schedule 80 main-recirculation-line pipe, had a diameter of 28 inches. The crack was in the base metal of the carbon steel pipe and in the center of a submerged arc weld in the stainless steel pipe . Both had machined surface cracks that extended 50

percent of the thickness and 25 percent of the circumference. The test data are presented in this report, but comparisons of the results with existing analyses are not completed yet.

An analysis of the earlier small-diameter surface-cracked pipe experiments on stainless steel pipe showed that there is a general correction factor on the net-section-collapse analysis as a function of the ratio R_m/t for the pipe. From these data and data from the Degraded Piping Program, this correction appears to be independent of the crack size. The trend is that as R_m/t increases, the maximum load decreases below the net-section-collapse analysis predictions. This result may be due to ovalization effects, wherein the net-section-collapse analysis assumes the pipe remains circular. This work points out some limitations of the ASME flaw evaluation solutions.

A final effort in this task was to extend the surface-cracked pipe J-estimation schemes to external cracks. This was to be used by Brookhaven National Laboratories (Ref. 11.3) to analyze low-cycle fatigue crack growth for a circumferential surface crack in Japanese pipe system experiments conducted at Tadatsu. As part of this effort, we reviewed how this analysis should be used in the Brookhaven analysis together with the fatigue crack growth data developed at DTRC (Ref. 11.4) for the Brookhaven effort. The pipe experiments and DTRC tests involved low-cycle fatigue under reversed loading. To make the low- and high-cycle laboratory specimen fatigue crack growth data consistent, the Dowling operational definition of J was used. This definition accounts for some of the compressive loads contributing to ΔJ. The difficulty is that when applying this lab specimen data to a structure, the deformation J analysis for the structure is not consistent with the Dowling J for negative R ratio loading. To overcome the differences, the Dowling definition of J must be used for the analysis of the structure (pipe) in order to be consistent with the laboratory specimen approach. Procedures for this methodology are discussed in this report and may be needed for evaluating fatigue crack growth under normal-plus-SSE loading.

11.3 Task 3 Bimetallic Weld Evaluations

This task is not scheduled to start until October 1992.

11.4 Task 4 Dynamic Strain Aging Effects on Toughness

Work on this task included consideration of several new experiments and tests that gave further insight into the phenomenon of dynamic strain aging (DSA). One experiment involved evaluation of a carbon steel B&W submerged arc weld. This weld behaved differently from all the base metals we tested in the past; based on strength and hardness data, the dynamic strain aging range appeared to be at a much higher temperature. This weld also had a higher toughness at seismic loading rates than at quasi-static rates, unlike base metals, which showed reduced toughness or no change in toughness at seismic rates. Because the weld metal exhibited DSA at a higher temperature than did the base metals, it is thought that the different effects of service loading rates in the weld and base metals may have reflected their different DSA behaviors. The reasons for the different DSA behavior of the weld remain uncertain but may be due to higher silicon and/or molybdenum levels than in the base metal. It is not known if other welds would behave similarly.

In this task, we also measured for the first time the velocity of an unstable crack jump, believed to be associated with dynamic strain aging. This test was conducted at 288 C. The velocity was approximately 0.5 meters per second, which is much slower than a cleavage crack, but is 40,000 times faster than the stable crack growth measured during the same C(T) test.

Additional efforts involved examination of the fracture surfaces of areas where there was stable and unstable crack growth in a C(T) specimen test at 288 C. The results showed similarities in fracture profile, microstructure, and failure mode (ductile dimple rupture) and differences in dimple size (larger in the unstable fracture regions) and coloration (distinct color difference on the oxidized stable and unstable crack surfaces).

Finally, we conducted an examination of the number of crack jumps that occurred in laboratory specimens and pipe tests on the same material. From a microstructural or local viewpoint, the results to date suggest that the precise location of the start of crack jumps appears to be probabilistic. From a global viewpoint, if crack jumps occurred in a laboratory specimen, then they occurred at some time during a pipe experiment, especially during through-wall-cracked pipe experiments. However, in 3 of 4 cases where there were no crack jumps in the laboratory specimens, there were crack jumps in the pipe experiments. Hence, unstable crack jumps at LWR temperatures are more likely to occur in a cracked carbon steel pipe than in laboratory specimen fracture tests. This is somewhat discouraging, in that the laboratory fracture specimen tests are not necessarily reproducing full-scale fracture behavior, and the full-scale behavior is worse than the laboratory specimen behavior.

11.5 Task 5 Effects of Anisotropy on Fracture of Piping

In this task data from this program and results from the literature were examined to see if a screening criterion could be developed to determine anisotropic fracture behavior. Anisotropic fracture properties are believed to be the cause of cracks turning away from the circumferential direction, even under pure axial membrane loading. This crack turning can be significant for LBB analyses where there are combined longitudinal, hoop, and torsional stresses. Frequently, only the longitudinal stresses are considered for circumferential cracks. However, if the low toughness direction and principal stresses are at an angle to the circumferential direction, the concern is whether the failure stresses could be lower than calculated in current LBB procedures.

The results of the literature review and assessment of our data showed that toughness anisotropy is more dependent on the shape of the nonmetallic inclusions content than any other manufacturing or metallurgical aspect. Anisotropy can best be minimized with sulfide shape control (i.e., titanium, zirconium, or rare earth additions such as cerium), although cross-rolling of plate for pipe fabricated from plate is another good option. The shape of the inclusions is more important than their volume fraction. Banded microstructures and crystallographic texture are less important sources of anisotropy. Hence, other than toughness testing, metallographic examination may be the best screening criterion to determine anisotropic fracture toughness. However, examination of chemical composition may give some good indications if the material has been modified by sulfide shape control practice.

Additionally, past pipe fracture test results were examined to correlate angular crack growth to anisotropy. Although there is a slight general trend toward less-angular crack growth with decreasing anisotropy, the results to date show a great deal of scatter. A closer evaluation of these data are planned.

11.6 Task 6 Crack-Opening-Area Analysis Improvements

The results in this reporting period are on a subtask to provide a technical basis for changes to NRC Regulatory Guide 1.45 on leakage detection systems. A probabilistic analysis is being conducted to assess safety margins that should be applied when using NRC LBB procedures such as in SRP 3.6.3. Changes to leakage detection system capabilities will be assessed relative to conditional failure probabilities.

Initial efforts involved examination of some deterministic aspects. The first was to assess the accuracy of current J-estimation schemes to predict the maximum load and crack opening of complex-cracked pipe. A complex crack is a long surface crack that penetrates the thickness only over a short part of its length, Ref. 11.5. Since leak-detection capabilities are used for pipe systems not approved for LBB, these systems may be susceptible to mechanisms that produce long surface cracks and hence a complex crack. The results showed that to make consistently conservative predictions of maximum load, a constraint factor on the toughness is needed when analyzing a complex-cracked pipe using the existing simple through-wall-cracked pipe analyses. Crack-opening-displacement predictions were much better using the constraint factor on toughness, but still overpredicted the crack opening significantly. This result is a nonconservative aspect for LBB evaluations of such cracks.

Another effort in the crack-opening-area analysis was to assess the potential for restraint of crack opening when the crack is close to a fixed terminal end. The fixed terminal end prevents the induced rotation of the pipe due to the eccentricity of the crack and axial membrane stresses (i.e., pressure loading). This assessment showed that if the crack is far (about 20 pipe diameters) from the fixed end or short in length (less than 1/8th of the pipe circumference), then there is no restraint of the axial membrane stress (pressure) component of the crack opening. In these cases, the existing crack-opening-area analyses can be used. However, for longer cracks that are close to a fixed end, the crack opening due to the pressure loading can be reduced significantly (up to a factor of 2). It may be advisable to account for this crack-opening restraint in an LBB analysis. This is the first time such an effect has been considered. The assessment consisted of a series of elastic finite element scoping analyses. No additional analyses are planned to develop a generalized correction factor for restraint at this time.

11.7 Task 7 NRCPIPE Code

Task 7 is the effort to formalize the fracture analyses into a computer code called NRCPIPE. The current NRCPIPE code was created during the Degraded Piping Program and contains only analyses for circumferential through-wall-cracked pipe. Some corrections to that code were made and released in Version 1.4e. An initial surface crack version called NRCPIPES has been created. It contains the

SC.TNP and SC.TKP J-estimation analyses for finite-length circumferential surface cracks. These analyses were developed in the Degraded Piping Program.

11.8 Task 8 Other Efforts

To date, the only effort that has been started in this task is being conducted by Professor Fong Shih on "Validation Limits in J-Resistance Curve Determination." The specific objective is to assess the use of the modified version of J proposed by Dr. H. Ernst versus the deformation theory J. This effort started on September 24, 1991 and will continue for two years.

11.9 Task 9 Interprogram Cooperation and Program Management

Several technical efforts are contained in this task. One of these is an analysis that is being conducted by Professor Jwo Pan at the University of Michigan. It involves a numerical evaluation of weld residual stresses on the crack driving force. The ASME Section XI pipe flaw evaluation criteria state that residual stresses should be considered, but contain no guidelines. The numerical analysis from this task will involve thermal plastic analysis to numerically create the residual stress field, then create the crack by node release and evaluate the J values as the welded structure is loaded. These results will be compared with simple approximate methods to assess potential Code techniques.

Another objective of this task is cooperation with the ASME Section XI pipe flaw evaluation criteria. Several different efforts were undertaken in this reporting period. The first involved developing equations to allow Charpy energy values to be used in an elastic-plastic fracture mechanics analysis of an axial surface crack in ferritic pipe. The second task is to develop a data base of past quasi-static pipe fracture data. This effort has been started and will be released when ready. Finally, Dr. Wilkowski was part of a special panel to evaluate the potential effect of changes proposed in Section III to eliminate inertial stresses from the design equations. Although the panelists had different reasons, the panel agreed that if inertial stresses are eliminated in the design stress, then in the flaw evaluation criteria they should be explicitly included. The Battelle assessment included technical justification from the NRC's International Piping Integrity Research Group (IPIRG) program, where DEGB fracture occurred in pipes tested under inertial loading, Ref. 11.6.

11.10 References

11.1 Wilkowski G. M. and others, "Analysis of Experiments on Stainless Steel Flux Welds," NUREG/CR-4878, April 1987.

11.2 Kumar, V., German, M. D., and Shih, C. F., "An Engineering Approach for Elastic-Plastic Fracture Analysis," EPRI report NP-1931, July 1981.

11.3 Park, Y. J., Curreri, J. R., and Hofmayer, C. H., "The High Level Vibration Test Program Final Report," NUREG/CR-5585, May 1991.

11.4 Joyce, J. A. and Hackett, E. M., "Elastic-Plastic Characterization of a Cast Stainless Steel Pipe Elbow Material," NUREG/CR-5774, January 1992.

11.5 Kramer, G. and Papaspyropoulos, V., "Assessment of Circumferentially Complex-Cracked Pipe Subjected to Bending," NUREG/CR-4687, October 1986.

11.6 Schmidt, R. A., Wilkowski, G. M., and Mayfield, M. E., "The International Piping Integrity Research Group (IPIRG) Program: An Overview," SMiRT-11, Paper G23/1, August 1991.

APPENDIX A WELD PROCEDURE

United McGill Corporation
Columbus Operations 2400 Fairwood Avenue, P.O. Box 820, Columbus, Ohio 43216, 614/443-0192, Telex: 245-384

QW-482 SUGGESTED FORMAT FOR WELDING PROCEDURE SPECIFICATION (WPS)
(See QW-201.1, Section IX, ASME Boiler and Pressure Vessel Code)

Company Name UNITED McGILL CORP. By: Donald Tackett
Welding Procedure Specification No. S.1.400 Date 4-18-85 Supporting PQR No.(s) S.1.400-1,2,3
Revision No. 0 Date 4-18-85
Welding Process(es) GTAW-SMAW-SAW Type(s) MANUAL & MACHINE-SAW
(Automatic, Manual, Machine, or Semi-Auto.)

JOINTS (QW-402)
Joint Design SINGLE or DOUBLE GROOVE & FILLET
Backing (Yes) YES (No) --
Backing Material (Type) ARGON/GTAW; WELD/SMAW & SAW

Sketches, Production Drawings, Weld Symbols or Written Description should show the general arrangement of the parts to be welded. Where applicable, the root spacing and the details of weld groove may be specified.

(At the option of the Mfgr., sketches may be attached to illustrate joint design, weld layers and bead sequence, e.g. for notch toughness procedures, for multiple process procedures, etc.)

Details

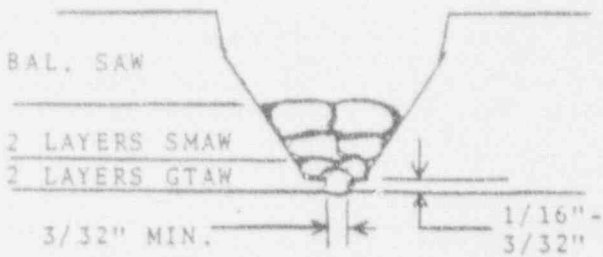

*BASE METALS (QW-403)
P-No. 8 Group No. 1 to P-No. 8 Group No. 1

Base Metal Thickness Range 3/16" to 2".
For GTAW and SMAW
Pipe Dia. Range Any.

For Submerge Arc-Pipe Dia. Range 6" and over.

Deposited Weld Metal Range
Groove GTAW 3/16"-7/16" Fillet ANY
Groove SMAW 3/16"-5/16" Fillet ANY
Groove SAW 3/16"-1-½" Fillet ANY
Other

*FILLER METALS (QW-404)
F-No. F-6 for GTAW & SAW Other F-5 for SMAW
A-No. A-8 Other A-8
Spec. No. (SFA) SFA-5.9 for GTAW & SAW SFA-5.4 for SMAW
AWS No. (Class) ER-308 E-308
Size of filler metals 3/32" for GTAW 1/8" for SMAW
1/8" - 3/32" For SAW
(Electrode, Cold Wire, Hot Wire, etc.)

Electrode-Flux (Class) ER-308/ST-100
Flux Trade Name LINCOLNWELD
Consumable Insert N/A

*Each base metal-filler metal combination should be recorded individually.

United McGill Corporation

Columbus Operations 2400 Fairwood Avenue PO Box 820 Columbus, Ohio 43216 614/443-0192 Telex 245-384

QW-484 MANUFACTURER'S RECORD OF WELDER OR WELDING OPERATOR QUALIFICATION TESTS

Welder Name RICHARD COOPER Check No. 1323 Stamp No. U4
Welding Process SUBMERGED ARC (SAW) Type MACHINE
In accordance with Welding Procedure Specification (WPS) S.1.400 REV.0
Backing (QW-402) YES WELD METAL
Material (QW-403) Spec. SA-240 to SA-240 of P No. 8 GROUP 1 to P No. 8 GROUP 1
Thickness 1" PLATE Dia. N/A
Filler Metal (QW-404) Spec. No. SFA-5.9 Class No. ER-308/ST-100 F No. 6
Other DEPOSITED WELD METAL SAW 5/8"
Position (QW-405) (1G, 2G, 6G) 1G
Gas (QW-408) Type N/A % Composition --
Electrical Characteristics (QW-409) Current DIRECT Polarity REVERSE
Weld Progression (QW-410) --
Other --

For Information Only
Filler Metal Diameter and Trade Name 1/8" L-18/8 LINCOLNWELD
Submerged Arc Flux Trade Name ST-100 LINCOLNWELD
Gas Metal Arc Welding Shield Gas Trade Name N/A

Guided Bend Test Results QW-462.2(a), QW-462.3(a), QW-462.3(b)

Type or Fig. No.	Result	
SIDE BEND QW-462.2 (a)	PASSED NO TEARS	QW-163
SIDE BEND QW-462.2 (a)	PASSED NO TEARS	QW-163
SIDE BEND QW-462.2 (a)	PASSED NO TEARS	QW-163
SIDE BEND QW-462.2 (a)	PASSED NO TEARS	QW-163
--	--	

Radiographic Test Results (QW-304 & QW-305)
For alternative qualification of groove welds by radiography
Radiographic Results: N/A

Fillet Weld Test Results (See QW-462.4(a), QW-462.4(b))
Fracture Test (Describe the location, nature and size of any crack or tearing of the specimen) N/A
Length and Per Cent of Defects -- inches -- %
Macro Test—Fusion --
Appearance—Fillet Size (leg) -- in. X -- in. Convexity -- in. or Concavity -- in.

Test Conducted by Philip A. Glaser Laboratory—Test No. UMC/QA
We certify that the statements in this record are correct and that the test welds were prepared, welded and tested in accordance with the requirements of Sections IX of the ASME Code.

Date 4-26-85 Organization UNITED McGILL CORP.
By Donald Tackett

United McGill Corporation

Columbus Operations 2400 Fairwood Avenue, P.O. Box 820, Columbus, Ohio 43216, 614/443-0192, Telex 245-384

QW-484 MANUFACTURER'S RECORD OF WELDER OR WELDING OPERATOR QUALIFICATION TESTS

Welder Name TOM M. SHAW Check No. 1737 Stamp No. 91
Welding Process GTAW & SMAW Type MANUAL
In accordance with Welding Procedure Specification (WPS) S.1.400 REV. 0
Backing (QW-402) YES ARGON/GTAW WELD/SMAW
Material (QW-403) Spec. SA-240 to SA-240 of P No. 8 GROUP 1 to P No. 8 GROUP 1
Thickness 1" PLATE Dia. N/A
Filler Metal (QW-404) Spec. No. SFA-5.9 SFA-5.4 Class No. ER-308 E-308 F No. 6, 5
Other DEPOSITED WELD METAL GTAW 7/32" SMAW 5/32"
Position (QW-405) (1G, 2G, 5G) 1G
Gas (QW-408) Type ARGON % Composition 100%
Electrical Characteristics (QW-409) Current DIRECT Polarity STRAIGHT/GTAW REVERSE/SMAW
Weld [illegible]ession (QW-410) --
Other --

For Information Only

Filler Metal [illegible] and Trade Name 3/32" McAY 1/8" LINCOLN
Submerged Arc Flux Trade Name N/A
Gas Metal Arc Welding Shield Gas Trade Name N/A

Guided Bend Test Results QW-462.2(a), QW-462.3(a), QW-462.3(b)

Type and Fig. No.	Result
SIDE BEND QW-462.2 (a)	PASSED NO TEARS QW-163
SIDE BEND QW-462.2 (a)	PASSED NO TEARS QW-163
SIDE BEND QW-462.2 (a)	PASSED NO TEARS QW-163
SIDE BEND QW-462.2 (a)	PASSED NO TEARS QW-163
--	--

Radiographic Test Results (QW-304 & QW-305)
For alternative qualification of groove welds by radiography

Radiographic Results: N/A

Fillet Weld Test Results (See QW-462.4(a), QW-462.4(b))

Fracture Test (Describe the location, nature and size of any crack or tearing of the specimen) N/A
Length and Per Cent of Defects -- inches -- %
Macro Test—Fusion --
Appearance—Fillet Size (leg) -- in. X -- in. Convexity -- in. or Concavity -- in.

Test Conducted by [signature] 4/26/85 Laboratory—Test No. UMC/CA

We certify that the statements in this record are correct and that the test welds were prepared, welded and tested in accordance with the requirements of Sections IX of the ASME Code.

Date 4-26-85 Organization UNITED McGILL CORP.
By [signature]

United McGill Corporation

Columbus Operations 2400 Fairwood Avenue, PO Box 820 Columbus Ohio 43216 614-443-0192 Telex 245-384

QW-484 MANUFACTURER'S RECORD OF WELDER OR WELDING OPERATOR QUALIFICATION TESTS

Welder Name JOHN HARNESS Check No 2304 Stamp No 40
Welding Process GTAW and SMAW Type MANUAL
In accordance with Welding Procedure Specification (WPS) 5.1.04 Rev. 0
Backing (QW-402) ARGON BACKING
Material (QW-403) Spec SA-240 TP 316 to SA-240-TP 316 of P No 8 GROUP 1 to P No 8 GROUP 1
Thickness 3/8" Dia PLATE
Filler Metal (QW-404) Spec. No. SFA.5.9 & 5.4 Class No. ER-308L E-308-16 F No 6 and 5
Other -----
Position (QW-405) (1G, 2G, 6G) 1G
Gas (QW-408) Type ARGON 100 % Composition WELDING GRADE
Electrical Characteristics (QW-409) Current DIRECT Polarity DCSP-GTAW/DCRP-SMAW
Weld Progression (QW-410) -----
Other -----

For Information Only

Filler Metal Diameter and Trade Name 3/32" N-S ER-308L & 1/8" E-308-16
Submerged Arc Flux Trade Name N/A
Gas Metal Arc Welding Shield Gas Trade Name N/A

Guided Bend Test Results QW-462.2(a), QW-462.3(a), QW-462.3(b)

Type and Fig. No.	Result
FACE BEND QW-452 & QW-466	SATISFACTORY NO TEARS
ROOT BEND QW-452 & QW-466	SATISFACTORY NO TEARS

Radiographic Test Results (QW-304 & QW-305)

For alternative qualification of groove welds by radiography

Radiographic Results: N/A

Fillet Weld Test Results [See QW-462.4(a), QW-462.4(b)]

Fracture Test (Describe the location, nature and size of any crack or tearing of the specimen) N/A

Length and Per Cent of Defects ----- inches ----- %

Macro Test—Fusion

Appearance—Fillet Size (leg) ----- in. X ----- in. Convexity ----- in. or Concavity ----- in.

Test Conducted by Alfred Gunn Co. Laboratory—Test No. N/A

We certify that the statements in this record are correct and that the test welds were prepared, welded and tested in accordance with the requirements of Sections IX of the ASME Code.

Date 8-26-82 Organization United McGill Corporation

By Orville Tackett

QW-483 (Back)

Tensile Test (QW-150) PQR No. S.1.400-1,2,3

Specimen No.	Width	Thickness	Area	Ultimate Total Load lb	Ultimate Unit Stress psi	Type of Failure & Location
A	.503	1.013	.5095	46,850	91,950	DUCTIL AT
						EDGE OF WELD
B	.495	1.011	.5004	45,980	91,890	DUCTIL AT
						EDGE OF WELD

Guided Bend Tests (QW-160)

Type and Figure No.	Result
SIDE BEND QW-462.2 (a)	PASSED QW-163 NO TEARS
SIDE BEND QW-462.2 (a)	PASSED QW-163 NO TEARS
SIDE BEND QW-462.2 (a)	PASSED QW-163 NO TEARS
SIDE BEND QW-462.2 (a)	PASSED QW-163 NO TEARS

Toughness Tests (QW-170)

Specimen No.	Notch Location	Notch Type	Test Temp.	Impact Values	Lateral Exp.		Drop Weight	
					% Shear	Mils	Break	No Break
N/A								
"								
"								
"								
"								

Fillet Weld Test (QW-180)

Result — Satisfactory: Yes N/A No " Penetration into Parent Metal: Yes " No "

Macro—Results "

Other Tests

Type of Test N/A

Deposit Analysis "

Other "

Welder's Name RICHARD COOPER/SAW THOMAS M. SHAW /GTAW & SMAW Clock No. 1323 1737 Stamp No. U4 91

Tests conducted by: [illegible] Laboratory Test No. UMC/QA

We certify that the statements in this record are correct and that the test welds were prepared, welded and tested in accordance with the requirements of Section IX of the ASME Code.

Manufacturer UNITED McGILL CORP.

Date 4-22-85 By Orville Tackett

(Detail of record of tests are illustrative only and may be modified to conform to the type and number of tests required by the Code.)

QW-483 SUGGESTED FORMAT FOR PROCEDURE QUALIFICATION RECORD (PQR)
(See QW-201.2, Section IX, ASME Boiler and Pressure Vessel Code)
Record Actual Conditions Used to Weld Test Coupon.

Company Name UNITED McGILL CORP.
Procedure Qualification Record No. S.1.400-3 Date 4-18-85
WPS No. S.1.400 rev. 0
Welding Process(es) SUBMERGED ARC (SAW)
Types (Manual, Automatic, Semi-Auto.) MACHINE

JOINTS (QW-402)

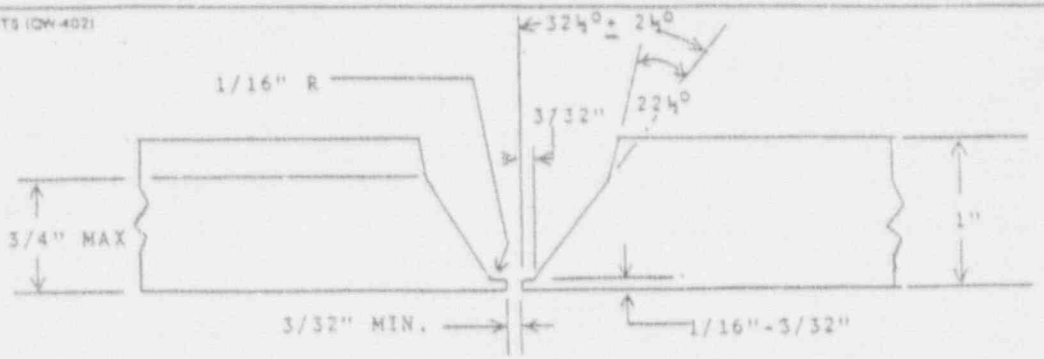

Groove Design of Test Coupon

(For combination qualifications, the deposited weld metal thickness shall be recorded for each filler metal or process used.)

BASE METALS (QW-403)
Material Spec. SA-240 to SA-240
Type or Grade 304 to 304
P-No. 8, GROUP 1 to P-No. 8, GROUP 1
Thickness of Test Coupon 1"
Diameter of Test Coupon PLATE
Other ONLY 5/8" of GROOVE WELDED

POSTWELD HEAT TREATMENT (QW-407)
Temperature NONE
Time --
Other --

GAS (QW-408)
Type of Gas or Gases N/A
Composition of Gas Mixture --
Other --

FILLER METALS (QW-404)
Weld Metal Analysis A-No. 8
Size of Filler Metal 1/8"
Filler Metal F-No. 6
SFA Specification 5.9
AWS Classification ER-308
Other DEPOSETED WELD METAL
12 PASSES 5/8" COMPLETE

ELECTRICAL CHARACTERISTICS (QW-409)
Current DIRECT
Polarity DCRP
Amps. 385 Volts 29
Tungsten Electrode Size N/A
Other --

POSITION (QW-405)
Position of Groove 1G
Weld Progression (Uphill, Downhill) --
Other --

TECHNIQUE (QW-410)
Travel Speed 18" - 20" I.P.M.
String or Weave Bead STRING
Oscillation N/A
Multipass or Single Pass (per side) MULTIPASS
Single or Multiple Electrodes SINGLE
Other --

PREHEAT (QW-406)
Preheat Temp. 60° F MIN.
Interpass Temp. 350° F MIN.
Other

QW-483 SUGGESTED FORMAT FOR PROCEDURE QUALIFICATION RECORD (PQR)
(See QW-201.2, Section IX, ASME Boiler and Pressure Vessel Code)
Record Actual Conditions Used to Weld Test Coupon

Company Name UNITED McGILL CORP.
Procedure Qualification Record No. 5.1.400-2 Date 4-18-85
WPS No. 5.1.400 rev. 0
Welding Process(es) SHIELDED METAL ARC (SMAW)
Types (Manual, Automatic, Semi-Auto.) MANUAL

JOINTS (QW-402)

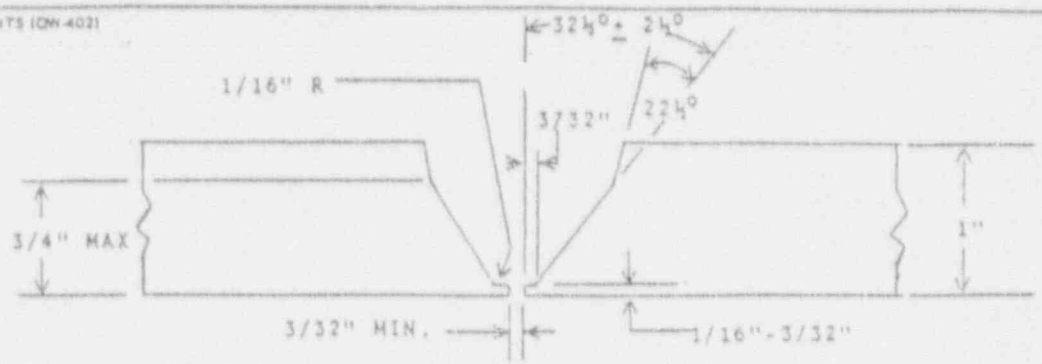

Groove Design of Test Coupon
(For combination qualifications, the deposited weld metal thickness shall be recorded for each filler metal or process weld.)

BASE METALS (QW-403)
Material Spec. SA-240 to SA-240
Type or Grade 304 to 304
P-No. 8, GROUP 1 to P-No. 8, GROUP 1
Thickness of Test Coupon 1"
Diameter of Test Coupon PLATE
Other ONLY 5/32" of GROOVE WELDED

POSTWELD HEAT TREATMENT (QW-407)
Temperature NONE
Time --
Other --

GAS (QW-408)
Type of Gas or Gases N/A
Composition of Gas Mixture --
Other --

FILLER METALS (QW-404)
Weld Metal Analysis A-No. 8
Size of Filler Metal 1/8"
Filler Metal F-No. 5
SFA Specification 5.4
AWS Classification E-308-16
Other DEPOSETED WELD METAL
4 PASSES 5/32" COMPLETE

ELECTRICAL CHARACTERISTICS (QW-409)
Current DIRECT
Polarity DCRP
Amps. 95 Volts 24
Tungsten Electrode Size N/A
Other --

POSITION (QW-405)
Position of Groove 1G
Weld Progression (Uphill, Downhill) --
Other --

TECHNIQUE (QW-410)
Travel Speed 10" I.P.M.
String or Weave Bead STRING
Oscillation N/A
Multipass or Single Pass (per side) MULTIPASS
Single or Multiple Electrodes SINGLE
Other --

PREHEAT (QW-406)
Preheat Temp. 60° F MIN.
Interpass Temp. 350° F MAX.
Other --

QW-483 SUGGESTED FORMAT FOR PROCEDURE QUALIFICATION RECORD (PQR)
(See QW-201.2, Section IX, ASME Boiler and Pressure Vessel Code)
Record Actual Conditions Used to Weld Test Coupon.

Company Name: UNITED McGILL CORP.
Procedure Qualification Record No.: S.1.400-1 Date: 4-18-85
WPS No.: S.1.400 rev. 0
Welding Process(es): GAS TUNGSTEN ARC (GTAW)
Type: (Manual, Automatic, Semi-Auto.): MANUAL

JOINTS (QW-402)

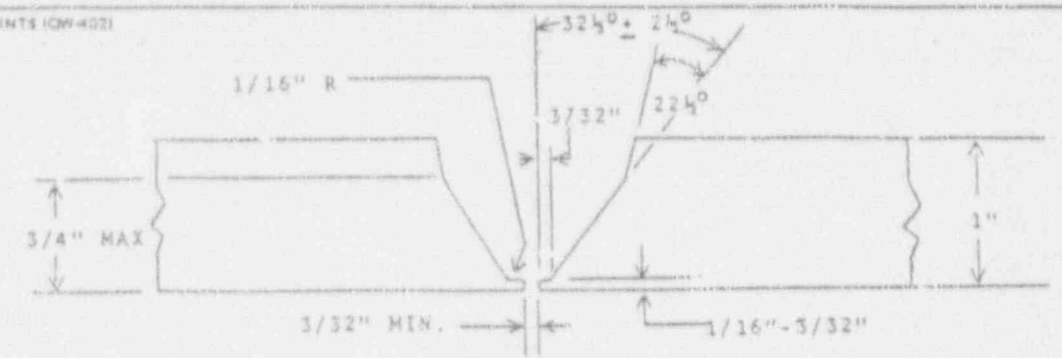

Groove Design of Test Coupon

(For combination qualifications, the deposited weld metal thickness shall be recorded for each filler metal or process used.)

BASE METALS (QW-403)
Material Spec.: SA-240 to SA-240
Type or Grade: 304 to 304
P-No.: 8 GROUP 1 to P-No.: 8 GROUP 1
Thickness of Test Coupon: 1"
Diameter of Test Coupon: PLATE
Other: ONLY 7/32" of GROOVE WELDED

FILLER METALS (QW-404)
Weld Metal Analysis A-No.: 8
Size of Filler Metal: 3/32"
Filler Metal F-No.: 6
SFA Specification: 5.9
AWS Classification: ER-308
Other: DEPOSITED WELD METAL
ROOT PASS FIRST LAYER - 2nd & 3rd
PASS 7/32" COMPLETE

POSITION (QW-405)
Position of Groove: 1G
Weld Progression (Uphill, Downhill): --
Other: --

PREHEAT (QW-406)
Preheat Temp.: 60° F MIN.
Interpass Temp.: 350° F MIN.
Other: --

POSTWELD HEAT TREATMENT (QW-407)
Temperature: NONE
Time: --
Other: --

GAS (QW-408)
Type of Gas or Gases: ARGON
Composition of Gas Mixture: 100% WELDING GRADE
Other: 22 CHF FLOW, # 7 CUP
ARGON for PURGING BACKSIDE
10 CHF FLOW

ELECTRICAL CHARACTERISTICS (QW-409)
Current: DIRECT
Polarity: DCSP
Amps: 105 Volts: 15
Tungsten Electrode Size: 3/32
Other: 2% THORIATED

TECHNIQUE (QW-410)
Travel Speed: 2" - 3" I.P.M.
String or Weave Bead: STRING
Oscillation: N/A
Multipass or Single Pass (per side): MULTIPASS
Single or Multiple Electrodes: SINGLE
Other: --

QW-482 (Back)

WPS No. S.1.400 Rev. 0

POSITIONS (QW-405)
Position(s) of Groove 1G
Welding Progression: Up N/A Down N/A
Position(s) of Fillet 1F & 2F

POSTWELD HEAT TREATMENT (QW-407)
Temperature Range NONE
Time Range --

PREHEAT (QW-406)
Preheat Temp. Min. 50° F
Interpass Temp. Max. 450° F
Preheat Maintenance TORCH NEUTRAL FLAME
(Continuous or special heating where applicable should be recorded)

GAS (QW-408)
Shielding Gas(es) N/A
Percent Composition (mixtures) --
Flow Rate --
Gas Backing --
Trailing Shielding Gas Composition --

ELECTRICAL CHARACTERISTICS (QW-409)
Current AC or DC DIRECT Polarity REVERSE
Amps (Range) PER TABLE Volts (Range) PER TABLE
(Amps and volts range should be recorded for each electrode size, position, and thickness, etc. This information may be listed in a tabular form similar to that shown below.)

MACHINE
SUBMERGED ARC WELDING
(SAW)

Tungsten Electrode Size and Type N/A
(Pure Tungsten, 2% Thoriated, etc.)
Mode of Metal Transfer for GMAW N/A
(Spray arc, short circuiting arc, etc.)
Electrode Wire feed speed range 50 - 60 I.P.M. 1/8", 55-65 I.P.M. 3/32"

TECHNIQUE (QW-410)
String or Weave Bead STRING
Orifice or Gas Cup Size N/A
Initial and Interpass Cleaning (Brushing, Grinding, etc.) ONLY WITH STAINLESS STEEL BRUSHES AND ALUMINUM OXIDE GRINDING WHEEL.
Method of Back Gouging AIR ARC and/or GRIND IF REQUIRED
Oscillation N/A
Contact Tube to Work Distance 5/8" - 1-1/2"
Multiple or Single Pass (per side) MULTIPLE
Multiple or Single Electrodes SINGLE
Travel Speed (Range) 14" - 24" I.P.M. 1/8", 12-22 I.P.M. 3/32"
Peening NONE
Other --

Weld Layer(s)	Process	Filler Metal Class	Filler Metal Dia.	Current Type Polar.	Current Amp. Range	Volt Range	Travel Speed Range	Other (e.g., Remarks, Comments, Hot Wire Addition, Technique, Torch Angle, Etc.)
1 & UP	SAW	ER-308	1/8"	DCRP	350-400	28-30	14-24 I.P.M.	
1 & UP	SAW	ER-308 ST-100 FLUX	3/32"	DCRP	275-325	24-26	12-22	

QW-482 (Back)

WPS No 5.1.400 Rev 0

POSITIONS (QW-405)
Position(s) of Groove 1G - 6G
Welding Progression: Up YES Down NO
Position(s) of Fillet 1F - 5F

POSTWELD HEAT TREATMENT (QW-407)
Temperature Range NONE
Time Range --

PREHEAT (QW-406)
Preheat Temp Min. 50° F
Interpass Temp. Max. 450 F
Preheat Maintenance TORCH NEUTRAL FLAME
(Continuous or special heating where applicable should be recorded)

GAS (QW-408)
Shielding Gas(es) N/A
Percent Composition (mixtures) --
Flow Rate --
Gas Backing --
Trailing Shielding Gas Composition --

ELECTRICAL CHARACTERISTICS (QW-409)
Current AC or DC DIRECT Polarity REVERSE
Amps (Range) PER TABLE Volts (Range) PER TABLE
(Amps and volts range should be recorded for each electrode size, position, and thickness, etc. This information may be listed in a tabular form similar to that shown below.)

MANUAL
SHIELDED MATAL ARC WELDING
(SMAW)

Tungsten Electrode Size and Type N/A (Pure Tungsten, 2% Thoriated, etc.)
Mode of Metal Transfer for GMAW N/A (Spray arc, short circuiting arc, etc.)
Electrode Wire Feed speed range N/A

TECHNIQUE (QW-410)
String or Weave Bead EITHER or BOTH
Orifice or Gas Cup Size N/A
Initial and Interpass Cleaning (Brushing, Grinding, etc.) ONLY WITH STAINLESS STEEL BRUSHES AND ALUMINUM OXIDE GRINDING WHEELS
Method of Back Gouging AIR ARC and/or GRIND IF REQUIRED
Oscillation MANUAL 2 FILLER DIA./ STRING 5-FILLER DIA./ WEAVE MAX.
Contact Tube to Work Distance N/A
Multiple or Single Pass (per side) MULTIPLE
Multiple or Single Electrodes SINGLE
Travel Speed (Range) 4" - 12" I.P.M.
Peening NONE
Other NO SINGLE PASS TO EXCEED 5" in THICKNESS

Weld Layer(s)	Process	Filler Metal Class	Filler Metal Dia.	Current Type Polar.	Current Amp. Range	Volt Range	Travel Speed Range	Other (e.g., Remarks, Comments, Hot Wire Addition, Technique, Torch Angle, Etc.)
1 -2	SMAW	E-308-16	1/8"	DCRP	80-110	22-26	4"-12" I.P.M.	
1-2	SMAW	E-308-16	3/32"	DCRP	60-80	18-22		

QW-482 (Back)

WPS No. 5.1.400 Rev. 0

POSITIONS (QW-405)
Position(s) of Groove 1G - 6G
Welding Progression: Up YES Down
Position(s) of Fillet 1F - 5F

POSTWELD HEAT TREATMENT (QW-407)
Temperature Range NONE
Time Range

PREHEAT (QW-406)
Preheat Temp. Min 50° F
Interpass Temp. Max 450° F
Preheat Maintenance TORCH, NEUTRAL FLAME
(Continuous or special heating where applicable should be recorded)

GAS (QW-40)
Shielding Gas(es) ARGON
Percent Composition (mixtures) 100%
Flow Rate 20 - 25 CFH
Gas Backing 8 - 12 CFH
Trailing Shielding Gas Composition N/A

ELECTRICAL CHARACTERISTICS (QW-409)
Current AC or DC DIRECT Polarity STRAIGHT
Amps (Range) PER TABLE Volts (Range) PER TABLE
(Amps and volts range should be recorded for each electrode size, position, and thickness, etc. This information may be listed in a tabular form similar to that shown below.)

MANUAL
GAS TUNGSTEN ARC WELDING
(GTAW)

Tungsten Electrode Size and Type 3/32" 2% THORIATED
(Pure Tungsten, 2% Thoriated, etc.)
Mode of Metal Transfer for GMAW N/A
(Spray arc, short circuiting arc, etc.)
Electrode Wire feed speed range N/A

TECHNIQUE (QW-410)
String or Weave Bead STRING
Orifice or Gas Cup Size #6 - #7
Initial and Interpass Cleaning (Brushing, Grinding, etc.) ONLY WITH STAINLESS STEEL BRUSHES AND ALUMINUM OXIDE GRINDING WHEELS
Method of Back Gouging N/A
Oscillation MANUAL 2 FILLER DIAMETERS MAX.
Contact Tube to Work Distance 1/16" - 3/32"
Multiple or Single Pass (per side) MULTIPLE
Multiple or Single Electrodes SINGLE
Travel Speed (Range) MANUAL 2 - 4 I.P.M.
Peening NONE
Other

Weld Layer(s)	Process	Filler Metal Class	Filler Metal Dia.	Current Type Polar.	Current Amp. Range	Volt Range	Travel Speed Range	Other (e.g., Remarks, Comments, Hot Wire Addition, Technique, Torch Angle, Etc.)
1-2	GTAW	ER-308	3/32"	DCSP	90-130	14-18	2-4 I.P.M.	
1-2	GTAW	ER-308	1/16"	DCSP	50-90	10-14		

APPENDIX B TOUGHNESS ANISOTROPY ABSTRACT

B.1 Nomenclature Used in Abstracts

In the extended abstracts which follow, a two-letter abbreviation is used to describe the orientation of fracture toughness specimens. The first letter indicates the direction of the principal tensile stress and the second letter indicates the direction of crack growth. For example, in specimens machined from a pipe, the designation C-L would denote a specimen oriented such that it was being stressed in the circumferential (C) direction and the crack would be growing in the longitudinal (L) direction.

For pipes and round bars, the letters R, C, and L indicate radial, circumferential, and longitudinal direction, respectively. For plates, the letters T, S, and L indicate transverse, short transverse, and longitudinal direction, respectively.

The term anisotropy coefficient as used in these abstracts refers to the following toughness ratios:

- For pipes and round bars

  E(C-L)/E(L-C) or E(R-L)/E(L-R)

- For plates

  E(T-L)/E(L-T) or E(S-L)/E(L-S)

where E is a quantitative measure of toughness and the letters within the parentheses indicate the specimen orientation. A value of 1.0 for the anisotropy coefficient means that the toughness is not orientation dependent, whereas low values indicate a high degree of toughness anisotropy.

B.2 Extended Abstracts

B.2.1 [Ref. 6.4] Matrosov, Yu. I. and Polyakov, I. E., "Improving Toughness and Ductility and Reducing Property Anisotropy in Low Alloy Steels," BISI Translation 14384, Stal', 1976 (2), pp. 162-167. [Ref. 6.4]

This document is a review paper that examines various factors determining the anisotropy of ductile and impact properties of carbon steels and low-alloys steels.

The effect of carbon on toughness anisotropy arises primarily through the development of banded microstructures. Decreasing the carbon content reduces the degree of banding and thereby, improves the anisotropy coefficient, defined as the ratio of transverse to longitudinal toughness. A steel which displayed no anisotropy would have a coefficient of 1.0. The authors state that banding alone can produce an anisotropy coefficient as low as approximately 0.8. In order for the effect of lower carbon to be significant in reducing anisotropy due to banding, it is necessary to go to reduced-pearlite steels (up to 0.08 percent carbon) or even to pearlite-free steels (up to 0.03 percent carbon). Reducing the carbon to these levels causes a substantial loss of strength, which can be

overcome by microalloying with elements such as niobium, vanadium, and titanium. The authors state that, even at the time of preparation of their review (1976), the beneficial effect of a reduction in carbon was being widely utilized in the development of a group of reduced-pearlite and pearlite-free precipitation hardening steels.

Sulfur has long been known to be one of the principal culprits in causing toughness anisotropy in plate because it combines with manganese to form MnS inclusions, which elongate during hot rolling of the steel to form long stringers within the microstructure. Fracture can occur much more readily along those inclusions than across them. Thus, these MnS stringers are the principal source of low anisotropy coefficients. There are a number of different ways to deal with the sulfur problem. These include reducing the sulfur content, reducing the manganese content, and making the sulfur-containing inclusions more brittle so that they do not elongate during deformation processing.

According to the authors, reducing the sulfur content produces a significant reduction in toughness anisotropy only when the sulfur content is below approximately 0.010 percent. Reducing the sulfur from 0.04 percent to 0.02 percent has relatively little effect. Sharp improvements are realized when sulfur is maintained at levels of 0.004 percent or below. Although the attainment of low sulfur levels was at one time difficult and expensive, the authors point out that, even in 1976, economical industrial methods were available for accomplishing this result.

With respect to manganese content, the authors note that reducing the manganese/sulfur ratio below a certain level (while adding silicon to maintain strength) can cause a significant reduction in the degree of anisotropy in rolled plate. For example, the anisotropy coefficient reached a value of 0.85 in a manganese-free steel which contained 0.028 percent sulfur. Nonetheless, the authors do not recommend the elimination of manganese from carbon steels because of its many useful characteristics as an alloying element.

The third method cited by the authors as being effective in lowering the degree of toughness anisotropy is to reduce the ductility of the sulfur-bearing inclusions. The role of oxygen in this regard is relatively modest but is worth noting prior to discussing the role of other elements. The authors state that, in balanced or rimmed steels, the sulfides contain significant amounts of oxygen which considerably reduces their plasticity and their ability to form stringers. Therefore, the authors state that rimmed steels are likely to show less toughness anisotropy than killed steels, in which most of the oxygen is present in the form of oxide inclusions and the sulfides are nearly pure MnS.

A more effective way to form low-plasticity sulfides, according to the authors, is to add titanium, zirconium, or rare-earth metals, especially cerium. Each of these elements has a higher affinity for sulfur than does manganese. The authors cite an investigation in which the cerium/sulfur ratio was varied from 0 to more than 3. When the ratio was zero, the anisotropy coefficient was approximately 0.4. The coefficient increased markedly as cerium was added, reaching a value of approximately 0.85 at a cerium/sulfur ratio of 1.5 to 2.0. Greater amounts of cerium led to a gradual reduction in the coefficient.

The authors conclude that a reduction of toughness anisotropy can be achieved "by reducing the sulfur content using thorough desulfurization outside the blast furnace or syathetic slag treatment of the steel and also by alloying the steel with elements which form low-plasticity sulfides. At the present time,

both these methods have been adequately investigated and developed for introduction into tonnage production of weldable structural steels."

B.2.2 [Ref. 6.5] Burnos, V. ..., Vaschilo, T. P., and Balandina, L. E., "Evaluation of the Quality of the Metal of Pipes According to Impact Toughness with Anisotropy Taken into Account," Industrial Laboratory (USSR); English translation of Zavodskaya Laboratoriya, Volume 54, No. 5, May 1988, pp. 548-550.

The authors conducted impact bend tests on specimens machined from two different heats of steel pipe. The pipe was of unspecified composition and had a diameter of 122 mm (4.8 inches) and a wall thickness of 6 mm (0.24 inch). Three different conditions were examined: (1) as cold formed, (2) after subsequent heat treatment at 250 C (482 F) for 1 hour, and (3) after subsequent heat treatment at 350 C (662 F) for 1 hour.

Bend specimens were machined in three orientations: (1) longitudinal (L-C), (2) transverse (C-L), and short transverse (C-R). The specimens were 5 x 10 x 55 mm (0.197 x 0.394 x 2.17 inches) (longitudinal) or 6 x 10 x 55 mm (0.236 x 0.394 x 2.17 inches) (transverse and short transverse arc-shaped specimens). The notch was U-shaped and of unspecified dimensions. The specimens were tested in a pendulum impact tester at room temperature and at -40 C (-40 F). Three to five specimens were tested at each temperature, but only average values of toughness, expressed as energy per unit area, were reported by the authors.

The results of this investigation confirm what many other investigators have reported, namely, that the transverse toughness of unidirectionally deformed steel is much lower than the longitudinal toughness. At room temperature, the transverse toughness of both heats of steel was 26 to 30 percent of the longitudinal toughness, regardless of the condition of the steel. At -40 C (-40 F), that ratio dropped to only 15 to 20 percent.

The authors found also that the toughness in the short transverse orientation (with the crack growing radially) was less, by approximately 15 to 20 percent, than in the longitudinal orientation (with the crack growing circumferentially).

B.2.3 [Ref. 6.6] Harada, S., Endo, T., and Kaseda, M., "Effects of Forging Ratio and Specimen Orientation on Elastic-Plastic Fracture Toughness of Thick Forged Steel Plates," Role of Fracture Mechanics in Modern Technology, G. C. Sih, H. Nisitani, and T. Ishihara, Eds., Elsevier Science Publishers, 1987, pp. 485-496.

While this reference contains much valuable information about the effects of forging ratio and specimen orientation on the toughness of thick, forged A533B Class 1 steel, the orientations investigated are of only limited interest relative to skewed fracture in pipe tests of steel. Only two orientations were studied, one of which was T-S, equivalent to the C-R orientation in a pipe, and the other was S-T, equivalent to the R-C orientation in a pipe. The orientations of principal interest in

pipe tests relative to the occurrence of skewed crack growth from circumferential notched are L-C and C-L, as well as orientations intermediate to those two.

The authors found that the upper-shelf toughness of the steel, hot forged to a thickness of 200 mm (7.9 inches), was always lower in the S-T orientation than in the T-S orientation, by approximately 20 percent in Charpy tests and 25 percent in J_{Ic} tests. The toughness difference between the two orientations was increased when additional hot forging was employed to reduce the thickness of the plates to 100 mm (3.9 inches). After the additional forging, the toughness in the S-T orientation was approximately 45 percent lower than that in the T-S orientation as determined from Charpy tests and approximately 55 percent lower as determined from J_{Ic} tests.

B.2.4 [Ref. 6.7] Kramer, G. S., Wilkowski, G. M., and Maxey, W. A., "Flaw Tolerance of Spiral-Welded Line Pipe," Battelle report to American Gas Association, NG-18 Report No. 154, January 1987.

The authors investigated specimen-orientation effects in two different lengths of spiral-welded pipe. The pipe was API 5LS-X52 having a diameter of 406 mm (16 inches) and a wall thickness of 7.9 mm (0.312 inch). The spiral-welded seam was oriented at a 52-degree angle to the pipe axis. The steel contained 0.025 percent sulfur but no other information was provided regarding thermal mechanical history or inclusion size and shape.

Two types of specimens were used to investigate orientation effects: (1) flattened straps to determine tensile properties, and (2) 2/3-size Charpy V-notch impact specimens to determine the upper-shelf toughness.

The results showed that the tensile properties, including the yield strength, the ultimate tensile strength, and the fracture elongation, were relatively independent of specimen orientation. Charpy values, on the other hand, were strongly dependent on specimen orientation. A graph of Charpy energy versus specimen angle was a sine wave whose maximum value was for specimens in the L-T orientation of the plate used to make the pipe and whose minimum value was for specimens in the T-L orientation. The ratio of minimum to maximum value was approximately 1/3, which is within the range that has been reported for many other plates and pipes.

B.2.5 [Ref. 6.8] Rosenfield, A. R., Hahn, G. T., and Markworth, A. J., "Effect of Metallurgical Variables on the Maximum Charpy Impact Energy of Structural Steels," Battelle report to the American Gas Association, NG-18 Report No. 27, September 1971.

These investigators examined two different contributors to toughness anisotropy in carbon steel plates: sulfide inclusion length and the presence of a banded microstructure. Upper-shelf Charpy energy was used to characterize the toughness in both the longitudinal (L-T) and the transverse (T-L) orientations. It was reported that the ratio of transverse to longitudinal toughness was approximately 0.5 for sulfide inclusion lengths of 8 μm. However, by extrapolating the data to shorter sulfide lengths,the toughness difference between the two orientations was predicted to vanish at inclusion

lengths of 3 to 4 μm. In addition, it was shown that the general level of toughness in both orientations increases as sulfide inclusion length decreases.

It also was shown in this report that a reduction of the degree of metallurgical banding present in ferritic steel plate, accomplished by a homogenizing heat treatment, can both increase the Charpy upper-shelf toughness and reduce the degree of anisotropy. The longitudinal toughness was reported to be increased by 5 to 10 percent and the transverse toughness by approximately 40 percent as a result of the homogenizing treatment. The ratio of transverse to longitudinal toughness was increased from 0.35 in the banded condition to 0.45 in the homogenized condition.

B.2.6 [Ref. 6.9] Williams, D. N., "Metallurgical Factors," in 6th Symposium on Line Pipe Research, American Gas Association Catalog No. L30175, October 29, 1979.

Williams conducted Charpy V-notch impact tests on specimens machined from tee fittings fabricated from carbon steel plates. Some of the specimens were oriented axially and the others circumferentially. In two different tee fittings, it was found that the ratio of energy values in the two directions was approximately 3 to 1. That ratio is typical of values reported by numerous other investigators. However, in one of the tees, the highest toughness was in the circumferential direction and in the other, the highest toughness was in the axial direction. The conclusion drawn from this investigation was that it is not safe to assume that tee fittings are always manufactured with a specified plate orientation.

B.2.7 [Ref. 6.16] Hodge, J. M., Frazier, R. H., and Boulger, F. W., "The Effect of Sulfur on the Notch Toughness of Heat-Treated Steels," Transactions of the Metallurgical Society of AIME, Volume 215, October 19: p. 745-753.

This paper reports an investigation designed to furnish quantitative information on the effect of sulfur on notch impact toughness and the factors affecting the anisotropy of impact properties in wrought heat-treated low-alloy steels.

A total of 12 melts were prepared, each weighing 2670 N (600 pounds). Their nominal compositions were: 0.30% C, 0.80% Mn, 0.25%Si, 2.5% Ni, 0.80% Cr, and 0.45% Mo. The sulfur contents ranged from 0.005% to 0.179%. The ingots, which were 203 mm (8 inches) square at the base and 229 mm (9 inches) square at the top, were hot rolled on a commercial mill to 48 mm (1.9 inch) slabs. Sections of the slabs were then rolled to 12.7 mm (0.5 inch) thickness according to one of three schedules: (1) straightaway rolled, (2) cross rolled 29 percent, or (3) cross rolled 46 percent. The plates were then hardened by quenching and tempering to obtain Rockwell C hardness levels of 25, 30, 35, or 40. Charpy V-notch specimens were taken both transverse (T-L orientation) and longitudinal (L-T orientation) to the main rolling direction and tested at various temperatures encompassing the ductile-to-brittle transition.

The authors concluded the following:

1. Increasing the sulfur content decreases Charpy V-notch impact resistance in a regular manner for both straightaway and cross-rolled conditions. When plotted on logarithmic coordinates, the Charpy values versus sulfur content describe straight lines.

2. Sulfur content did not markedly affect the ductile-brittle transition temperature.

3. Directionality of toughness properties depends on rolling practice and not on sulfur content. Cross rolling decreases the spread in Charpy values between longitudinal and transverse specimens proportional to its amount (46 percent cross rolling eliminated directionality entirely) and independent of sulfur content. (Note added by reviewer: It was not completely accurate for the authors to state that directionality is independent of sulfur content. Their data showed that the anisotropy coefficient in straightaway rolled plates was approximately 0.29 at 0.060% S, 0.33 at 0.02% S, and 0.50 at 0.005% S, and it is likely that the coefficient would increase even further at sulfur contents below 0.005%. Nonetheless, it is striking to find such a high degree of anisotropy at a sulfur level of only 0.005%.)

4. The effect of sulfur on impact properties is similar in steels with pearlitic or slack-quenched microstructures to that in steels with tempered martensitic microstructures, for steels with sulfur contents of 0.060% or below.

5. Charpy values are improved by an homogenization treatment of 10 hours at 1290 C (2350 F), independent of sulfur content, but directionality of properties is relatively unaffected. This treatment results in a rounding of sulfide inclusions, which is believed to be the principal factor in the improved impact properties.

B.2.8 [Ref. 6.11] Tomita, Y., "Effect of Decreased Hot-Rolling Reduction Treatment on Fracture Toughness of Low-Alloy Structural Steels," Metallurgical Transactions A, Vol. 21A, September 1990, pp. 2555-2563.

Tomita investigated the effect of decreasing the amount of hot-rolling reduction from 98 percent to 80 percent on the fracture toughness of quenched and highly tempered [650 C (1200 F) for 2 hours] low-alloy structural steels. The steels were AISI 1045, AISI 4140, and AISI 4340. Each steel contained 0.018 to 0.020 percent sulfur and a volume fraction of MnS inclusions ranging from 0.14 to 0.18 percent.

Tomita found that reducing the amount of hot-rolling reduction from 98 to 80 percent produced a number of effects: (1) the sulfide inclusions were modified from a stringer (aspect ratio of approximately 17) to an ellipse (aspect ratio of approximately 4), (2) the tensile yield and tensile ultimate strengths were not significantly changed, (3) the upper-shelf Charpy toughness in the transverse (T-L) orientation, which originally was only about 30 percent of the toughness in the longitudinal (L-T), was increased by a factor of approximately 2.3 to a level of approximately 70

percent of the toughness in the longitudinal orientation, (4) upper-shelf J_{Ic} values in the T-L orientation, which originally were less than 25 percent of the values in the L-T orientation, were increased by a factor of approximately 3.0, and (5) the ductile-to-brittle transition temperature was not strongly influenced.

These results show clearly that inclusion shape is of paramount importance in controlling the degree of toughness anisotropy.

B.2.9 [Ref. 6.12] Garwood, S. J., "The Effect of Temperature, Orientation, and Constraint on the Toughness of A533B Class 1 Steel," Application of Fracture Mechanics to Materials aad Structures, Martinus Nijhoff Publishers, 1984 pp. 939-950.

Garwood conducted precracked, 3-point bend tests on specimens machined from 90-mm (3.5-inch)-thick A533B Class 1 plates. He investigated four different specimen orientations -- L-T, L-S, T-L, and T-S -- and determined four different fracture toughness parameters. Those parameters were J_i (J at crack initiation), dJ/da (the slope of the J-R curve), δ_i (the crack tip opening displacement at crack initiation), and dδ/da (the slope of the graph of crack-tip-opening displacement versus crack extension). The sulfur content of the steel was stated to be less than 0.005 percent, but little information was provided about the thermal mechanical history or the shape of the nonmetallic inclusions.

The two orientations in Garwood's study that are of major interest with regard to toughness anisotropy in pipe tests are L-T and T-L. Regardless of which toughness parameter was used, Garwood found, as expected, that the T-L orientation was consistently less tough than the L-T orientation. However, the difference between the two orientations was not as pronounced as has been reported by numerous investigators. If a value of 1.0 is assigned to each toughness parameter measured in the L-T orientation, the corresponding values in the T-L orientation were found to be: J_i 0.74, dJ/da 0.51, δ_i 0.63, and dδ/da 0.66. These toughness reductions of approximately 25 to 50 percent are far less than reductions in upper-shelf Charpy energy of 50 to 75 percent that are commonly found in carbon and low-alloy steels. The reason for the smaller effect of specimen orientation in Garwood's tests is not known because no information is available about the size and shape of the inclusions.

B.2.10 [Ref. 6.13] Park, J. W., Kim, J. S., and Moon, I. G., "The Effect of Banded Structure and Sulfide Morphology on the Anisotropy of Tensile Ductility and Impact Toughness," Journal of the Korean Institute of Metals, Vol. 22, No. 7, July, 1984, pp. 588-595.

It was not possible to do a thorough review of this paper because the text was in Korean. Only the abstract, figures, and tables were in English.

The authors studied the effects of pearlite banding and sulfide morphology on the anisotropy of tensile properties and impact toughness in three different hot-rolled C-Mn steels. Each of the steels contained 0.17 to 0.19% carbon, 1.25% manganese, and 0.02 to 0.022% sulfur. One of the steels

was treated with a rare-earth addition to modify the shape of the sulfide inclusions. Homogenizing treatments for different lengths of time at a temperature which was not given in the English portion of the reference were used to change the pearlite distribution, i.e. to reduce the degree of banding. Tensile specimens were tested in the longitudinal and in the transverse orientation. Notched, 3-point impact bend specimens were machined in four different orientations: L-T, T-L, L-S, and T-S. They were tested at, presumably, room temperature.

The effect of the rare-earth addition was to reduce the degree of anisotropy in the as-rolled condition. The ratio of toughness in the T-L orientation to that in the L-T orientation was 0.67 when the rare earth was added; without the rare earth, the ratio was 0.54. Homogenization treatments to reduce the degree of banding of the pearlite improved that ratio for both steels. The rare-earth treated steel improved to a ratio of 0.85, while the untreated steel improved to a ratio of 0.58.

It is the authors' belief that the planar anisotropy of tensile ductility is due primarily to the elongated sulfides rather than to pearlite banding, based on the effects of homogenization treatments. However, they believe the anisotropy in toughness is associated with both the pearlite banding and sulfide morphology. The pearlite banding is the cause of anisotropy associated only with notch orientation, while the elongated sulfides are the cause of anisotropy associated with both notch and specimen orientation.

B.2.11 [Ref. 6.14] Fegredo, D. M., Faucher, B., and Shehata, M. T., "Influence of Inclusion Content, Texture and Microstructure on the Toughness Anisotropy of Low Carbon Steels," Strength of Metals and Alloys, Volume 2, Pergamon Press, Ltd., 1985, pp. 1127-1132.

The objective of these investigators was to determine how the fracture toughness anisotropy of low-carbon (0.06 to 0.09 percent) steels containing two levels of sulfur (0.007 and 0.02 percent), with and without added rare-earth elements (cerium and lanthanum) to modify the sulfides, is affected by soaking and rolling temperature. It is the authors' belief that low rolling temperatures, particularly below A_{r3}, produce the most severe toughness anisotropy due to a combination of pancaked microstructures, crystallographic texture (preferred orientation of individual grains), and flattened and elongated sulfide inclusions.

The authors studied steels that had been rolled to 67% reduction in thickness at six different soaking temperatures, ranging from 680 to 1200 C (1256 to 2192 F). They tested Wedge Opening Load specimens at several temperatures, many of which did not produce ductile fracture. Only two orientations were examined -- S-L and T-L. It is not clear why the two higher toughness orientations -- L-T and L-S -- were not investigated.

The occurrence of pancaked microstructures and several strong rolling plane textures was demonstrated for the lower soaking temperatures. At the higher soaking temperatures, the grains became equiaxed and the crystallographic texture was greatly reduced.

It is difficult to interpret the authors' results, both because they did not include specimens in the high-toughness orientations and because the test temperatures of specimens rolled at different temperatures and having different orientations were not always the same. Nonetheless, the authors

concluded that the main contributors to reduced toughness in the S-L orientation, resulting from rolling at low temperatures, are pancaked microstructures and flattened sulfides. They state their belief that pancaked microstructures probably is the more damaging component; however, the two contributors behave synergistically when both are present.

B.2.12 Lai, M. O. and Ferguson, W. G., "Relationship Between Fracture Topography and Fracture Toughness of a High Strength Steel," Journal of Materials Science, Vol. 20, 1985, pp. 1985-1992.

The main thrust of this investigation was to study fracture topography as a function of tempering temperature and specimen orientation. Only a limited study of property variations with specimen orientation was reported.

The steel investigated was Comsteel En25, a high-strength low-alloy steel in the form of 125-mm (4.9-inch)-diameter bar. It contained 0.31% carbon, 0.26% silicon, 0.58% manganese, 0.025% phosphorus, 0.032% sulfur, 2.22% nickel, 0.59% chromium, and 0.53% molybdenum. No information was provided on the reduction ratio of the bar or on the shape and size of the MnS inclusions.

The only fracture toughness data that dealt with the anisotropy question were K_{Ic} values obtained from the R-L and L-R orientations in material that had been hardened and tempered at 500 C (932 F). The fracture toughness in the L-R orientation was reported to be 150.4 MPa$\sqrt{m}$ (136.7 ksi$\sqrt{in}$), while that in the R-L orientation was 83.7 MPa$\sqrt{m}$ (76.1 ksi$\sqrt{in}$), yielding an anisotropy coefficient of 0.56.

With respect to fracture topography, the authors reported that terrace-type fracture prevailed in the R-L orientation, but this frequently was observed to change to zigzag-type fracture in the R-C orientation. Both of these fracture mechanisms were absent in the L-R orientation.

APPENDIX C FRACTURE PATHS IN CARBON STEEL PIPES

Abbreviations used in Figure C-1:

- c = half-crack length
- D = pipe diameter
- d = depth of surface crack
- t = pipe wall thickness
- SS = single shear fracture
- DS = double shear fracture
- A = blue oxide
- B = no oxide
- C = bronze-colored oxide

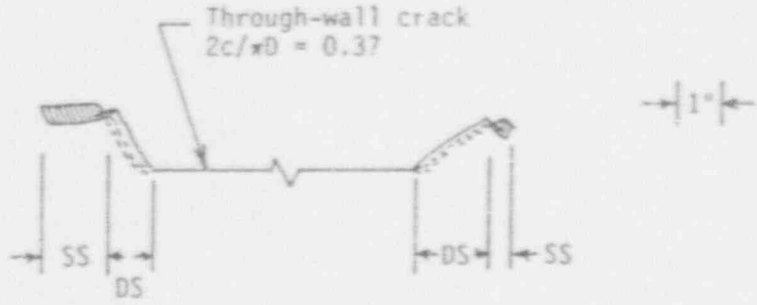

(a) Experiment 4111-1, four-point bending
Pipe DP2-F11, A333 Grade 6, 4.5-inch diameter, Schedule 80

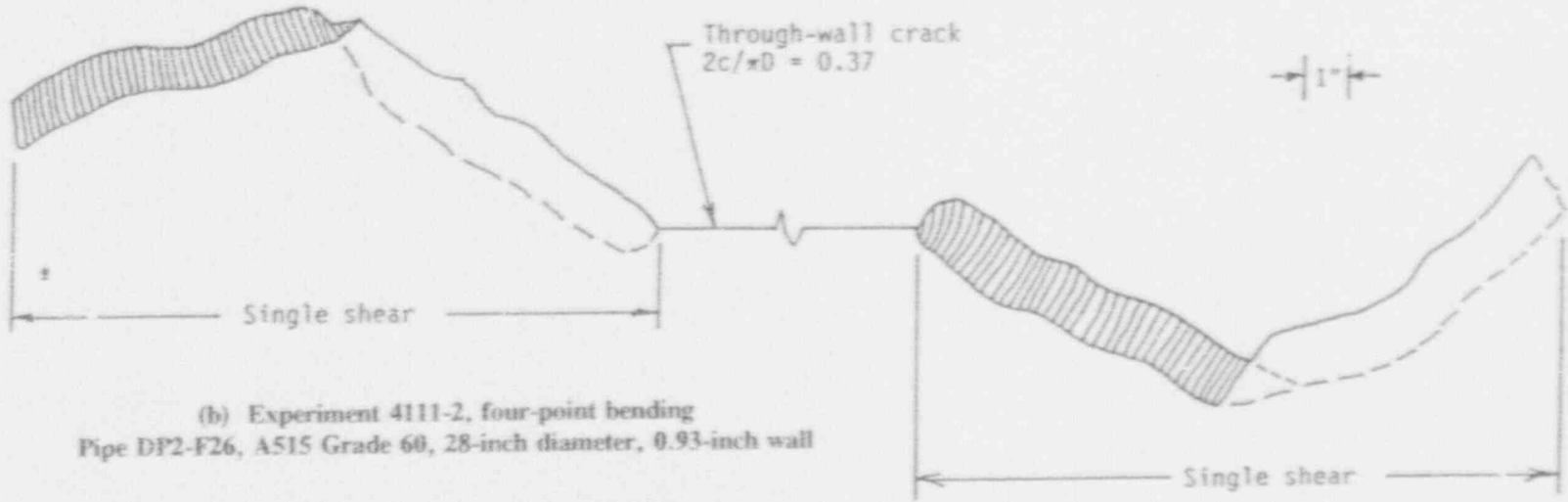

(b) Experiment 4111-2, four-point bending
Pipe DP2-F26, A515 Grade 60, 28-inch diameter, 0.93-inch wall

Figure C.1 Illustration of fracture paths in carbon steel pipes which contained circumferential flaws

The sketches were made from outside the pipe as if the pipe had been flattened. The shaded areas indicate fracture surfaces visible from outside the pipe.

SC-SA-5/92-FC.1a,b

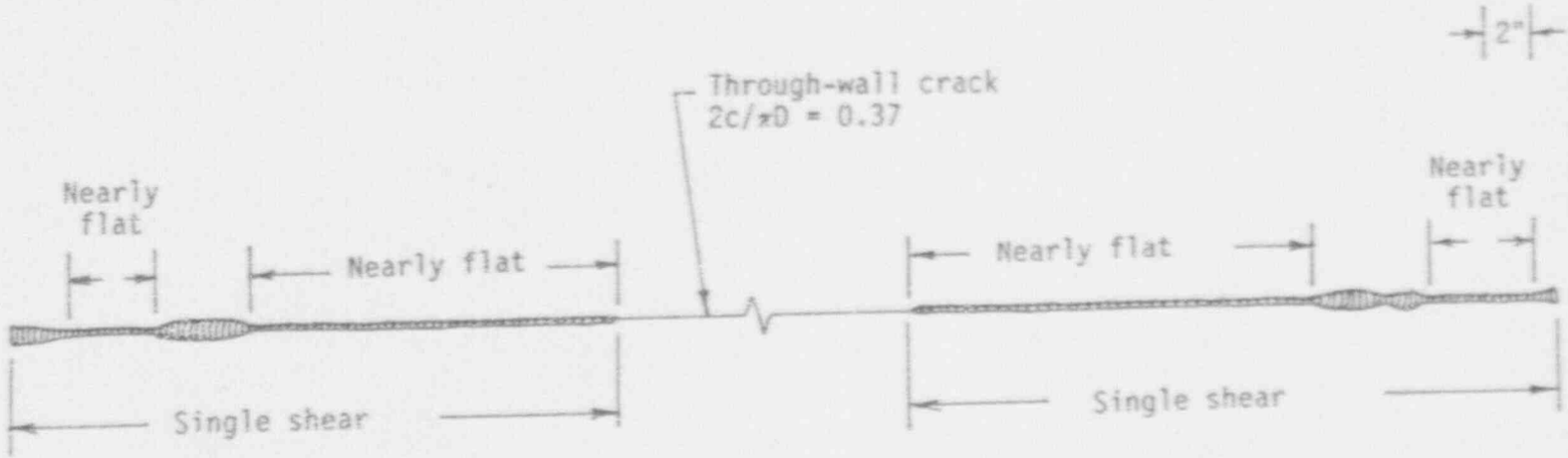

(c) Experiment 4111-4, four-point bending
Pipe DP2-F32, API 5LX65, 42-inch diameter by 0.625-inch wall

Figure C.1 (Continued)

SC-SA-5/92-FC.1c

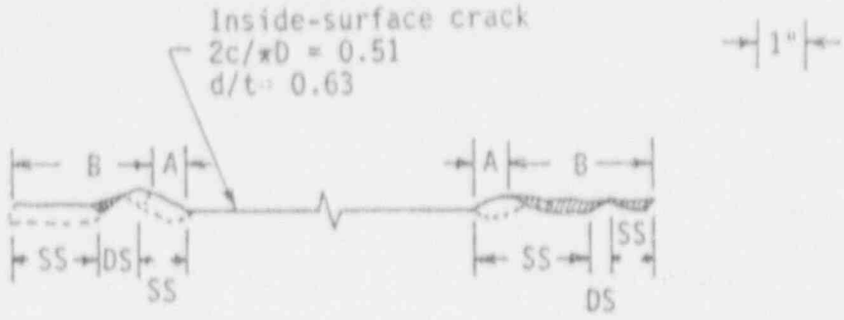

(d) Experiment 4112-5, four-point bending
Pipe DP2-F1, A106 Grade B, 6-inch diameter, Schedule 40

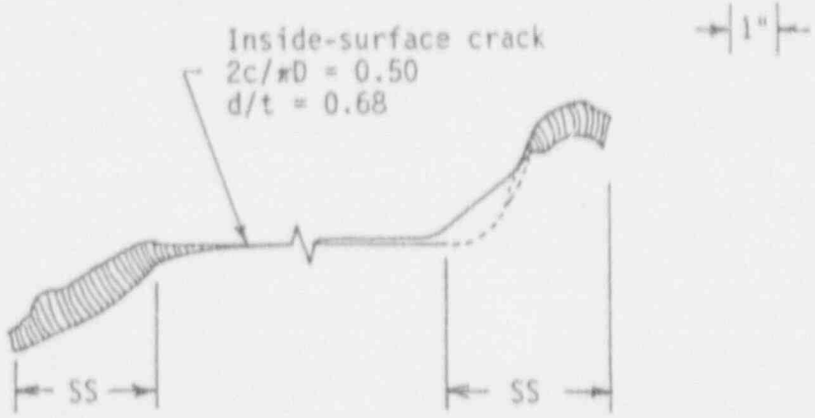

(e) Experiment 4112-6, four-point bending
Pipe DP2-F30, A106 Grade B, 6-inch diameter, Schedule 120

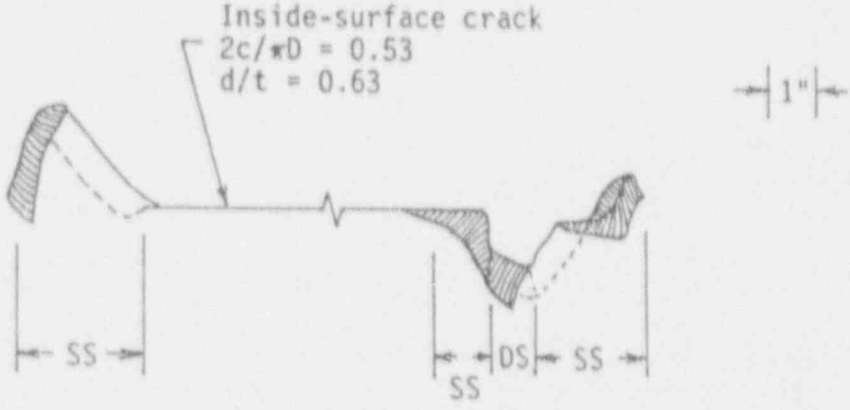

(f) Experiment 4112-7, four-point bending
Pipe DP2-F2, A106 Grade B, 6-inch diameter, Schedule XXS

Figure C.1 (Continued)

SC-SA-5/92-FC.1d,e,f

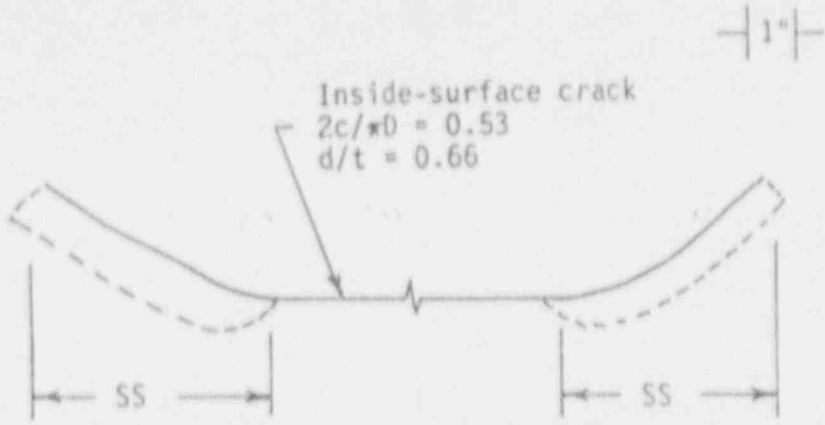

(g) Experiment 4112-8, four-point bending
Pipe DP2-F29, A106 Grade B, 16-inch diameter, Schedule 100

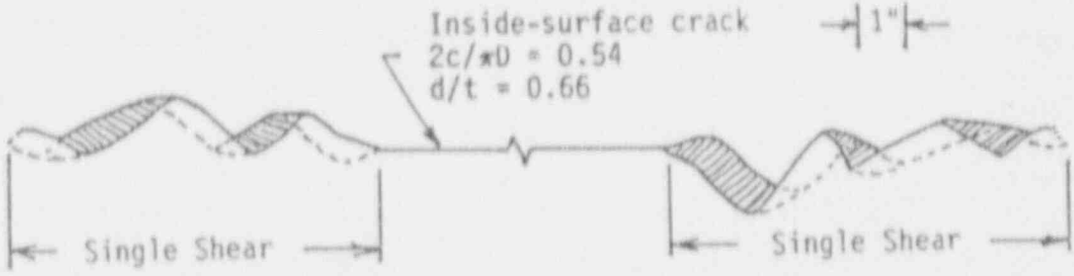

(h) Experiment 4112-9, four-point bending
Pipe DP2-F13, A106 Grade B, 16-inch diameter, Schedule 40

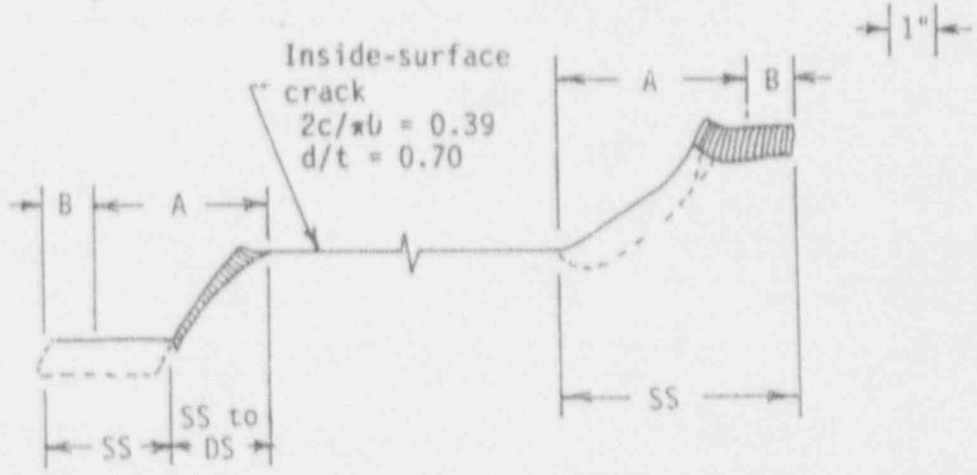

(i) Experiment 4115-1, four-point bending
Pipe DP2-F9, A333 Grade 6, 10-inch diameter, Schedule 100

Figure C.1 (Continued)

SC-SA-5/92-FC.1g,h,i

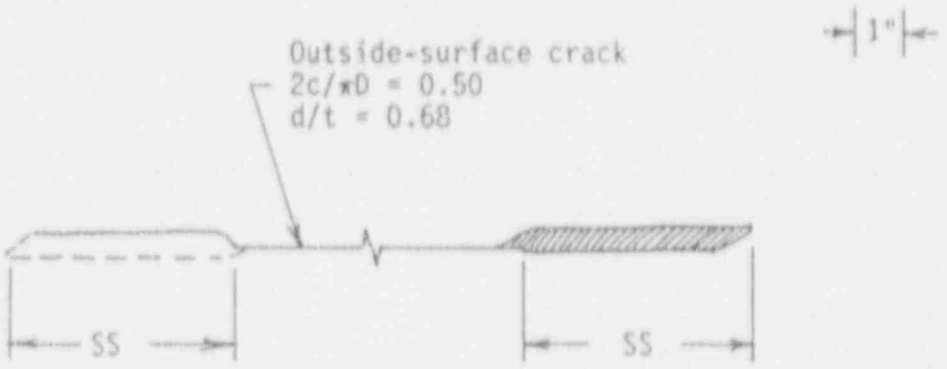

(j) Experiment 4121-6, internal pressure
Pipe DP2-F9, A333 Grade 6, 10-inch diameter, Schedule 100

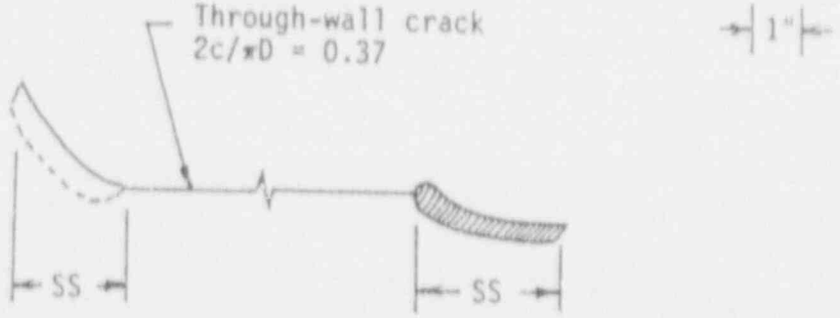

(k) Experiment 4131-3, four-point bending plus internal pressure
Pipe DP2-F9, A333 Grade 6, 10-inch diameter, Schedule 100

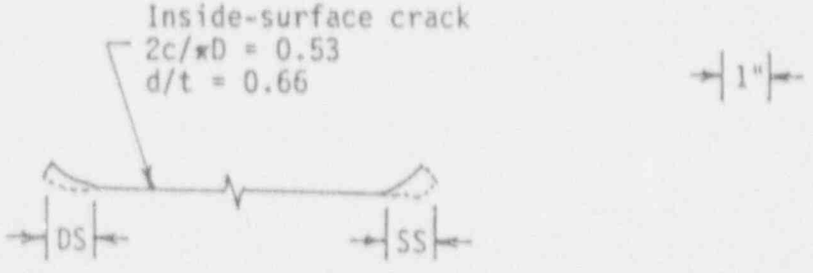

(l) Experiment 4131-4, four-point bending plus internal pressure
Pipe DP2-F9, A333 Grade 6, 10-inch diameter, Schedule 100

Figure C.1 (Continued)

SC-SA-5/92-FC.1j,k,l

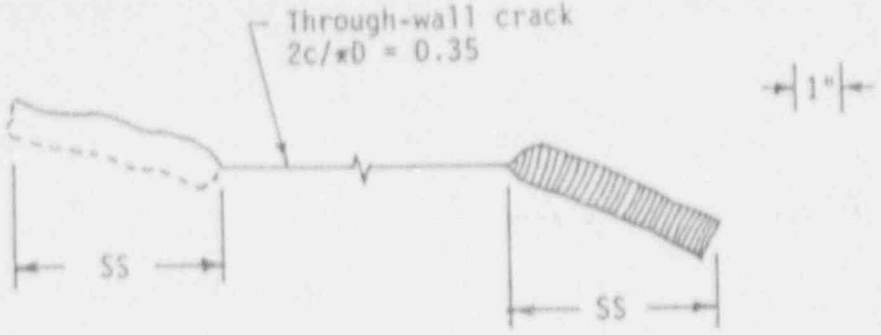

(m) Experiment 4131-7, four-point bending
Pipe DP2-F9, A333 Grade 6, 10-inch diameter, Schedule 100

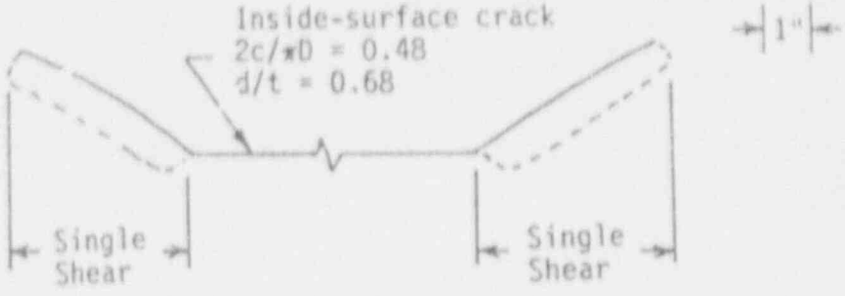

(n) Experiment 4131-8, four-point bending
Pipe DP2-F9, A333 Grade 6, 10-inch diameter, Schedule 100

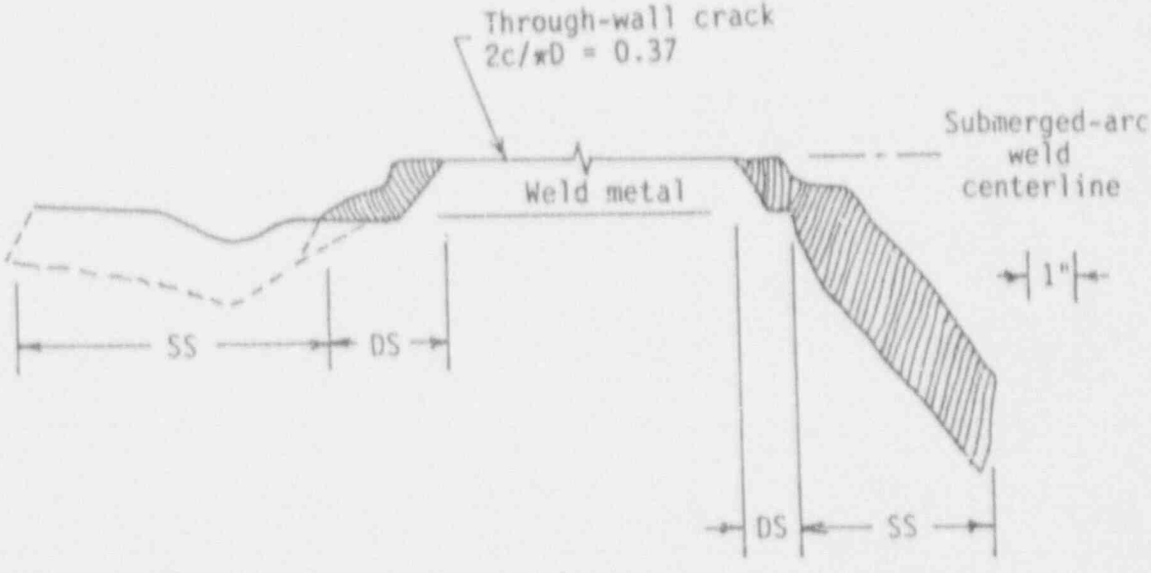

(o) Experiment 4141-9, four-point bending plus internal pressure
Pipe DP2-F29W, SAW in A106 Grade B, 16-inch diameter, Schedule 100

Figure C.1 (Continued)

SC-SA-5/92-FC.1m,a,o

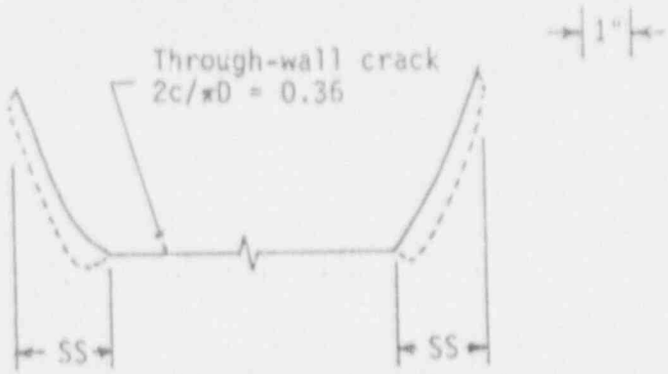

(p) Experiment IPIRG 1.2-2, four-point bending, quasi-static cyclic (R = 0)
Pipe DP2-F30, A106 Grade B, 6-inch diameter, Schedule 120

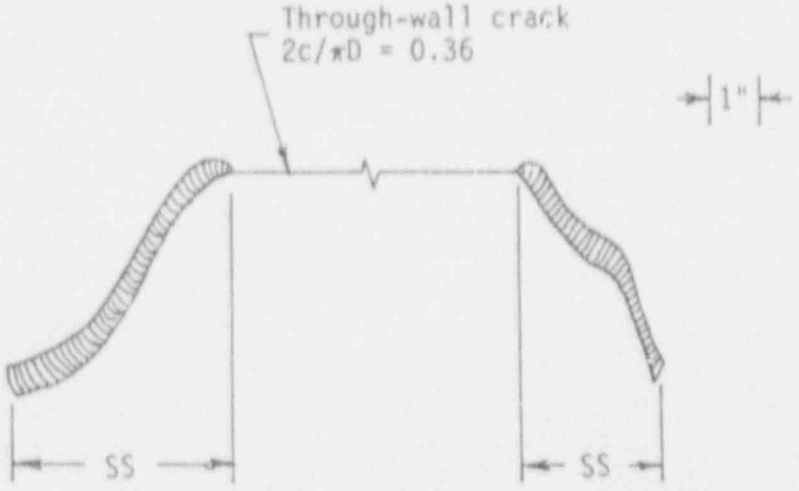

(q) Experiment IPIRG 1.2-4, four-point bending, quasi-static cyclic (R = -1)
Pipe DP2-F30, A106 Grade B, 6-inch diameter, Schedule 120

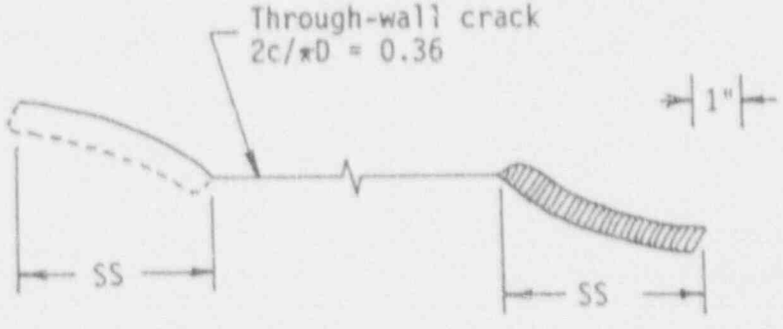

(r) Experiment IPIRG 1.2-6, four-point bending, dynamic cyclic (R = -1)
Pipe DP2-F30, A106 Grade B, 6-inch diameter, Schedule 120

Figure C.1 (Continued)

SC-SA-5/92-FC.1p,q,r

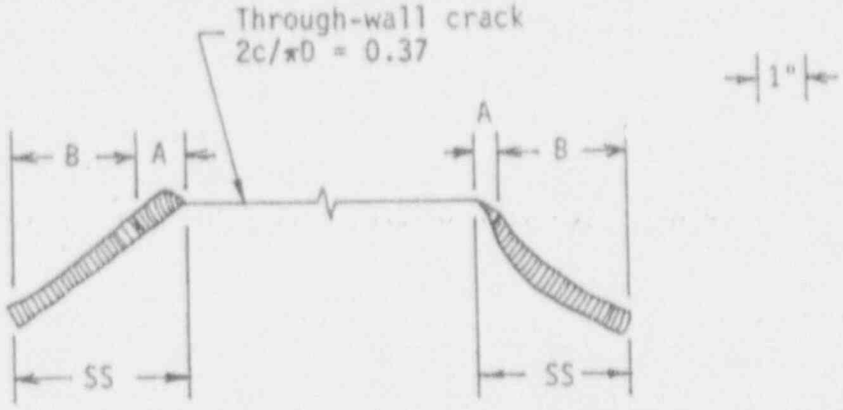

(s) Experiment IPIRG 1.2-6A, four-point bending, dynamic monotonic
Pipe DP2-F30, A106 Grade B, 6-inch diameter, Schedule 120

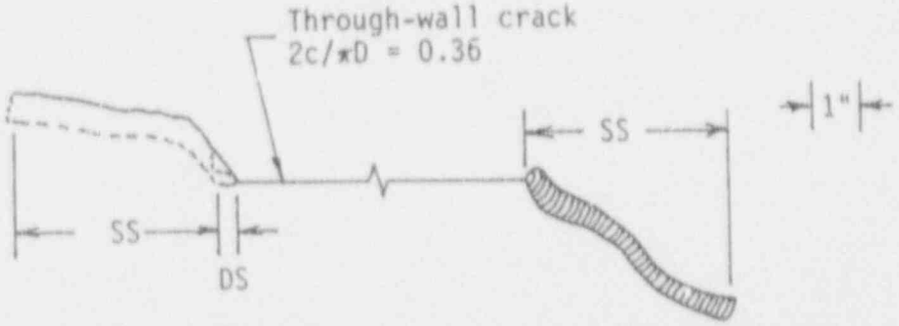

(t) Experiment IPIRG 1.2-7, four-point bending, quasi-static monotonic
Pipe DP2-F30, A106 Grade B, 6-inch diameter, Schedule 120

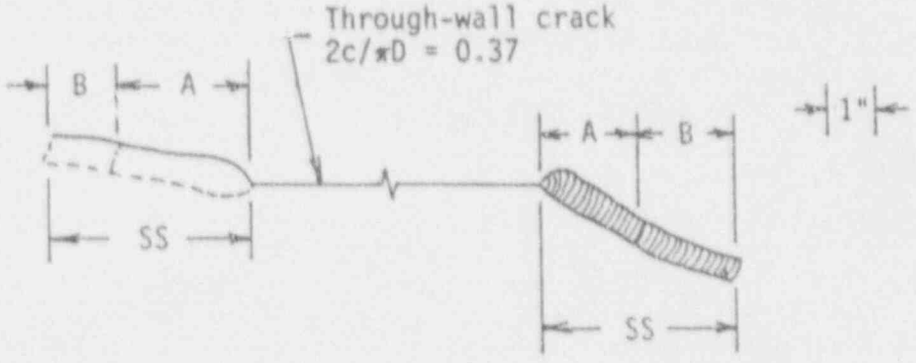

(u) Experiment IPIRG 1.2-8, four-point bending, dynamic monotonic
Pipe DP2-F30, A106 Grade B, 6-inch diameter, Schedule 120

Figure C.1 (Continued)

SC-SA-5/92-FC.1s,t,u

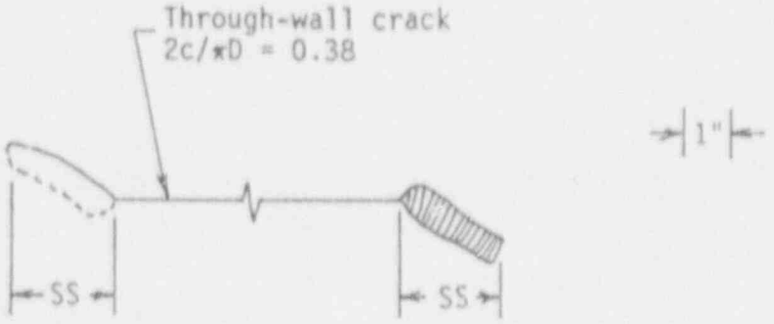

(v) Experiment IPIRG 1.2-10, four-point bending, dynamic cyclic (R=0)
Pipe DP2-F30, A106 Grade B, 6-inch diameter, Schedule 120

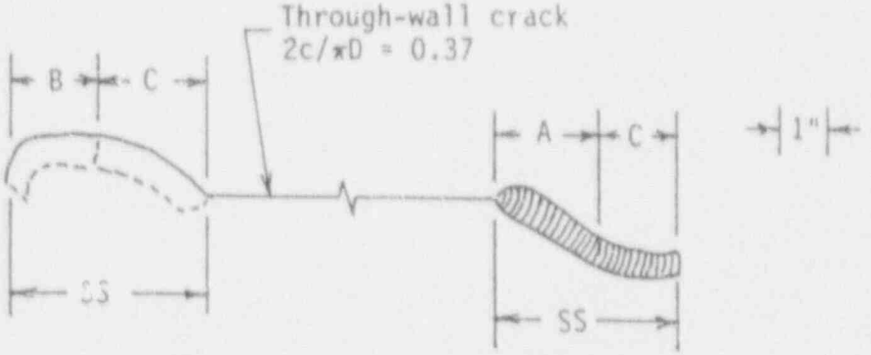

(w) Experiment IPIRG 1.2-11, four-point bending, dynamic monotonic
Pipe DP2-F30, A106 Grade B, 6-inch diameter, Schedule 120

Figure C.1 (Continued)

SC-SA-5/92-FC.1v,w

NRC FORM 335 (2.89) NRCM 1102, 3201, 3202

U.S. NUCLEAR REGULATORY COMMISSION

BIBLIOGRAPHIC DATA SHEET

(See instructions on the reverse)

1. REPORT NUMBER (Assigned by NRC, Add Vol., Supp., Rev., and Addendum Numbers, If any.)

NUREG/CR-4599
BMI-2173
Vol. 2, No. 1

2. TITLE AND SUBTITLE

Short Cracks in Piping and Piping Welds
Semiannual Report
April - September 1991

3. DATE REPORT PUBLISHED

MONTH: September | YEAR: 1992

4. FIN OR GRANT NUMBER

B5702

5. AUTHOR(S)

G. M. Wilkowski, F. Brust, R. Francini, N. Ghadiali, T. Kilinski, P. Krishnaswamy, M. Landow, C. W. Marschall, S. Rahman, P. Scott

6. TYPE OF REPORT

Technical

7. PERIOD COVERED (Inclusive Dates)

8. PERFORMING ORGANIZATION - NAME AND ADDRESS (If NRC, provide Division, Office or Region, U.S. Nuclear Regulatory Commission, and mailing address; if contractor, provide name and mailing address.)

Battelle
505 King Avenue
Columbus, Ohio 43201

9. SPONSORING ORGANIZATION - NAME AND ADDRESS (If NRC, type "Same as above"; if contractor, provide NRC Division, Office or Region, U.S. Nuclear Regulatory Commission, and mailing address.)

Division of Engineering
Office of Nuclear Regulatory Research
U.S. Nuclear Regulatory Commission
Washington, D.C. 20555

10. SUPPLEMENTARY NOTES

11. ABSTRACT (200 words or less)

This is the third semiannual report of the U.S. Nuclear Regulatory Commission's Short Cracks in Piping and Piping Welds research program. This 4-year program began in March 1990. The overall objective of this program is to verify and improve fracture analyses for circumferentially cracked large-diameter nuclear piping with crack sizes typically used in leak-before-break analyses or in-service flaw evaluations.

12. KEY WORDS/DESCRIPTORS (List words or phrases that will assist researchers in locating the report.)

Pipe, Fracture Mechanics, Cracks, J-Integral/Tearing Modulus, Leak Rate, Elastic-Plastic Fracture Mechanics, Nuclear Piping Steels

13. AVAILABILITY STATEMENT

Unlimited

14. SECURITY CLASSIFICATION

(This Page)
Unclassified

(This Report)
Unclassified

15. NUMBER OF PAGES

16. PRICE

Federal Recycling Program

UNITED STATES
NUCLEAR REGULATORY COMMISSION
WASHINGTON, D.C. 20555-0001

OFFICIAL BUSINESS
PENALTY FOR PRIVATE USE, $300

SPECIAL FOURTH-CLASS RATE
POSTAGE AND FEES PAID
USNRC
PERMIT NO. G-67

UNITED STATES
NUCLEAR REGULATORY COMMISSION
WASHINGTON, D.C. 20555-0001

OFFICIAL BUSINESS
PENALTY FOR PRIVATE USE, $300

SPECIAL FOURTH-CLASS RATE
POSTAGE AND FEES PAID
USNRC
PERMIT NO. G-67